Energy transfer and fluorescence quenching in the lightharvesting complexes of photosystem II from higher plants

Cristian Ilioaia

Energy transfer and fluorescence quenching in the light-harvesting complexes of photosystem II from higher plants

Cristian Ilioaia

PhD Thesis

Department of Molecular Biology and Biotechnology

The University of Sheffield

February 2008

The University Of Sheffield.

Abstract

Non-photochemical quenching (NPQ) is the process by which plants exposed to high light conditions dissipate the potentially harmful excess energy as heat. It is thought to involve conformational changes in the light-harvesting complexes of photosystem II (LHCII). The work reported here involves an investigation of LHCII from various perspectives, describing energy transfer between the pigments bound as well as the role of the protein in NPQ.

The 510 nm band in the 77K absorption spectra of LHCII trimers belongs to one of the luteins (lutein 2) in each monomer. The red-shift of this band may be caused by specific interaction(s) between the monomers during their association into trimers. The presence of the red-shifted lutein 2 in the unusual Lhcb3-Lhcb5 trimers from antisense *Lhcb2 Arabidopsis* plants is consistent with this interpretation. This lutein was found to be efficient in transferring energy to chlorophyll *a*. Analysis of the spectroscopic features of spinach thylakoids before and after de-epoxidation suggests the occurrence of a conformational change in the light-harvesting antenna, resulting in the remaining violaxanthin becoming more strongly involved in energy transfer to the PSII core.

The quenching mechanism in LHCII was investigated. LHCII immobilised in a gel matrix showed quenching without protein aggregation, the transition to the quenched state involving a conformational change in which the neoxanthin and lutein 1 domains were affected. By monitoring the twisting of the neoxanthin molecule detected by resonance Raman spectroscopy, the same conformational change that accompanies the formation of the quenched state *in vitro* was observed *in vivo* upon NPQ induction. Transient absorption spectroscopy applied to purified LHCII in the quenched state showed the pathway for energy dissipation, involving energy transfer from chlorophyll *a* to the S1 excited state of lutein 1, which then decays to its ground state, dissipating the energy as heat.

Acknowledgements

I would like to thank my supervisor Professor Peter Horton for all his help, advice and support, and for giving me the opportunity to work in his lab, which is something I will always be grateful for. Also, I want to thank him for trusting me when he appointed me for the PhD position, someone with no background and no practical experience in the photosynthesis field. I would like also to thank him for the patience he had with me during the writing up process; I hope I was not the worst PhD student he ever supervised.

Thanks also must go to Dr. Alexander (Sasha) Ruban, for introducing me to the world of spectroscopy, for guidance, for suggestions and for sharing with me his ideas (not only scientific). A special thank you to Anett for sharing with me all the good and bad things throughout the 2 years we spent together in Sheffield, and for supplying the plants for the Nature paper experiments. I am also grateful to Pam Scholes for her everyday invaluable assistance and to Sveta Solovieva for assistance with sample preparation. Thanks also to Dr. László Kovács for help with the CD measurements, as well as to Marisa, Sophie, Sonia, Matt and all the past members of the Horton Lab.

I would also like to thank my Amsterdam collaborators - Rudi Berera for his assistance with the femtosecond transient absorption spectroscopy, Dr. Ivo van Stokkum for the hard work done with the data analysis, Dr. John Kennis and Professor Rienk van Grondelle.

Special thanks go to the people in Saclay in particular to: Dr. Bruno Robert who is a really great person and to Dr. Andy Pascal who helped me a lot with the thesis preparation and being such a good proof-reader. I must mention here also Dr. Andrew Gall for the chats and beers that we had together and for helping me to find a flat in Paris, Dr. Ghada Ajlani for asking me almost everyday when I am going to finish my thesis, Dr. Thibaut Desquilbet who helped me with the (French) administrative issues.

Many thanks to my family who have demonstrated incredible understanding and patience during the last three years (or so)!

Finally, I would like to thank the INTRO2 Marie Curie Research Training Network for my PhD studentship, courses and conferences during these years.

To Oana & Alexia

"A pessimist sees the difficulty in every opportunity;
an optimist sees the opportunity in every difficulty."

Sir Winston Churchill

Abbreviations

ΔA	absorbance change
ADP	adenosine di-phosphate
Anth	antheraxanthin
APS	ammonium persulphate
ATP	adenosine tri-phosphate
ATPase	adensosine tri-phosphate synthase complex
BBO	*β*- barium borate
BSA	bovine serum albumin
***β* –car**	*β* –carotene
[Chl]	chlorophyll concentration
CD	circular dichroism
cDNA	complimentary DNA
Chl	chlorophyll
Chl*a*	chlorophyll a
Chl*b*	chlorophyll b
Cyt b_{559}	cytochrome b_{559} complex
Cyt b_6f	cytochrome b_6f complex
DCCD	dicyclohexylcarbodiimide
DCMU	3-(3,4-dichlorophenyl)-1,1-dimethylurea
DES	de-epoxidation state
DGDG	digalactosyldiacylglycerol
dH_2O	distilled water
***α* – DM**	*n*-dodecyl-*α*-D-maltoside
***β* – DM**	*n*-dodecyl-*β*-D-maltoside
DTT	dithiothreitol
EADS	evolution associated difference spectra
EDTA	ethylenediaminetetraacetic acid
EM	electron microscopy
ESA	excited state absorption
Fd	ferredoxin
FeS	iron-sulphur centre
FLIM	fluorescence lifetime imaging microscopy

FNR	ferredoxin NADP reductase
FPLC	fast protein liquid chromatography
FWHM	full width at half maximum
HEPES	*N*-(2-hydroxyethyl)piperazine-*N'*-2-ethanesulphonic acid
HPLC	high performance liquid chromatography
IEF	isoelectric focusing
k_d	quenching strength
kDa	kilodalton
LD	linear dichroism
L17	PsbS overexpressor line 17
LHCI	light harvesting antenna of photosystem I
LHCII	light harvesting antenna of photosystem II
LHCs	light harvesting complexes
Lut	lutein
MES	2-(N-Morpholino)-ethanesulfonic acid
MeV	methyl viologen
MGDG	monogalactosyldiacylglycerol
NADP	nicotinamide adenine dinucleotide phosphate
NADPH	nicotinamide adenine dinucleotide phosphate (reduced)
Neo	neoxanthin
NPQ	non-photochemical quenching of chlorophyll fluorescence
OD	optical density
OEC	oxygen evolving complex
OPA	optical parametric amplifier
PAM	pulse amplitude modulated
PB	photobleaching
PC	plastocyanin
Pheo	pheophytin
Pi	inorganic phosphate
PMF	proton motive force
PQ	plastoquinone
PQH_2	plastoqinol
PSI	photosystem I
PSII	photosystem II

qE	rapidly relaxing, energy dependent quenching component of NPQ
qI	very slowly relaxing, photoinhibitory quenching component of NPQ
qP	photochemical quenching
qT	slowly relaxing quenching component of NPQ caused by state transitions
RC	reaction centre
RR	resonance Raman spectroscopy
SADS	species associated difference spectra
SDS-PAGE	sodium dodecyl sulphate-polyacrylamide gel electrophoresis
SE	stimulated emission
SEP	stress enhanced protein
SQDG	sulfoquinovosyldiacylglycerol
TA	transient absorption
ΔpH	transthylakoid pH gradient
TEMED	tetramethylethylenediamine
Tris	trishydroxymethylaminomethane (2-amino-2-hydroxymethyl-1,3-propanediol)
Vio	violaxanthin
VDE	violaxanthin de-epoxidase
Wt	wild type
Zea	zeaxanthin
ZE	zeaxanthin epoxidase
XC	xanthophyll cycle

Table of Contents

CHAPTER ONE

General introduction

1.1 Introduction

Photosynthesis is the process by which green plants, algae and some species of bacteria utilize light energy to synthesise organic compounds. The process of photosynthesis can be either oxygenic or anoxygenic. The difference between these two processes is tha,t in the former water is oxidised and oxygen is released and in the latter water is not oxidised and no production of oxygen takes place.

In higher plants, photosynthesis is an oxygenic process where light energy is used to convert the simple molecules, water (H_2O) and carbon-dioxide (CO_2) into complex organic sugars, releasing oxygen (O_2) as a by-product. The process may be basically described by the following chemical reaction:

$$6H_2O + 6CO_2 + \text{ light energy} \rightarrow C_6H_{12}O_6 + 6O_2$$

The energy of the light is absorbed by the photosynthetic pigments (chlorophylls and carotenoids) and converted into chemical energy (adenosine triphosphate, ATP) and the reducing equivalents (in the form of reduced nicotinamide adenine dinucleotide phosphate, NADPH), which are subsequently used in the synthesis of carbohydrates from carbon dioxide in Calvin-Benson cycle.

1.2 Two phases of photosynthesis: the 'light' and 'dark' reactions

Chlorophyll and carotenoid molecules are bound to numerous multi-subunit pigment-protein complexes that are specifically organised to maximise the efficiency of light capture and the transfer of energy to the electron transport chain. The vast majority of these pigments function to harvest light energy and increase the effective surface area for light absorption. Photons of light excite the pigment molecules of the light-harvesting complexes (LHC) into a higher singlet excited state, this excitation energy being further directed to the reaction centres of the two photosystems: photosystem I (PSI) and photosystem II (PSII). The excitation energy is used in the reaction centres to produce a charge separation resulting in the release of the electrons which are passed along a series of electron carriers as seen in Figure 1.

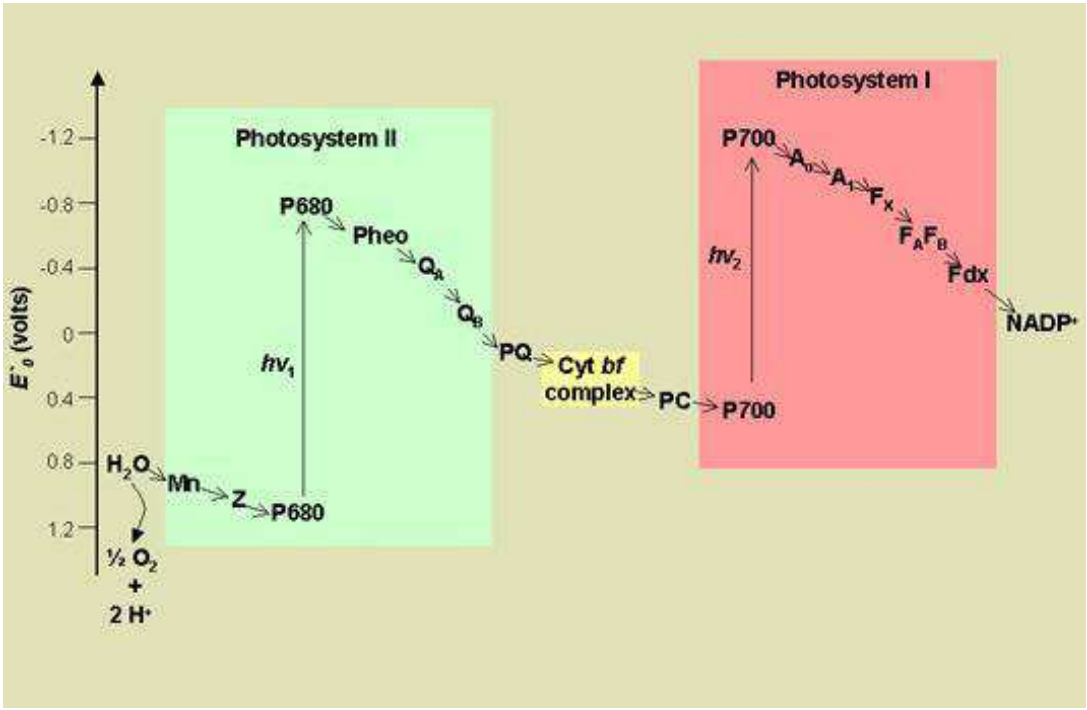

Figure 1. The Z-scheme for linear electron transport in the thylakoid membrane: Mn=manganese cluster; Z= tyrosine Z; P680=PSII reaction centre special pair chlorophyll; P680*=excited singlet state of special pair (primary donor); Pheo=pheophytin (primary acceptor)=Q_A^-=plastoquinone A; Q_B=plastoquinone B; PQ= pastoquinone pool; Cyt b*f*=cytochrome b6*f* complex; PC=plastocyanin; P700=PSI reaction centre special pair chlorophyll; P700*=excited singlet state of special pair (primary donor); A_0=primary acceptor chlorophyll; A_1=secondary acceptor phylloquinone; F_x=iron sulphur cluster; F_AF_B=iron sulphur cluster; Fdx=ferredoxin (Berg et al., 2002).

Higher plants transfer electrons from H_2O to ferredoxin, the latter being able to reduce $NADP^+$ to NADPH due to its oxidation-reduction potential of approximately –0.42 V. At the same time, protons are transferred across the thylakoid membrane from the stroma to the lumen, creating a proton motive force, which is employed by the ATP-synthase complex to drive ATP synthesis. In the 'dark' reactions that occur in the chloroplast stroma ATP and NADPH produced during the 'light' reactions are used to assimilate CO_2 into carbohydrates.

1.2.1 The electron transport chain in higher plants

The excitation energy absorbed by the LHC antenna is funnelled to the reaction centres (RCs) of both photosystems (PSI and PSII), where it is used to produce a charge separation reaction between a special chlorophyll molecule (P680 in PSII and P700 in PSI) and an acceptor molecule (see also Figure 1). An electron is transferred to Q_A via a molecule of pheophytin (Pheo), forming the highly oxidised species, $P680^+$. The electron on Q_A is transferred further to a molecule of plastoquinone bound to the Q_B site which, after accepting a second electron, becomes protonated and is then released as

plastoquinol. Electrons from plastoquinol are then transferred via the cytochrome b_6f (cyt b_6f) complex to a mobile electron carrier called plastocyanin (PC). A second charge separation event within the reaction centre of PSI liberates a second electron, which is passed along a series of carriers to the terminal electron acceptor ferredoxin (Fdx). Fdx is used by ferredoxin NADP reductase (FNR) to reduce $NADP^+$ to NADPH. The linear electron transport chain is completed by the reduction of the P680 special pair in PSII, via the oxidation of H_2O to O_2. Translocation of protons across the thylakoid membrane occurs concomitantly with the transport of electrons from water to $NADP^+$. A pH gradient is formed by the release of protons into the thylakoid lumen through water splitting in the oxygen-evolving complex of PSII, the oxidation of plastoquinol to plastoquinone (PQ) by the cyt b_6f complex and the uptake of protons in the reduction of plastoquinone and NADP.

1.3 Photosynthetic apparatus

Photosynthesis in higher plants is carried out by leaves. Within the leaf, the apparatus of photosynthesis is located in chloroplasts, a specialised organelle, consisting of three membranes, two forming a smooth outer envelope, which surround the elaborately folded inner membrane known as the thylakoid (Figure 2). The surrounding aqueous phase called the stroma is a dense protein gel located between the outer membrane and the thylakoids and contains the enzymes that catalyse the 'dark' reactions. The thylakoid membrane is a continuous double membrane system, which is differentiated into stacked (appressed) and unstacked (non-appressed) regions, and which accommodates all the light harvesting proteins and the electron transport chain.

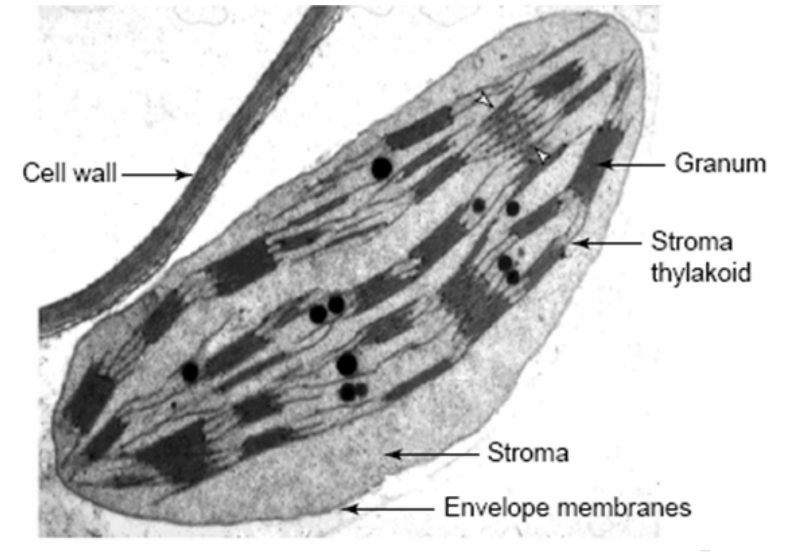

Figure 2 Thin section electron micrograph of a chloroplast. The internal membrane is divided into grana and stroma thylakoids. Stromal thylakoids are indicated between 2 white arrowheads (Mustárdy & Garab, 2003).

The thylakoid consists of a continuous membrane organised into a 3 dimensional network with an interior aqueous phase, known as the lumen. The generally accepted model was proposed by Paolillo (1970), and later confirmed by Brangeon & Mustárdy (1979). The model depicts the thylakoid membranes with multiple right-handed helices of stroma lamellae wrapped around cylindrical grana forming a contiguous system. An updated version of this model was recently proposed (Figure 3), based upon electron micrographs from serial sections of grana-stroma assemblies (Mustardy & Garab, 2003).

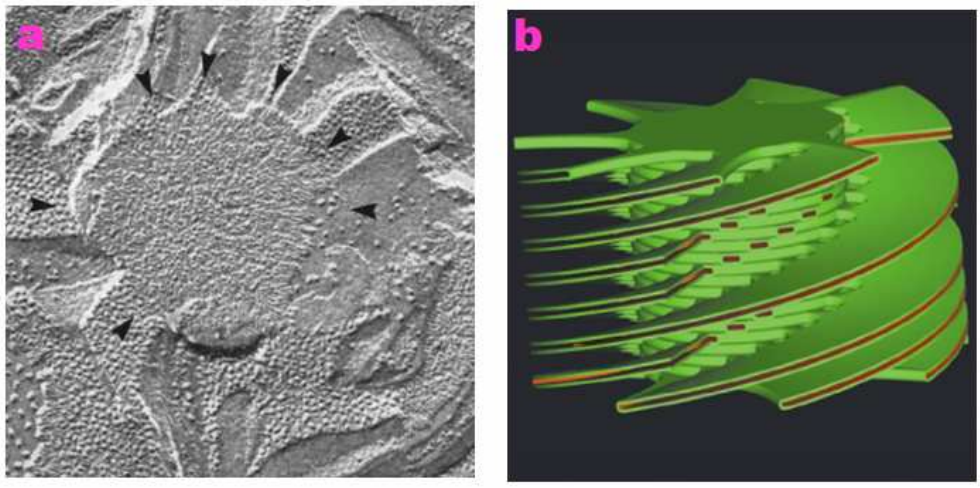

Figure 3. Freeze-fractured chloroplast (a) when the fracture plane is parallel with the granum thylakoid, arrowheads showing stroma thylakoid junctions, which are arranged in a circular fashion surrounding the granum membrane; 3-D computer model of the granum constructed from electron micrographs of full serial sectioning of a granum–stroma assembly (b).

The functional justification of the thylakoid architecture is the lateral heterogeneity of the appressed and non-appressed regions within the thylakoid membrane, where the protein compostion varies considerably. Photosystem I and ATPase dominate the unstacked regions of the membrane whilst the majority of Photosystem II is located in the grana stacks. The abundance of LHCII in the grana has led to suggestions that these antennae complexes play a vital role in the lateral organisation of the thylakoid.

1.4 Photosynthetic pigments

1.4.1 Chlorophylls

Chlorophylls *a* and *b* are the major light harvesting pigments found in the photosynthetic antenna. Chlorophylls are molecules which have a magnesium (Mg) atom as its central atom, forming a chlorin ring (Figure 4).

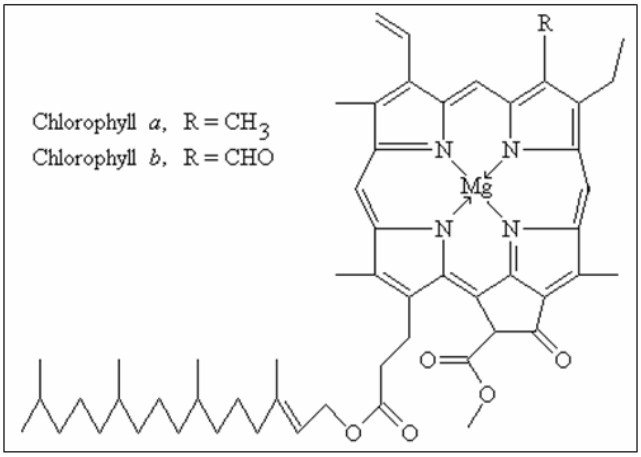

Figure 4. Molecular structure of chlorophyll pigments. The difference between the two chlorophyll forms is within the side chain (R) of the 7th carbon atom (Scheer, 2003).

Chlorophylls are planar, with a large conjugated π-system, the only difference between chlorophyll *a* and chlorophyll *b* being the extra C=O group in case of chlorophyll *b*. The differences between the absorption spectra of these 2 molecules (Figure 5) are large: the red-most absorption band in the absorption spectrum (also known as the Q_y band) of chlorophyll *a* is located at ~662 nm, whereas the red most absorption band for chlorophyll *b* is located at ~642 nm; and the so-called Soret band (in the blue region of the spectrum) for chlorophyll *a* is situated at ~430 nm and at 460 nm for chlorophyll *b*. The difference in the absorption spectra of the chlorophyll *a* and chlorophyll *b* increases the absorption cross-section of the chlorophyll *a*-chlorophyll *b*

containing complexes. All the chlorophylls present in the thylakoid membrane are bound by proteins, which provide a specific local environment, resulting in red shifts of the absorption spectra, further increasing the absorption cross-section.

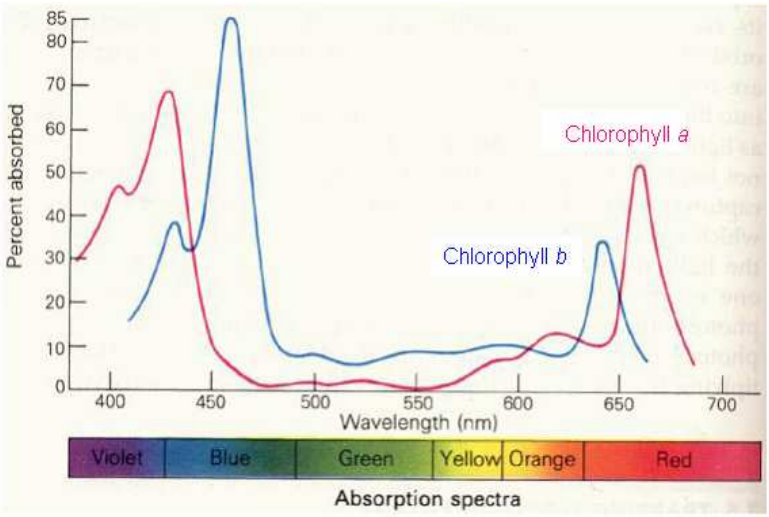

Figure 5. Room temperature absorption spectra of chlorophyll *a* (magenta) and chlorophyll *b* (blue) molecules in acetone (Berg et al., 2002).

1.4.2 Carotenoids

Carotenoids are molecules containing extended conjugated double bond systems and cyclic ring structures, most commonly C_{40}. They are derived from isoprenoid precursors and are divided into two groups, the carotenes (cyclic hydrocarbons) and xanthophylls (oxygenated derivatives of the carotenes). Lycopene, a red pigment, is synthesised from geranylgeranyl pyrophosphate and the remainder of the carotenoid biosynthesis pathway follows 2 branchesleading to α xanthophylls and β xanthophylls (Figure 6).

Carotenoids are involved in light harvesting, absorbing light of different wavelengths to that of chlorophyll, and passing the energy on to chlorophyll. A major function of carotenoids is in photoprotection, removing chlorophyll triplet states, quenching singlet oxygen species and dissipating chlorophyll singlet states under excess light conditions. The role of carotenoids in photoprotection will be discussed in detail in section 1.7.1.

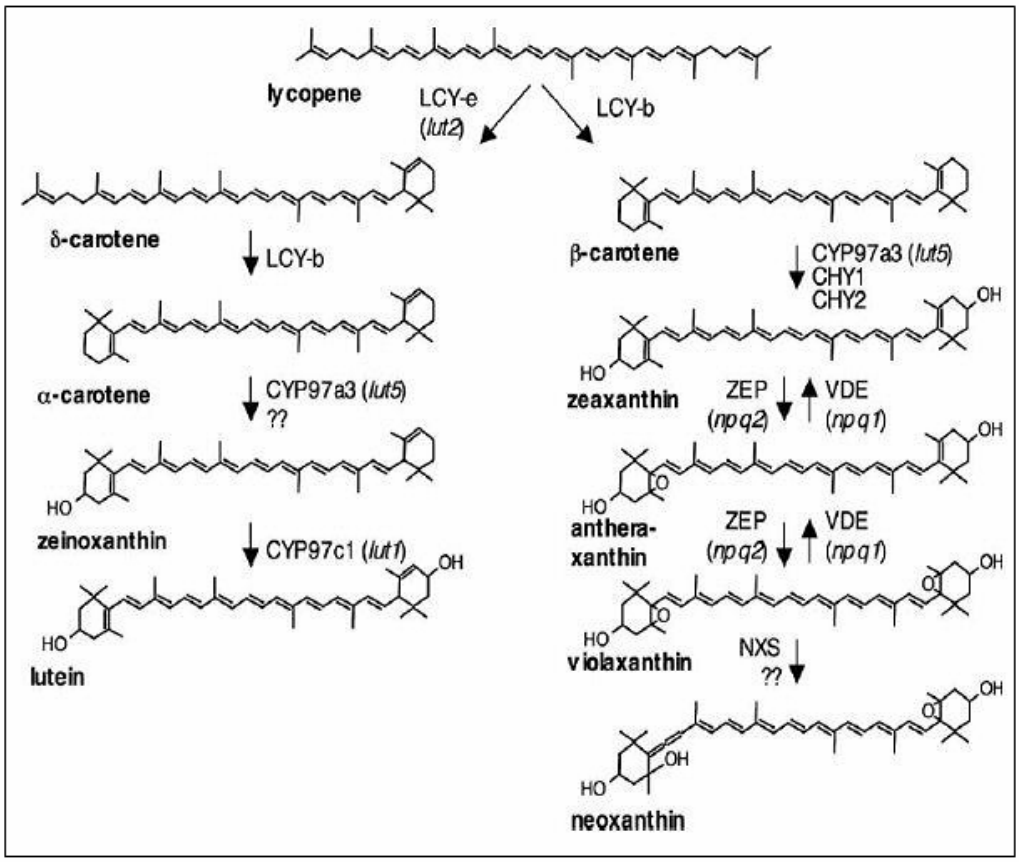

Figure 6. The carotenoid biosynthetic pathway in higher plants. Key enzymes are in capitals, *Arabidopsis* mutants that led to their identification in italics: LCY-e=lycopene ε-cyclase (*lut2*); LCY-b=lycopene β-cyclase; Chy1/Chy2=β-carotene hydroxylase; ZEP=zeaxanthin epoxidase; VDE=violaxanthin de-epoxidase; NXS=neoxanthin synthase; CYP97a3 (*lut5*)=β-ring hydroxylase activity; CYP97c1 (*lut1*)=ε-ring hydroxylase activity (Fiore et al., 2006).

1.5 The protein complexes of the thylakoid membrane

1.5.1 Photosystem I

Photosystem I (PSI) is a large, multi subunit protein complex, which comprises a reaction centre core and peripheral antenna. It is located in the non-appressed stromal lamellae regions of the thylakoid membrane (Dekker & Boekema, 2005) where it catalyses the light-induced oxido-reduction of plastocyanin and ferredoxin (Jensen et al., 2003). The 3-D crystal structure of higher plant *Pisum sativum* (pea) PSI at 4.4 Å shows 12 core subunits and 4 different light harvesting proteins (LHCI), assembled together in a half-moon shape on one side of the core (Ben-Shem et al., 2003). The complex binds 167 chlorophylls, 3 Fe-S clusters and 2 phylloquinones, and consists of 45 transmembrane helices (Ben-Shem et al., 2003). The structure of plant PSI is shown in Figure 8. The large subunits PsaA and PsaB comprise the catalytic core and bind the majority of the chlorophylls, including the P700 special pair, which forms the primary

electron donor. Light absorption causes charge separation, the P700 transfers an electron to the electron acceptor A_0 (a chlorophyll *a* molecule). The electron then passes to A_1 (a phylloquinone) and then through 3 iron-sulphur centres (F_X, F_A and F_B), to ferredoxin on the stromal side of the membrane (Jordan et al., 2001). The electron reduces ferredoxin, which binds in a pocket on the stromal side of PsaA and is surrounded by PsaC, PsaD and PsaE. Oxidised $P700^+$ is reduced by an electron from plastocyanin on the lumenal side of PSI.

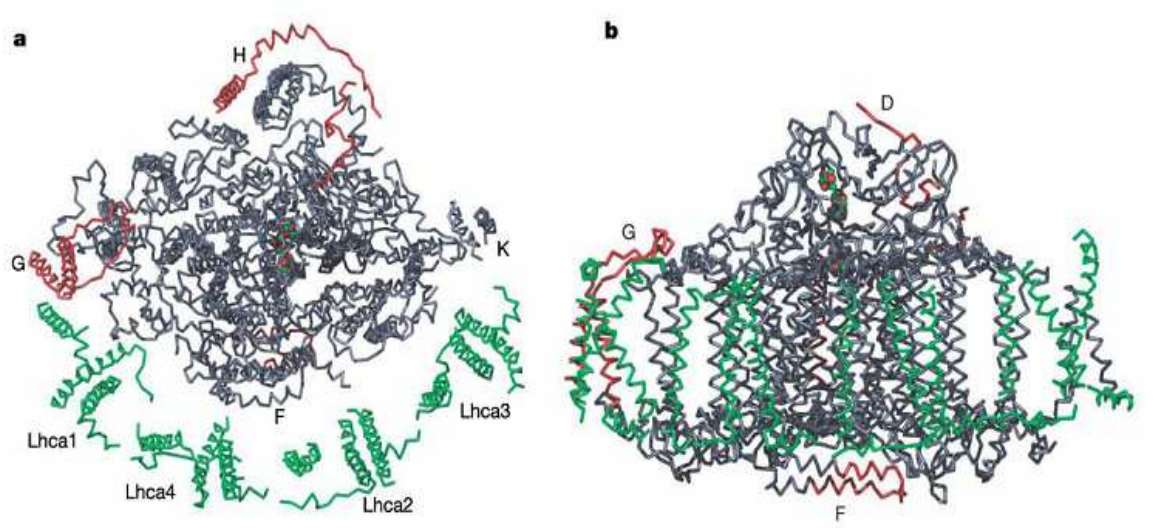

Figure 8. Structural model of the plant photosystem I. View from the stromal side of the thylakoid membrane (a) and view from the LHCI side (b). Lhca antenna proteins are shown in green, PSI core proteins (PsaA and PsaB) in grey and the minor subunits in red (Ben-Shem et al., 2003).

Four light-harvesting proteins (Lhca1-4) form LHCI and they are arranged as two dimers (LHCI-730 and LHCI-680) that bind asymmetrically to the RC, via associations between a number of different subunits (Ben-Shem et al., 2003). The LHCI-730 dimer (named after the 77K fluorescence emission maximum) is formed by association of the Lhca1 and Lhca4 polypeptides, while Lhca2 and Lhca3 form the LHCI-680 dimer (Klimmek et al., 2005). Together, these dimers bind 56 chlorophyll molecules. The red shifted fluorescence emission spectrum of PSI is caused by a few so-called 'red' chlorophylls, which have an energy level lower than the RC. The antenna serves to capture light and funnel it to the PSI core. The amount of LHCI bound to the PSI core was shown to vary with environmental conditions (Bailey et al., 2001). PSI is also the binding site for phosphorylated LHCII following the state 1 to state 2 transition, described in section 1.8.2 (Lunde et al., 2000).

1.5.2 Cytocrome b_6f

The cytochrome *b6f* (cyt *b6f*) connects the two photosystems in linear electron flow and is located in both granal and stromal regions of the membrane (Dekker & Boekema, 2005). It functions as a plastoquinol-plastocyanin oxidoreductase, simultaneously translocating protons into the lumen (for review, see Cape et al., 2006). The complex is dimeric, consisting of 4 large (cytochrom *b6*, cytochrom *f*, Rieske iron-sulfur, and subunit IV) and 4 smaller (PetG, PetM, PetL and PetN) polypeptide subunits (Widger et al., 1984; Kurisu et al., 2003). The cyt *b6f* monomer is composed of 13 transmembrane helices and binds four haem molecules (Kurisu et al., 2003), one chlorophyll *a* (Pierre et al., 1997) and one β-carotene (Zhang et al., 1999). The ferredoxin NADP reductase (FNR) binds to the cyt *b6f* complex, providing the means for cyclic electron transport around PSI (Joliot et al., 2004; Munekage et al., 2004).

1.5.3 ATP-synthase complex

The plant ATP-synthase complex is a large macromolecular multisubunit enzyme of approximately 600 kDa that is responsible for the generation of ATP, utilising the proton gradient created by electron transport. ATP is formed from adenosine di-phosphate (ADP) and inorganic phosphate (Pi). The complex is formed by the association of nine polypeptides organised in the CF_1 and CF_0 main subunits (for review, see Groth & Pohl, 2001). The CF_1 subunit is found on the stromal surface of the thylakoid membrane, where it is associated with the CF_0 intrinsic membrane subunit. CF_1 is water soluble and CF_0 is hydrophobic (Mc Carty et al., 2000). CF_1 is the largest, contains the active site and consists in 5 different polypetides in a stoichiometry of $\alpha_3\beta_3\gamma\delta\varepsilon$ (Abrahams et al., 1994; Groth & Pohl, 2001). CF_0 is formed from 4 subunits (I-IV), and its function is to use a proton driving force to rotate the γ subunit of CF_1 (Junge et al., 1997), a process that is a key part of the ATP synthase mechanism (Noji et al., 1997). Muller et al. (2000) showed by atomic force microscopy that the 4 subunits are present in a 1:1:14:1 stoichiometry.

1.5.4 Photosystem II

Photosystem II (PSII) is a multisubunit protein-cofactor complex found abundantly in the appressed (granal) regions of the thylakoid membrane, having a water-plastoquinone oxidoreductase function (Hankamer et al., 1997; Barber, 1998). PSII contains a reaction

centre (RC), which together with inner antenna constitutes the PSII core complex, the proteins of the oxygen-evolving complex (OEC), and those of the peripheral light-harvesting antenna. The structure of the PSII core complex of the cyanobacterium *Synechococcus elongatus* has been resolved using X-ray crystallography to a 2.5Å resolution (Zouni et al., 2001). Situated at the heart of PSII, the RC incorporates the chloroplast encoded D1 and D2 polypeptides (products of *psb*A and *psb*D genes, respectively), which form a heterodimer. The dimer contains 35 chlorophyll *a*, 11 β-carotene molecules and 14 lipid molecules namely 6 MGDG, 4 DGDG, 3 SQDG and 1 PG (Loll et al., 2005). Each of the D1 and D2 subunits contains five membrane spanning helices, which each have N-termini on the stromal side of the membrane. The D1 and D2 subunits are homologues of the L and M subunits of the purple bacterial RC (Deisenhofer et al., 1985; Rhee et al., 1998). The cofactors involved in charge separation and electron transport bind to the RC's dimeric core, and include the primary electron donor P680 reaction centre chlorophyll (probably P_{D1}), P_{D2}, Chl_{D1}, Chl_{D2}, Chl_{ZD1}, Chl_{ZD2} chlorophylls, two pheophytins ($Pheo_{D1}$ and $Pheo_{D2}$), the secondary electron acceptors plastoquinones Q_A and Q_B (situated close to pheophytins), two β-carotenes and finally a non-haem iron molecule situated between the plastoquinones molecules. The RC also contains cytochrome b559 (situated at the periphery), which consists of two subunits (9kDa and 4kDa) encoded by the chloroplast *psb*E and *psb*F genes, respectively. These polypeptides ligate a single haem group. The function of cytochrome b559 still remains unproven but it is thought to have a role in the protection of the RC against photodamage (Whitmarsh & Pakrasi, 1996; Stewart & Brudvig., 1998).

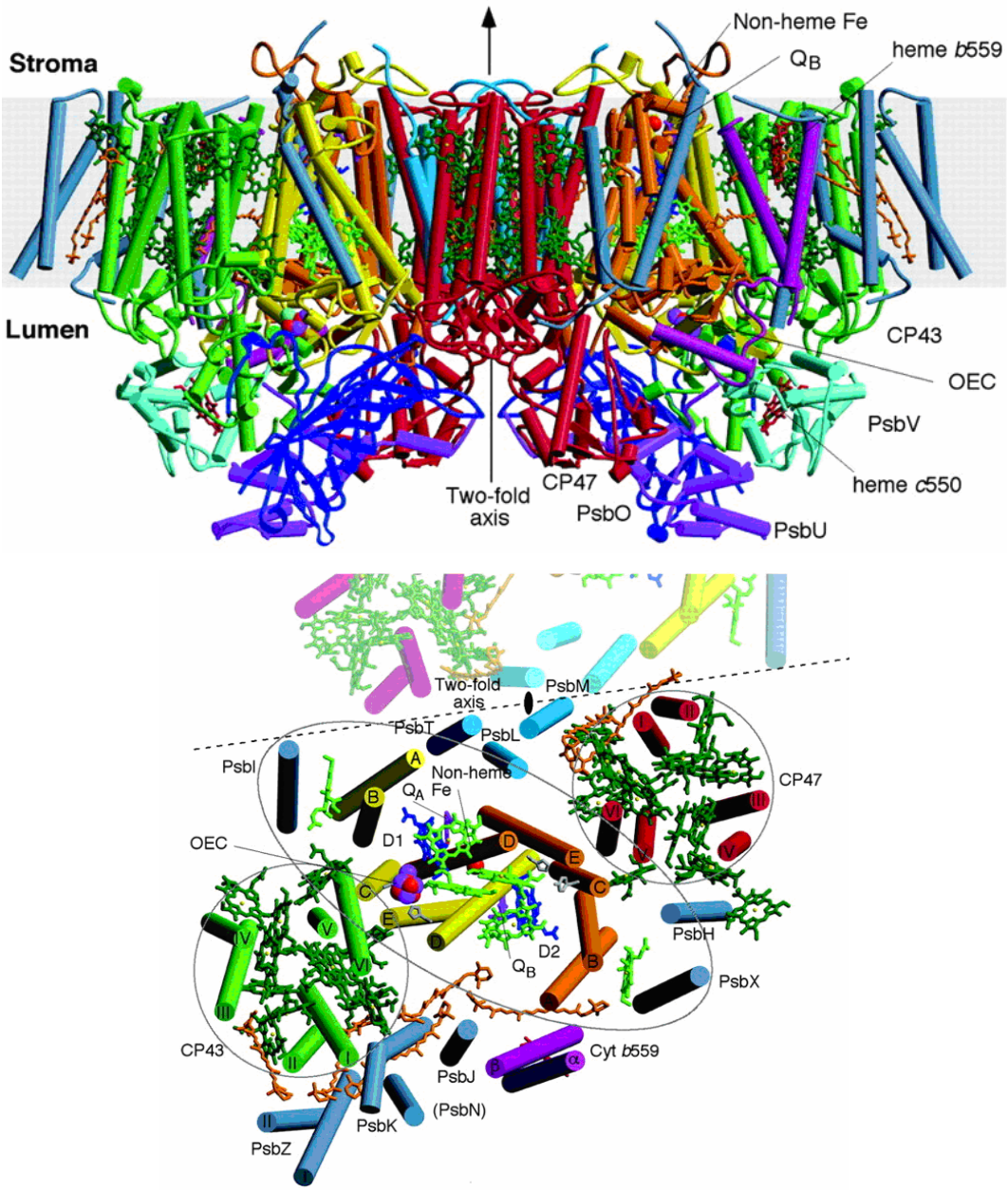

Figure 7. Structural organisation of the Photosystem II core complex. View perpendicular to the membrane plane, showing the minor lumenal exposed subunits (top). Helices are represented as cylinders with D1 in yellow; D2 in orange; CP47 in red; CP43 in green; cyt *b*559 in red; PsbL, PsbM, and PsbT in medium blue; and PsbH, PsbI, PsbJ, PsbK, PsbX, PsbZ, and PsbN in gray. The extrinsic proteins are PsbO in blue, PsbU in magenta, and PsbV in cyan. Chlorophylls of the D1/D2 reaction center are light green, pheophytins are blue, chlorophylls of the antenna complexes are dark green, β-carotenes are in orange, hemes are in red, nonheme Fe is red, Q_A and Q_B are purple. The oxygen-evolving center (OEC) is shown as the red (oxygen atoms), magenta (Mn ions), and cyan (Ca^{2+}) balls. View vertical from the membrane plane (bottom). Coloring is the same as for the top view (Ferreira et al., 2004).

Several other small subunits are present in the PSII dimer, the roles of most of them also being unclear. It is thought that PsbL, PsbM, and PsbT are involved in dimer formation and that PsbJ, PsbK, PsbN and PsbZ might facilitate the carotenoid binding since they are located close to β-carotene molecules (Ferreira et al., 2004). Cross-linking experiments (Tomo et al., 1993; Shi et al., 1999; Zouni et al., 2001) have located the

low molecular weight PsbI and PsbX proteins close to the reaction centre D2 and cytochrome b559 proteins, perhaps having a role in stabilising the peripheral Chl_{ZD1} and Chl_{ZD2} chlorophylls (Ferreira et al., 2004).

The D1 and D2 proteins bind the inner antenna proteins, CP43 and CP47, products of the *psb*C (CP43) and *psb*B (CP47) genes binding 14 and 16 chlorophyll *a* molecules, respectively. These pigments form two layers close to the stromal and lumenal sides of the membrane. This is consistent with the observation by Barry et al. (1994) that the majority of conserved histidines, known to coordinate the Mg atoms in the chlorophyll molecules, are located towards the stromal and lumenal parts of the proteins. CP43 and CP47 are also thought to bind β-carotene and lutein (Bassi, 1996), although structural data can not confirm the latter (Zouni et al., 2001; Kamiya & Shen 2003). The 2.5 Å structure of CP47, from Zouni et al. (2001) reveals 6 membrane spanning helices as predicted by the topology of both CP43 and CP47 (Rhee et al., 1998). The transmembrane α-helices form a trimer of dimers. CP47 and CP43 function not only as light harvesters, but also to transfer excitation energy from the peripheral antenna to the RC, via the Chl_{ZD1} and Chl_{ZD2} chlorophylls (Fereira et al., 2004).

On the lumenal side of the PSII complex close to the D1 subunit are located the extrinsic proteins, PsbO, PsbP and PsbQ (Zouni et al., 2001), which form a 'cap' over the OEC (De Las Rivas et al., 2004). The OEC splits water into molecular oxygen, electrons and protons. The extrinsic proteins have a structural role, keeping the peripheral antenna at an appropriate distance from OEC (Boekema et al., 2000b), but their main role is in oxygen evolution. The Mn and Ca ions seen in the cyanobacterial PSII structure form a cuban-like Mn_4CaO_3 cluster that plays a catalytic role in the water splitting (Ferreira et al., 2004). The PsbO subunit is critical for stabilising the Mn cluster (Ono & Inoue, 1984) and has been suggested to form a hydrophilic "pore" connecting the OEC with the lumenal surface (Ferriera et al., 2004). PsbO attaches to the PSII core via the large extrinsic loops of CP43 and CP47 (Bricker & Frankel, 2002). The catalytic cycle of water oxidation involves five intermediate oxidation states, S_0 to S_4, each transition driven by a photon of light (Kok et al., 1970; Goussias, 2002). Each of four incoming photons results in a charge separation event, removing 4 electrons from the Mn cluster, with concurrent de-protonation of 2 water molecules, resulting in

liberation of one O_2 for each completed cycle.

1.5.4.1 The peripheral light-harvesting antenna of Photosystem II

Peripheral light-harvesting complexes of PSII collect and transfer the light energy towards the PSII core. The peripheral light-harvesting antenna of plant PSII comprises multiple pigment binding proteins, which together with the LHCI complexes are encoded by members of the *Lhc* gene family (Jansson, 1994). The proteins can be divided into two groups – the major antenna complex known as LHCIIb (encoded by the *Lhcb1*, *Lhcb2* and *Lhcb3* genes) and the 3 minor antenna complexes CP29 (encoded by the *Lhcb4* genes), CP26 (encoded by the *Lhcb5* gene) and CP24 (encoded by the *Lhcb6* gene) (Jansson, 1994). The most abundant complex, the trimeric LHCIIb binds more than 50% of the PSII chlorophylls, while the minor monomeric complexes bind altogether approximately 20% (Peter & Thornber, 1991). All complexes bind chlorophyll *a* and chlorophyll *b* and also xanthophylls. The complexes increase the capacity of PSII for light capture, the minor antenna forming a link between the PSII core and the LHCII outer antenna. This function of the light-harvesting antenna is subject to regulation by a number of processes including state transitions and non-photochemical quenching, both discussed in more detail below.

1.5.4.1.1 LHCII

Early biochemical analyses showed that trimeric LHCIIb (often called just LHCII) has a molecular weight of 72 kDa and a chlorophyll *a*/*b* ratio of 1.33 and that each monomer binds 3.5 xanthophylls, comprising 2 molecules of lutein, 1 of neoxanthin and 0.5 of violaxanthin (Peter and Thornber, 1991). The Lhcb1, Lhcb2 and Lhcb3 polypeptides are organised in either homo or hetero-trimers (Jansson, 1994; Jansson, 1999). Only Lhcb1 is able to form homotrimers and it is also present in all heterotrimeric forms such as $Lhcb1_{(2)}$/ Lhcb2, $Lhcb1_{(2)}$/ Lhcb3 and Lhcb1/Lhcb2/Lhcb3 (Jackowski et al., 2001). The first structural information about the monomeric subunit came from studies of Burgi et al. (1987), in which it was suggested from hydropathy analysis that each subunit consists of 3 transmembrane helices. The first structural model of trimeric LHCII obtained at 6 Å resolution by electron crystallography of 2-D crystals confirmed the presence of 3 transmembrane helices and indicated 15 chlorophylls in each subunit (Kuhlbrandt & Wang, 1991). Later, the structure was refined by the same method

(Kuhlbrandt et al., 1994) to a 3.4 Å resolution, revealing the interaction between two of the 3 membrane-spanning α-helices. Additionally, a short helix was observed, located at the interface between the membrane and the lumen. In the centre of the complex there is evidence of 2 xanthophylls and 12 chlorophylls. In this model, chlorophyll *a* and chlorophyll *b* cannot be distinguished, but their positions were inferred from consideration of energy transfer efficiencies. The 3-D structures of the LHCII from spinach at 2.72 Å resolution (Liu et al., 2004), and pea at 2.5 Å (Standfuss et al., 2005) provide much more detail about the protein and pigments. The spinach structure confirmed the early biochemical results where it was suggested that each monomeric LHCII binds 13-15 chlorophyll *a* and chlorophyll *b* molecules (Peter & Thornber, 1991) and 3-4 xanthophylls (Ruban et al., 1999). The structure is depicted in Figure 9.

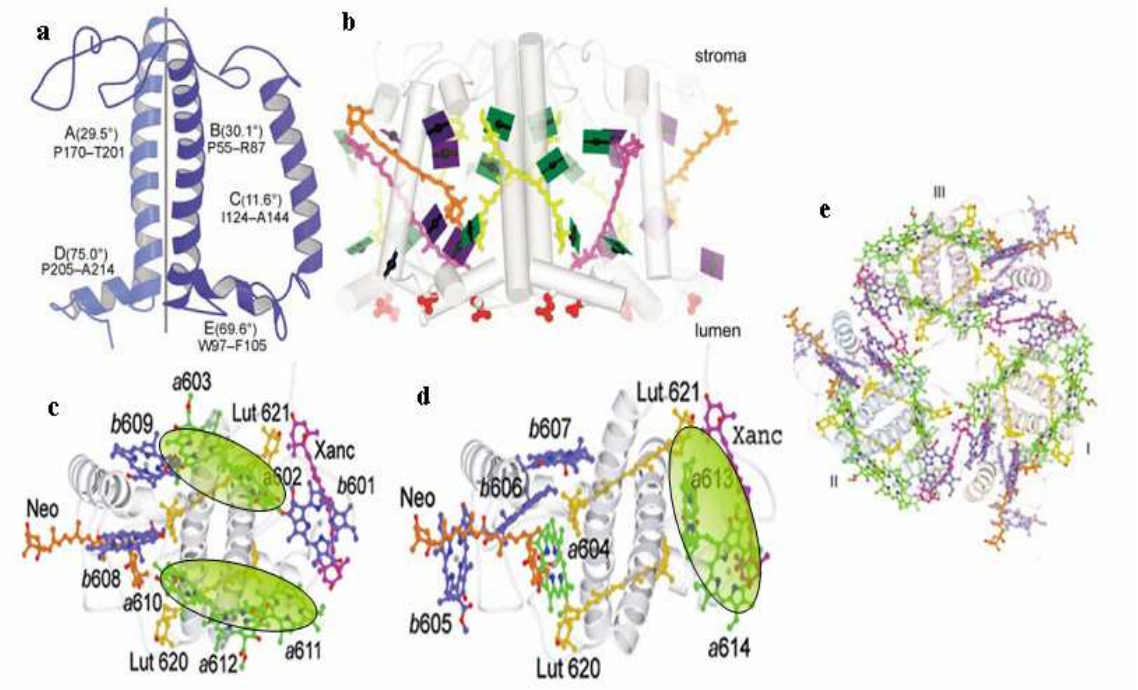

Figure 9. Structural model of the LHCII obtained by X-ray crystallography (a). Side view of monomer showing the pigments: lutein (yellow), neoxanthin (orange), violaxanthin (purple), chlorophyll *a* (green), chlorophyll *b* (blue) (b). Pigment pattern in an LHCII monomer at the stromal and lumenal sides, respectively, displaying the strongly coupled chlorophyll clusters shown by green ovals (*a*610-*a*611-*a*612, *a*602-*a*603 and *a*613-*a*614) (c,d). Top view of LHCII trimer (e) ,(Liu et al., 2004).

It was therefore established that each monomer binds 8 molecules of chlorophyll *a*, 6 chlorophyll *b*, 2 all-*trans* luteins forming a cross-brace, 1 molecule of 9-*cis* neoxanthin present in a highly selective binding site and 1 all-*trans* violaxanthin at the monomer-monomer interface. The chlorophylls are located at specific binding sites for either chlorophyll *a* or chlorophyll *b* molecules, with no sites available for both (Liu et al.,

2004). The chlorophylls are organised into 2 layers within the membrane, one layer (8 chlorophylls) close to the stroma and the other one (6 chlorophylls) near the lumen. In the trimer, chlorophylls on the stromal side form two rings, the inner one thought to be involved in energy transfer between monomers (Gradinaru et al., 1998), and the outer one thought to provide broad absorption of light energy and be involved in energy transfer to the RC (Liu et al., 2004). The lumenal side chlorophylls are suggested to function upstream of the stromal chlorophylls (Liu et al., 2004). There are three clusters of strongly coupled chlorophyll *a* molecules, to which fast energy transfer from chlorophyll *b* can occur (Figure 9): the *a*610-*a*611-*a*612 trimer and the *a*602- *a*603 and *a*613-*a*614 dimers (Novoderezhkin et al., 2005). The *a*610-*a*611-*a*612 cluster is located at the outer side of the LHCII trimer, providing a good connection with other subunits of PSII. This cluster, together with the adjacent lutein (lut 620) forms the terminal emitter domain, which is proposed as the possible energy quenching site in LHCII (Wentworth et al., 2003; Pascal et al., 2005) - see below.

The structural model again confirmed the presence of the three transmembrane helices (A-C), and the α-helix along the lateral plane of the membrane (D), but also revealed a new, short amphipathic helix (E) inclined to the membrane plane by 30^0. In the native membrane, LHCII is arranged as a trimer (Figure 9e), and the trimerisation region was found to cover both the N-terminal and C-terminal domains, the stromal end of helix B and some residues of helix C. A phosphatidylglycerol (PG) molecule appears to stabilise the trimer in the crystal structure (Liu et al., 2004; Standfuss et al., 2005), in agreement with previous reports (Remy et al., 1982; Nussberger et al., 1993) that this lipid is essential for stability of the trimer, its hydrolysis with phospholipase A_2 resulting in the monomerisation of the complex (Remy et al., 1982). The lipid digalactosyl diacylglycerol (DGDG) mediates the interaction between adjacent trimers through van der Waals contacts (Nussberger et al., 1993; Liu et al., 2004).

Biochemical studies suggest that LHCII has four carotenoid binding sites, 2 for lutein (L1 and L2) bound tightly within the complex, a neoxanthin binding site (N1) and one site on the periphery of the complex, where violaxanthin is bound only loosely (V1) (Ruban et al., 1999). The high resolution crystal structure confirmed the biochemical results. Lutein had previously been found to be essential for correct *in vitro* folding and

stability LHCII (Plumley & Schmidt, 1987; Croce et al., 1999; Phillip et al., 2002) and was also suggested to be involved in non-photochemical quenching (see section 1.8.2) (Lokstein et al., 2002). The neoxanthin molecule is present in a chlorophyll *b* rich region close to helix C, a site which was previously shown to be selective for neoxanthin, although this pigment is not essential for protein folding (Croce et al., 1999). Neoxanthin is suggested to have a role in protection of the chlorophyll against photodamage (Standfuss et al., 2005). Thus, lutein and neoxanthin appear to be involved in both light harvesting and photoprotection (Kühlbrandt et al., 1994). Violaxanthin has a role in non-photochemical quenching (Demmig-Adams, 1990) via the xanthophyll cycle (discussed in detail in section 1.7.2) but its role in light harvesting is unclear (discussed in Chapter 3).

1.5.4.1.2 CP29 (Lhcb4)

CP29 is the largest of the minor light-harvesting proteins, containing approximately 257 amino acids, giving a molecular weight of approximately 29 kDa (Peter & Thornber, 1991; Bassi, 1996). It is always present in its monomeric form and is the product of the *Lhcb4* genes (Jansson et al., 1994). Three *Lhcb4* genes exist in *Arabidopsis*, two (*Lhcb4.1* and *Lhcb4.2*) have similar expression levels but the third (*Lhcb4.3*) appears to be expressed at a low level (Jansson et al., 1999). CP29 binds 8 chlorophyll molecules, 6 chlorophyll *a* and 2 chlorophyll *b* (Sandona et al., 1998; Bassi et al., 1999), and approximately 3 carotenoids: one lutein molecule, 0.77 neoxanthin and 1.54 violaxanthin (Peter & Thornber, 1991). This ratio of carotenoid binding is disputed, and for example, *in vitro* reconstitution of recombinant CP29 produced in *Escherichia coli* showed that only 1 lutein and 1 violaxanthin are bound to the complex (Bassi et al., 1999). However, Ruban et al. (1999) showed that there are two populations of violaxanthin that are bound differently to the complexes, one tightly bound, unavailable for de-epoxidation, and one loosely bound, which can be de-epoxidised. In contrast, studies using site directed mutagenesis of pigment binding sites again suggested only 2 carotenoid binding sites in CP29, one binding lutein and the other site occupied by either violaxanthin or neoxanthin (Bassi et al., 1999). In addition to its role in light harvesting and energy transfer, CP29 is proposed to have a regulatory function. Lhcb4 has been shown to bind dicyclohexylcarbodiimide (DCCD), indicating that the protein may be protonated, and indeed a putative protonation site has been located on the

lumenal loop (Pesaresi et al., 1997). These results together with the evidence of the enrichment in violaxanthin (compared to LHCII) have lead to a suggested role for CP29 in non-photochemical quenching. Additionally, Lhcb4 is phosphorylated in the N-terminal domain under some photoinhibitory conditions (Bergantino et al., 1995).

1.5.4.1.3 CP26 (Lhcb5)

The minor antenna protein Lhcb5 is a 26 kDa protein consisting of 247 amino acids, which binds pigments to form the CP26 complex (Peter & Thornber, 1991, Bassi, 1996). The protein binds 9 chlorophyll molecules, 6 chlorophyll *a* and 3 chlorophyll *b*, and contains three binding sites specific for chlorophyll *b* (Croce et al., 2002). Peter & Thornber (1991) found that CP26 binds also 1 neoxanthin, 2 luteins and 0.5 violaxanthin. In a later study, Ruban et al. (1999) reported 7-8 molecules of chlorophyll *a* and 3 of chlorophyll *b* as well as one molecule each of the three carotenoids lutein, neoxanthin and violaxanthin, consistent with the results of Wehner et al. (2006). These results contrast with those found in reconstitution studies carried out by Sandona et al. (1998), which suggest only 2 binding sites exist in CP26, L1 (occupied by lutein) and L2 (occupied by violaxanthin). It is proposed that the L2 violaxanthin plays a key role in non-photochemical quenching (NPQ) (Dall'Osto et al., 2005). Of the three minor complexes, Lhcb5 shares the most sequence homology with Lhcb1 (Jansson et al., 1999), and it has been shown to form trimers together with Lhcb3, substituting for LHCII trimers in antisense plants lacking Lhcb1 and Lhcb2 (Ruban et al., 2003).

1.5.4.1.4 CP24 (Lhcb6)

Lhcb6 is the smallest of the Lhcb proteins and contains 210 amino acids, having a molecular mass of 24 kDa (Morishige et al., 1990). Lhcb6 is thought to bind 5 chlorophyll *a* together with 5 chlorophyll *b* molecules (Peter & Thornber, 1991; Pagano et al., 1998) to form CP24, thus, having the lowest chlorophyll *a*/*b* ratio of all the antenna complexes. It is also thought to bind lutein and violaxathin but possibly not neoxanthin (Bassi et al., 1993, Ruban et al., 1999). Reconstitution studies also suggest that neoxanthin is absent from the complex, the L1 and L2 sites being occupied by lutein and violaxanthin respectively (Sandona et al., 1998; Wehmer et al., 2006). As is the case for CP29, there is evidence that CP24 has regulatory and structural roles. Plants expressing an *Lhcb6* antisense gene and knock-out Lhcb6 mutants that are both depleted

in the CP24 complex show partial inhibition of NPQ and disruption of the macro-organisation of the PSII-LHCII supercomplexes (Kovacs et al., 2006, see section 1.6).

1.5.4.1.5 Other LHC-related proteins

In addition to the light-harvesting complexes of the two photosystems, there are also numerous 'LHC-like' proteins, which share some sequence homology with LHC proteins (Grimm et al., 1989; Jansson et al., 2000). These include the one-helix proteins (OHP), the two-helix stress enhanced proteins (SEP), the three-helix early light induced proteins (ELIP) and the four-helix PsbS protein. The PsbS protein is essential for the rapidly relaxing component of NPQ (see section 1.8.2) (Li et al., 2000), and has been found to bind zeaxanthin *in vitro* (Aspinall O'Dea et al., 2002). In early studies Peter & Thornber (1991) found a small 13 kDa protein in barley thylakoids; it was present very close to the free-pigment band in a native deriphat-PAGE gel, it had a high violaxanthin content and it was called 'LHCIIe'.

1.6 Macro-organisation of the photosystem II

Details of the macro-organisation of PSII and its associated light-harvesting antenna were first revealed by electron microscopy (EM) and single particle analysis of mildly solubilised PSII-enriched particles from spinach (Boekema et al., 1995). A rectangular-shaped PSII supercomplex was seen, which was suggested to be a dimer formed from 2 PSII cores (C), along with two tightly bound LHCII trimers (S), two CP29, and two CP26 monomers per PSII core. This supercomplex was referred to a C_2S_2 and was found to lack the Lhcb3 containing trimer and the *Lhcb6* gene product. A following study on partially solubilised membranes (gentle isolation of PSII particles by gel filtration chromatography) located all three minor complexes and revealed the existence of one more pair of LHCII trimers in the supercomplex, symmetrically associated with each PSII monomer. This new supercomplex was called $C_2S_2M_2$ complex, indicating the presence of two moderately bound LHCII trimers (M) in addition to the core complexes and strongly bound trimers.

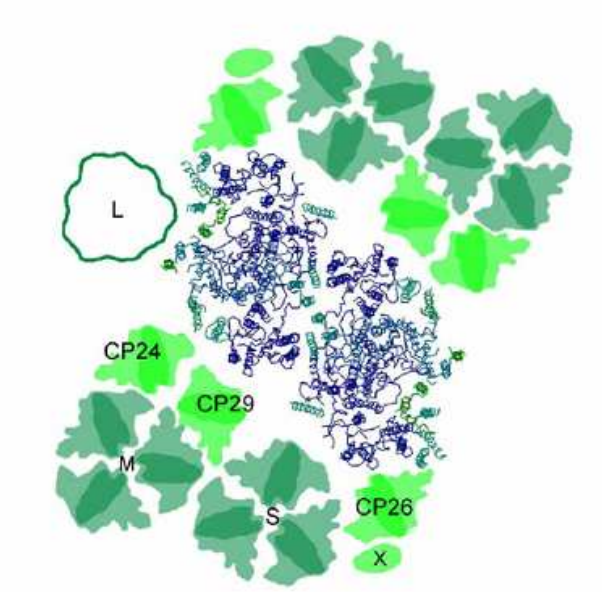

Figure 10. Top view of the spinach $C_2S_2M_2$ supercomplex (Dekker & Boekema, 2005). "S" and "M" refer to strongly and moderately bound LHCII, respectively. "L" indicates the loosely bound trimer, found only in spinach. The central part indicates the protein backbone in the membrane-intrinsic part of the PSII core complex (calculated from the structure of the PSII core complex from *S. vulcanus*). Also shown the minor complexes CP29, CP26 and CP24. "X" denotes a possible small peripheral subunit according to fitting and a comparison of slightly different types of supercomplexes (Boekema et al., 1999).

More detailed analysis revealed a third type of LHCII binding, denoted as loosely bound (L) complexes (Boekema et al., 1999) (Figure 10). No supercomplexes were observed with six LHCII trimers bound ($C_2S_2M_2L_2$), and the frequency of five bound trimers ($C_2S_2M_2L$ supercomplex) was extremely low.

In solubilised grana membranes from spinach, large associations of mainly C_2S_2M LHCII/PSII supercomplexes were observed organised into 2-D semi-crystalline arrays (Boekema et al., 2000). Analysis of pairs of membranes with large-spaced crystalline macrodomains indicated that PSII complexes in one layer face only LHCII complexes in the other layer (Boekema et al., 2000a), suggesting that the organisation of the supercomplex membranes is also optimised for energy transfer between layers (Dekker & Boekema, 2005). Dekker et al. (1999) showed the presence of oligomeric associations of 7 LHCII trimers, which they suggested represent the native structure in the LHCII-only domains.

Interestingly in *Arabidopsis* a larger unit cell is observed that has a composition of $C_2S_2M_2$ (Figure 11c). The semi-crystalline fragments are highly ordered (Yakushevska et al., 2001) and after alignment and averaging of 450 crystal fragments, a unit cell was revealed (indicated within the rectangular shape) (Figure 11a). A density map shows the

likely positions of LHCII S and M trimers (indicated in yellow) and the minor complexes, CP29, CP26 and CP24 (indicated in green) (Figure 11b), modelled from the map of the isolated complex (Figure 11c) (Yakushevska et al., 2001).

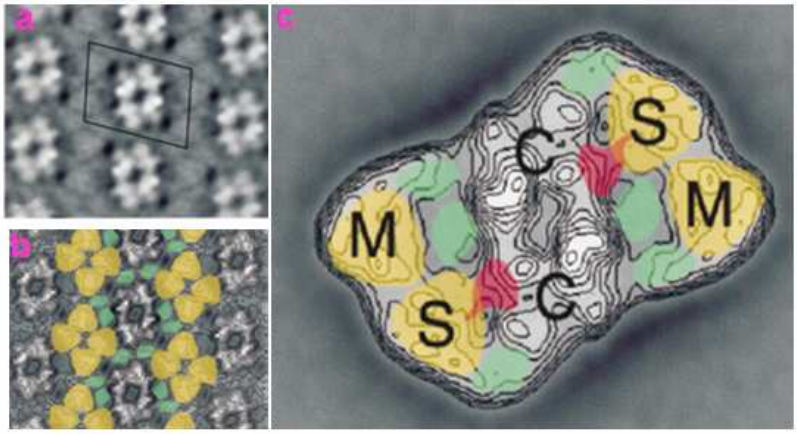

Figure 11. EM images of grana fragments from *Arabidopsis* showing PSII-LHCII macrostructure (Yakushevska et al., 2001). Sum of 450 aligned crystal fragments; the unit cell is indicated by the rectangular shape (a). Image of (a) showing the S and M trimers (yellow) and CP29, CP26 and CP24 (green). C2S2M2 supercomplex (c).

Evidence for the location of the minor, monomeric light-harvesting proteins came from cross-linking studies and studies on various antisense plants. Cross-linking studies revealed CP29 to be in close contact with CP47 on one side of the supercomplex and CP26 to be located close to CP43 on the other side (Harrer et al., 1998, Hankamer et al., 1997). Analysis of antisense plants lacking CP26 revealed this complex to be located on the periphery of the supercomplex, and the position of CP29 was identified by elimination (Yakushevska et al., 2003). CP24 (Lhcb6) was located close to CP29 after analysis of antisense plants lacking Lhcb4 (CP29), results which also showed a decrease in the level of Lhcb6 protein (Andersson et al., 2003). Recently, studies of the knockout mutant lacking Lhcb6 confirmed the location of CP24 and established its role in binding the M trimer to the supercomplex (Kovacs et al., 2006). CP29 is thought to be unique and it is essential for the formation of supercomplexes, since in its absence no supercomplexes are isolated following membrane solubilisation (Yakushevska et al., 2003). In the absence of CP26, supercomplexes are still formed, although the thylakoid membranes are more easily solubilised and the resulting supercomplexes less stable (Yakushevska et al., 2003). Supercomplexes isolated from *Arabidopsis* plants lacking the major light-harvesting protein LHCII (antisense *asLhcb2*) are almost identical in structure to those isolated from wild type plants (Ruban et al., 2003). Synthesis of both

Lhcb1 and Lhcb2 in these plants is abolished, and the expression of the minor antenna protein Lhcb5 (CP26) greatly increases, although levels of all other Lhcb proteins remain the same. The extra Lhcb5 protein appears to replace Lhcb1 and Lhcb2 by forming trimers with Lhcb3, binding at both the S and M binding sites. The plants also show the same extent of grana stacking as the wild type and similar photosynthetic characteristics, although non-photochemical quenching is reduced (Andersson et al., 2003). This evidence that the major light-harvesting protein can be functionally and structurally replaced by a different protein underlines the importance of the supermolecular organization of PSII and LHCII in light-harvesting and electron transport (Ruban et al., 2003).

1.7 Photoprotection in higher plants

Exposure of plants to conditions of excess light intensity increases the rate of formation of excited states, increasing the probability of triplet-state excitation of chlorophylls within the antenna. Triplet chlorophyll can transfer energy to the ground state of O_2 to generate singlet oxygen ($^1O_2$), which can in turn lead to irreparable damage to pigments, proteins and lipids, a process known as photoinhibition. As a result, plants have evolved both biochemical and physiological responses to excess light that enable optimisation of photosynthesis and continued growth. Mechanisms that reduce the amount of light absorbed include movement of the leaves and chloroplasts away from the light and reduction in the size of the PSII antenna (Horton et al., 2001). At the thylakoid level, the dynamic regulation of light-harvesting efficiency is required in order to balance the absorption and utilisation of light energy and prevent photo-oxidative damage. Thus, under excess light conditions, protective non-photochemical mechanisms quench the excited state of the chlorophyll molecules and dissipate excess excitation energy as heat, therefore reducing the population of triplet states.

1.7.1 The role of carotenoids in photoprotection

Carotenoids fulfil numerous important functions in higher plants. They play at least four different roles: accessory pigments in light harvesting, absorbing the light in the region of the electromagnetic spectrum where the chlorophyll absorption is poor; triplet chlorophyll and singlet oxygen scavenging; excess energy dissipation; and structure stabilisation/assembly. As mentioned above, photo-oxidative damage of the thylakoid

membrane and its components is caused by the formation of highly reactive ^{3}Chl and $^1O_2$ species. Carotenoids quench both ^{3}Chl and $^1O_2$ species by energy transfer to form the triplet state of the carotenoid (^{3}Car) (Krinsky et al., 1971), followed by the non-destructive thermal dissipation of the triplet energy (Mathis 1969, Mathis et al., 1979, Cogdell & Frank, 1987). This photoprotective process appears to be universal in chlorophyll-based photosynthetic organisms. In higher plants, photoprotective roles have been described for β-carotene (two molecules providing photoprotection of the PSII RC chlorophylls (Telfer et al., 1994)), lutein (Kuhlbrandt et al., 1994; Pogson et al., 1998; Niyogi et al., 2001), and neoxanthin (Lockstein et al., 2002; Dall'Osto et al., 2007).

These roles of carotenoids rely upon their specific chemical structures and electronic properties. Energy level diagrams for carotenoids consist of at least two singlet excited states denoted 2^1Ag (S_1) and 1^1Bu (S_2) according to their symmetry (Figure 12).

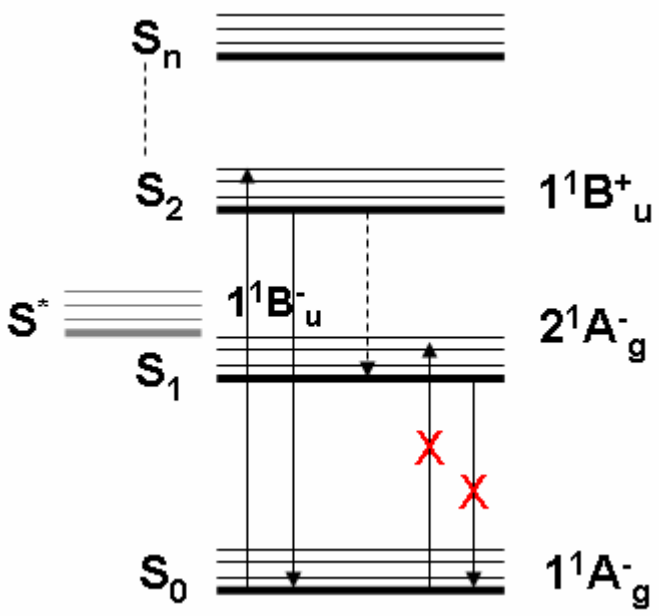

Figure 12. The general energy level scheme of carotenoids. S_0 ground state, S_1, S_2,…S_n excited electronic states. S^* denotes an intermediate excited state.

Although direct transition from the ground state (S_0) to the first excited state (S_1) is forbidden (because of symmetry properties), there can be transition from S_0 to the S_2 excited state. The S_0 to S_2 transition is followed by internal conversion between S_2 and S_1 and subsequent return to the ground state by dissipation of energy as heat or by

resonance energy transfer to chlorophyll molecules (Cogdell & Frank, 1987; Ricci et al., 1996). Differences in the extent of the conjugated double bond system affects the carotenoid S_2 and S_1 energies, with a lowering of the singlet excited state energies in carotenoids with longer conjugated double bonding systems. It has been suggested that the longer the conjugated double bond system the more reactive the carotenoid becomes to $^1O_2$ (Edge & Truscott, 1999). The differences in the structure of each carotenoid also determine other physical properties such as polarity (Ruban et al., 1993a).

1.7.2 Xanthophyll cycle carotenoids

The xanthophyll cycle (XC) was first characterised by Yamamoto et al. (1962) as the reversible two-step de-epoxidation of violaxanthin to zeaxanthin via an intermediate molecule called antheraxanthin. The XC is organised across the thylakoid membrane with the de-epoxidation reaction (violaxanthin to zeaxanthin) lumenally located, whilst the epoxidation reaction (zeaxanthin to violaxanthin) occurs on the stromal side of the membrane (Yamamoto, 1999). Violaxanthin de-epoxidation occurs in the light and is catalysed by the nuclear encoded enzyme violaxanthin de-epoxidase (VDE).

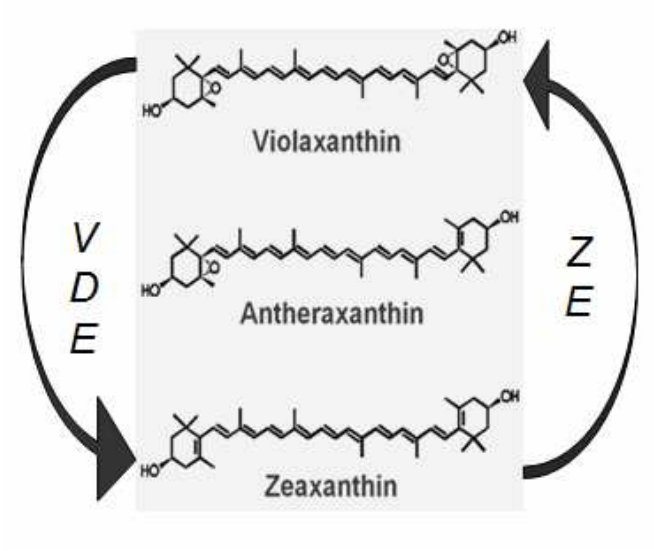

Figure 13. The xanthophyll cycle in higher plants. See text for details.

VDE was purified from spinach using a combination of gel filtration and anion chromatography (Arvidsson et al., 1996) and from lettuce using lipid-affinity precipitation with monogalactosyldiacylglyceride (MGDG) (Rockholm & Yamamoto, 1996). The enzymes from both species have an apparent molecular weights of approximately 43 kDa on SDS-PAGE. VDE activity is controlled by the lumenal pH of

the thylakoid, with maximum activity between pH 4.8 – 5.2, whilst being completely inactive above pH 6.3 (Eskling et al., 1997). Additionally, the enzyme requires the presence of ascorbate (Neubauer & Yamamoto, 1994) and the thylakoid lipid MGDG for maximal activity. The XC is completed by a reaction catalysed by the nuclear-encoded enzyme zeaxanthin epoxidase (ZE). While this enzyme has not been purified directly, cDNA encoding ZE has been extracted from tomato and pepper and the enzyme successfully synthesised in *Escherichia coli* (Bouvier et al., 1996; Burbridge et al., 1997). ZE has similar behaviour as VDE, displaying a strong pH dependency, but with optimum activity occurring around pH 7.0 – 7.5 (Siefermann & Yamamoto, 1975). Additional components are required for the reaction including molecular oxygen (Takeguchi & Yamamoto, 1968) and the cofactors NADPH (Siefermann & Yamamoto, 1975) and FAD (Büch et al., 1995), together with the presence of ferredoxin or 'ferredoxin' like reductants (Yamamoto, 1999).

As mentioned previously, the XC carotenoids are not freely located within the thylakoid membranes, but are specifically bound to the light harvesting complexes, mainly at the V1 site (Thayer & Bjorkmann, 1992; Lee & Thornber, 1995; Ruban et al., 1999; Ruban et al., 2002a). However, other studies suggest that some part of the pool is free in the lipid phase under certain conditions (Havaux & Tardy, 1997; Morosinotto et al., 2002), although this suggestion is refuted by Johnson et al. (2007). Most of the violaxanthin molecules are bound to the antenna complexes at readily accessible sites. However, not all of the violaxanthin pool can be converted into zeaxanthin (Ruban et al., 1999). The maximum de-epoxidation state (defined as DES=A+Z/A+Z+V, where A, Z, V are the content of antheraxanthin, zeaxanthin and violaxanthin, respectively) is typically around 60%, although much higher values (up to 90%) are found in some plant species, especially under stress conditions (Demmig-Adams & Adams, 1992).

The level of zeaxanthin formed from the light induced de-epoxidation of violaxanthin has been shown to have a strong correlation with NPQ (Demmig-Adams, 1990). More details about the role of the XC in NPQ will be presented in section 1.8.4.

Additionally, the XC appears to have a number of other important roles. In particular, there is evidence that under high light stress zeaxanthin has a role in protection against

the peroxidation and degradation of thylakoid lipids (Havaux et al. 1991). Studies of the *npq1* mutant of *Arabidopsis*, which is unable to convert violaxanthin to zeaxanthin, show that whilst the rate of photosynthesis is unaffected in the mutant, the plants have increased lipid peroxidation, pigment loss and photoinhibition (Havaux & Niyogi, 1999). Overexpression of the *chyB* gene encoding the β-carotene hydroxylase enzyme (a component of the zeaxanthin biosynthetic pathway) in *Arabidopsis*, results in a specific two fold increase in the size of the xanthophyll cycle pool (Davison et al., 2002). These plants possess an increased tolerance to excess light conditions, showing a reduction in lipid peroxidation, along with decreased leaf necrosis and anthocyanin levels (Johnson et al., 2007). Such evidence highlights a strong link between zeaxanthin and the protection of thylakoid lipids from photodegradation. Finally, the presence of zeaxanthin reduces the fluidity of the membrane and protects against heat-induced increases in lipid bilayer permeability (Gruszecki & Strzalka, 1991; Havaux et al., 1996). These observations suggest that a third role of the XC is to regulate membrane stability.

1.8 Chlorophyll fluorescence and non-photochemical quenching (NPQ)

1.8.1 Chlorophyll fluorescence

Upon absorption of a photon of light energy, electrons (present in the conjugated π-system) of chlorophyll molecules are promoted from the S_0 ground state to a higher energy level, followed by rapid decay to the first excited singlet state S_1. Electrons at S_1 will decay eventually back to the ground state (S_0) by: re-emission as fluorescence (k_F); transfer of energy to a low or non-fluorescent chlorophyll molecule situated in the vicinity (k_T); utilisation of energy in photochemistry (k_P); and by dissipation of the energy through non-irradiative process as heat (k_D). In solution, up to 30% of the light absorbed by chlorophyll is emitted as fluorescence, but under physiological conditions, this is around 3% (Krause & Weis, 1991). The quantum yield of fluorescence (Φ_F) of any single chlorophyll (or a group of molecules) is givin by the energy remaining after competition with all the above processes according to the following equation:

$$\Phi_F = \frac{k_F}{k_F + k_P + k_D + k_T}$$

A decrease of the fluorescence yield occurs in two ways: firstly, through photochemical quenching of chlorophyll fluorescence (qP), caused by an increase in k_P, as a result of photosynthetic electron transport; and secondly, an increase in the qN (non-photochemical quenching or NPQ) due to an increase in k_T or k_D. Since the fluorescence yield of PSI at room temperature is much lower than PSII, the observed changes in fluorescence result only from effects of these processes on PSII.

Separation of the photochemical and non-photochemical components of chlorophyll fluorescence quenching is achieved using two techniques. The first is described by Krause et al. (1982), who blocked qP using 3-(3,4-dichlorophenyl)-1,1-dimethylurea (DCMU), which inhibits electron transport from Q_A to Q_B in PSII. The second method uses a strong light pulse to saturate PSII photochemistry and is called the 'light doubling' technique (Bradbury & Baker, 1981). The use of modulated fluorescence, which allows continuous visualisation of the fluorescence yield during application of the saturating pulses, enabled qP and qN to be directly probed (Quick & Horton, 1984). This approach is the basis of PAM (Pulse-Amplitude-Modulation) fluorimetry (Schreiber, 1984). Using a range of inhibitors and monitoring the relaxation of NPQ in the dark following illumination, Horton & Hague (1988) classified NPQ as being made up from 3 components: qE (the rapid relaxing phase), qT (slowly relaxing phase) and qI (very slow relaxing phase), each of which represents regulation of light-harvesting. The resolution of qP and these components is the aim of chlorophyll fluorescence quenching analysis (Figure 13). When a dark adapted sample such as leaf is illuminated with a measuring beam of low intensity, a minimum level of fluorescence is reached (F_0), at which point all RCs are open and photochemistry is operating at maximum efficiency. When actinic light (AL) is applied, a fast fluorescence increase is observed due to the progressive closing of the PSII RCs. When all RCs are closed and photochemistry is at minimum (high light conditions), the maximum fluorescence level is achieved (F_m). From this point fluorescence starts to decline due to the increase in photochemical quenching that begins as the rate of photosynthesis accelerates, and the slow induction of non-photochemical quenching.

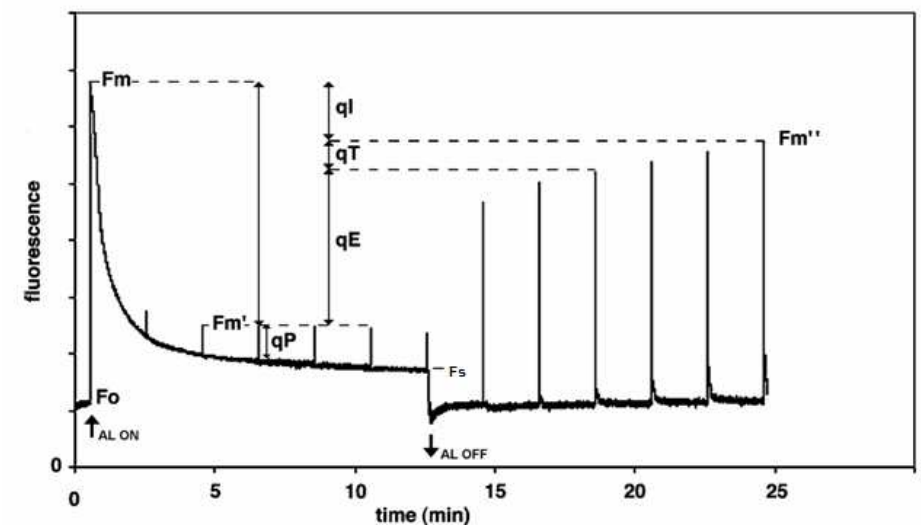

Figure 13. A typical fluorescence trace used for quenching analysis. F_0 is the minimum and F_m maximum fluorescence. F_m' represents maximum fluorescence in light and Fs the steady state fluorescence in light. F_m'' is the maximum fluorescence during dark relaxation. AL=actinic light; qP=photochemical quenching; qE=energy dependent quenching; qT=state transition; qI=photoinhibition components of NPQ (Muller et al., 2001).

The quantum yield of PSII is calculated during the actinic light illumination as the ratio $(F_m'-F_s)/F_m'$, where F_m' is the maximum fluorescence in the light and F_s the steady state fluorescence in light. It provides information on the proportion of the light used in photochemical processes. qP is given by $(F_m'-F_s)/F_m'-F_0$, where F_0 is the fluorescence level in dark (Figure 13). NPQ is usually calculated as $(F_m-F_m')/F_m'$.

1.8.2 Non-photochemical quenching of chlorophyll fluorescence

Energy dependent quenching – qE

qE is the largest component of NPQ and is caused by the formation of a proton gradient during illumination (Briantais et al., 1979). The formation of qE is rapid and it has a relaxation half-time in the dark of approximately 30-60 seconds (Horton & Hague, 1988). qE is usually estimated as $F_m/F_m'-F_m/F_m''$, where F_m'' is the maximum fluorescence after about 10 min of dark relaxation (as shown in Figure 13).

Papageorgiou & Govindjee (1968) first described the participation of non-photochemical components in the second wave of fluorescence quenching in *Chlorella pyrenoidosa*. The dependence of qE on the rate of the photosynthetic electron transport was ruled out. Chlorophyll fluorescence quenching was also shown to be unrelated to photochemistry by Murata & Sugahara (1969) who described it as arising from a high energy state of photophosphorylation that may influence in some way the state of

chlorophyll *a* molecules in the chloroplasts, and as a result decrease the fluorescence yield. Fluorescence quenching was further investigated by Wraight & Crofts (1970), who found that this 'energy-dependent' quenching was sensitive to uncouplers, suggesting its dependence on the ΔpH. They proposed that chlorophyll fluorescence quenching occurs by an increase in the rate of non-radiative dissipation of the chlorophyll excited singlet state via thermal degradation. These results were corroborated by Briantais et al., (1979) who found a linear correlation between intra-thylakoid proton gradient and level of chlorophyll fluorescence in broken pea protoplasts, firmly establishing the link between the energy dependent chlorophyll fluorescence quenching (called qE) and the ΔpH formed during photosynthesis. Furthermore, Krause (1973) found that the influx of protons into the lumen is accompanied by efflux of Mg cations and is associated with changes in the thylakoid membrane structure that were proposed to be responsible for the appearance of an absorption band around 535 nm. It was suggested that these membrane changes were directly responsible for changes in fluorescence.

Krause and Behrend (1986) first established that elimination of the rapidly relaxing component of NPQ led to an increase in photoinhibition, proposing that qE had a physiological function. Horton & Hague (1988) similarly found that in isolated chloroplasts photoinhibition is inversely proportional to the level of qE present. It was proposed that qE prevents build-up of reduced Q_A in high light conditions, thereby preventing photoinhibition. This notion was also based upon the observation that, as the light intensity increases and the PSII quantum yield decreases, the level of qP remained high and Q_A remains oxidised (Weis & Berry, 1987; Genty et al., 1989). This showed that the decrease in quantum yield was not due to feedback from reduced components of the photosynthetic electron transport system, but due to an increase in dissipation of the energy absorbed by the antenna that was reflected in NPQ. Together, the above data firmly established qE as a regulatory mechanism that provides photoprotection.

A second effect of the formation of the ΔpH that is important in qE is the activation of the xanthophyll cycle, detailed in section 1.7.2. The conversion of violaxanthin to zeaxanthin correlates with the level of qE in numerous plants under different conditions (Demmig-Adams, 1990) and in isolated chloroplasts (Gilmore & Yamamoto, 1992). Inhibition of VDE using dithiothreitol results in inhibition of qE (Bilger et al., 1989; Adams et al., 1990). Study of NPQ mutants provided important

insights into the mechanisms of qE. *Npq1* mutants of *Arabidopsis*, unable to convert violaxanthin to zeaxanthin, showed greatly reduced qE, and induction of qE in the *npq2* mutant, which constitutively accumulates zeaxanthin, was faster than in wild type plants (Niyogi et al., 1998).

Spectroscopic studies of isolated thylakoids and leaves showed that high light induction of qE correlates with two separate absorbance changes. One absorbance change at 505 nm is a result of the conversion of violaxanthin to zeaxanthin (Yamamoto, 1972), and this change is a quantitative measure of the de-epoxidation reaction (Siefermann & Yamamoto, 1974). The second absorbance change, frequently referred to as a light scattering change, has a maximum at 530-540 nm and is designated ΔA_{535}. It is dependent on ΔpH and the presence of zeaxanthin (Bilger et al., 1989). ΔA_{535} is correlated with qE in both leaves and chloroplasts, (Noctor et al., 1993; Ruban et al., 1993b) and absent in mutants lacking qE (Li et al., 2000a). As discussed above, ΔA_{535} was initially thought to be a light scattering change resulting from a ΔpH-dependent conformational change in the thylakoid membrane (Heber, 1969; Krause, 1973) possibly associated with aggregation of LHCII (Ruban et al., 1993b). However, further studies showed that it is, at least in part, a "real" absorbance change, reflecting a change in the electronic absorption of zeaxanthin. This is a complex change, resulting from the "activation" of zeaxanthin molecules by some type of modification of their local environment (Ruban et al., 2002b), possibly head-to-tail aggregation (Polivka et al., 2002). An absorption spectral shift giving rise to a similar ΔA_{535} has been reproduced *in vitro* upon association between isolated PsbS and zeaxanthin, suggesting that this interaction may be crucial for the functioning of zeaxanthin in NPQ (Aspinall O'Dea et al., 2002).

The PsbS protein has an essential role in qE. The *npq4* mutant, which is deficient in PsbS, was found to be deficient in the qE component of NPQ (Li et al., 2000a). Some NPQ still occurs in this mutant but is very slow in both formation and relaxation. The absorption changes associated with ΔA_{535} are also slower and smaller in amplitude, but interestingly, the change is blue shifted to around 520 nm suggesting a defect in zeaxanthin activation. Based on these observations, it was suggested that PsbS may act to promote conformational changes within LHCII to bring about NPQ *in vivo* (Horton et al., 2000; Horton & Ruban, 2005). A number of site directed mutations of

PsbS have been investigated. Most important were those in which mutation of certain lumen-facing glutamate residues resulted in inhibition of qE (Li et al., 2002c; Li et al., 2004). It was suggested that protonation of these residues is a key event in the ΔpH-dependent induction of qE, consistent with DCCD binding to this protein (Ruban et al., 1992; Dominici et al., 2002). PsbS over-expressor plants have also been created, and these plants exhibit a larger amplitude of qE that found in wild type (Li et al., 2002b). Although this was used as evidence for a direct role of PsbS in NPQ, providing the binding site for zeaxanthin, it was subsequently shown that the stimulatory effect of PsbS is independent of the presence of zeaxanthin (Crouchman et al., 2006). Therefore, at present the mode of action is unclear. In fact there is still uncertainty about where this protein is located: some reports indicate it is associated with either LHCII (Kim et al., 1994) or the PSII core (Funk et al., 1995; Donminici et al., 2002; Bergantino et al., 2003); and others even suggest high mobility within the thylakoid membrane (Neild et al., 2000; Yakushevska et al., 2001; Teandro et al., 2007).

Quenching related to state transitions – qT

The qT component of NPQ, which relaxes with a half time of around 5-10 minutes is a small proportion (15-20%) of the maximum quenching, although under very low light it is the major component (Horton & Hague, 1988; Walters & Horton, 1993). It was assigned to the state 1 to state 2 transition. The state transition is a process by which an imbalance in the rates of excitation of PSII and PSI is removed. It involves the reversible phosphorylation of LHCII in PSII complexes, resulting in LHCII migration from PSII to PSI. State transitions are important only at low light intensities and they are inhibited in high light (Aro et al., 1993). Consistent with this, qT does not make a significant contribution to quenching in high light conditions (Walters & Horton, 1991). However, qT can be difficult to measure from chlorophyll fluorescence alone since it overlaps with slower components of qE (Walters & Horton, 1991), as well as with the dark-induced inactivation of certain electron transport reactions (Schansker et al., 2006).

Photoinhibitory, irreversible quenching – qI

The NPQ component that relaxes over a longer period, of greater than 10-20 minutes, is known as qI. The slowly reversible qI may be sustained for several hours, but interestingly some of it is rapidly reversed on addition of nigericin (Ruban & Horton,

1995). A part of qI is thought to reflect photoinhibition of PSII reaction centres, but mostly it is unrelated to PSII RC activity and is thought to reflect a sustained quenching of the antenna (Lee et al., 1990; Gilmore & Bjorkman, 1994; Horton et al., 1996). It is suggested that qI originates from a structural change caused by illumination (similar to qE), but one that is stable in the dark for a longer period of time than the change required for qE (Ruban & Horton, 1995). qI has been correlated with the persistence of zeaxanthin, which is only slowly epoxidised in darkness (Demmig et al., 1987; Jahns & Miehe, 1996). Dall'Osto et al. (2005) suggested that some of this zeaxanthin is bound to the CP26 complexes and therefore proposed these minor antenna complexes are the sites for qI.

1.8.3 The site of qE

qE has been suggested to take place both in the RC and the light harvesting antenna. Weis & Berry (1987) and later Krieger et al. (1992) observed that the quantum yield of PSII was correlated with the amount of qE and proposed that quenching occurs due to the increased population of Q_A^-, which facilitates non-radiative recombination via a back reaction with $P680^+$, suggesting that the quencher was the PSII RC itself. The back reaction would be promoted by a low pH-induced Ca^{2+} release from the OEC (Krieger & Weis, 1993). Even though there are results suggesting that such an NPQ process is present in RCs (Finazzi et al., 2004), most evidence indicates that, under physiological conditions, the qE component of NPQ occurs within the antenna (Horton & Ruban, 1992; Ruban & Horton, 1995; Wentworth et al., 2000). Some of this evidence is as follows:

a) the qE inhibitor DCCD (Ruban et al., 1992) has been shown to bind antenna polypeptides (Walters et al., 1994; Ruban et al., 1998a), although it should be noted that recent evidence shows that DCCD also binds to PsbS protein (Dominici et al., 2002);

b) the XC carotenoids are also associated with the peripheral light harvesting antennae, (Peter & Thornber, 1991; Ruban et al., 1999);

c) heat emission kinetics measured directly using laser-induced optoacustic spectroscopy show completion within 1.4 μs (Mullineaux et al., 1994), significantly faster than the Q_A^- and $P680^+$ recombination reaction (~120 μs);

d) *in vitro* quenching in isolated antenna complexes reproduces many features of qE observed in leaves and chloroplasts, such as the kinetics of fluorescence change, the

enhancement by zeaxanthin, and the absorbance changes accompanying the *in vivo* quenching process (Ruban & Horton, 1992; Wentworth et al., 2000; Wentworth et al., 2001);

e) preferential quenching of excitation energy within the antenna complexes has been observed by analysis of PSII fluorescence at 77K (Ruban & Horton, 1995) and, following the induction of qE, the fluorescence emission spectrum of PSII resembled that of partially aggregated LHCII, with an enhanced band at 700 nm.

Although these data strongly suggests that the light-harvesting antenna is the site for qE, the RC could be involved under certain physiological conditions, for example, under conditions of high ΔpH or when antenna quenching is inhibited or slowed down.

1.8.4 The mechanism of qE

Two types of mechanisms have been proposed to account for quenching in the antenna. In part these arose as a result of experiments conducted in order to elucidate the exact role of zeaxanthin, a key player in the NPQ process. The first is so-called the direct quenching mechanism, where zeaxanthin is proposed to be the direct quencher by accepting the excitation energy from the chlorophyll excited state. In the second, the indirect quenching mechanism, zeaxanthin is postulated to act as an allosteric regulator of a quenching process that is an intrinsic property of the antenna complexes.

The strong correlation between qE and the formation of zeaxanthin (Demmis-Adams 1989; Demmig-Adams, 1990) gave rise to the simple idea that zeaxanthin is the direct quencher. The obligatory requirement for the pH gradient was explained by it activating the zeaxanthin binding site within PSII light-harvesting antenna (Gilmore et al., 1995). A theory for how quenching could be switched on by the de-epoxidation of violaxanthin was first put forward by Owens (1994). This was later described as the so-called "molecular gear shift model" (Frank et al., 1994). As mentioned previously (see section 1.7.1) a carotenoid molecule displays at least 2 excited states namely S_1 and S_2. Direct transition from the ground state S_0 to S_1 is symmetry forbidden, but S_2 to S_1 transfer is possible and is employed by carotenoids as a means of energy transfer to chlorophylls. The S_1 energy level of carotenoids relative to the chlorophyll *a* Q_y band can be calculated/approximated using the energy gap law (Frank et al., 1994), and crucially it depends upon the length of the conjugated double bond chain of the molecule. The

conversion of violaxanthin to zeaxanthin means the removal of 2 epoxy groups, thereby increasing the number of conjugated double bonds from 9 to 11. The molecular gear shift model suggests that because the zeaxanthin S_1 state is lower than the chlorophyll *a* Q_y band, it can act as a quencher by accepting energy from the first excited state of chlorophyll and then dissipating this energy as heat upon its re-conversion to the ground state. Since the violaxanthin S_1 state was found to be significantly higher than the chlorophyll *a*, it would be more likely that this pigment acts as a light harvester than as quencher. In this way this model proposes that violaxanthin which predominates in the low light conditions would act as an accessory pigment, whilst in high light conditions, its conversion to zeaxanthin would enable dissipation of the excess energy.

Although the results of Phillip et al. (1996), which show a relationship between the increase in the conjugated double bond chain and the pH induced quenching in LHCII *in vitro* provide support for the molecular gear shift model. However, it was subsequently shown that this relationship was more likely due to differences in carotenoid configuration rather than in S1 excited state energy level (Ruban et al., 1998b, see below). Furthermore, transient absorption (Polivka et al., 1999) and fluorescence (Frank et al., 2000) spectroscopy measurements allowed the direct measurement of the violaxanthin and zexanthin energy levels. These measurements show that the S_1 states of both xanthophylls were far lower than those calculated before, both lying below the level of chlorophyll *a* Q_y band, so undermining the basic tenet of this hypothesis. *In vitro* studies using low temperature fluorescence spectroscopy have accurately measured the S_1 energy levels of the xanthophyll cycle carotenoids (Josue & Frank, 2002). The results obtained are similar with those previously reported (Frank et al., 1994), but it has been suggested that low temperature may cause a change in the protein that would create a significant distortion of the carotenoid (Josue & Frank, 2002).

In the artificial conjugated dyad model system, direct proof was obtained that energy dissipation may occur by energy transfer from a porphyrin ring to the S_1 state of a carotenoid, coupled with an internal charge transfer state (Berera et al., 2006). In this study, it was shown that the addition to the conjugated double bond chain of the carotenoid of only one double bond turns the carotenoid from a non-quencher into a powerful quencher.

1.8.4.1 The carotenoid radical cation model

As an alternative to singlet-singlet energy transfer, it has been proposed instead that electron transfer between carotenoids and chlorophylls could be a mechanism for chlorophyll fluorescence quenching. Carotenoid cation radicals have been transiently observed after photoexcitation of bacterial light harvesting complexes (Frank & Brudvig, 2004) and most significantly also in measurements performed on thylakoid membranes (Holt et al., 2005). A new version of a direct quenching model was proposed (Figure 14). In this model, the protonation-induced formation of a zeaxanthin/PsbS complex, leads to the quenching of the major light harvesting antenna chlorophylls directly (Figure 14a). Effective energy transfer from chlorophyll to carotenoids is possible if the excited state of the carotenoid is lower than the lowest excited state of the chlorophyll (Qy band). This carotenoid excited state was found by transient absorption measurements performed on isolated thylakoids, where a carotenoid excited state was detected (either S1 or S*), which was theoretically of a lower energy than the Qy band (Ma et al., 2003). The authors then suggested that quenching can occur via energy transfer from chlorophyll to a carotenoid (zeaxanthin) or alternatively via formation of a chlorophyll xanthophyll heterodimer. The qE-dependent changes were observed only when zexanthin and PsbS were present and therefore the signal was suggested to arise from zeaxanthin that is bound to PsbS (Holt et al., 2004).

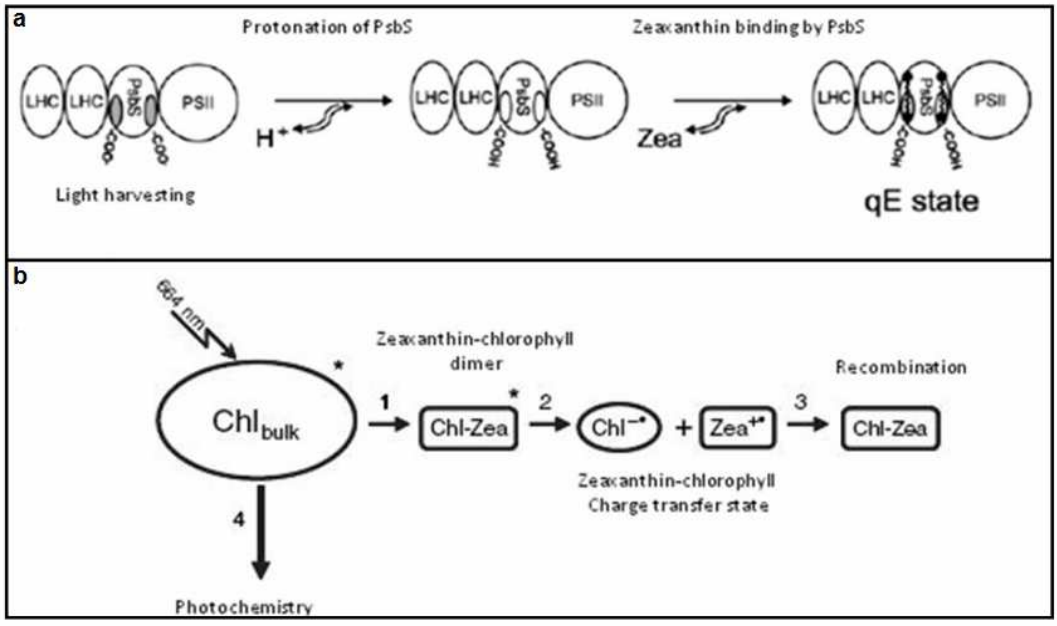

Figure 14. The PsbS-zeaxanthin model for non-photochemical quenching (a) (Holt et al., 2004). The hypothesis for the zeaxanthin cation formation and the dissipation of energy by charge recombination (b) (Holt et al., 2005).

Application of transient absorption spectroscopy showed the appearance of an qE-related absorption band in the near-IR region, indicating the formation of a carotenoid cation. The signal, which appears only in chloroplasts showing qE and containing zeaxanthin (Holt et al., 2005), was interpreted as arising from a chlorophyll-zeaxanthin (Chl-zea) heterodimer formed when qE is induced (Figure 14b). The heterodimer quenches the bulk of chlorophylls (Chl_{bulk}) via the formation of a charge separated ground state $Chl^{\cdot -}$ plus $Zea^{\cdot +}$, which decay further to the ground state by charge recombination. Consistent with this model, it was calculated that zeaxanthin has the lowest ionization potential of the xanthophyll cycle carotenoids (Dreuw et al., 2003). A carotenoid (zeaxanthin mainly) radical cation was also found in transient absorption studies of the isolated minor light-harvesting complexes that bind zeaxanthin, and therefore it was proposed that these complexes may be the site of qE *in vivo* (Avenson et al., 2007).

1.8.4.2 The allosteric model

The LHCII aggregation model of qE was first proposed by Horton et al. (1991) as an alternative to the direct quenching model. The authors proposed that qE arises from ΔpH induced aggregation of the LHCII, which causes a conformational change in each LHCII sub-unit that modifies the environment of the complex, resulting in the appearance of a dissipative state. Early studies on isolated chloroplasts in absence or in presence of zeaxanthin showed that a different ΔpH is required for the formation of the qE state (Rees et al., 1989; Noctor et al., 1991). Most importantly, qE was observed in isolated chloroplasts (Rees et al., 1989; Noctor et al., 1991) that do not contain zeaxanthin. These results indicate that this carotenoids is not the quencher itself, rather it has an indirect role, lowering the ΔpH necessary for qE. The initial model, which has been updated (Horton et al., 2000; Horton et al., 2005) describes 4 LHCII states, depending on the de-epoxidation state of the xanthophyll cycle and the lumenal pH (Figure 15).

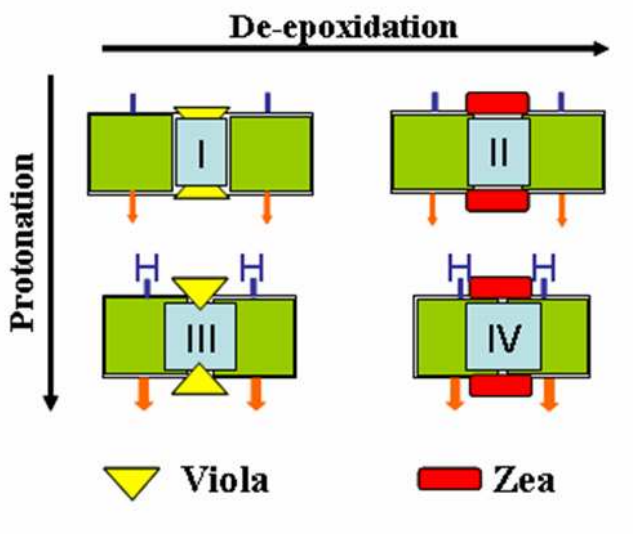

Figure 16. The LHCII model for NPQ. LHCII is represented in green; violaxanthin in yellow; zeaxanthin, red; orange arrows indicate energy dissipation; H denotes protonation; (Horton et al., 2000; Horton et al., 2005).

State I represents the unquenched, light harvesting state where violaxanthin is bound to the complex and the pH difference between the stroma and the lumen is minimal. State III is the protonated state binding only violaxanthin and forms a weakly quenching complex. State II represents the light activated state of the LHCII, unprotonated but partially quenched, with zeaxanthin bound. Finally, state IV represents the maximally quenched state when both protonation and zeaxanthin binding to LHCII occur. In isolated LHCII, quenching occurs when protein is in the aggregated form, induced by the removal of the detergent (Ruban et al., 1991) or by addition of Mg ions (Arntzen & Ditto, 1976), and this was suggested to be a molecular basis for NPQ. Several lines of evidence support this idea:

a) violaxanthin prevents and zeaxanthin induces both the *in vitro* quenching and the aggregation of the complexes (Ruban et al., 1991);

b) the band at 700 nm in fluorescence emission spectra has been found in both quenched LHCII and leaves where qE was present (Ruban et al., 1991; Horton et al., 1996);

c) the aggregated *minus* trimeric associated difference in the absorption spectrum is very similar to the qE light *minus* dark difference spectrum (Ruban & Horton, 1992);

d) qE inhibitors and enhancers have similar effects on quenching in LHCII (Horton & Ruban, 1992; Ruban et al., 2001).

Evidence was found that the opposing effects of violaxanthin and zeaxanthin in qE could arise from difference in their structures rather than in their excited energy levels

(as suggested by the molecular gear shift model). Ruban et al. (1998b) found that the ability to induce quenching is not dependent on the number of conjugated double bonds. Auroxanthin, an isomer of violaxanthin with only 7 double bonds was found to stimulate quenching in the isolated LHCII with even greater efficiency than zeaxanthin. This observation is explained by the structural similarity between auroxanthin and zeaxanthin – in both, the head groups are in the same plane with respect to the double bond chain, but they are twisted in violaxanthin. The head group configuration was therefore proposed to control the interaction of the molecules with LHCII (Horton et al., 1999). This observation is in contradiction to the direct quenching model of qE, but in complete agreement with the indirect model.

In vitro quenching is a property of all of the PSII light harvesting complexes. In fact, the minor complexes produce higher levels of quenching and quench more rapidly than does the major trimer LHCII (Ruban et al., 1996; Wentworth et al., 2001). Hence, it was suggested that quenching is a property of the whole antenna, rather than of one particular complex (Horton et al., 1996). Important insights into this question were found following the investigation of various *Lhc* mutants. These mutants were obtained by expression of anti-sense *Lhcb* genes and t-DNA insertions in *Lhcb* genes. The first antisense mutant lines were lacking CP29 or CP26, but neither was NPQ deficient, showing only a 30% and 10% reduction, respectively. The CP29-defficient mutant has found to have an unstable macro-organisation, no PSII-LHCII supercomplexes being found, and there is a slight decrease in stability of the supercomplexes in the CP26-defficient mutant (Yakushevska et al., 2003). An antisense *Lhcb2* line was also constructed (Andersson et al., 2003) resulting in plants lacking both the *Lhcb1* and *Lhcb2* gene products (the major constituents of the trimeric LHCII). This mutant again shows only a 30% qE reduction, but, as discussed above (see section 1.5.4.1.3) replacement of Lhcb1 and Lhcb2 proteins with Lhcb5 preserved the macro-organisation of the PSII (Ruban et al., 2003). The most marked change in NPQ occurs in the antisense and knock-out CP24 (Lhcb6) plants, which show a 60% reduction of qE (Kovacs et al., 2006). Here, the PSII macro-organisation is drastically altered with the elimination of the $C_2S_2M_2$ supercomplexes, due to the absence of CP24 and the M-trimer. These results together confirm that no single Lhcb protein is the unique site of qE and suggest the importance of the macro-structure of the LHCII antenna system for maximal NPQ *in vivo* (Horton et al., 2005; Kovacs et al., 2006).

Spectroscopic analysis of quenched LHCII gives rise to suggestions about the mechanism of quenching. Wentworth et al. (2001) emphasise the importance of the terminal emitter domain (consisting in Chl *a*611, Chl *a*612, Chl *b*608 and lutein 1), and suggest that a conformational change could create a quenching interaction between the chlorophylls and lutein. The crystal structure model of LHCII of Liu et al. (2004) allowed the first detailed insights into how quenching may occur. Spectroscopic analysis performed on these crystals by Pascal et al. (2005) showed that they are in a highly quenching state. The lifetimes measured with the fluorescence lifetime imaging technique (FLIM) were found to be 0.89 ns for crystals compared to 4.2 ns for the isolated trimers. The fluorescence emission spectra revealed a characteristic 680 nm band along with a maximum situated at around 700 nm, identical to previous results on quenched aggregated LHCII. Resonance Raman analysis showed changes in the pigment interactions when comparing crystal and trimers; the neoxanthin molecule in each monomer in the crystal is twisted relative to its state in the trimer. Also changes in the chlorophyll *b* region were found, indicating an extra hydrogen bond between a formyl group of a chlorophyll *b* with a water molecule in the crystal (Pascal et al., 2005). These observations provided conclusive proof that a conformational change occurs in LHCII upon transition to the quenched state. According to the orientation of the pigments in the crystal structure, several possible quenching sites were proposed (Pascal et al., 2005):

- terminal emitter domain consisting in chlorophylls: Chl *a*611, Chl *a*612, Chl *b*608 and lutein 1 (lut 620); Figure 16a
- neoxanthin domain: neoxanthin (neo), lutein 2 (lut 621), Chl *b*606 and Chl *b*607; Figure 16b
- xanthophyll cycle binding domain (V1):violaxanthin (Xanc), Chl *a*611 and Chl *a*601; Figure 16c

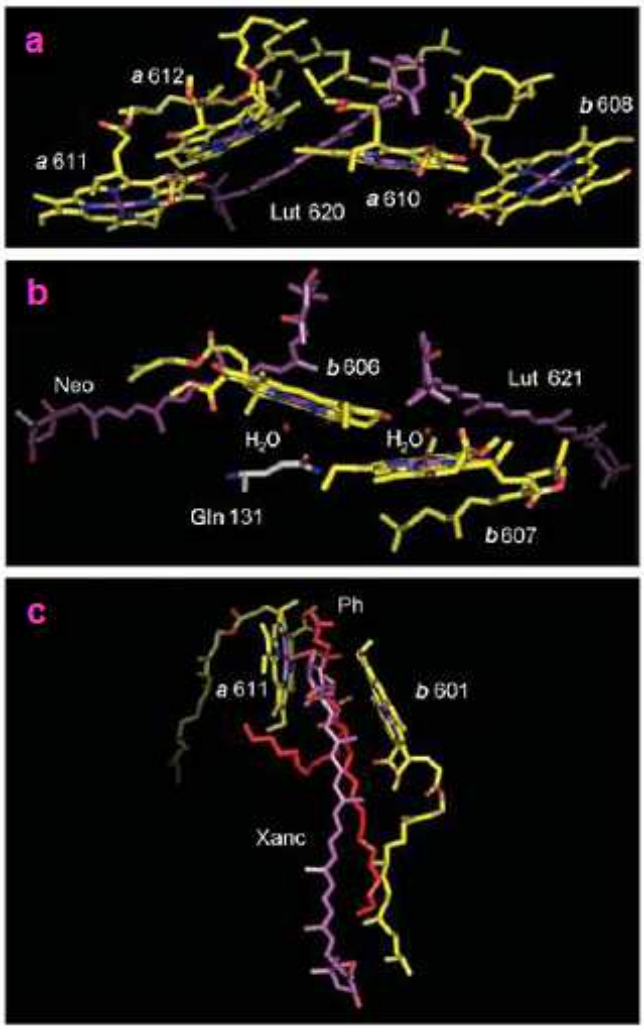

Figure 16. Possible quenching sites in the LHCII crystal structure. The Lutein 1 terminal emitter domain (a), the Lutein 2-neoxanthin-chl*b* domain (b) and the XC binding site (c) (Pascal et al., 2005).

In a subsequent examination of the crystal structure, the different configuration of lutein 1 and lutein 2 is highlighted; it was suggested that rotation the lutein 1 molecule relative to the Chl *a*611 and Chl *a*612 molecules could be the conformational change creating the quencher (Yan et al., 2007).

1.9 Project outline

The overall aim of the work presented in this thesis is to investigate using different spectroscopic and biochemical approaches the dynamics of LHCII and the energy transfer from xanthophylls to chlorophylls *in vitro* and *in vivo*.
The work is divided in 4 chapters as follows:

Chapter 3

- Estimation of the energy transfer from xanthophylls to chlorophyll *a* in LHCII using 2nd derivative and curve fitting analysis;
- Exploration of the origin and the role of lutein 2 band in absorption and fluorescence excitation spectra;
- Analysis of the thylakoid membrane before and after the conversion of the violaxanthin to zeaxanthin by absorption and fluorescence excitation spectroscopy;
- Investigation of the isolated complexes and thylakoid membranes from antisense *Lhcb2* Arabidopsis plants.

Chapter 4

- Development and spectral properties of a solid-state gel system where quenching can be induced without protein aggregation.

Chapter 5

- Resonance Raman studies of the LHCII complexes in different quenching states and of chloroplasts and leaves after qE induction.

Chapter 6

- Transient absorption spectroscopy on LHCII in different quenching states.

CHAPTER TWO

Materials and Methods

2.1 General laboratory chemicals

Chemicals and reagent used for carrying out the experiments were obtained from Sigma unless stated otherwise.

2.2 Plant material

Spinach leaves were purchased fresh from a local supermarket and stored at 4ºC in the dark until required for use. *Arabidopsis thaliana*, *cv Columbia*, *npq4-1* mutant, Lhcb2 antisense *aslhcb2-12* line and PsbS overexpressing (L17) lines were grown for 10-12 weeks in Conviron controlled environment growth rooms with an 8 hour photoperiod at a light intensity of 200 μmol quanta m^{-2} s^{-1} and a day/night temperature of 22/18 ^{0}C in a mixture M_3 soil and perlite with a ratio not higher than 2:1.

2.3 Sample preparation

2.3.1 Preparation of intact chloroplasts

Intact chloroplasts were prepared by homogenizing fresh *Arabidopsis* leaf tissue in ice-cold grinding medium (450 mM sorbitol, 20mM Tricine, 10mM EDTA, 10mM $NaHCO_3$, and 0.1% BSA at pH 8.4) with a Polytron (Kinematica GmbH), applying 3-4 short bursts at full power. The homogenate was then filtered on ice through four layers of muslin followed by two layers of muslin and one layer of cotton wool. The filtrate was centrifuged for 30 s at 4000 g (MSE Mistral, 6L). The chloroplast-enriched pellet was washed and resuspended in the resuspending medium (330 mM sorbitol, 20 mM Tricine, 5 mM $MgCl_2$ and 2.5 mM EDTA, pH 7.6). The resuspended sample was applied to a 2 cm Percoll cushion mixed with double osmotic strength resuspension medium, and centrifuged for 10 minutes at 3500 x g. The pellet was then resuspended with a small volume of resuspension medium and kept on ice until used.

2.3.2 Preparation of thylakoid membranes

Stacked thylakoids were prepared by homogenizing fresh dark adapted *Arabidopsi*s leaves in ice-cold grinding medium (330 mM sorbitol, 5 mM $MgCl_2$, 10 mM $Na_4P_2O_7$, pH 6.5, 2 mM D-*iso*-ascorbate) with a polytron. The homogenate was then filtered through four layers of muslin followed by two layers of muslin and one layer of cotton

wool. The filtrate was centrifuged for 10 min at 4000 x *g*, and the chloroplast-enriched pellet was resuspended in wash buffer (330 mM sorbitol, 10 mM MES, pH 6.5), followed by a further 10 minutes centrifugation at 4000 x *g*. The pellet was then resuspended in 5 mM $MgCl_2$ for 30 s to lyse any remaining intact chloroplasts, followed by an equal volume of medium containing 660 mM sorbitol, 20 mM KCl, 2 mM EDTA, and 100 mM HEPES, pH 6.5 medium. After further centrifugation, thylakoids were resuspended in 20 mM Bis-Tris (pH 6.5), 5 mM $MgCl_2$. Unstacked thylakoids were preparing using the same protocol and but removing $MgCl_2$ from the media.

2.3.3 PSII membrane preparation (BBYs)

Preparation of PSII particles preparations was carried out using the method of Berthold et al. (1981). Approximately 80g of fresh leaves (spinach) with the midrib removed were homogenised in 300 ml of slushy grinding medium (330 mM sorbitol, 10 mM $Na_4P_2O_7x10H_2O$, 5 mM $MgCl_2$, 2 mM sodium D-iso-ascorbate, pH 6.5) with 2-3 short bursts from a polytron. The homogenate was initially filtered through 2 layers of muslin followed by 8 layers of muslin surrounding a central layer of highly absorbent cotton wool. The sample was then centrifuged at 4000 x g for 5 minutes, the supernatant discarded and the pellet resuspended in washing medium (330 mM sorbitol, 10 mM MES, pH 6.5) before centrifugation for 7.5 minutes at 4000 g. The resulting pellet was resuspended in 30 ml of resuspension medium (330 mM sorbitol, 5 mM $MgCl_2$, 40 mM MES, pH 6.5) and osmotically shocked by the addition of 50 ml of breaking medium (5 mM $MgCl_2$, pH 7.6). The osmotic potential was restored after 30 seconds by the addition of 50 ml of a double osmotic strength medium (660 M sorbitol, 5 mM $MgCl_2$, 40 mM MES, pH 7.6). The thylakoids were then centrifuged for 10 minutes at 4000 x g and the pellet resuspended in stacking medium (5 mM $MgCl_2$, 15 mM NaCl, 2 mM MES, pH 6.3). A 0.5 ml aliquot was used for chlorophyll determination (see section 2.5), and the rest of the sample was resuspended to a final chlorophyll concentration of 3 mg/ml in stacking medium. The sample was left on ice in the dark without stirring for a minimum period of 45 minutes to promote membrane stacking. Following this, the sample was then diluted with half its volume of 10 % (v/v) Triton X-100 in stacking medium to give a final detergent concentration of 3.33 % (v/v). The sample was then incubated on ice for 30 minutes with occasional gentle inversions to help membrane digestion. After this step, the digestion was stopped by dilution of the detergent with the addition of at least 6 ml of stacking medium. The sample was then centrifuged -*for 30

minutes at 30000 x g (4 °C) in a Beckman J2 centrifuge using a J2-21 rotor. The pellet was resuspended in particle wash medium (2 mM EDTA, pH 7.5) and again centrifuged as in the previous step (30000 x g, 30 minutes at 4 °C). The supernatant was discarded and the final pellet resuspended in deionised water. Samples were used as required or frozen in liquid nitrogen and stored at –80 °C.

2.3.4 LHCII isolation

Non denaturing IEF (iso elecrtic focusing)

IEF was carried out using a Multiphor II Electrophoresis system (Pharmacia) following the method of Bassi et al. (1991) as modified by Ruban et al. (1994b). A slurry of volume 100 ml containing 4% Ultradex (Amersham Biosciences), 2% ampholine carrier ampholites (pH 3.5–5.0), 1% glycine and 0.06% *n*-dodecyl *β*-D-maltoside was prepared. Electrode strips were soaked in 2 % (w/v) ampholine solution (pH range 3.5-5.0), excess solution was removed with tissue and the strips placed at each end of the 24.5 by 11.0-cm gel tray. The slurry was poured into the gel tray and, after carefully removing air bubbles, the tray was placed on a balance, 70 cm below a small fan for approximately 2 hours in order to evaporate 30g of water. The anode and cathode strips were prepared by soaking the strip in either anode solution (5.6 % (v/v) H_3PO_4) or cathode solution (1 M NaOH). The excess solution was removed with a tissue and the strips were carefully placed at either end of the gel on top of the electrod strips. A 0.1 % (v/v) solution of Triton X-100 was applied to the surface of the Multiphor II cooling plate to improve heat transfer from the gel tray. The gel tray was then placed on the cooling plate and the electrodes connected to the electrode strips. Pre-focusing of the gel was carried out at ~8 W (13 mA, 600 V) for 1-2 hours. Freshly prepared PSII particles, with a total chlorophyll concentration of 2.5mg/ml, were resuspended in 1 ml of deionised water. 0.5 ml of 3% *n*-dodecyl *β*-D-maltoside was added on ice and the sample incubatied with occasional stirring for 30 minutes. The sample was centrifuged at 35000 x *g*, and the supernatant was applied 2 cm from the cathode of the pre-cooled and pre-focused gel using a sample applicator (10 by 2 cm). After sample application the gel was allowed to equilibrate for 3 minutes before the start of focusing. The focusing procedure was carried out for 18 h (overnight) at a constant power of 8W at 4 °C. The initial and final current values were normally ~15 and 5 mA, respectively. Each

green band corresponding to the different light harvesting complexes was carefully collected using a spatula. The samples were eluted using a minimum volume of a solution containing 100 mM HEPES (pH 7.6) and 0.01% *n*-dodecyl *β*-D-maltoside using a plastic Pasteur pipette. The samples were then loaded onto a desalting column to remove the ampholine, using a desalting buffer (25 mM HEPES and 0.01-0.03 % (w/v) *n*-dodecyl *β*-D-maltoside as required).

Sucrose gradient separation

Further purification (removing monomers and free pigments) of LHCII was carried out by sucrose density gradient centrifugation. Seven step exponential sucrose gradients from 0.15 to 1.0 M sucrose were used.. Two 60 ml sucrose stock solutions of 0.1 M and 1.5 M in 20 mM HEPES buffer containing 20 mM *n*-dodecyl *β*-D-maltoside (pH 8.0) were prepared for a total of six tubes. 1.5 ml of 0.1 M sucrose was pipetted into each of the six tubes (9 ml total). Subsequently, 9 ml of the 1.5 M stock solution was added to the 0.1 M stock and mixed. Again, a total of 9 ml of the latter stock are added to the tubes. This process was repeated six times to form the gradient. 200 to 500 µl of sample are loaded onto each tube and centrifuged at 200 000 x g in a SW41 rotor for 18 h at 4°C.

For monomer preparation, the trimeric LHCII was treated with phospholipase A_2 from bee venom for 48 h at room temperature in the presence of 20 mM $CaCl_2$ in a sterilized eppendorf tube at a chlorophyll concentration of 500 µmol/ml. Immediately after the treatment, the sample was applied onto a seven-step exponential sucrose gradient as described above. After centrifugation, the monomer band was located at approximately 0.25 M sucrose with a yield of 60%. The remaining LHCII trimers were located at around 0.45 M sucrose. The monomeric LHCII were loaded onto a desalting column as for the trimers onto a desalting column, and then either immediately frozen in liquid N_2 or used for analysis.

Quenched LHCII were obtained by incubation with ~50mg of SM-2 Absorbent (Bio-Rad) in a 1 cm (optical path length) cuvette, allowing fine control over the extent of quenching by simultaneous fluorescence measurements with a Walz PAM1000 fluorimeter. Samples were taken from the cuvette at different levels of quenching.

2.4 De-epoxidation procedure

De-epoxidation experiments were carried out using a modification of the method described by Rees et al. (1992). Spinach leaves were floated on water at ~20 °C with their cut petioles under water and light treated with 200μE m^{-2} s^{-1} for ~2 hours under an atmosphere of 98% N_2, 2% O_2. A ~10 min equilibration period was allowed before and after treatment. The same procedure was applied to *Arabidopsis col-0* plants. 8-9 weeks old plants were taken from their pots, the soil gently removed and the plants immersed immediately in water. Plants were light treated for ~ 2 hours as for spinach leaves.

2.5 Determination of the chlorophyll concentration

The chlorophyll concentration of the samples was measured using the method of Porra et al. (1989). Pigments were extracted with 80 % (v/v) acetone and centrifuged at 3000 g for 3 minutes to remove debris. Sample absorption was measured at 663 nm (A_{663}), 645 nm (A_{645}) and 470 nm (A_{470}) using a Beckman DU650 spectrophotometer. Chlorophyll concentration and chlorophyll *a*/*b* ratio were estimated using the following equations:

$$[\text{Chl } a] = 12.7\,(A_{663}) - 2.69\,(A_{645})$$

$$[\text{Chl } b] = 22.9\,(A_{645}) - 4.68\,(A_{663})$$

$$\text{Total } [\text{Chl}] = 20.2\,(A_{645}) - 8.02\,(A_{663})$$

$$\text{Chl } a/b \text{ Ratio} = \frac{[\text{Chl } a]}{[\text{Chl } b]}$$

2.6 Determination of pigment composition (HPLC)

The pigment composition of leaves and thylakoid membranes was determined using high performance liquid chromatography (HPLC). All solvents used were HPLC grade. For pigment extraction thylakoid membranes were mixed with 0.5 ml 100% acetone. The debris was pelleted by centrifugation for 5 minutes at 3000 g in a microfuge.

Samples were loaded into glass vials, which were sealed with caps containing PTFE (polytetrafluoroethylene) septa. A Dionex HPLC instrument in combination with a LiChroCART RP-18 column (Merck, Darmstadt, Germany) was used. Two solvents were used: Solvent A (87% Acetonitrile, 10% Methanol, 3 mM Tris pH 8.0) and Solvent B (80% Methanol, 20% Hexane) at 1 ml/min flow rate with the following run profile:

0 – 18 minutes: 100% Solvent A
18 – 25 minutes: 0% to 100% Solvent B
25 – 36 minutes: 100% Solvent B
36 – 38 minutes: 100% to 0% Solvent B
38 – 46 minutes: 100% Solvent A

Spectra were recording between 280 and 750 nm using a Dionex PDA-100 photodiode array detector. Data analysis was carried out using Chromeleon Version 6.50 software (Dionex). Each individual peak was integrated and the area recorded at the optimum wavelength. Conversion factors allowing the calculation of pigment concentration from the integrated peak area were determined by calibration with pure pigments.

2.7 Spectroscopy

Low temperature absorption and fluorescence measurements were carried out using an Optistat^{DN}LN-2 cooled bath cryostat (Oxford Instruments). The samples were diluted in a medium containing 80% glycerol (w/v), 20 mM HEPES buffer at pH 7.8, and 0.03% *n*-dodecyl *β*-D-maltoside for isolated complexes. The chlorophyll concentration for absorption measurements was 1-4 μmol Chl/ml, and for the fluorescence emission and fluorescence excitation measurements was 1 μmol Chl/ml. Measurements were performed using polymethyl methacrylate 1 cm (optical path length) cuvettes. The temperature of the sample was monitored with a thermocouple sensor (Comark) immersed directly into the sample.

2.7.1 Absorption

Absorption measurements were carried out using a Cary 500 UV-visible NIR spectrophotometer (Varian) modified to accept the cryostat when required. The spectra were recorded from 350-700 nm with a 2 nm slit width. The spectral resolution was 1

nm with a signal-to-noise ratio of 10000. The single spectral beam mode was employed to focus the measuring beam on the sample only, and to obtain the maximum light output. The spectra were corrected for the cuvette and buffer medium using Gramms/32 software (Galactic Industries Corporation).

2.7.2 Fluorescence

Low temperature

Fluorescence emission and excitation spectra were recorded using a SPEX FluoroLog FL3-22 spectrofluorimeter (SPEX Industries Inc.). The excitation light was provided from a Xenon light source. For fluorescence emission measurements the excitation was set at 435 nm with a 5 nm spectral bandwidth. The fluorescence spectral resolution was 1 nm. For fluorescence excitation measurements fluorescence was detected at 685 nm with a 5 nm spectral bandwidth. The excitation spectral resolution was 1 nm. The spectra were automatically corrected for the spectral distribution of the exciting light during data acquisition. For the LHCII samples immobilised in gel or gelatine, low temperature fluorescence emission spectra were measured using a holder consisting of two flat, round pieces of glass (14 mm diameter) sealed with a metal ring. The samples were immersed in liquid nitrogen in a purpose-build cryostat during data acquisition. Broad band excitation of 50 μE m^2 s^{-1} centred on 435 nm was provided by a Wotan tungsten halogen 150 W lamp defined by Corning filters (4-46 and 5-57) with heat-absorbing glass. Fluorescence was detected by a 1024-channel silicon photodiode detector (Model 1455), via a Jarrell-Ash Monospec 27 monochromator, and analysed by a PARC 1461 multichannel analyser (EG&G Instru. Corp., Princeton Appl. Res., Princeton, USA) using EG&G OMA-Vision-PDA software. This gave a resolution of 0.3 nm and a signal to noise ratio 10000:1 (Ruban et al., 1991). Data analysis was carried out using Gramms/32 software (Galactic Industries Corporation).

Room temperature

Room temperature chlorophyll fluorescence quenching analysis of detached leaves and isolated chloroplasts was carried out using a Walz PAM 101 fluorimeter (see section 5.2 for details).). For the NPQ induction, chloroplasts were treated with 1500 μmol m^{-2} s^{-1} light for approximately 5 minutes. 100 μM methylviologen was added as electron

acceptor for the chloroplast measurements. The fluorescence intensity of the LHCII-gel system was monitored with a Walz PAM 1000 fluorimeter.

Fluorescence images of gels were acquired with a FluorCam 690M from PSI (Photon System Instruments) after 1min exposure time. The scale of fluorescence intensity was colour-coded from the blue (low fluorescence) to the red (high fluorescence).

2.7.3 CD

Circular dichroism spectra were recorded between 400 and 750 nm at room temperature in a J810 (Jasco) dichrograph using a band pass of 3 nm and a resolution of 1 nm. The chlorophyll content was adjusted to 20 μg/ml and spectra were recorded in a glass cuvette with a 1 cm optical path length. For gel samples a home made sample holder was used. Temperature was maintained by an attached PFD425S Peltier system.

2.7.4 Resonance Raman

Low temperature resonance Raman spectra were obtained in a liquid nitrogen flow cryostat (Air liquid, Paris, France) using a Jobin-Yvon U1000 Raman spectrophotometer equipped with a liquid nitrogen-cooled charge-coupled device (CCD) detector (Spectrum One, Jobin-Yvon, Paris, France) as described by Ruban et al. (2001). Intact chloroplasts and isolated LHCII samples were frozen on glass plates and a grazing incidence was used in order to prevent re-absorption of the Raman photons by the sample (Robert & Lutz 1986). For leaf measurements a home made sample holder was used. After the induction of NPQ the samples were immediately frozen in liquid nitrogen to conserve the quenching state. Excitation at 488.0 nm was provided by Coherent Argon (Innova 100) laser. Laser power was maintained at about 20mW, with less than 2mW penetrating the sample (Robert & Lutz 1986). Typical spectral resolution at 1000 cm^{-1} was 8 cm^{-1}.

2.7.5 Transient absorption

Time-resolved transient absorption spectroscopy was carried out at the Vrije Universiteit (VU) Amsterdam, with the assistance of Rudi Berera. LHCII isolated from dark adapted spinach leaves and in different quenched oligomeric states (see section 2.3.4 for preparation) were subject to transient absorption measurements (see Chapter 6 for details).

CHAPTER THREE

Spectral characteristics and energy transfer properties of LHCII-bound xanthophylls

3.1 Introduction

Photosynthetic light-harvesting antennae of green plants bind two types of pigments: chlorophylls and carotenoids. Xanthophylls are a specific class of oxygenated carotenoids that are present in the photosynthetic apparatus of higher plants, associated with the light-harvesting complexes of the chloroplasts membranes (Yamamoto & Bassi, 1996). Five types of xanthophylls are present in the light-harvesting antenna: lutein, neoxanthin, violaxanthin, zeaxanthin and antheraxanthin (the latter three are interconverted in the so-called xanthophyll cycle).

The crystal structure of the major light-harvesting complex of PSII from spinach has shown that each monomer of the trimeric complex binds 14 chlorophylls (8 chlorophyll *a* and 6 chlorophyll *b*) and 4 xanthophylls: 1 neoxanthin, 2 luteins and 1 violaxanthin (Liu et al., 2004). When isolated in detergent micelles the complex is present in its trimeric form, the pigment composition of this preparation being similar to that of the crystal, except the content of violaxanthin, which varies between 0.1 and 1 per monomer depending of the isolation procedure (Sandona et al., 1998; Ruban et al., 1999), showing that this xanthophyll is only loosely bound to the complex.

Energy transfer in LHCII has been widely studied by transient absorption spectroscopy (Gradinaru et al., 2000; Croce at al., 2001), time resolved fluorescence spectroscopy (Ide et al., 1987; Du et al., 1994), photon echo spectroscopy (Salverda et al., 2003) and other spectroscopic techniques. Energy transfer from carotenoids and chlorophyll *b* to chlorophyll *a* is very efficient (van Amerongen & van Grondelle, 2001). Using the crystal structure (Liu et al., 2004), van Grondelle & Novoderezhkin (2006) recently analysed numerous spectroscopic data by modified Redfield theory. They propose a precise assignment of the energy transfer pathways, leading to a visualization of the excitation dynamics in this complex. However, the model based on the modified Redfield relaxation theory applied to the limited set of data is not unique. In the case of LHCII the fit of the linear spectra can produce more than 30 models, which can reproduce quantitatively the absorption and LD spectra, but not the time-scales and the kinetics of the transient absorption measurements. Only after including in the model the 650 and 662 nm excitation kinetics, the model can be used to specify the site energies (van Grondelle & Novoderezhkin, 2006).

The aim of the work described in this chapter was to investigate energy transfer to chlorophylls from the different xanthophylls in the thylakoid membrane. This was

carried out firstly by investigation of purified LHCII trimers in which only neoxanthin and lutein were bound, and secondly by study of intact thylakoid membranes in which the extent of de-epoxidation of xanthophyll cycle carotenoids was different. The experimental approach was to analyse absorption and fluorescence excitation spectra recorded at 77K, applying second derivative and curve fitting analysis. Comparing these spectra allows an estimation of the efficiency of energy transfer from xanthophylls to chlorophyll *a*. The experiments were also designed to provide more information about the 510 nm absorption band, which arises from lutein 2 (Ruban et al., 2000). Finally, thylakoid membranes and isolated complexes from the antisense *asLhcb2* plants, which lack the main light-harvesting complexes, were investigated using the same spectroscopic techniques.

3.2 Results

3.2.1 Analysis of the xanthophylls to chlorophyll a energy transfer in purified LHCII trimers

LHCII was prepared from unstacked thylakoids isolated from *Arabidopsis thaliana* wild type. Detergent (*n*-dodecyl *β*-D-maltoside) solubilised thylakoids were fractioned by IEF (see 2.3.4 for details) and the dark green band LHCII was collected (Figure 1a). This preparation contains mostly trimers but is contaminated with monomers and some traces of minor complexes (Ruban et al., 1999). Furthermore, the occupancy of the V1 site by violaxanthin is variable and on average about 0.2 (Ruban et al., 1999). For the analysis of the absorption spectrum it is essential to have pure LHCII trimers with a defined and uniform xanthophyll composition. Therefore, to improve purification and to remove completely violaxanthin, monomers and minor complexes (Ruban et al., 1999), the IEF preparation was loaded on a sucrose gradient (Figure 1b) and the purified LHCII trimers harvested. This preparation was then investigated by low temperature measurements: fluorescence (emission and excitation) and absorption.

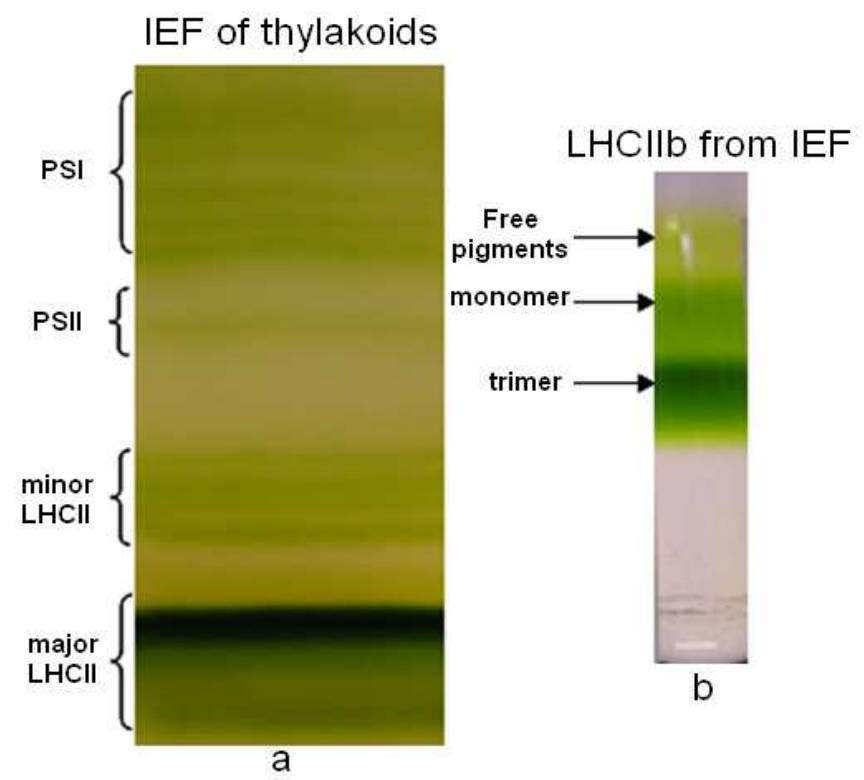

Figure 1. Isolation and purification of LHCII. (a) Iso electric focusing gel of isolated solubilised thylakoid showing the position of the chlorophyll containing complexes(b). Sucrose gradient centrifugation profile of the LHCII band from IEF showing the free pigment, monomer and trimer bands.

Figure 2 shows the absorption spectra of LHCII recorded at room temperature (a) and at 77K (b) along with their second derivatives. For clarity the 2nd derivatives are presented inverted.

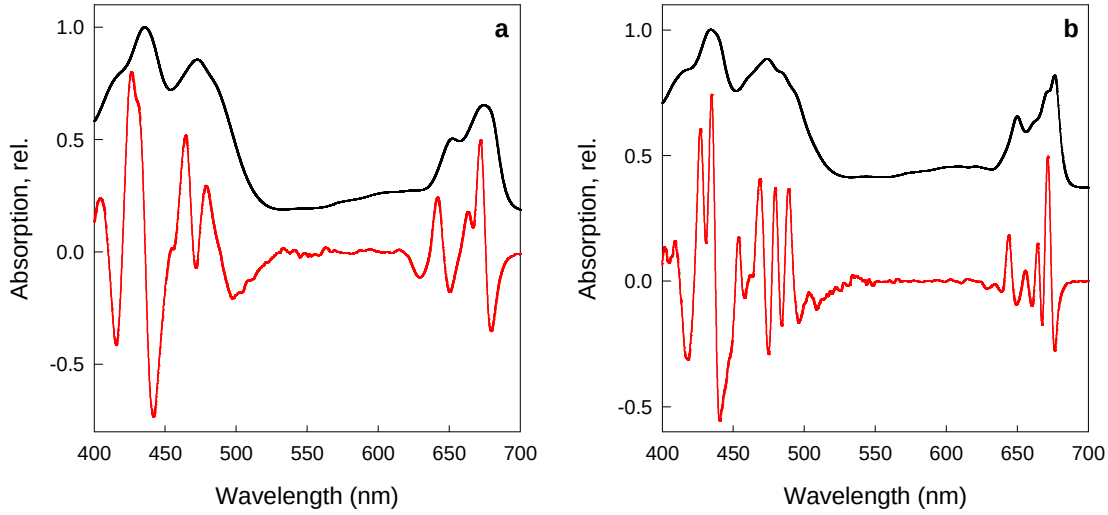

Figure 2. Absorption spectra of purified LHCII trimers. Room temperature (a) and 77K (b) absorption spectra of LHCII trimers (black) and the inverted 2nd derivatives (red). Samples were prepared as shown in Figure 1.

At room temperature the spectrum displays a number of bands and is rather complex in the Soret region because the absorption bands from both chlorophylls and xanthophylls are overlapping. The room temperature spectrum shows in the Qy region the typical chlorophyll *a* absorption bands at around 669 and 672 nm, and the chlorophyll *b* absorption at 641 nm (Figure 2a). In the Soret region the spectrum exhibits bands arising from both chlorophylls and carotenoids molecules: a 485 nm carotenoid band, a chlorophyll *b* band at 474 nm and chlorophyll *a* bands at around 437 nm and 413 nm. The spectral resolution was improved by decreasing the temperature to 77K, when more fine structure appears (Figure 2b). Also, more information about the position of the bands in the spectrum was provided by the calculation of the 2nd derivative. At low temperature, new bands can be seen: 510, 495 and 486 nm carotenoid bands, which replace the 485 nm band seen in the room temperature spectrum, along with the bands arising at 457, 465 (chlorophyll *b*), and 433 nm (chlorophyll *a*). In the red region of the spectrum, additional bands are present from chlorophyll *b* at around 650 and from chlorophyll *a* at 662 nm.

Figure 3 shows the absorption spectrum of a carotenoid (β-carotene) in tetrahydrofuran (THF) and the inverted second derivative. Second derivative spectrum clearly shows that the carotenoid spectrum contains three electronic transition, namely 0-0, 0-1 and 0-2 transitions. The electronic transition of the xanthophylls present in the trimeric and monomeric LHCII were identified by Ruban et al. (2000) using a combination of ultra-low-temperature absorption, circular dichroism and resonance Raman spectroscopies. It was found that 0-0, 0-1 and 0-2 electronic transition for neoxanthin and lutein in monomers are situated at 486, 457, 403 nm and 495, 466, 437 nm, respectively. Using selective excitation lines for resonance Raman spectra the band at 510 nm in the low temperature absorption spectrum of trimers has been shown to arise from one of the lutein molecules (lutein 2), which is distorted in this complex, according to the analysis of the resonance Raman spectra in the ν_4 region (Ruban et al., 2001). Note that this distortion is accompanied by a red shift in its 0-0 transition, from 495 to 510 nm. The 0-1 and 0-2 transition for lut2 were found to be situated at around 476 nm (0-1) and 445 nm (0-2). According to these assignments for all the xanthophylls present in LHCII trimer, the 0-0 absorption transition does not significantly overlap the absorption transition of any chlorophyll. Therefore, this band provides information about the

absorption for each individual carotenoid. The following data analysis in this section only focuses on the investigation of the xanthophyll 0-0 transition.

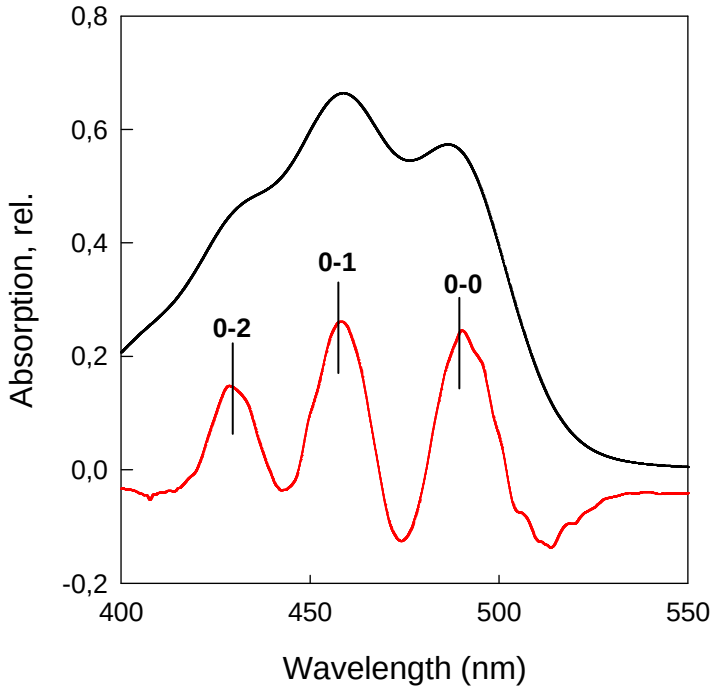

Figure 3. Absorption spectrum of β-carotene in tetrahydrofuran (THF) (black trace) and the inverted second derivative showing the 0-0, 0-1 and 0-2 electronic transitions (red).

Figure 4 shows the comparison between the 2nd derivative of the 77K absorption spectrum in the Soret region for the LHCII trimers and a preparation of monomerised LHCII (see 2.3.4 for details). It can be seen that there is an additional band in the trimeric preparation, situated at 510 nm, which was assigned to an absorption transition (0-0) of one of the two luteins (lutein 2) present in the preparation (see also above). This 510 nm band has small amplitude in the 2nd derivative compared to the other lutein (lut1) band at 495 nm and for this reason it was at first considered to be a minor band, possibly from contaminating violaxanthin, (Peterman et al., 1997). Since the preparation used here contains no violaxanthin, this can not be the case. Another possible explanation for the difference in the amplitudes might be a difference in their extinction coefficients. Alternatively, the 0-0 absorption transition of the lut2 may be broader, much broader than either lut1 or the neoxanthin band (486 nm), as suggested by Ruban et al. (2001). This latter possibility was investingated further.

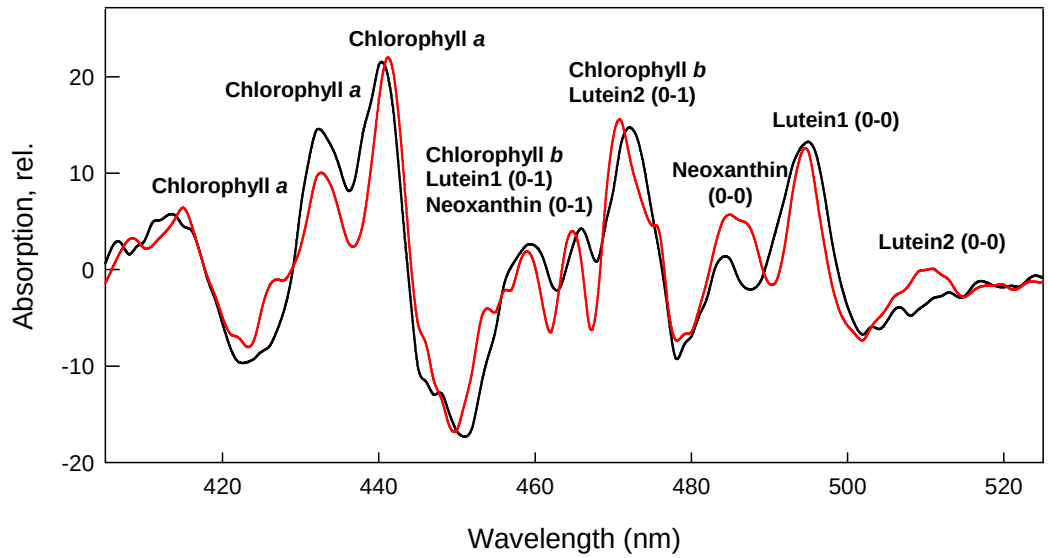

Figure 4. Inverted 2nd derivatives calculated for 77K absorption spectra for LHCII trimers (red) and monomers (black). Spectra were normalised to the chlorophyll *a* band at 440 nm. The bands are labelled for the 0-0 and 0-1 transitions according to Ruban et al 2000.

It can be proven that the amplitude of a 2nd derivative band is reciprocal to its width. This proof was achieved by calculation of the 2nd derivative of a Gaussian contour. Firstly, the first derivative of the Gaussian function was calculated and then the derivative calculation was applied to the result.

First derivative:

$$f(x) = a \cdot e^{-\frac{(x-b)^2}{2c^2}}$$

$$\frac{d}{dx} f(x) = \frac{d}{dx}\left(a \cdot e^{-\frac{(x-b)^2}{2c^2}} \right) = a \frac{d}{dx}\left(e^{-\frac{(x-b)^2}{2c^2}} \right) = a \cdot e^{-\frac{(x-b)^2}{2c^2}} \frac{d}{dx}\left(-\frac{(x-b)^2}{2c^2} \right) =$$

$$= -\frac{a \cdot e^{-\frac{(x-b)^2}{2c^2}}}{2c^2} \frac{d}{dx}\left((x-b)^2 \right) = -\frac{a \cdot e^{-\frac{(x-b)^2}{2c^2}} (x-b)}{c^2} \frac{d}{dx}(x-b) =$$

$$= -\frac{a \cdot e^{-\frac{(x-b)^2}{2c^2}} (x-b)\left(\frac{d}{dx}(-b) + \frac{d}{dx}(x) \right)}{c^2} = -\frac{a \cdot e^{-\frac{(x-b)^2}{2c^2}} (x-b)}{c^2} \frac{d}{dx}(x) =$$

$$-\frac{a \cdot e^{-\frac{(x-b)^2}{2c^2}} (x-b)}{c^2} = \frac{a \cdot e^{-\frac{(x-b)^2}{2c^2}} (b-x)}{c^2}$$

Second derivative:

$$\frac{d}{dx}\left(\frac{a\cdot e^{-\frac{(b-x)^2}{2c^2}}(b-x)}{c^2}\right)=\frac{a}{c^2}\frac{d}{dx}\left(e^{\frac{(b-x)^2}{2c^2}}(b-x)\right)=\frac{a\cdot\left((b-x)\frac{d}{dx}\left(e^{\frac{(b-x)^2}{2c^2}}\right)+e^{\frac{(b-x)^2}{2c^2}}\frac{d}{dx}(b-x)\right)}{c^2}=$$

$$=\frac{a\cdot\left((b-x)\frac{d}{dx}\left(e^{\frac{(b-x)^2}{2c^2}}\right)+e^{\frac{(b-x)^2}{2c^2}}\left(\frac{d}{dx}(b)+\frac{d}{dx}(-x)\right)\right)}{c^2}=\frac{a\cdot\left(e^{\frac{(b-x)^2}{2c^2}}\left(\frac{d}{dx}(b)-1\right)+(b-x)\frac{d}{dx}\left(e^{\frac{(b-x)^2}{2c^2}}\right)\right)}{c^2}=$$

$$=\frac{a\cdot\left((b-x)\frac{d}{dx}\left(e^{\frac{(b-x)^2}{2c^2}}\right)-e^{\frac{(b-x)^2}{2c^2}}\right)}{c^2}=\frac{a\cdot\left(e^{\frac{(b-x)^2}{2c^2}}(b-x)\frac{d}{dx}\left(-\frac{(b-x)^2}{c^2}\right)-e^{\frac{(b-x)^2}{2c^2}}\right)}{c^2}=$$

$$=\frac{a\cdot\left(-\frac{e^{\frac{(b-x)^2}{2c^2}}(b-x)}{2c^2}\frac{d}{dx}\left((b-x)^2\right)-e^{\frac{(b-x)^2}{2c^2}}\right)}{c^2}=\frac{a\cdot\left(-\frac{e^{\frac{(b-x)^2}{2c^2}}(b-x)^2}{2c^2}\frac{d}{dx}(b-x)-e^{\frac{(b-x)^2}{2c^2}}\right)}{c^2}=$$

$$=\frac{a\cdot\left(-\frac{e^{\frac{(b-x)^2}{2c^2}}\left(\frac{d}{dx}(b)+\frac{d}{dx}(-x)\right)(b-x)^2}{c^2}-e^{\frac{(b-x)^2}{2c^2}}\right)}{c^2}=\frac{a\cdot\left(-\frac{e^{\frac{(b-x)^2}{2c^2}}(b-x)^2}{c^2}\frac{d}{dx}(-x)-e^{\frac{(b-x)^2}{2c^2}}\right)}{c^2}=$$

$$=\frac{a\cdot\left(\frac{e^{\frac{(b-x)^2}{2c^2}}(b-x)^2}{c^2}\frac{d}{dx}(x)-e^{\frac{(b-x)^2}{2c^2}}\right)}{c^2}=\frac{a\cdot\left(\frac{e^{\frac{(b-x)^2}{2c^2}}(b-x)^2}{c^2}-e^{\frac{(b-x)^2}{2c^2}}\right)}{c^2}=\frac{ae^{\frac{(b-x)^2}{2c^2}}\left(b^2-2xb+x^2-c^2\right)}{c^4}=$$

$$=\frac{a}{c^4}\left(e^{\frac{(b-x)^2}{2c^2}}\left(b^2-2xb+x^2-c^2\right)\right)$$

In the above equation *a, b, c* are constants, *a* representing the amplitude of the Gaussian peak, *b* the position of the centre of the peak and *c* is related to the width (FWHM) by the equation: $FWHM = 2\sqrt{2\ln 2}\cdot c \approx 2.35\cdot c$. Hence, in the 2nd derivative calculation the amplitude (*a*) is inversely proportional to the width and it can be concluded that when the width is larger the amplitude will be smaller. This conclusion was confirmed by calculating the 2nd derivative for two Gaussian bands (one band having FWHM twice larger than the other one, Figure 5) and comparing their amplitudes. The amplitude of

the 2nd derivative (calculated using Gramms/32 software) was found to be approximately 3 times smaller for the broader band (FWHM=2x).

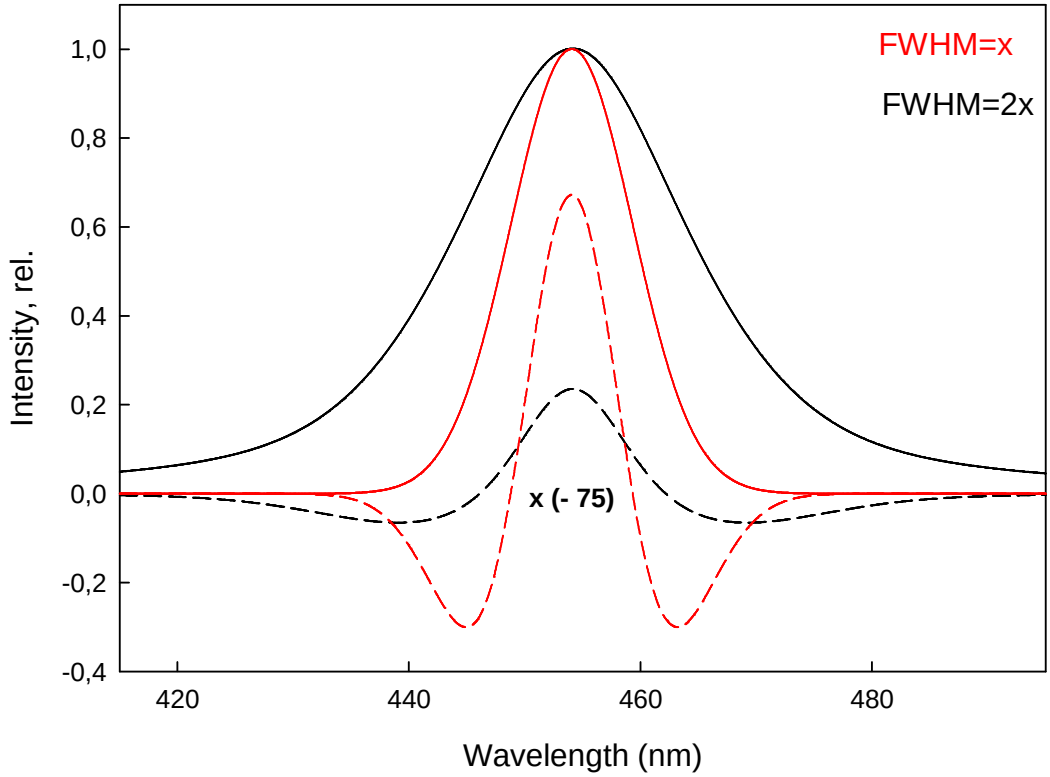

Figure 5. Gaussian bands (solid) and inverted 2nd derivative (short dash) with x2 difference in FWHM (red and black). The Gaussians were normalised to their maxima. Both 2nd derivatives were multiplied by a factor of (-75).

Applying this rationale to the 2nd derivative of the LHCII absorption spectrum, it would be predicted that the estimated width of the 510 nm band would be 2-3 times larger for lutein 2. An estimation of the band widths from the 2nd derivative of the absorption spectrum of the trimeric preparation presented in Figure 4 (red trace) showed that lutein 2 band has a width of 18 nm, lutein 1 10 nm and neoxanthin 11 nm, which is consistent with the results presented above.

In order to investigate this further, a curve fitting procedure was used. Using Gramms/32 software (Galactic Industries Corporation) absorption (1-T) spectra recorded for LHCII trimers at 77K were fitted with a mixture Gaussian and Lorentzian contours. The numbers of the peaks, each corresponding to the absorption transition of a population of the pigments present in the samples, and their width for the fitting analysis were taken from the 2nd derivative spectrum. Twelve peaks with an average

width of 10 nm were used for the first iteration of the fitting procedure. After several iterations another 2 peaks were added in order to obtain the best fit. During the fitting, the positions of the peaks were checked not to be in disagreement with either their position in the 2nd derivative or the results reported in the literature. The results of the fitting are presented in Figure 6, where it can be seen that there is a good fit to the recorded spectrum. The xanthophyll peaks are depicted in blue, dark-green and dark-yellow for neoxanthin, lut1 and lut2, respectively. Because the peaks have different widths a comparison of the amplitude is not appropriate, instead the area under each band was calculated. Calculation of the area revealed a ratio 1:1.35:0.85. From these results it can be concluded that the lut2 band is not minor, but it has an absorption area comparable to the other xanthophylls.

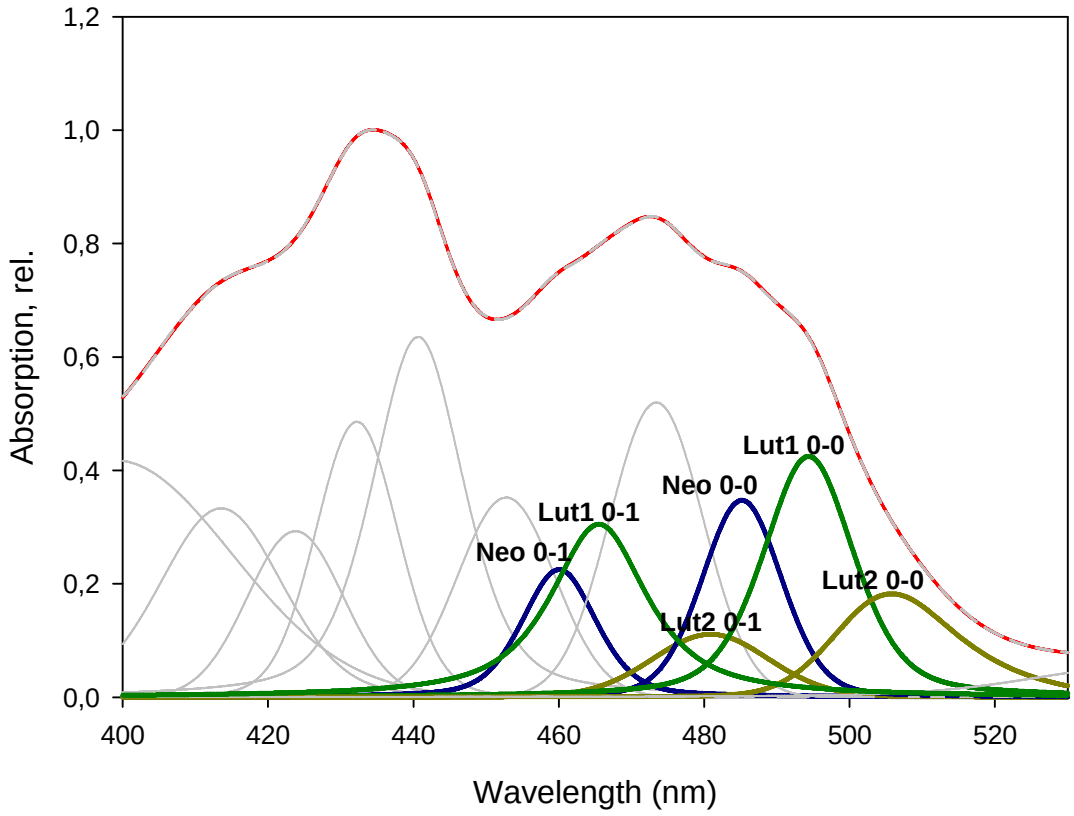

Figure 6. Curve fitting applied on the LHCII trimer 1-T spectrum. The 0-0 and 0-1 xanthophyll absorption transitions are depicted in blue for neoxanthin, dark-green for lut1 and dark-yellow for lut2. The 0-2 transitions could not be resolved by the fitting probably being part of the chlorophyll peaks.

The quantum yield of energy transfer can be estimated by comparing the absorption (1-T) with the fluorescence excitation spectrum (Gruszedski et al., 1999). The comparison was made with the 1-T (where T is transmittance) not with the absorption since the

absorbance is a logarithmic function and it can not be compared with the excitation which is a linear function. Figure 7 shows the 2nd derivatives of these spectra normalized to the chlorophyll *a* band (440 nm), making the assumption that the efficiency of the energy transfer between chlorophyll *a* molecules is 100%. The coefficient of energy transfer (k) for a given pigment can be calculated as the ratio between the amplitude of band estimated from the 2nd derivative excitation spectrum and the amplitude of the same band in the 2nd derivative of 1-T spectrum, knowing that the excitation is a convolution of 1-T with the energy transfer coefficients:

$$E_n(\lambda) = \sum_{i=1}^{n} (1 - T_i(\lambda))k_i$$

If the bands in the spectrum have different widths, then the ratio between the areas of the bands is calculated.

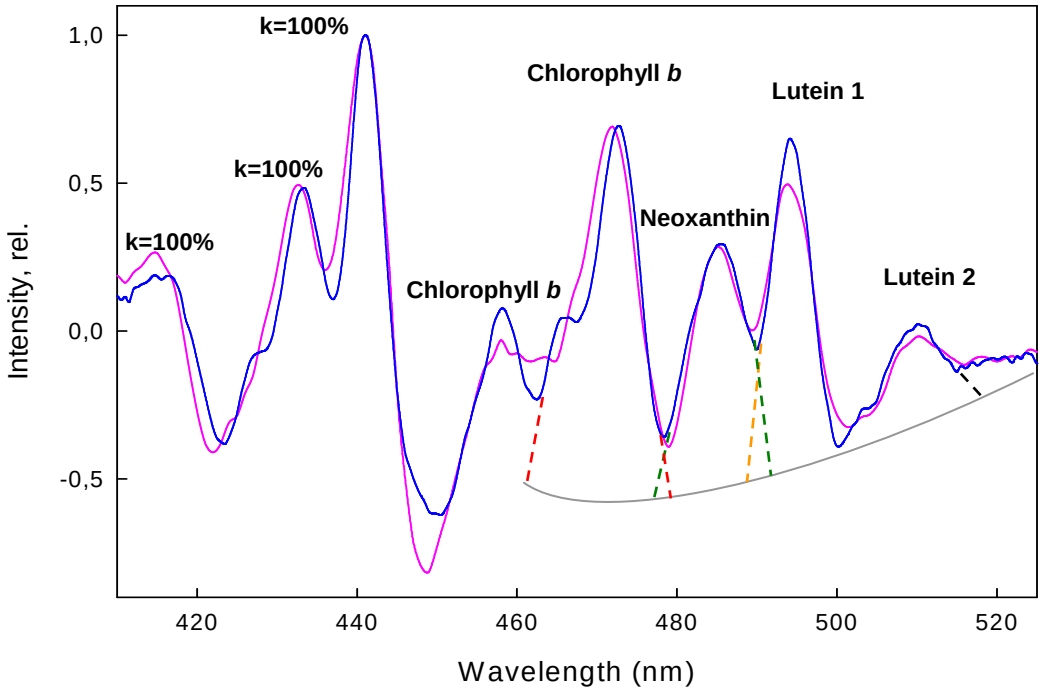

Figure 7. Inverted 2nd derivatives for 77 K fluorescence excitation (pink) and 1-T (blue) spectra of an LHCII trimer (trimers2 in Table1). For the estimation of the coefficient of energy transfer the traces were normalised to the 440 nm chlorophyll *a* band. Spectra were baseline (gray line) corrected. Dashed lines represent the limits taken for the aproximation of the areas: red for chlorophyll b band, green for neoxanthin orange for lutein 1 and black for lutein 2. The areas were estimated using (integration function) Gramms/32 software (Galactic Industries Corporation).

Table 1 presents the estimation of energy transfer efficiencies determined from 4 different preparations of LHCII trimers. The results presented were obtained by

calculation using only the 0-0 absorption band of the xanthophylls. However, in the case of the energy transfer coefficient for chlorophyll *b* band at 471 nm, there is a contribution from the lutein 2 0-1 transition at 476 nm (Ruban et al., 2000). This contribution was not taken in account in the calculation.

k (%)					
	trimers1	trimers2	trimers3	trimers4	Mean±SEM
Chl*b* (471 nm)	99	95	100	88	96 ± 2.23
Neo	85	98	81	83	85 ± 2.96
Lut1	93	86	100	92	93 ± 2.72
Lut2	85	80	89	61	79 ± 5.36

Table 1. Estimation of the coefficients of energy transfer (k) from chlorophyll *b* and xanthophylls to chlorophyll *a* for different LHCII trimeric (trimers 1-4) preparations, and the mean value and SEM. Data were obtained by measurement of the areas of appropriate bands in the second derivative spectra shown in Figure 7.

3.2.2 Analysis of xanthophylls to chlorophylls energy transfer in thylakoids.

Having established a method to measure the efficiency of energy transfer between xanthophylls and chlorophyll *a* in isolated LHCII, an attempt was made to apply the same procedure to more complex systems like thylakoid membranes. Then, it could be possible to study the properties of xanthophyll cycle carotenoids, violaxanthin and zeaxanthin. For this, unstacked thylakoids membranes (see section 2.3.2 for details) from *Arabidopsis* and spinach were isolated from both the dark-adapted state (containing only violaxanthin) and after light treatment designed to induce violaxanthin de-epoxidation (see 2.4 for details). HPLC analysis confirmed the complete absence of zeaxanthin in the dark-adapted *Arabidopsis* samples. There were trace amounts of antheraxanthin present in both preparations. In dark-adapted spinach samples the levels of these two xanthophylls (zeaxanthin and antheraxanthin) were slightly higher, but nevertheless the de-epoxidation state (DES) was still of less than 4%. In contrast, in the light treated sample a large part of the violaxanthin was converted to zeaxanthin and antheraxanthin (Figure 8, Table 2). The DES was approximately 50% and 65% in *Arabidopsis* and spinach respectively.

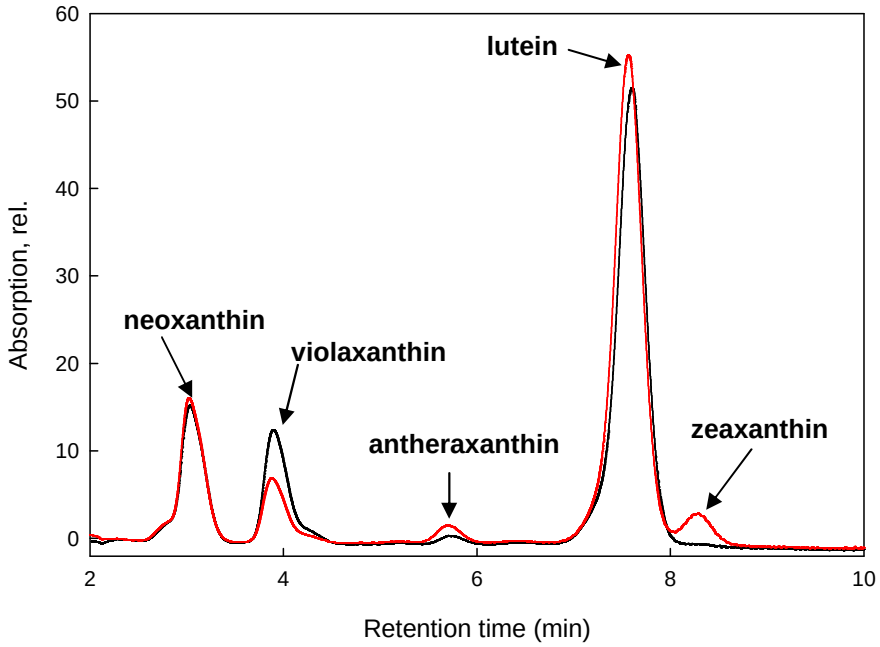

Figure 8. HPLC traces for *Arabidopsis* thylakoids before (black trace) and after light treatment (red trace). The traces show the absorption at 446 nm as a function of elution time

Pigment content (% of total pigments)										
Pigments	Lut	Anth	Zea	Neo	Vio	β-car	Chl *b*	Chl *a*	a / b	DES
Arabidopsis dark	12.36	0.07	0	4.04	2.73	8.13	17.9	54.9	3.09	1.29
Arabidopsis light	12.42	0.4	1.11	4.05	1.13	8.17	18	54.7	3.04	49.71
Spinach dark	9.33	0.37	0.15	4.36	6.74	7.16	17.8	54.08	3.04	3.65
Spinach light	9.15	0.69	3.67	4.25	1.87	7.62	17.53	55.22	3.15	64.36

Table 2. Pigment analysis of thylakoids before and after light treatment. The data represent the pigment content for the samples with the highest DES of each type of plant; 5 replicate samples were analysed for *Arabidopsis* and 3 for spinach.

Immediately after isolation the thylkoids were frozen, ready for analysis by 77K absorption and fluorescence excitation measurements, so that epoxidation of zeaxanthin back to violaxanthin was prevented. Figure 9 shows the differences between the excitation (a) and 1-T (b) spectra in the Soret region before and after de-epoxidation. It can be seen that changes occurs in this region in both excitation and 1-T spectra after de-epoxidation, but they were more pronounced in the excitation spectra (Figure 9a). This difference between excitation and 1-T spectra might indicate a change in the efficiency of the energy transfer from xanthophylls to chlorophylls in these two states.

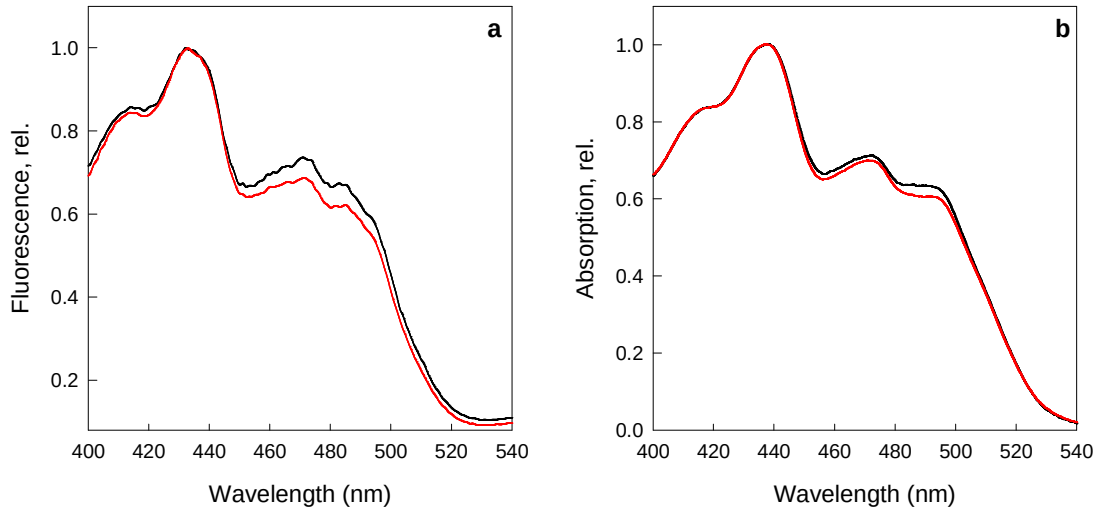

Figure 9. 77K fluorescence excitation (a) and 1-T (b) spectra of thylakoids isolated from *Arabidopsis* dark- adapted (red traces) and light-treated (black traces) leaves. No normalisation was performed since the same chlorophyll concentration was used for both excitation and absorption measurements.

Figure 10 shows the inverted second derivatives calculated for *Arabidopsis* and spinach thylakoids before and after de-epoxidation. However, accurate estimation of the amplitudes/areas of bands needed to determine the efficiency of energy transfer from xanthophylls to chlorophyll was found to be impossible. The complexity of the spectra is caused by both the abundance of the pigments present in the thylakoid membrane (much more than in isolated LHCII), and the contribution of more than one pigment to some bands (these bands overlapping with each other). It is noticeable that the 2nd derivative is less resolved for light-treated samples, particularly in the blue region between 480-520 nm, in both excitation and 1-T. This may arise from the presence of the new carotenoids antheraxanthin and zeaxanthin, formed as a result of the de-epoxidation of violaxanthin. Another interesting feature is the fact that the 2nd derivative is less resolved for the spinach thylakoids, possibly because of the higher DES present in spinach samples (see Table 2) or due to some unknown differences in the antenna composition and stoichiometries and/or different scattering artefacts (Figure 9b).

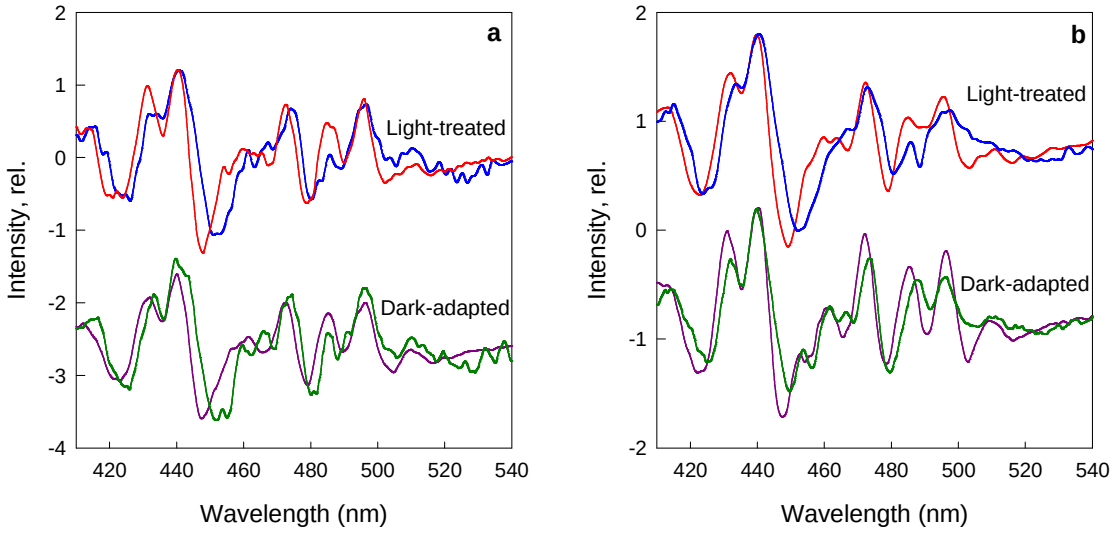

Figure 10. Inverted 2nd derivatives of the excitation and 1-T spectra for *Arabidopsis* (a) and spinach (b) thylakoids. Top: blue (1-T) and red (fluorescence excitation) for light-treated thylakoids. Bottom: dark-green (1-T) and dark-pink (fluorescence excitation) for dark-adapted thylakoids.

Since analysis of the 2nd derivatives was not possible, a different approach was attempted. The changes in the spectra shown in Figure 9 following the de-epoxidation procedure are clearly seen when a difference light-treated *minus* dark-adapted spectrum was calculated. Figure 11a shows the difference associated spectra for fluorescence excitation and 1-T for spinach thylakoids. The green trace has the features expected of a 1-T (absorption) difference spectrum zeaxanthin *minus* violaxanthin. The spectrum has three positive bands situated at around 508, 474 and 445 nm (from zeaxanthin formation) and three negative at around 488, 455 and 428 nm (from violaxanthin disappearance). This is consistent with the room temperature difference spectra light-treated *minus* dark-adapted measured on plants grown under intermittent light (Pfündel, 1993) and with the 4K difference spectrum, except that the latter revealed more fine structure, with the negative bands mentioned above showing a doublet structure (Ruban et al., 2001). The most surprising observation was that the 1-T and excitation differences do not have the same shape, as would be expected. The excitation difference (black trace) shows two pronounced minima at around 440 and 465 nm with a small gap around 500 nm. The same features were again reported by Pfündel (1993). These minima correspond to maxima in the 1-T difference spectrum. Three positive bands are present in the excitation difference at around 424, 455 and 489 nm, along with a weak one at around 508 nm and two shoulders at 474 nm and 445 nm. It is important to note that the bands corresponding to violaxanthin (489, 455 and 424 nm) are positive and not

negative as would be expected when the difference zeaxanthin *minus* violaxanthin is taken. This suggests that after de-epoxidation the remaining violaxanthin population in the light-adapted state is more involved in energy transfer than the total violaxanthin pool in the dark-adapted sample.

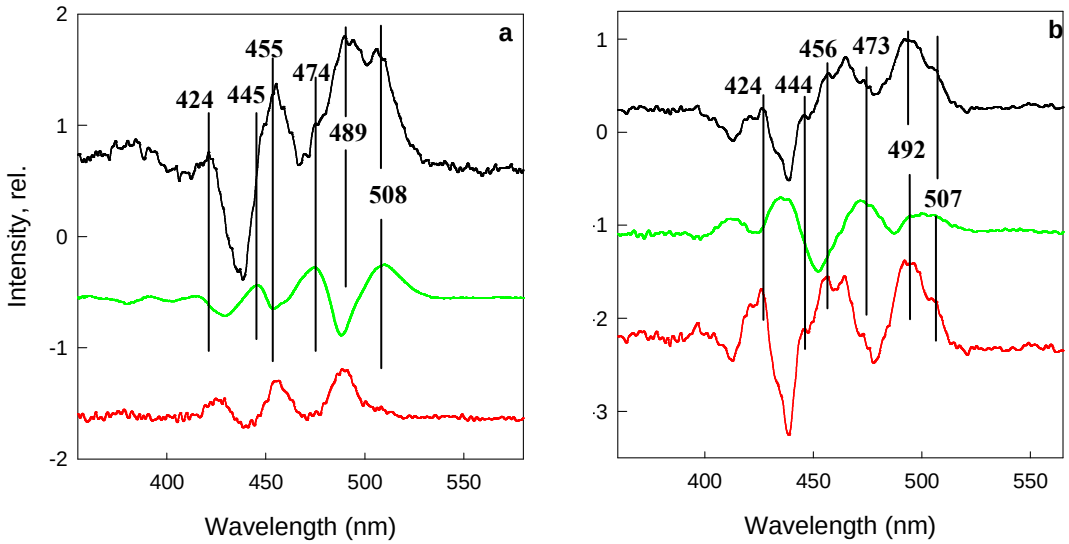

Figure 11. Difference spectra of spinach (a) and *Arabidopsis* (b) thylakoids. Fluorescence excitation light *minus* dark (black trace), 1-T light *minus* dark (green trace). Red trace is the difference black *minus* green trace.

These unexpected features were further revealed after subtracting of the green spectrum from the black one. The 'double' difference depicted in red in Figure 10a shows the features which are likely to arise from the non-de-epoxidised violaxanthin population, which becomes more active in energy transfer after the illumination. The difference between the excitation and 1-T difference can therefore be explained by the changes that occur when violaxanthin is converted to zeaxanthin; these may create a destabilising effect on the complexes or result in a change in pigment conformation that might lead to alteration in the efficiency of energy transfer from the remaining violaxanthin to chlorophyll.

Similar results were obtained when the same analysis were applied on the *Arabidopsis* thylakoids after de-epoxidation was induced (see above, Figure 11b). The excitation difference was on largely the same as for spinach, only to a lesser extent, because of the lower DES in *Arabidopsis*. Hence, the 'double' difference was not so well-resolved, with shoulders at around 507, 473 and 424 nm, but it similarly resembled the non-de-epoxidised violaxanthin pool as in spinach.

3.2.3 Investigation of spectral properties and energy transfer in plants lacking LHCII

Low temperature absorption and fluorescence steady-state spectroscopy were further used to analyse *lhcb2* antisense *Arabidopsis* (*asLhcb2*) plants. These plants were constructed by introducing a region of the *lhcb2.1* gene into the plant genome in the antisense orientation, resulting in the absence not only of the Lhcb2 but also of the Lhcb1 polypeptides (Andersson et al., 2003). Western blot analysis of PSII membrane preparation from wild-type (wt) and *asLhcb2* plants showed that Lhcb1 is completely absent and the amount of Lhcb2 is less than 5% of that found in wild type (Ruban et al., 2003). Remarkably, it has been found that in the absence of the major LHCII polypeptides, new types of trimers are formed from greatly increased amounts of Lhcb5, this polypeptide being found only in the monomeric minor CP26 complex in wild type plants (Ruban et al., 2003). Biochemical analysis has subsequently shown the presence of 2 new types of trimers in the antisence plants, one homotrimer of Lhcb5 and one heterotrimer of Lhcb5 and Lhcb3 (Ruban et al., 2006). The proportion of these trimers was calculated to be 65% homotrimers and 35% heterotrimers, homotrimers being less stable than the heterotrimers (Ruban et al., 2006).

An important question is whether the efficiency of energy transfer was different in these new types of light-harvesting trimers. To investigate this, thylakoid membranes were isolated from *asLhcb2* and wt *Arabidopsis* plants and absorption spectra were recorded at 77K (Figure 12a).

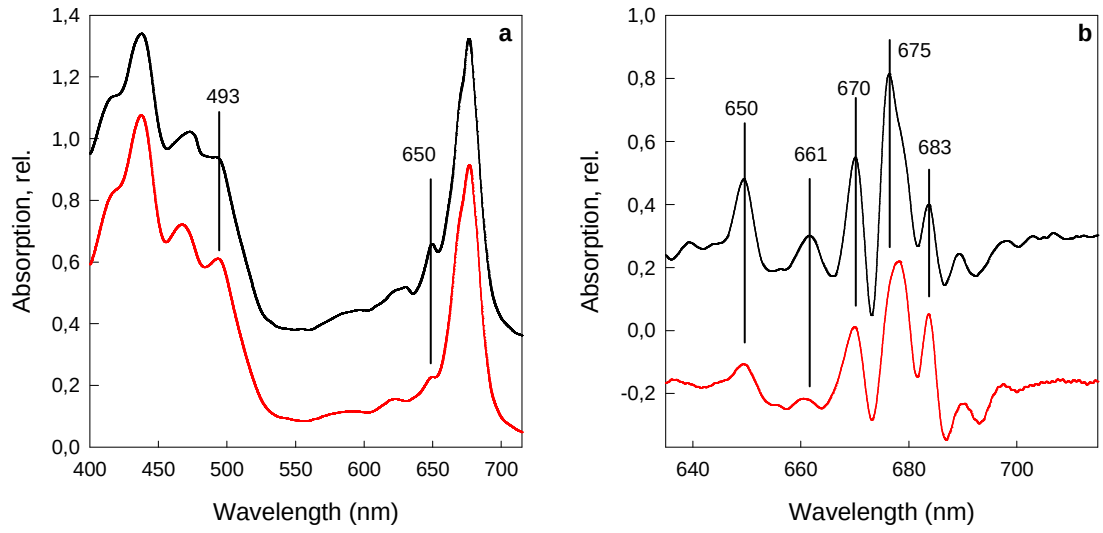

Figure 12. 77K absorption spectra (a) and the inverted 2nd derivatives in the red region (b) of the thylakoids from wt (black) and *asLhcb2* (red) plants. Normalisation was made at 700 nm.

In the Soret region, the spectra are very similar, with a slight increase in the carotenoid band at around 493 nm in the antisense thylakoids. This might be caused by the difference in the carotenoid content, which was found to be higher in the antisense plants thylakoids (Ruban et al., 2006). In the red chlorophyll region, the major change in the spectra was in the chlorophyll *b* band at 650 nm. In order to resolve the complex structure present in the absorption spectra, 2nd derivatives of the spectra were calculated (Figure 12b). The 2nd derivative spectrum of the antisense thylakoids clearly showed the reduction in the absorption of the chlorophyll *b*, along with the decrease in the chlorophyll *a* bands at 661 nm and 670 nm. The drop in absorption in the chlorophyll *b* was caused by the absence of the major LHCII, which was reported to have a well defined absorption at around 650 nm caused by the extra chlorophyll *b* present in the complexes (Bassi, 1996). Another feature revealed in the 2nd derivatives was that the major band at 675 nm in the wild type was shifted (by about 3 nm) in the antisense thylakoids. There was also an increase in the relative absorption of the band at around 683 nm, which can be explained by the 50% increase in the expression of PSII core proteins (Andersson et al., 2003), CP43 having an absorption transition in this region (de Weerd et al., 2002).

Figure 13 shows the 77K fluorescence emission spectra of wt (black) and *asLhcb2* (red) thylakoids and the calculated difference *wt* minus *asLhcb2* (blue). There was a small difference in the PSI fluorescence emission, whereas major changes appeared in the PSII fluorescence region (670-700 nm) caused mainly by the absence of the major LHCII. The reduced amount of the LHCII polypeptides reduces the energy transferred to the reaction centre of PSII and consequently the intensity of PSII fluorescence emission is decreased. Hence, the wild type *minus* asLhcb2 difference spectrum had a maximum at 685 nm and shoulders at around 693 and 699 nm, features that have been attributed to LHCII (Ruban & Horton, 1992).

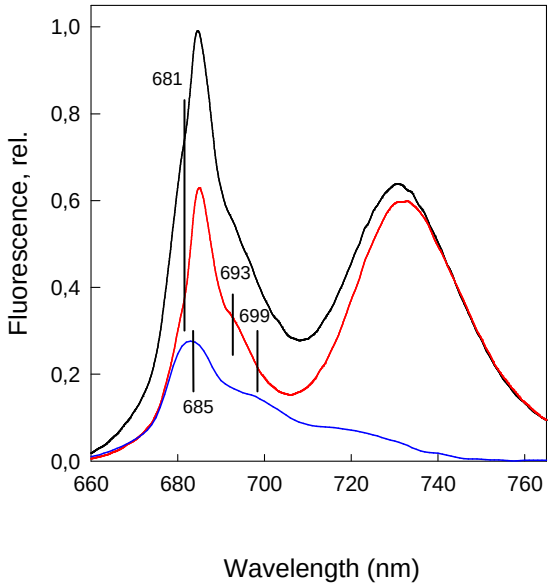

Figure 13. 77K fluorescence emission spectra of wt (black), *asLhcb2* (red) thylakoids and the difference *wt* minus *asLhcb2* (blue). The spectra were normalised at 750 nm.

Using a combination of isoelectric focusing (IEF) and chromatographic techniques (FPLC) the trimers from *asLhcb2* thylakoids were purified (this was kindly carried out by Sveta Solovieva). The isolated trimers were then analysed by low temperature absorption spectroscopy. Figure 14 presents the red region of the absorption spectrum of trimers (a) and monomers (b) isolated from wt and *asLhcb2* plants. As seen in the absorption spectra of the thylakoids, the 650 nm region where chlorophyll *b* absorbs is less pronounced in the antisense timers. Estimation of the area of the 650 nm band (from the 2nd derivative) gave a ratio of 1:0.87:0.53 for wt trimers, Lhcb5/Lhcb3 trimers and Lhcb5 trimers. This is consistent with the trimers being formed by either 3 Lhcb5 monomers or by 2 Lhcb5 and one Lhcb3 (Ruban et al., 2006). It is known that the wt monomer binds 6 chlorophyll *b* molecules (Liu et al., 2004), Lhcb5 only 3 (Bassi, 1996) and Lhcb3 monomer 6 (Caffarri et al., 2004). Hence, a wt trimer will bind 18 chlorophyll *b*, a trimer built from 2 Lhcb5 and one Lhcb3 15 chlorophyll *b*, and an Lhcb5 trimer 9 chlorophyll *b* giving a 1:0.83:0.5 ratio, similar to the ratio obtained from the area calculation.

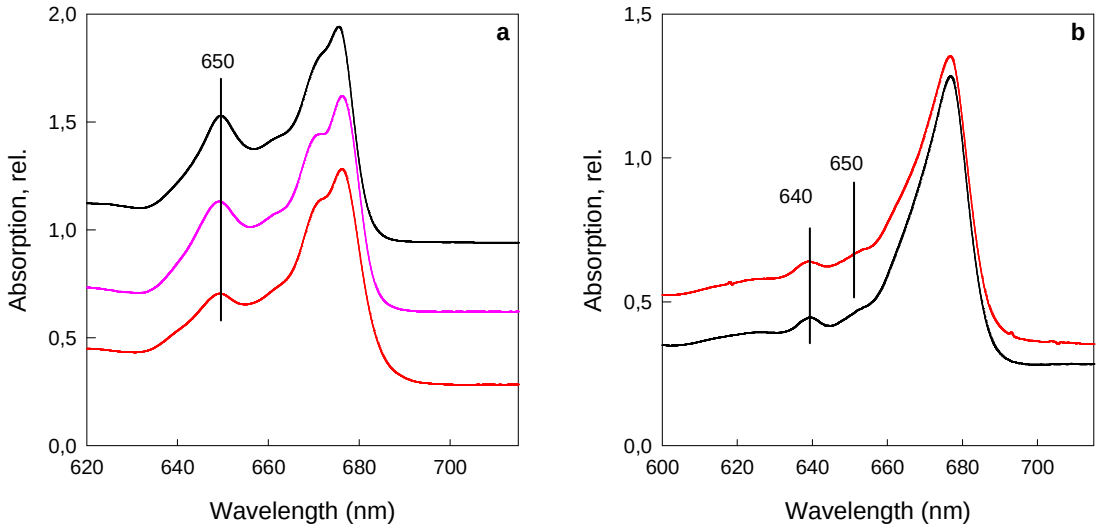

Figure 14. 77K absorption spectra of trimers and monomers: (a) red region for trimers from wt (black) and from *asLhcb2* plants; Lhcb5/Lhcb3 are shown in pink and Lhcb5 in red. (b) red region for wt (black) and antisense Lhcb5 monomers (red).

In contrast with that of the trimers, in the spectrum of Lhcb5 monomers from the wt and antisense plants the 650 nm band is practically missing, and there is an increase in the band around 640 nm arising from absorption by another chlorophyll *b* population. The difference between the monomer Lhcb5 (red trace, Figure 14b) and trimer Lhcb5 (red trace, Figure 14a) consists of an enhancement of the band absorbing at 650 nm, which suggests the presence of the extra chlorophyll *b*, present only when the monomers are organised in trimeric structures (Bassi, 1996).

The Soret region of the spectrum of Lhcb5 trimer (red trace, Figure 15a) resembles that of the wt trimers (black trace, Figure 15a), but there were minor differences around 486 and 495 nm regions that indicated a change in the absorption of neoxanthin and lutein 1, which have absorption transitions at these wavelengths (Ruban et al., 2000). Indeed, the 2nd derivative spectra revealed a small drop in the neoxanthin band (486 nm), with a slight increase in the lutein 1 band (495 nm) for the antisense Lhcb5 trimers (red trace, Figure 15b). The lutein 2 band at 510 nm, which was thought to be characteristic for the major trimeric LHCII (Ruban et al., 2000) was seen in the spectra of these trimers (and was also found in the thylakoids spectra). The 510 nm band was not present on the spectrum of the Lhcb5 monomers, only a broad 495 nm band being present (blue trace, Figure 15b). It is suggested that this lutein might be involved in the stability of the trimer, trimerisation changing the conformation of the lutein, resulting in a red

absorption, shifted in comparison to the lut1. A similar conclusion was reached from the analysis of the lut2 band in LHCII (see section 3.2.1 above). Studies of both the native wild type CP26 complex and one reconstituted from Lhcb5 polypeptide have suggested that violaxanthin or neoxanthin bind to the L2 site (Croce at al., 2002), which is inconsistent with the evidence presented here that lutein is bound at this site.

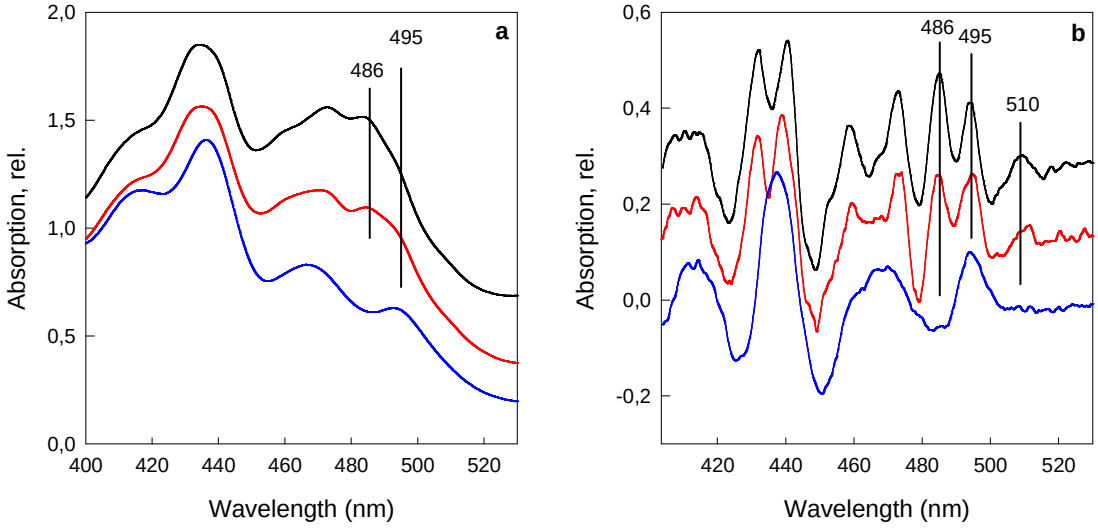

Figure 15. 77K absorption spectra in the Soret region. (a) wt trimers (black), antisense Lhcb5 trimers (red) and Lhcb5 monomers (blue). (b) Associated inverted 2nd derivatives for the spectra presented in (a).

In order to investigate the energy transfer in the antisense plants the PSII fluorescence excitation spectra (emission was set at 685 nm) of the thylakoid membranes were recorded and compared to the 1-T spectrum.

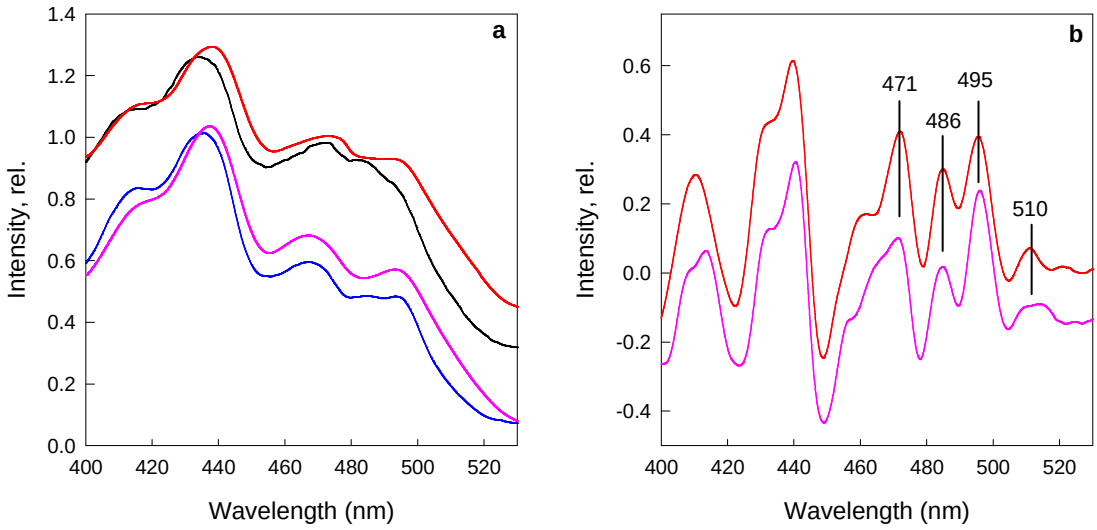

Figure 16. 77K fluorescence excitation and 1-T spectra. (a) wt thylakoids, excitation measured at 685 nm (black) and 1-T spectra (red); *asLhcb2* thylakoids, excitation measured at 685 nm (pink) and 1-T (blue). (b) the inverted 2nd derivatives of the excitation spectra wt thylakoids (red) and *aLhcb2* thylakoids (pink).

Figure 16 shows this comparison between the fluorescence excitation spectra and 1-T for thylakoids from wt (red and black traces) and *asLhcb2* (pink and blue traces) plants. It can be seen that the excitation spectra for the antisense thylakoids followed closely the 1-T spectra, even better than for wt thylakoids. Thus, it can be concluded that there was no major alteration in the energy transfer from the antenna pigments of the *asLhcb2* plants to the PSII reaction centre. Second derivatives calculated for the excitation spectra depicted a slightly increased contribution of xanthophylls neoxanthin (485 nm) and lut1 (495 nm) in *asLhcb2* (pink trace, Figure 15b) as compared to the wt thylakoids (red trace, Figure 16b). The chlorophyll *b* profile at around 471 nm was slightly reduced and no detectable differences were seen in the chlorophyll *a* bands (439 and 410 nm). The 510 nm band was also found in the excitation spectrum suggesting an efficient involvement of lutein 2 in energy transfer. Energy transfer from lutein 2 appears to be more efficient in the antisense plants judging from the relative areas under 510 nm band which showed a 20% increase in *asLhcb2* compared to the wt thylakoids.

3.3 Discussion

In the first part of the chapter the spectral features of LHCII-bound xanthophylls were investigated. There has been considerable debate about the origin the 510 nm band, which appears as a low amplitude band in the absorption (1-T) spectrum of LHCII trimers. This band was originally assigned to the LHCII bound xanthophyll violaxanthin, because the amount of violaxanthin was significantly reduced compared to that of the other xanthophylls in trimeric preparations (Peterman et al., 1997), but it has been demonstrated (Ruban et al., 2000) and confirmed (Caffari et al., 2001) that the band can be assigned to one of the two luteins. The different absorption spectrum of these luteins can be explained by the fact that one of them undergoes a conformational change (twisting) during the trimerization process (Ruban et al., 2001). Indeed close examination of the crystal structure of the LHCII trimer reveals the different configurations of lutein 1 and lutein 2 (Yan et al., 2007).

Analysis of the absorption spectrum of LHCII trimers first involved calculation of the 2nd derivative, which showed the presence of the lutein 1, lutein 2 and neoxanthin bands. The amplitudes of these bands were different. Calculation of the second derivative of a Gaussian contour showed that the amplitude in the second derivative is inversely proportional to the width, meaning that the amplitude of the second derivative

is smaller for broader bands. Thus, the second derivative analysis showed that although the lutein 2 band was small in the second derivative, it is also broad (the width was almost twice that of lutein 1 and neoxanthin) suggesting that the area under this band could be approximately the same as for lutein 1 and neoxanthin. By fitting the absorption spectrum with Gaussian and Lorentzian contours having the width (FWHM) and position obtained from the second derivative spectra to the absorption spectrum, it was indeed proven that the areas of the absorption bands of lutein 1, lutein 2 and neoxanthin were almost identical.

With this information about the absorption spectrum it was then possible to determine the efficiency of energy transfer from each xanthophyll to chlorophyll *a*. Second derivatives of the fluorescence excitation spectrum and the 1-T spectrum were compared. It was found that all three xanthophylls transferred energy with high efficiency, around 80-90 %. These estimated efficiencies of the energy transfer were higher than those found by Gruszedski et al. (1999) studying monolayers of light harvesting complexes from *Secale cereale* (rye), where they found 97% efficiency for chlorophyll *b*, 85% for neoxanthin, but only 62% for lutein 1 and 54% for violaxanthin/lutein 2, assuming then that the band at 510 nm band came from violaxanthin. However, the high overall efficiencies of xanthophyll energy transfer to chlorophyll are in good agreement with those found by Connelly et al. (1997) using time-resolved femtosecond transient absorption measurements and with those published by Holt et al. (2003) from measurements of fluorescence upconversion. It should be noted that these latter results were obtained at room temperature where it is possible that the energy transfer may be more favourable than at 77 K.

The same methodology was applied to thylakoid membranes. However, the complexity of the spectrum prevented similar quantification of the bands from individual xanthophylls in the second derivative. Instead other analytical approaches were used, which were found to be useful in understanding the changes that occurs during the de-epoxidation of the antenna complexes. Here, very interesting results were obtained by comparing the de-epoxidation dependent difference excitation and 1-T spectra. Whereas the 1-T spectrum displayed the typical zeaxanthin-*minus*-violaxanthin features, the excitation spectra had several additional bands. These bands probably arose from violaxanthin, suggesting that the pool of this xanthophyll which was not de-epoxidised transferred energy to the PSII core complexes more efficiently. This

population of violaxanthin active in transferring energy may be one which was tightly bound to the minor antenna complex CP29, and therefore not readily de-epoxidised (Ruban et al., 1994; Ruban et al., 1999).

Studies of the antisense plants *asLhcb2* have showed the plasticity of the light-harvesting antenna, where, even when the major LHCII polypeptides are missing the minor complexes tend to organize in trimeric structures. The new population of trimers in these plants has specific features which were thought to belong only to native major LHCII: the red shifted 510 nm band of lutein 2 and an extra chlorophyll *b*. Therefore, it can be proposed that there is a similar environment in these Lhcb5-containing trimers as in the major LHCII trimer. Recently, from the crystal structure of LHCII from cucumber at 2.66 Å, it was found that the lutein 2 molecule shows a left-handed twist along the polyene chain from the lumenal side to the stromal side as compared to lutein 1 (Yan et al., 2007). The end ring of lutein 2 is situated in a cavity formed by the chlorine ring and phytyl tail of chl *a*602 in vicinity of the indole ring of Trp46 and chl *a*603 from the adjacent monomer. These exert steric constraints, which may twist the lutein molecule upon trimerisation (Yan et al., 2007). Previously, the results from resonance Raman spectroscopy indicated the presence of one distorted lutein molecule in trimeric LHCII (Ruban et al., 2001). This was suggested to be lutein 2, since lutein 1 in the crystal structure is located at the periphery of the complex and therefore unlikely to be affected by trimerisation.

3.4 Conclusions

The red-shifted 510 nm band is not a minor component of the absorption spectrum of LHCII trimers isolated from *Arabidopsis* plants, but it arises from lutein 2, its charactertistics being consistent with a xanthophyll composition of equal amounts of lutein 1, lutein 2 and neoxanthin. Lutein 2 is involved in energy transfer to chlorophyll *a* with a ~79% efficiency. The red shifted lutein 2 is found in the Lhcb5-containing trimers from *asLhcb2* plants, which lack the Lhcb1 and Lhcb2 polypeptides of the major LHCII, supporting the hypothesis that it arises from specific events resulting from trimerisation. Studies of the thylakoids isolated from spinach leaves, before and after de-epoxidation suggest a conformational change in the PSII antenna which leads to an involvement of the remaining violaxanthin in energy transfer to the PSII core complexes.

CHAPTER FOUR

Investigation of quenching in LHCII incorporated into a gel matrix

4.1 Introduction

Light harvesting in plants is a controlled process, well-integrated into the light phase of photosynthesis. Along with the collection of light energy essential for photosynthetic processes, the light-harvesting complexes of photosystem II (LHCII) carry out a vital photoprotective function. Under conditions of excess illumination LHCII undergoes a transition into an inefficient, photoprotective mode, in order to dissipate the potentially harmful excess absorbed light energy (Ruban & Horton, 1995; Horton et al., 1996; Pascal et al., 2005). The excess absorbed energy is thereby efficiently dissipated as heat. This process has been quantified by chlorophyll fluorescence measurements in the form of a calculation of the non-photochemical quenching component, NPQ (Muller et al., 2001). The quenching state is a response to the acidification of the thylakoid lumen, which signals saturation in the light energy conversion capacity of the photosynthetic membrane (Horton et al., 1991; Horton & Ruban, 1992).

The mechanism of NPQ has not yet been determined, although several hypotheses have been put forward (Holt et al., 2005; Standfuss et al., 2005; Horton et al., 2005). Spectroscopic and structural analysis (Pascal et al., 2005; Yan et al., 2007) has suggested that NPQ involves changes in configuration of certain pigments, resulting from a protein conformational change. A wide range of evidence has indicated that one or more proteins of the PSII light-harvesting antenna are involved. Early experiments on the major antenna trimeric complex, LHCII, suggested that a dissipative, low fluorescent state strongly resembling the *in vivo* NPQ state, could be achieved by means of exposure of isolated complexes to a low-detergent medium (Ruban et al., 1997; Ruban et al., 1999). These conditions induced gradual and pronounced aggregation of LHCII (Ruban & Horton, 1992). However, it has been argued that this aggregation process causes atypical interactions between exposed pigments on LHCII trimers, resulting in artefactual chlorophyll fluorescence quenching (Standfuss et al., 2005). Alternatively, it has also been suggested that the quenching originates from a small population of (unusual) complexes in the preparation, which are always in the quenched state, connectivity brought by aggregation being the only factor which triggers fluorescence quenching (Barzda et al., 2001). Recently, the finding that LHCII crystals for which the structure has been published at 2.72Å (Liu et al., 2004) have significantly reduced chlorophyll fluorescence lifetimes allowed detailed proposals for the location of the quenching pigment species and provided evidence for conformational change in individual LHCII subunits, by comparison of solubilised and crystallised LHCII.

However, although artefactual pigment interactions between neighbouring complexes in the crystals was ruled out, the possibility of non-physiological protein-protein interactions giving rise to the changes in pigment configuration and resultant quenching can not be discounted. Furthermore, crystals are clearly not suitable for many of the experimental approaches that are needed to unravel the NPQ mechanism: crystals can not be prepared quickly or reliably in large amounts or under a range of conditions. Also, such a condensed system as a crystal is not suitable for many spectroscopic analyses and the dynamics and regulation of the any conformational change can not be easily studied in these systems. Hence, there is an urgent need to develop a new approach to study the quenching mechanism in LHCII, which excludes protein-protein interactions and yet is amenable to a range of spectroscopic analyses.

4.2 Results

LHCII incorporated into polyacrylamide or gelatine gels were analysed based upon the proposition that a dilute solution of protein (OD of the samples was ~0.1, which corresponds to a concentration of ~1 μg chl/ml) in detergent would thereby be immobilised, and could not form aggregates. LHCII trimers were diluted in a solution containing 20mM HEPES buffer at pH 7.8, and 0.03% *n*-dodecyl *β*-D-maltoside. The sample was mixed with a solution of Acrylamide/Bisacrylamide (37.1:1 ratio), then polymerised with 0.05% APS (ammonium persulphate) and 0.03% TEMED for approximately 20 minutes using a BIORAD^{TM} mini-protein system, with a 1mm gel thickness. Trials were made with different gel concentration in order to find the most suitable environment for the protein, since there may be harmful effects from the polyacrylamide itself and from local heating during the polymerization. Upon increasing the concentration of the polyacrylamide a drop in absorption in the blue region at around 472 and 486 nm was observed (Figure 1). Also, a decrease in the red region of the spectrum occurred at around 675 nm. All of these suggested that chlorophylls and carotenoids were affected by the polyacrylamide gel. Alternative explanations may be that the higher concentration of the gel had a disturbing, destabilizing effect on the protein or that scattering effects lead to the distortion of the spectrum. Finally, a 6% concentration was chosen for the investigation, because no effect was seen in the absorption spectrum of the LHCII-gel (red trace), the spectrum being very similar to that of the solubilised LHCII (black trace).

Gelatine gels were also used for some measurements. Gelatine with a 6.6% final concentration was dissolved in the same buffer as for the polyacrylamide gels by heating up to 50-60^{0}C. When the temperature fell back to 25-30^{0}C the LHCII trimers and 0.03% β-DM were added and left it for approximately 30 minutes at 4^{0}C until the gel was set. However, the gelatine gels were not stable and manipulation of the gels was difficult to do at room temperature without damaging the sample. Therefore, all subsequent experiments were carried out only on the polyacrylamide gels.

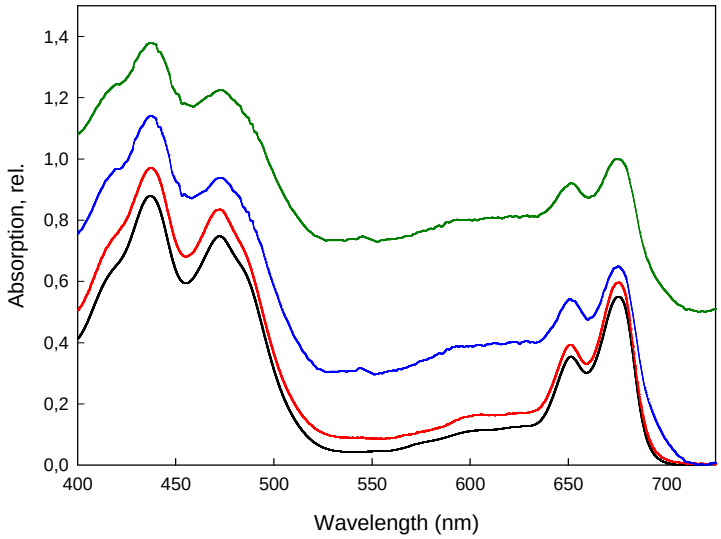

Figure 1. Absorption spectra of LHCII trimers in gel containing 15% polyacrylamide (dark-green), 10% (blue), 6% (red) and in solution (black) for comparison.

Strips of set 6% polyacrylamide gels (1 by 1.2 cm) were used to investigate the properties and dynamics of the new system. LHCII-gels were highly fluorescent, but after 6 hours of incubation in detergent-free buffer the fluorescence level of the sample was decreased about 10 times (Figure 2).

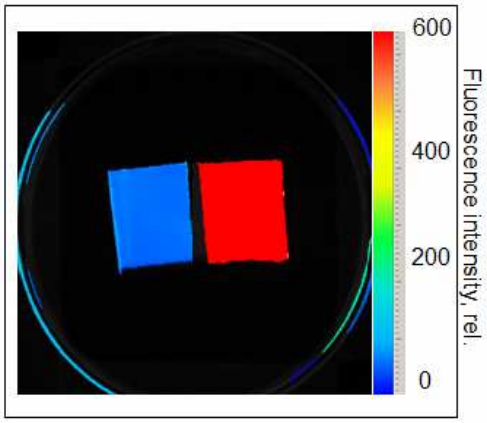

Figure 2. FluorCam image of LHCII-gel before (right) and after 6 hours incubation in detergent-free buffer (left). The fluorescence intensity is colour-coded from blue (low values) to red (high values).

The fluorescence level of the control LHCII-gel, incubated in detergent, was stable for several hours, showing only a ~10% decline (black trace, Figure 3). For the LHCII-gel in detergent-free buffer, quenching developed rapidly after an initial lag period, reaching a maximum level in approximately 1 hour with a half time of quenching of ~40 minutes (red trace, Figure 3). Most importantly, the quenching was almost completely reversed when the quenched LHCII-gel was immersed in buffer containing detergent (red trace, Figure 3). The increase in fluorescence was completed in about 2 hours, with a half time of approximately 45 minutes.

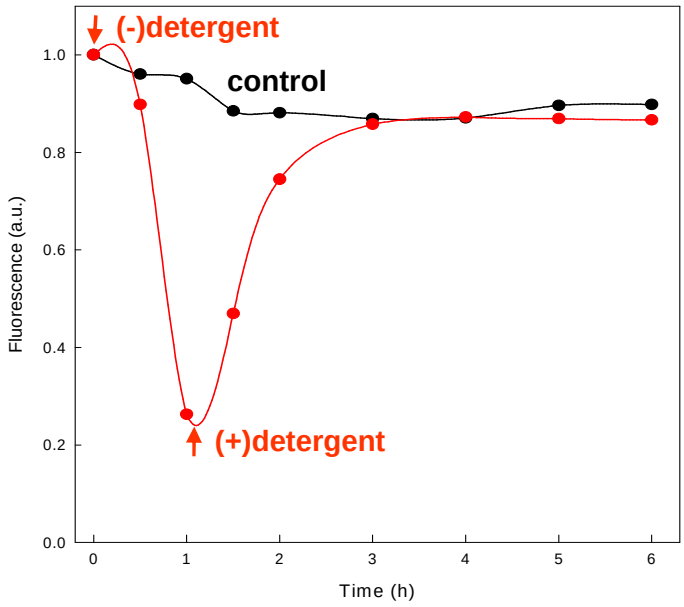

Figure 3. Quenching and recovery of LHCII-gels. Control LHCII-gel in buffer with 0.03% β-DM detergent (black); 1 hour incubation in detergent-free buffer (↓), followed by recovery in detergent buffer (↑) (red). Fluorescence was measured with a Waltz PAM1000 fluorimeter.

It should be pointed out that the extent of quenching observed in the LHCII-gel was very large. This drop in the fluorescence (~90%) had previously been associated with the formation of very large LHCII aggregates (Mullet & Arntzen, 1980; Ruban & Horton, 1992) and it is highly unlikely that such aggregates could be formed when the complexes are immobilized in the pores of the gel.

In order to obtain direct evidence of the state of aggregation of the low-fluorescent sample, LHCII-gels were placed on a polyacrylamide gel electrophoresis system in the stacking gel area and run for approximately 60 minutes. The stacking gel was composed of 0.375 M Tris pH 7.8, 0.05% APS, 0.03% TEMED, and 4% polyacryamide. The running gel had the same composition except that the

polyacrylamide concentration was 6%. The gels were run at 100V for 1 hour in a reservoir buffer containing 0.375M Tris, 0.15 mM glycine and 0.005% deriphat detergent at pH 7.8. Figure 4 displays the results of electrophoresis of LHCII-gels in 3 different quenching states (qtr1, qtr2, qtr3) at the beginning of the experiment, at an intermediate step after 30 minutes incubation and after 60 minutes of incubation. Also shown are LHCII aggregates (a), timers (tr) and monomers (m) set in the gel.

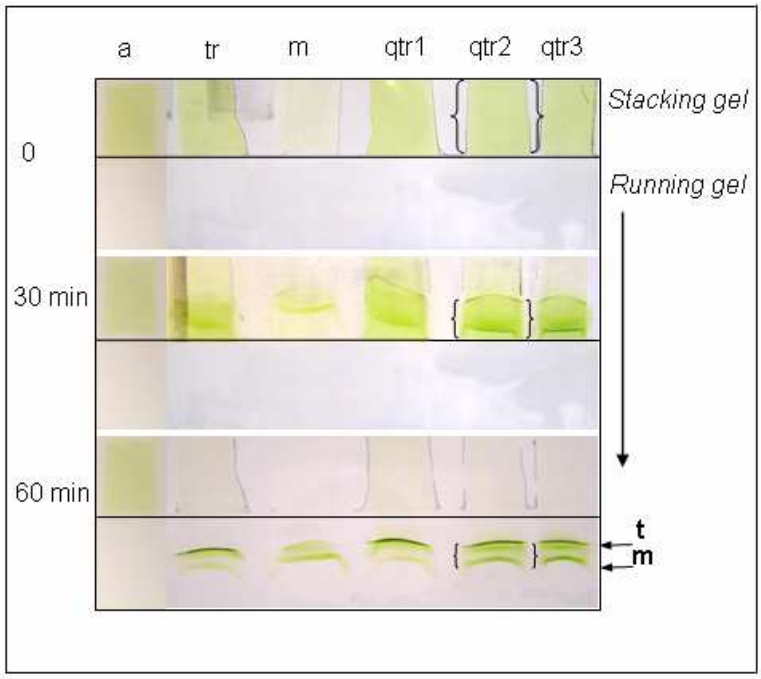

Figure 4. Non-denaturating gel electrophoresis of the LHCII-gel: a=aggregates in gel; tr=unquenched LHCII-gel (trimers); m=unquenched LHCII-gel (monomers); qtr1=quenched LHCII-gel with k_d=0.2 (~17% fluorescence decrease); qtr2=quenched LHCII-gel with k_d=2 (~67% decrease); qtr3=quenched LHCII-gel with k_d=9 (~90% decrease). Vertical arrow represents the direction of the migration.

Quenched LHCII-gels were obtained by incubation in detergent-free buffer allowing a slow diffusion of the detergent from the gel, until reaching the k_d stated in the legend of Figure 4. Aggregates of LHCII were obtained by incubation of the trimers with 50mg of SM-2 Absorbent (Bio-Rad) allowing a 10-times decrease in the fluorescence intensity (~90% decrease), before setting into the gel. Fluorescence quenching was described as k_d (quenching strength), which is numerically equivalent to the *in vivo* NPQ parameter, and calculated using the equation following:

$$k_d = \frac{F_{unquenched} - F_{quenched}}{F_{quenched}},$$

where $F_{unquenched}$ is the fluorescence intensity at time 0 in isolated LHCII trimers or in the LHCII-gel after polymerisation, and $F_{quenched}$ is the fluorescence intensity at different

times after induction of quenching. It is clear that for all LHCII-gels, the complex moved out of the gel into the running gel area. In contrast, LHCII aggregates remained in the stacking gel area.

The complex that moved in the gel appeared as a mixture of LHCII monomers (m) and trimers (t), as can be seen from the positions of the complexes that were run separately (Figure 4). The quenching conditions appear to have had a slight destabilising effect on the trimer, which can be seen from the relative increase in the ratio of monomer to trimer bands in the more highly quenched LHCII-gels (qtr2 and qtr3) compared to the mostly unquenched LHCII-gel (qtr1) and the unquenched LHCII-gel (tr). The fact that the quenched LHCII was present in the running gel in the trimeric/monomeric state not in a higher oligomeric state, suggests that there was no aggregation involved in the establishment of the quenched state in the gel. Rather, it points towards a conformational transition within individual LHCII trimers.

To understand the changes in pigment properties, which accompany the formation of the quenched state of LHCII, room temperature absorption spectra of unquenched LHCII-gel (black trace), quenched LHCII-gel (red) and recovered LHCII-gel (blue) were measured and analysed (Figure 5).

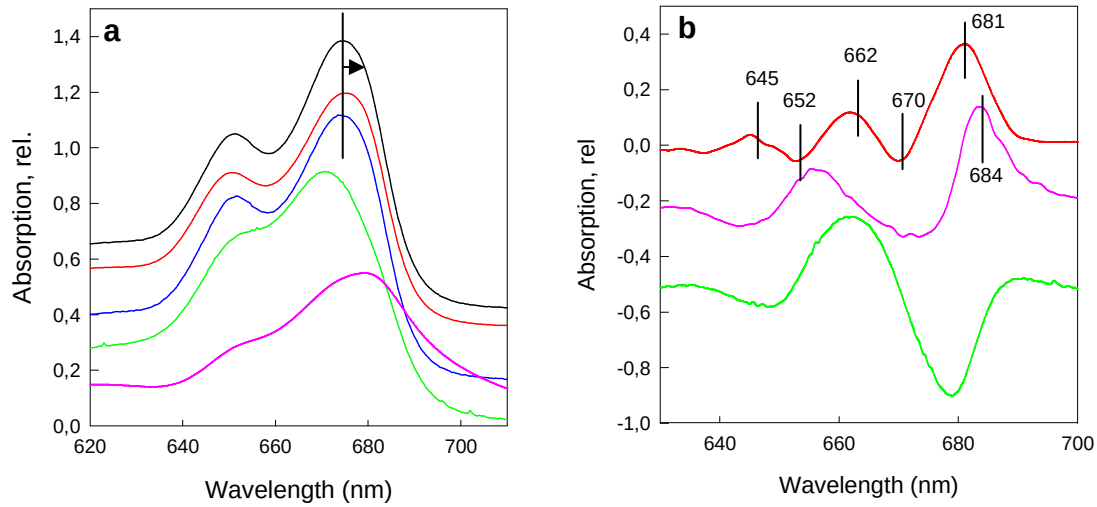

Figure 5. Absorption spectra of LHCII-gels. (a) Room temperature absorption spectra in the Qy region: unquenched LHCII-gel (black); quenched LHCII-gel (red); recovered LHCII-gel (blue). Also shown the spectra of LHCII aggregates (pink) and of the heat-treated trimers (green). Spectra were normalised to the maximum and are presented offset for clarity. (b) Difference absorption spectra: quenched LHCII-gel *minus* recovered LHCII-gel (red), aggregates *minus* trimers (pink), heat-treated *minus* trimers (green). Normalisation was performed at 620 nm before difference was taken.

The absorption spectrum of the quenched LHCII-gel was slightly red shifted in the chlorophyll Qy region around 680 nm (shown by the arrow) compared to the

unquenched LHCII-gel. This shift was reversed in the gel in which quenching had also been reversed (blue trace). In contrast, a strong blue shift of the Qy region of the spectrum was seen in a heat-treated sample (green trace, Figure 5a). The heat-treated sample was obtained by heating LHCII trimers (in solution) above 60^0C, when unfolding of the helical secondary structure of the protein upon denaturation occurs (Wentworth et al., 2003 Hence, the pigment changes associated with the transition to the quenching mode were different from those that occurred during the complex denaturation. This can clearly be observed in the difference spectra, quenched LHCII-gel *minus* recovered LHCII-gel (red), compared to heat-treated *minus* control trimers (green) (Figure 5b). A spectrum of aggregated LHCII was measured and the difference spectrum aggregates *minus* trimeric LHCII was also calculated (pink trace). This latter difference spectrum was similar to the quenching-associated difference spectrum calculated for LHCII-gels (red trace). The distinct feature of both difference spectra was the appearance of a positive band in the chlorophyll *a* region at 681nm for quenched LHCII-gel, with a 3 nm red shift to 684 nm for the aggregates. In contrast, the heat-treated *minus* trimers spectrum is completely different, displaying only 2 bands in the chlorophyll *a* region at around 680 nm (negative) and 662 nm (positive). The difference spectrum indicated that the absorption changes associated with the quenching in the gel (red trace, Figure 5b) were more pronounced in chlorophyll *a* regions at 681 nm, 662 nm (positive) and 670 nm (negative), than in chlorophyll *b* regions, 645 nm (positive) and 652 nm (negative).

The spectrum of the aggregates exhibited a pronounced 'tail' in the Qy region above 700 nm as a result of light scattering, a typical feature of the room temperature absorption spectra of highly scattered aggregates (pink trace, Figure 5a; dark-yellow & pink trace, Figure 6). In contrast, the absorption spectrum of the quenched LHCII-gel (red trace, Figure 6) has a very small 'tail', consistent with the absence of aggregation, or, if aggregation had occured, the aggregates formed were very small (such an association of few trimers). Therefore, the quenching in the gel can not be caused only by aggregation: although the same drop in fluorescence was achieved in the gels as in large aggregates, the gel spectrum did not display the red 'tail' indicative of aggregate formation.

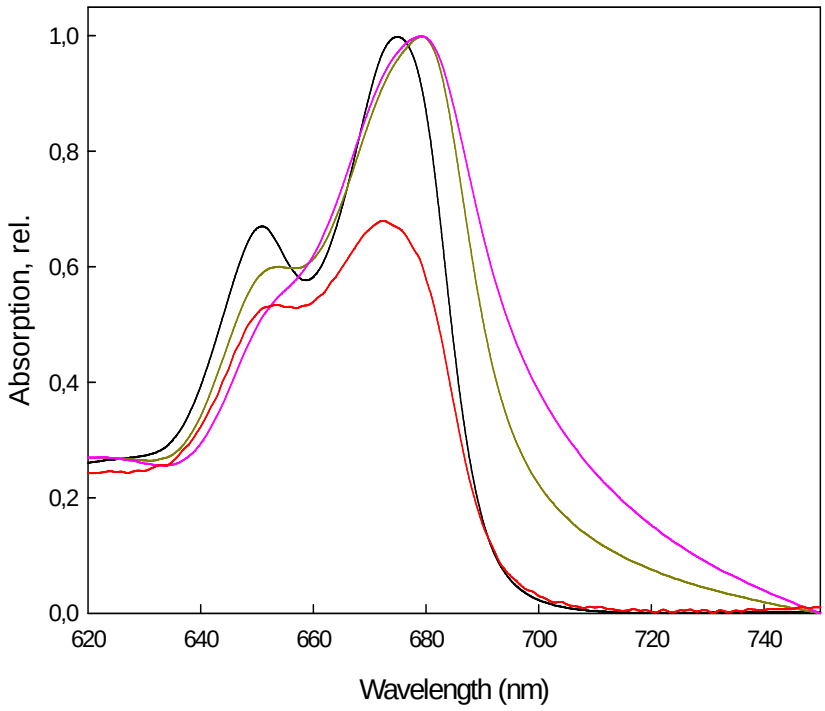

Figure 6. Room temperature absorption spectra of different samples in the red Qy region: unquenched LHCII-gel (black), quenched LHCII-gel with k_d=9 (red); medium aggregates with k_d=3 (dark-yellow); large aggregates with k_d=9 (pink). Spectra were normalized to the maximum amplitude, except the quenched LHCII-gel spectrum, which is presented without normalization.

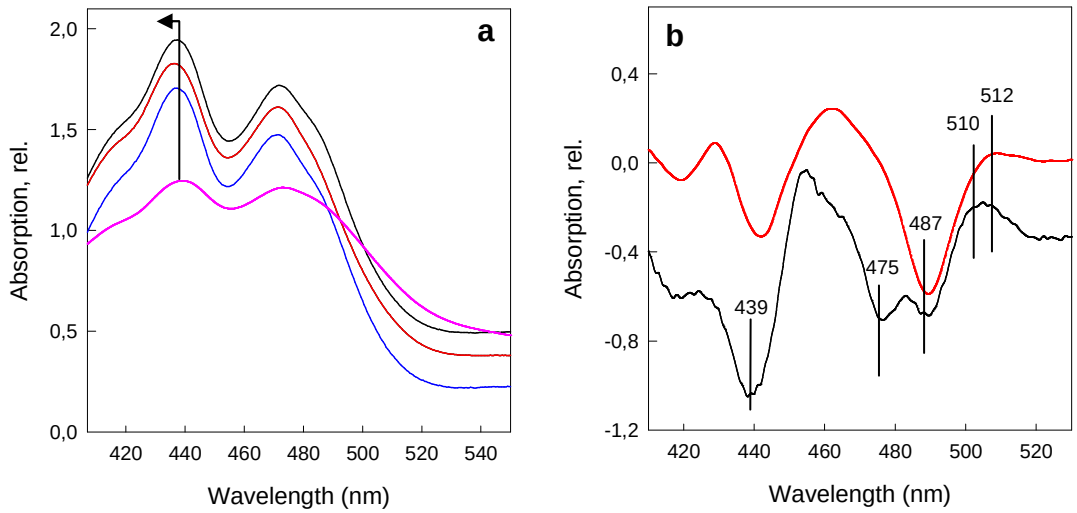

Figure 7. Room temperature absorption spectra of LHCII in the blue region. (a) unquenched LHCII-gel (black trace), quenched LHCII-gel (red); recovered LHCII-gel (blue). Spectra were normalised at the 440 nm band. (b) Difference absorption spectra: quenched LHCII-gel *minus* unquenched LHCII-gel (red); aggregates *minus* trimers (black). Spectra were normalised in the Qy region (680 nm) before the differences were taken.

In the blue region, quenching was associated with changes arising in both chlorophyll and carotenoid populations (Figure 7a). A slight blue shift of the

chlorophyll *a* band at around 439 nm (indicated by the arrow) was found in the spectrum of quenched LHCII-gel (red trace) in comparison to the one for unquenched LHCII-gel (black trace), this shift being reversed after recovery (blue trace). The spectrum of aggregates displayed a drastic drop in absorption in the chlorophyll and carotenoid regions (pink trace).

Difference spectra aggregates *minus* trimers and quenched LHCII-gel *minus* unquenched LHCII-gel showed similar changes (Figure 7b). A strong negative band was found from chlorophyll *a* at 439 nm and in the carotenoid region at 487 nm, with a small positive broad maximum at 512 nm for the gel difference spectrum. In addition, in the difference spectrum for aggregates, an extra band at 475 nm from chlorophyll *b* was found, the broad positive maximum above 500 nm being situated at ~510 nm.

As it can be seen in Figure 4, a slight monomerisation occurred in the gels following the transition to the quenched state, the size of the monomer band appearing to be proportional to the degree of quenching (k_d). It is possible that monomerisation of LHCII timers in the gel could complicate the room temperature absorption data shown in Figure 5 and 7. Therefore, to investigate if the monomerisation had contributed to the induced changes in absorption, the experiments were repeated using monomeric LHCII prepared by phospholipase treatment (see section 2.3.4 for details). In order to increase the accuracy the absorption spectra, they, were recorded at 77K and several differences spectra, quenched *minus* recovered, were taken. Figure 8 shows these difference spectra for LHCII monomers in a gel with k_d of 0.3 (~25% fluorescence decrease), 2.5 (~69% decrease) and 10 (~91% decrease).

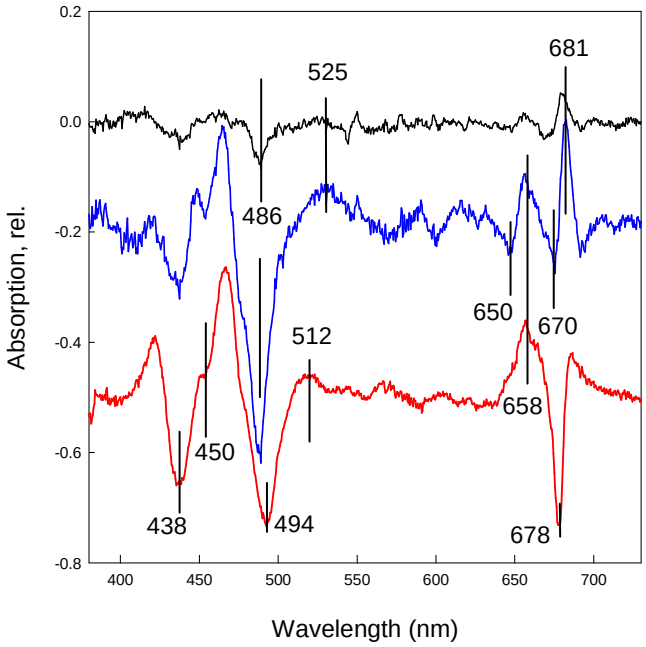

Figure 8. 77K difference absorption spectra, quenched LHCII-gel *minus* recovered LHCII-gel using LHCII monomers. The quenched LHCII-gels had the following quenching strength: k_d=0.3 (black), k_d=2.5 (blue), k_d=10 (red).

All the major absorption changes were found to be similar to those observed for the trimeric LHCII incorporated in the gel. A negative band arising from chlorophyll *a* at around 438-439 nm, and a negative carotenoid band at 486-487 nm were present. In the Qy region chlorophyll *b* negative bands were found at 650-652 nm and 670 nm, with positive bands from chlorophyll *a* at 658-662 and 681 nm bands. It was found that the spectral structure was dependent upon the amount of quenching. Even at the lowest level of quenching, the 681 nm feature emerged (black trace) and this grew in intensity as the level of quenching increased, along with the other bands, until, at the highest level of quenching, the 681 nm feature collapsed, and a negative band at 678 nm appeared (red trace). In the blue region the negative band from carotenoid at 486 nm grew in the same way, and it was shifted towards 494 nm in the sample with the highest k_d. Also, the carotenoid band situated at around 512 nm in the trimeric preparations was present in the monomeric sample displaying the highest k_d. It is interesting to notice that this band was absent in the samples with a low degree of quenching, then as the quenching increases, it was situated at around 525 nm, being blue shifted to 512 nm after further increase in the quenching strength. Previously it has been suggested that there was no change in the structure of the absorption spectrum upon formation of the

quenched state of LHCII – rather it was proposed that the observed changes arose from light scattering artefacts (Naqvi et al., 1999). However, using the LHCII-gel, the absorption changes are very clearly displayed and conclusively establish the occurrence of specific pigment alterations upon formation of the quenched state of LHCII.

It was similarly important to measure the 77K fluorescence emission spectra in order to investigate the origin of the unusual long wavelength band at around 700 nm, which is characteristic of the quenched state of LHCII aggregates (Ruban & Horton, 1992; Mullineaux et al., 1993; Vasiliev et al., 1997).

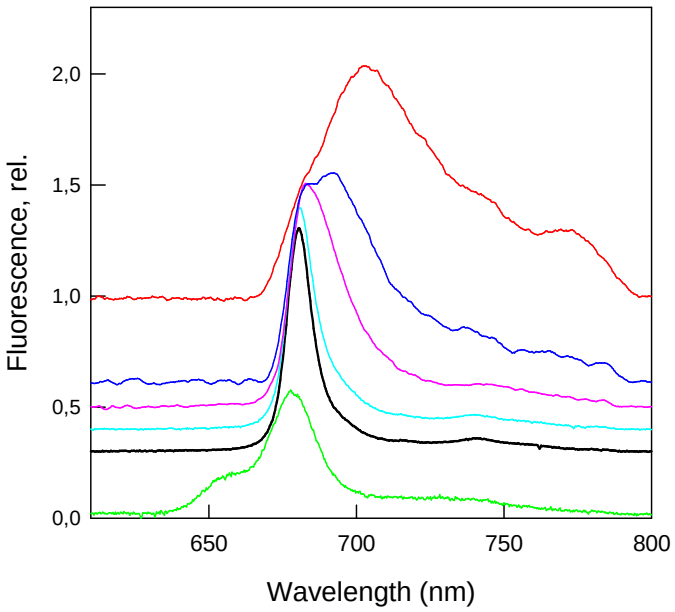

Figure 9. 77K fluorescence emission spectra (435 nm excitation): unquenched LHCII-gel (black); quenched LHCII-gel with k_d=1 (~67% fluorescence decrease, cyan); k_d=5 (~80% decrease, pink); k_d=12 (~92% decrease, blue); k_d=23 (96% decrease, red). Also shown is the spectrum of the heat-treated sample (green). Spectra were normalised to 680 nm band and are displayed offset for clarity.

Figure 9 shows a number of fluorescence emission spectra recorded for LHCII-gels with a range of quenching strengths. A gradual broadening of the 681 nm band for the first 2 quenched samples took place. Then, when the quenching strength increased, the appearance and the development of the 700 nm was associated with a decrease in the amplitude of the 680 nm band along with an enhancement of the vibronic satellite contribution at around 740 nm and 770 nm. All these features have been shown in the 77K fluorescence spectrum of LHCII aggregates (Ruban et al., 1999). In contrast to these changes, denaturation of LHCII lead to a blue shift of the chlorophyll *a* fluorescence and the appearance of the chlorophyll *b* fluorescence band at around 655 nm, indicative of the uncoupling of chlorophyll *b* from chlorophyll *a* (green trace).

Therefore, it can be concluded that the 700 nm band neither originates from a damaged and partially denatured complex nor is a result trimer-trimer interactions.

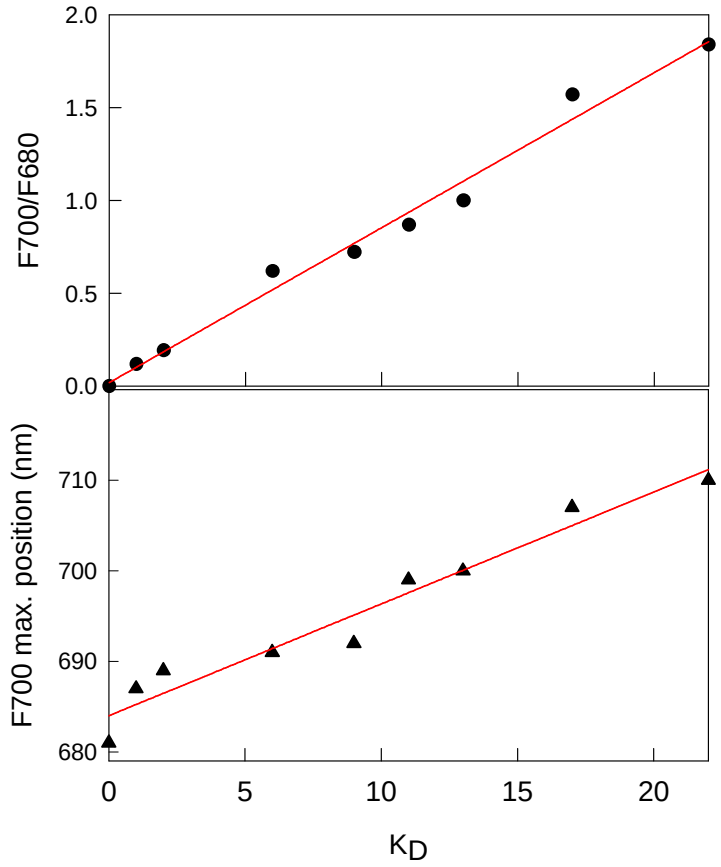

Figure 10. Relative amplitude (top) and maximum peak position (bottom) of 77K fluorescence emission spectra for different quenching states shown in Figure 9.

The relative amplitude and maximum position of the fluorescence emission was linearly proportional to the quenching strength, k_d (Figure 10). The progressive shift in peak position suggests that the development of the quencher is a gradual process, rather than an on/off switch between two LHCII states. Most likely, this shift involves transitions within a group of pigments.

Alterations in pigment configurations and interactions during transition into the quenched state were further explored using circular dichroism (CD) spectroscopy. Figure 11 shows CD spectra for unquenched LHCII-gel (black trace), quenched LHCII-gel (red trace), recovered LHCII-gel (blue) and heat-treated trimers (green). The most affected regions in the spectrum of quenched LHCII-gel were around 440 and 680 nm, suggesting that there occurred specific changes in the pigments showing optical activity in those regions. The CD spectrum of unquenched LHCII-gels (black trace), showed in

the red region the main negative bands situated at 650 and 680 nm, with a positive band at 667 nm. Also a weak shoulder was present at ~640 nm.

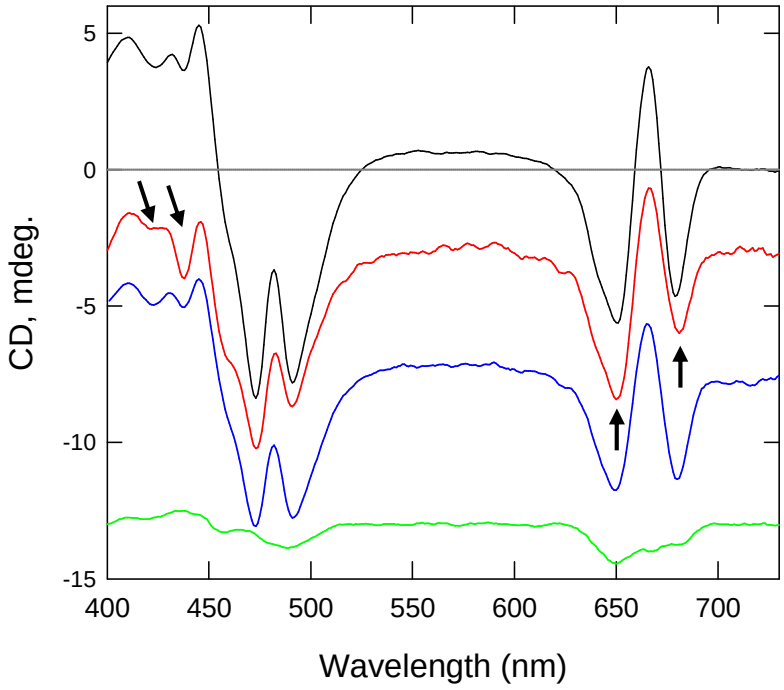

Figure 11. Circular dichroism spectra of LHCII-gels: unquenched LHCII-gel (black); quenched LHCII-gel (red); recovered LHCII-gel (blue) and heat-treated trimers (green). Arrows indicate the most affected regions of the spectrum. Spectra are normalised to their maximum and presented as offset.

In the blue region the CD spectrum revealed the main excitonic bands at 424 and 438 nm (positive), two characteristic negative peaks at 472 and 491 nm, along with a shoulder at around 460 nm. The CD spectrum of the unquenched LHCII-gel was very similar to those published for solubilised trimers (Ruban et al., 1997; Lambrev et al., 2007), indicating that the complexes present in gel are in a native condition without any change in the excitonic interactions between pigments. When quenching was induced the CD spectrum changed (red trace). In the red region the ratio of the bands situated at 650 and 680 nm (650/680) increased. In the blue region there was an enhancement of the bands peaking at 438 nm, the 460 nm shoulder became more pronounced and the ratio 472/491 increased. It should be noted that after the recovery (blue trace) these features were no longer present and the spectrum was similar to that of trimers. Thus, the processes which occurred during quenching were completely reversible. Thermal denaturation of LHCII led to a strong decrease in the CD spectrum (green trace) and elimination of its excitonic features (Wentworth et al., 2003), again showing that no denaturation occurred in the gel sample.

Figure 12 shows the difference spectra associated with quenching in gel and in aggregates.

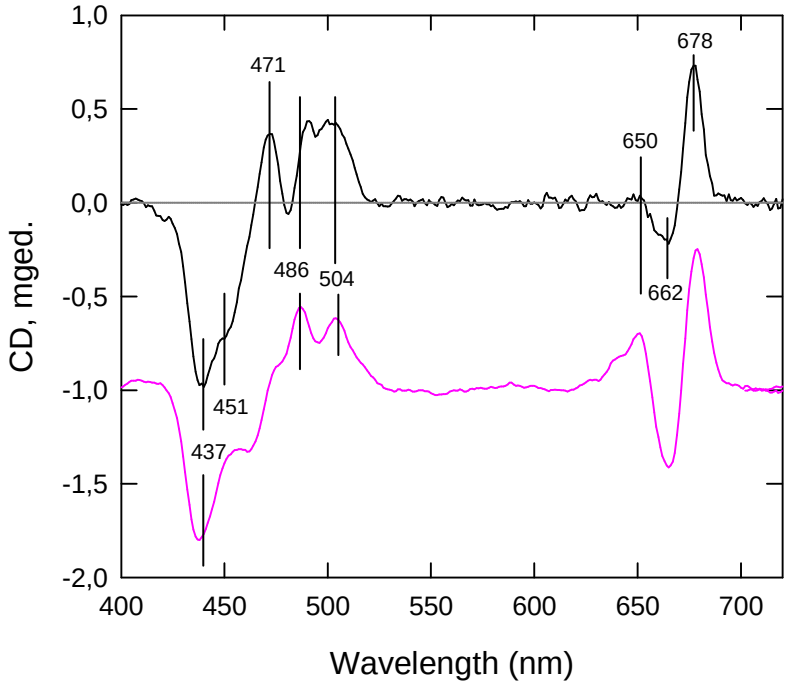

Figure 12. Difference CD spectra quenched LHCII-gel *minus* unquenched LHCII-gel (black) and aggregates *minus* trimers (pink). Spectra were normalised to 700 nm before difference was taken.

Both spectra displayed a strong negative band at 437 nm and a shoulder at around 451 nm which was more pronounced in the difference spectrum of the aggregates. In the chlorophyll *b* Soret and carotenoid regions a group of bands was present: a positive band at 471 nm in the gel difference spectrum, present only as a shoulder in the aggregates difference; a negative band at around 480 nm only in the gel difference; a positive band at 486 nm in the difference spectrum of the aggregates, slightly (3nm) red shifted in the gel difference; and also a positive band at around 504 nm in both spectra. There were also similarities between the difference spectra in the red region, with the main positive maxima at 678 nm. The negative band at 662 nm (chlorophyll *a*) and the group of smaller bands in the chlorophyll *b* region around 650 nm were observed, these being more pronounced in the aggregates difference.

Apart from the spectroscopic analysis presented above, the LHCII-gel was found to be suitable for exploration of other important features of the quenching process. The cross-linker glutaraldehyde (GA), which reacts with amino groups of lysyl residues and the amino termini, was used to test the involvement of a protein conformation change.

The blue and dark-green traces in Figure 13 show the quenching and recovery behaviour of the LHCII-gel after GA treatment. Pre-incubation for 5-10 minutes of the LHCII trimers with GA before setting the gel gave rise to a reduction of the maximum level of quenching after incubation in the detergent-free medium and also a reduction in recovery (dark-green trace). Furthermore, incubation of the pre-quenched LHCII-gel in a detergent medium containing GA (blue trace) showed much less recovery compared to the control sample (black dotted trace). These results suggest that the structure of LHCII undergoes conformational changes during the transitions between the unquenched and the quenched states.

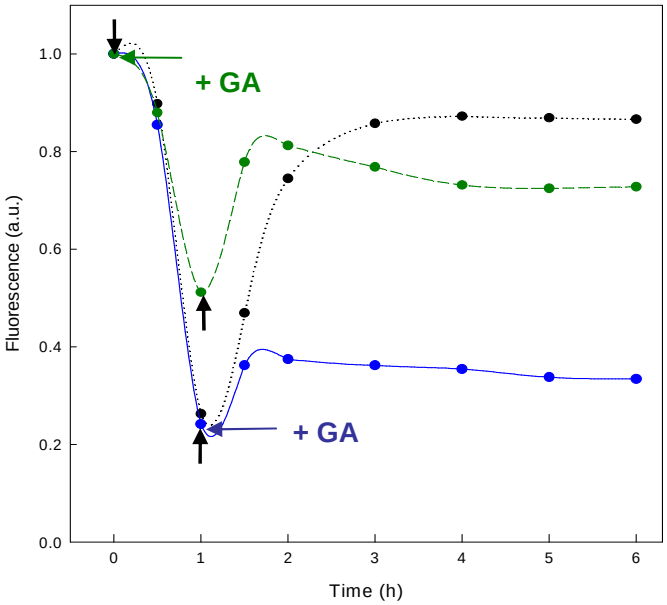

Figure 13. Effect of glutaraldehyde on quenching in the LHCII-gel. 2.5% Glutaraldehyde pre-treatment of LHCII followed by incorporation in gel, quenching in detergent-free buffer (↓) and recovery in detergent buffer (↑) (dark-green); quenching (↓) followed by recovery in 2.5% glutaraldehyde and detergent buffer (↑) (blue). Also shown is a LHCII-gel incubated for 1 hour in detergent- free buffer (↓) followed by recovery in detergent buffer (↑) (dotted trace) as showed in Figure 3.

4.3 Discussion

The discovery that fluorescence quenching can be induced in LHCII immobilised in a solid state gel is an important advance in our understanding of the processes that occur when the antenna changes from an efficient light-harvesting state to a dissipative state. Firstly, strengthening the evidence obtained from the study of LHCII crystals it is becoming increasingly clear that quenching does not require interactions between complexes. Rather, it appears to be a process occurring within individual LHCII subunits. Furthermore, the LHCII-gel provides a new experimental system, free from

the various optical artefacts that occur in aggregated states. The spectral analysis of the gels yielded for the first time information about the character of the changes in absorption and CD spectra of pigments associated with the transition to the quenching state.

The results presented in this chapter unambiguously showed that florescence quenching in the LHCII trimers is not artefactual, and is not caused by the aggregation or by a partial denaturation of the protein. Analysis of the absorption spectra in the Qy region clearly showed that the quenched LHCII-gels did not display the red 'tail' typical of aggregated samples (having the same magnitude of quenching). This 'tail' is present in the spectra of aggregates and is due to the light scattering that occurs when complexes are found in large associates. When detergent micelles were not present in the proteins immobilised in gel, it seems that the gel matrix has a restrictive effect, not allowing protein interaction. Furthermore, when ran in an electrophoresis gel, the LHCII in the quenched LHCII-gels have the same mobility as those in the unquenched LHCII-gel, although there was an increase in the fraction of monomers relative to trimers in proportion to the degree of quenching. This suggests that there was a destabilising effect during gel formation that separated the trimeric complexes into its monomeric subunits. Aggregates of LHCII showed no electrophoretic mobility, indicating that in the quenched LHCII-gels no aggregates were present. This is in agreement with the recent results of Tang et al. (2007) using heat stress induced aggregates of LHCII *in vivo*, where they showed that the aggregates remained in the stacking area of the electrophoresis gel.

Studies of the 77K fluorescence emission spectra of the quenched LHCII-gels showed the presence of the typical 700 nm emission that is associated with the quenching induced by aggregation (Ruban & Horton, 1992). Since there was no evidence of aggregation in the quenched gel, it is concluded that the 700 nm band in fluorescence emission spectrum is a typical fingerprint of the quencher, independent of the presence or absence of the aggregation.

The cross-linker glutaraldehyde (GA) was used to test the involvement of a conformational change during the transition to the quenched state. Pre-treatment of the LHCII with GA inhibited both the formation of fluorescence quenching and the subsequent recovery. Furthermore, GA inhibited the reversal of quenching when it was added to the quenched gel. These results provide good evidence that a conformational change occurred in the protein during the transitions between the unquenched and

quenched states. Hence, the treatment with GA 'froze' the protein conformation, the result being much less quenching and recovery.

4.4 Conclusions

The work presented in this chapter have conclusively demonstrated that the photoprotective switch in the function of photosystem II antenna of higher plants occurred in individual protein subunits without protein interaction. Thus, a new system has been described which allowed studies of light harvesting complexes in different quenching states without protein aggregation, suitable for different experimental techniques and allowing studies in a range of conditions. Of course, it could not be excluded that aggregation in the gel was completely absent. New techniques such as freeze-fracture electron microscopy, atomic force microscopy and chlorophyll fluorescence annihilation experiments could be used in the future to further explore this issue.

CHAPTER FIVE

In vitro and *in vivo* investigation of LHCII by resonance Raman spectroscopy

5.1 Introduction

Resonance Raman spectroscopy has been used for determining the chemical identity, molecular conformation and state of interactions of pigment molecules in all types of photosynthetic organisms: purple and green bacteria (Robert, 1996; Robert, 1999), brown algae (Pascal et al., 1998) and the light harvesting proteins of higher plants (Lutz et al., 1977; Ruban et al., 1995; Ruban et al., 2001; Robert et al., 2004).

The Raman effect is the phenomenon of a change in light frequency when it is scattered by a molecule, and it may only happen if there is energy exchange between the molecule and the photon (Robert, 1999). When a photon of light collides with a polyatomic molecule the major part of the re-emitted or scattered light has the same energy (wavelength) as the incident light (green arrow, Figure 1) and the molecule returns to its ground state, as depicted in the energy level diagram in Figure 1.

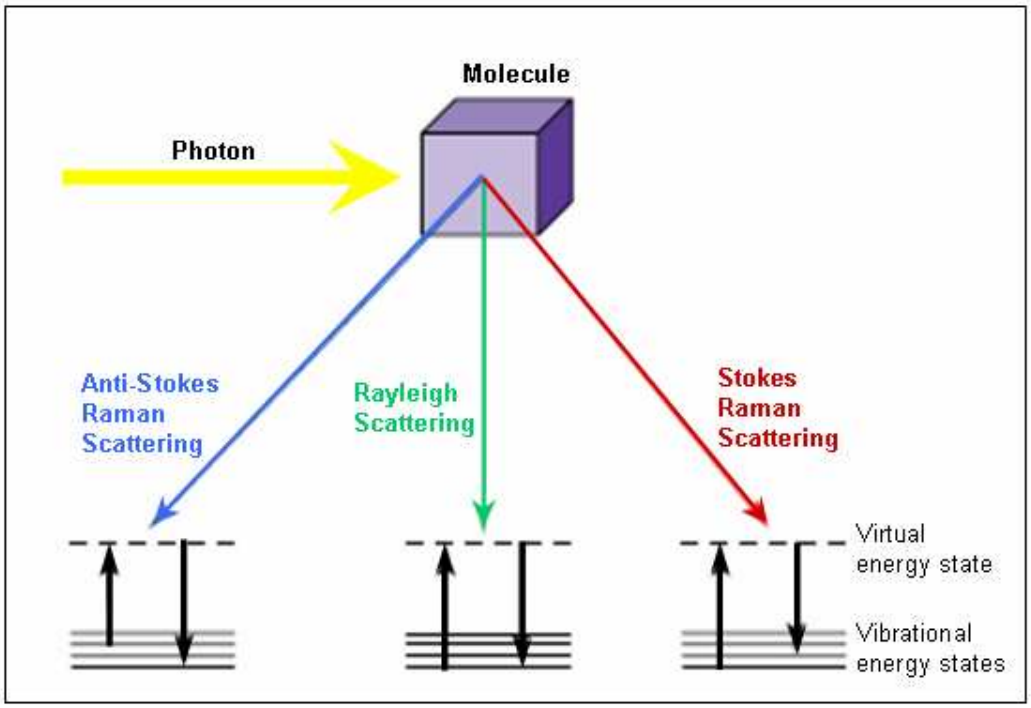

Figure 1. Principle of Raman spectroscopy (after Robert et al., 2004).

After the collision the molecule can be moved to a higher vibrational energy level, when the emitted photon will be of lower energy (shifted towards longer wavelength-red arrow), a process called Stokes' Raman. Anti-Stokes' Raman is also possible when the molecule starts at a higher vibrational level than that after the collision, the emitted photon then being of higher energy (shifted towards shorter wavelength-blue arrow).

Because the change in the energy of the photon corresponds with a change in the vibrational energy of the molecule, measuring the wavelength shift of the scattered light gives information about the vibrational energy levels of the molecule involved (Robert et al., 2004). A Raman spectrum is a plot of the intensity of Raman scattered radiation as a function of its frequency difference from the incident radiation (usually in units of wavenumbers, cm^{-1}). This difference is called the Raman shift.

In resonance Raman spectroscopy, the energy of the incoming photons used to produce the Raman effect is adjusted such that it coincides with an electronic transition of the molecule. The result is that the probability of scattering dramatically increases, leading to a ~ 10^6 fold increase in the Raman signal – this is the resonance effect. Therefore, resonance Raman spectroscopy is a highly selective technique, enabling studies not only of the different pigment molecules in complex media (e.g. different xanthophylls in chloroplasts membranes), but also the same molecule in different environments (e.g. neoxanthin in quenched and unquenched LHCII trimers as will be described in this chapter).

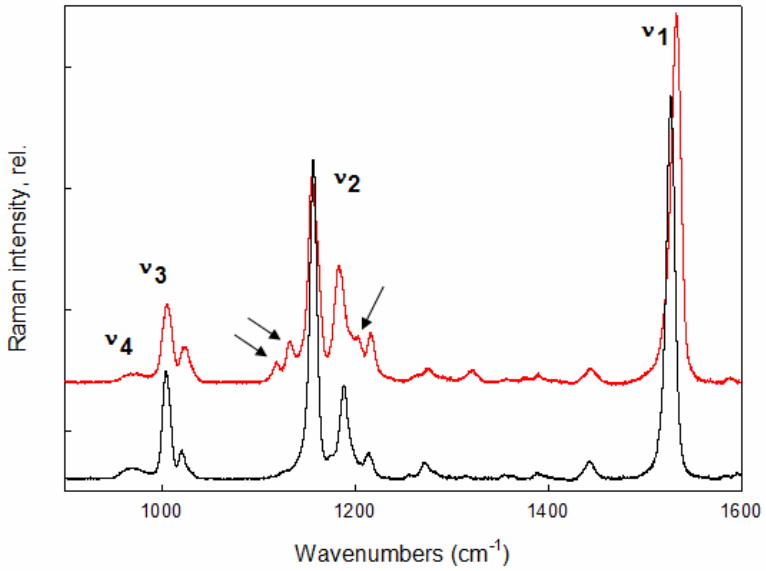

Figure 2. Resonance Raman spectra of neoxanthin (red), a 9-*cis*, and lutein (black), an all-*trans* carotenoid in pyridine. Excitation was at 501.6 nm. The arrows indicate the characteristic band in the neoxanthin spectrum.

The resonance Raman spectra of carotenoid molecules have 4 main groups of intense bands, namely ν_1, ν_2, ν_3, and ν_4 as shown in Figure 2. These bands provide information on the conformation and configuration of the molecule. In the results reported in the early 1970s by Rimai et al. (1973) from a model derived from an infinite polyenic chain, these groups of bands were assigned. The ν_1 mode at ~ 1530 cm^{-1} was

attributed to the stretching modes of the conjugated C=C bonds, and its frequency is therefore sensitive to both the conjugated chain length and the molecular configuration (*trans* or *cis*) of the carotenoid. Thus, in Figure 2 a downshift of the ν_1 band is observed for lutein relative to neoxanthin, as the latter carotenoid has one less conjugated double bond (9 instead of 10) and also exhibits a *cis* configuration at position 9 of the chain. The ν_2 region is situated at 1120-1200 cm^{-1} and corresponds to a mixture of C=C and C-C bond stretching modes with C-H bending modes, the arrows in Figure 2 showing characteristic frequencies present in the ν_2 region of the neoxanthin spectrum that are probably due to the 9-*cis* conformation (Ruban et al., 2001). The ν_3 region is situated at ~1000 cm^{-1} and corresponds to stretching modes of C-CH_3 bonds between the main-chain and the side methyl carbon. Finally, the ν_4 band at ~950 cm^{-1} results from out-of-plane C-H wagging modes. As these modes are formally uncoupled from the electronic transitions of a perfectly-planar carotenoid, the intensity of the ν_4 band depends of the distortion from planarity of the molecule (Robert et al., 2004).

Application of the resonance Raman technique to the light harvesting complexes of higher plants gave valuable information about identification, conformation and dynamics of the pigments within these complexes. Using of combination of ultra-low-temperature absorption, circular dichroism and resonance Raman spectroscopies, Ruban et al. (2000) were able to identify the major electronic transitions and the configurations of all of the xanthophylls in both trimeric and monomeric LHCII. It was found that 0-0, 0-1 and 0-2 electronic transitions for neoxanthin and lutein in monomers are situated at 486, 457, 403 nm and 495, 466, 437 nm respectively. Using selective excitation lines for resonance Raman spectra the band at 510 nm in the low temperature absorption spectrum of trimers has been shown to arise from one of the lutein molecules which is distorted in this complex, according to the analysis of the Raman spectra in the ν_4 region (Ruban et al., 2001). This distortion is accompanied by a red shift in its 0-0 transition, from 495 to 510 nm. Moreover, application of the resonance Raman technique to the thylakoid membrane led to identification of the absorption transitions of the xanthophyll cycle carotenoids, violaxanthin and zeaxanthin. Zeaxanthin was found to have a broad 0-0 transition situated around 503-511 nm, whereas two populations of violaxanthin were identified, the major one absorbing at 488 nm with a minor contribution at 497 nm (Ruban et al., 2001).

Resonance Raman spectroscopy was also applied to investigate the changes that occur when aggregation is induced in LHCII. When the excitation is set to a value where mainly carotenoid molecules are excited, which also coincides with an absorption difference between the aggregated and trimeric LHCII (488 nm), the ν_4 region of the aggregated spectrum exhibits a different structure (Ruban et al., 1995). Aggregation induced an increase in band structure for ν_4 - specifically in the ratio between the main bands situated at around 951 and 963 cm^{-1}, the 951 cm^{-1} band being more intense in the aggregates than in the trimers. These changes have been attributed to a carotenoid population which is affected by the oligomerization process, and becomes twisted in the aggregates (Ruban et al., 1995). Later this carotenoid was identified as neoxanthin (Ruban et al., 2001). In the higher frequency region of the spectrum of the aggregates obtained with a 441.6 nm excitation line, (when contribution from chlorophyll *a* and chlorophyll *b* can be observed), a 1639 cm^{-1} band (attributed to a chlorophyll *b* carbonyl stretching mode) was found, a feature not present in the trimeric samples. This band is absent when the chlorophyll *a* pigments were excited (413.1 nm), where a 1672 cm^{-1} band attributed to a keto carbonyl group involved in intermolecular interactions is present. It was then concluded that the aggregation induces the formation of an H-bond to a formyl group of a chlorophyll *b* molecule and to a keto group of a chlorophyll *a* molecule (Ruban et al., 1995).

Recently, similarities were reported between the resonance Raman spectra of LHCII aggregates and LHCII crystals (Pascal et al., 2005), for which the 2.72 Å structure has been determined (Liu et al., 2004). Fluorescence analysis showed that the crystals are in a highly quenched state (Pascal et al., 2005). Resonance Raman spectra indicated that the quenched structure of the LHCII in crystals significantly differs from that of the unquenched, solubilised protein and it is similar to the one present when the protein is present in the aggregated form (Robert et al., 2004). In particular, in the crystallised LHCII, the bound carotenoid neoxanthin exhibits a distorted configuration which is not present in the solubilised protein. When excitation was set at 488 nm which is specific for neoxanthin, an increase in the intensity of the ν_4 region was observed with an enhancement in the Raman band at around 953 cm^{-1}. This clearly indicates a deviation of this molecule from a planar structure (Pascal et al., 2005). The increase in the crystal was more pronounced than the one reported for the aggregates (Ruban et al., 1995). Also, similar to the findings for the aggregated forms, differences in the

chlorophyll *b* molecules are found in crystals, spectral changes showing that at least one chlorophyll *b* in the crystal becomes involved in a hydrogen bond, whereas the trimeric forms is free from this interaction (Pascal et al., 2005).

It is well-known that, when trimeric LHCII complexes are isolated from the thylakoid membranes they display a high fluorescence yield, indicating a very low rate of energy dissipation. The excited state lifetime was found to be around 4ns (Moya et al., 2001). When trimers form aggregates the fluorescence is highly quenched, having lifetimes between 0.2 and 1.5 ns (Mullineaux et al., 1993; Moya et al., 2001). Using FLIM (fluorescence lifetime imaging microscopy) the lifetime of the LHCII crystals mentioned above was measured, showing an average fluorescence lifetime of 0.89 ns (Pascal et al., 2005). Thus, the LHCII crystal was in a quenched state.

These measurements of LHCII aggregates and crystals proved that LHCII may exist in different conformational states, each state having different capacities for energy dissipation. Hence, it was suggested that changes in conformation of LHCII regulate the switch between energy utilisation and energy dissipation underlying the process of NPQ (Horton et al., 1991; Horton et al., 1996; Pascal et al., 2005). However, there was no direct proof that the proposed conformational changes occur *in vivo*, when NPQ is induced. From the studies discussed above it was concluded that the changes in the intensity of the resonance Raman band situated at around 953 cm^{-1} are correlated with the fluorescence lifetimes. Consequently, this twist can be considered as a 'quenching fingerprint'. Because resonance Raman spectroscopy is a highly selective technique that can be applied to chloroplasts membranes and leaves in their natural state of NPQ, it could provide information about the existence of quenching-associated conformational changes *in vivo* and hence give new insights into the process.

The aim of the work presented in this chapter was to investigate by resonance Raman spectroscopy isolated LHCII complexes in different quenching states (e.g. different fluorescence intensities), and chloroplasts and leaves with different NPQ levels. Investigating the changes in the configuration of the LHCII-bound carotenoid neoxanthin, via the resonance Raman spectra of intact chloroplasts and whole leaves should provide evidence for, or against the conformational change hypothesis for NPQ, as well as indicating the extent of these changes.

5.2 Results

LHCII trimers were prepared from dark-adapted spinach leaves after solubilisation of PSII-enriched particles with *n*-dodecyl *β*-D-maltoside and IEF fractioning (see section 2.3.4). Previous studies using isolated LHCII have provided important information into the possible mechanism of energy dissipation. LHCII can be isolated from the thylakoid membrane in detergent micelles and manipulated to display large differences in fluorescence yield, by formation of oligomers of trimers. In order to investigate the changes that occur in the neoxanthin Raman signal, and how they correlate with the extent of quenching, isolated LHCII trimers and 5 quenched oligomeric samples were obtained, covering up to a 10-times decrease in the fluorescence intensity. To obtain these samples, trimeric LHCII was incubated in a 2 ml cuvette in the presence of *n*-dodecyl *β*-D-maltoside. Biobeads were added in order to gradually remove the detergent, the degree of quenching being monitored by fluorescence measurements. The quenched samples, each having a different fluorescence intensity (k_d, see Figure 3 legend) were immediately frozen in liquid nitrogen to conserve their state of quenching state. 77K resonance Raman spectra with 488 nm excitation were then recorded for each sample. Figure 3a shows the ν_4 region for these samples, with two major bands, one at around 952-953 cm^{-1} and the second one at 964 cm^{-1}. It can be seen that there was a progressive increase in the intensity of the band situated at 953 cm^{-1} as quenching grew larger. This showed that the neoxanthin Raman signal was affected by the oligomerisation-induced quenching; the structure of the neoxanthin was altered, becoming more distorted, the twisting of the molecule reducing its planarity and the out-of-plane modes becoming more coupled with the electronic transition. A plot of the intensity at the band situated at 953 cm^{-1} relative to the intensity of the 964 cm^{-1} band as a function of the percentage change in the fluorescence intensity, showed a linear relationship between them (Figure 3b).

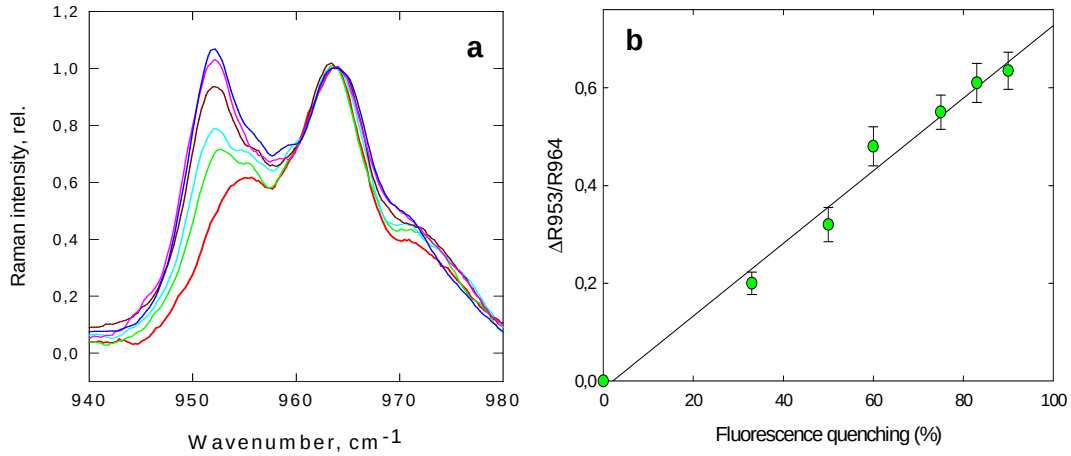

Figure 3. (a) ν_4 region of Raman spectra for LHCII trimer (red) and different quenched states (green- k_d=0.5; cyan- k_d=1; brown- k_d=2; pink- k_d=5; blue- k_d=9). Excitation was set at 488 nm. (b) Relationship between the change in Raman intensity at 953 cm^{-1} relative to that at 964 cm^{-1} (obtained from (a) and fluorescence quenching expressed as a percentage change in the fluorescence. The error bars represents the amplitude of the noise for each spectrum. Normalization was made at 964 cm^{-1}.

In order to determine if the same changes occur *in vivo* when NPQ is induced, intact chloroplasts were isolated from wild type (wt) *Arabidopsis thaliana* plants. The resonance Raman spectra were recorded for the samples with and without NPQ. NPQ was induced by illuminating dark-adapted chloroplasts with strong white light (1500 µmol m^{-2} s^{-1}) for about 5 minutes (Figure 4). Saturating light pulses were used at approximately 60 seconds intervals to assay the development of NPQ. In order to generate maximum ΔpH and NPQ 0.1mM methyl viologen was added as artificial electron acceptor. Figure 4 shows the fluorescence traces recorded for chloroplasts prepared from wt and L17 PsbS overexpressor plants which have higher NPQ levels.

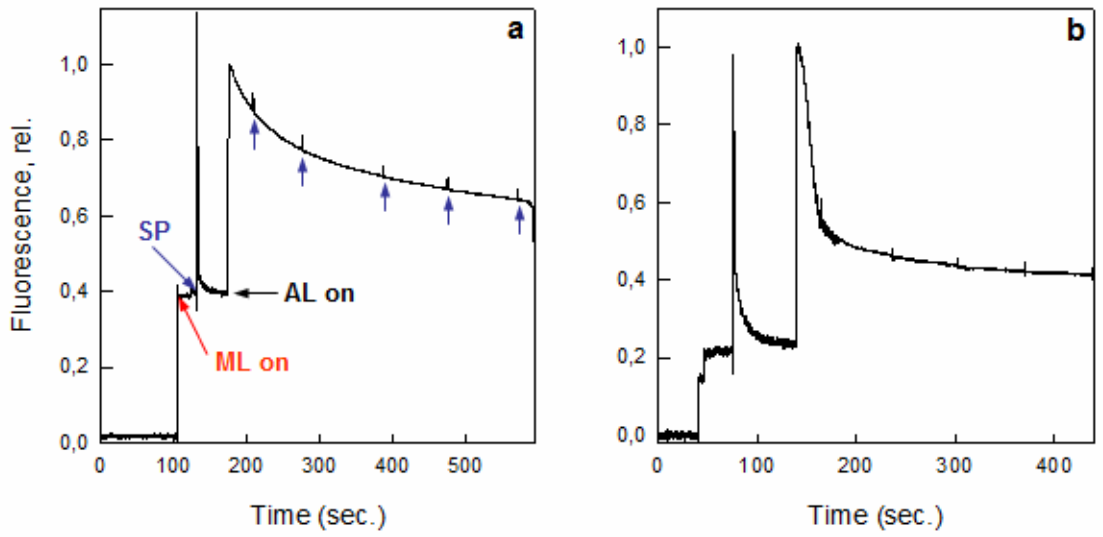

Figure 4. Selected fluorescence traces for quenching analysis for wt (a) and L17 (b) chloroplast preparations. ML=measuring light beam; SP=saturated pulse (blue ↑) (3000 µmol m^{-2} s^{-1}); AL=actinic light; light intensity was 1500 µmol m^{-2} s^{-1}.

Figure 5 shows the resonance Raman spectra in the ν_4 region of chloroplasts isolated from wt (a) and L17 (b), with (red trace) and without (black trace) NPQ. The Raman spectra displayed two distinct bands at around 953 cm^{-1} and 964 cm^{-1}. In the presence of NPQ, there was an enhancement of the 953 cm^{-1} band relative to 964 cm^{-1}. The proportional increase of the 953 cm^{-1} was 5-7 % for wt and 8-9% for overexpressor chloroplasts. This increase in the 953 cm^{-1} band was similar to that found in samples of quenched LHCII (Figure 1a; Ruban et al., 2000; Pascal et al., 2005).

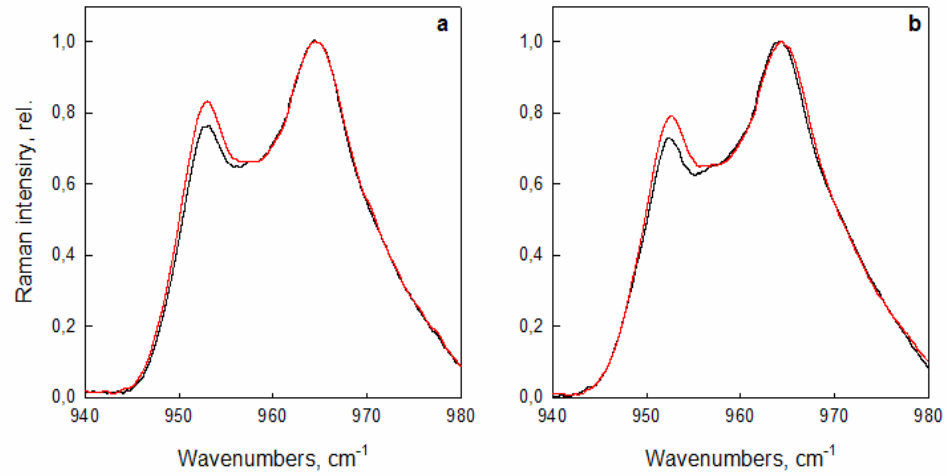

Figure 5. The ν_4 region of the Raman spectra of isolated chloroplasts from *Arabidopsis* wt (a) and L17 (b) plants. Spectrum after illumination (+NPQ, red spectra) and before illumination (-NPQ, black spectra) are displayed. Normalisation was performed at 964 cm^{-1} band. Each spectrum represents an average of 25 individual spectra. Excitation was at 488 nm.

In order to compare the observed quenching-associated differences in the spectra for chloroplasts and isolated LHCII, the quenched-*minus*-unquenched difference spectra were calculated for each. Figure 6 shows the difference spectrum associated with quenching in LHCII (black) and wt chloroplasts (red), after normalisation was made in the ν_3 region. The spectrum calculated for chloroplasts clearly exhibited the same features as the difference taken for LHCII, with three characteristic bands at around 953, 958 and 965 cm^{-1}.

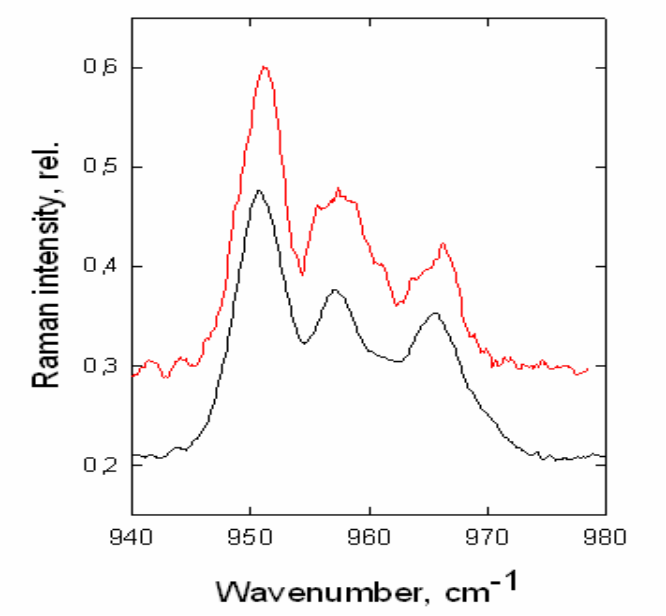

Figure 6. Quenching-associated difference resonance Raman spectra for LHCII (black) and wt chloroplasts (red). Spectra were obtained by calculating quenched-*minus*-unquenched difference after normalization in the ν_3 band (at 1003cm^{-1}). Spectra are presented as offset.

These similarities observed in the difference spectra strongly suggest that the same twisting of neoxanthin occurs in both isolated chloroplast when NPQ is induced and in the quencxhed state of LHCII.

The resonance Raman spectra of leaves from L17, the *npq4* mutant with much reduced NPQ, and wt leaves are presented in Figure 7, along with the fluorescence traces recorded during NPQ induction. It should be emphasized that the samples described as without NPQ were not dark-adapted, but samples after illumination followed by a period of dark relaxation (about 5 minutes). During this period the ΔpH which is formed upon illumination collapses, allowing the relaxation of the major component (qE) of NPQ while more long-lived forms (such as qI) will remain. Illumination can also cause de-epoxidation of violaxanthin to zeaxanthin in the

thylakoid membrane, which could potentially interfere with the resonance Raman measurement. The experimental design ensured that the changes in the Raman spectra were associated with qE, not with the qI component of NPQ, and also did not arise from changes in the level of zeaxanthin: firstly, no epoxidation of zeaxanthin or reversal of qI occur during the 5 minute dark relaxation period (Ruban & Horton 1995; Ruban et al., 2002); and secondly, measurement of the *npq4* mutant showed that although the same level of violaxanthin de-epoxidation and qI formation occurred as the wt and L17 mutant (Kiss A., personal communication), the amplitudes of the Raman change was much less, in line with the much reduced levels of qE (see below).

The differences in qE in the three plant types were compared to the change in the relative intensity of the 953 cm^{-1} Raman band. For the spectra presented in Figure 5 and Figure 7 (right panel) an average of the individual spectra (see figure legends) has been calculated in order to increase the signal to noise ratio. It can be seen that the magnitude of the change in Raman signal was greatly reduced in the *npq4* mutant, in which the reversible component of NPQ is almost absent. Conversely, in the L17 leaves, both the Raman signal and qE were larger.

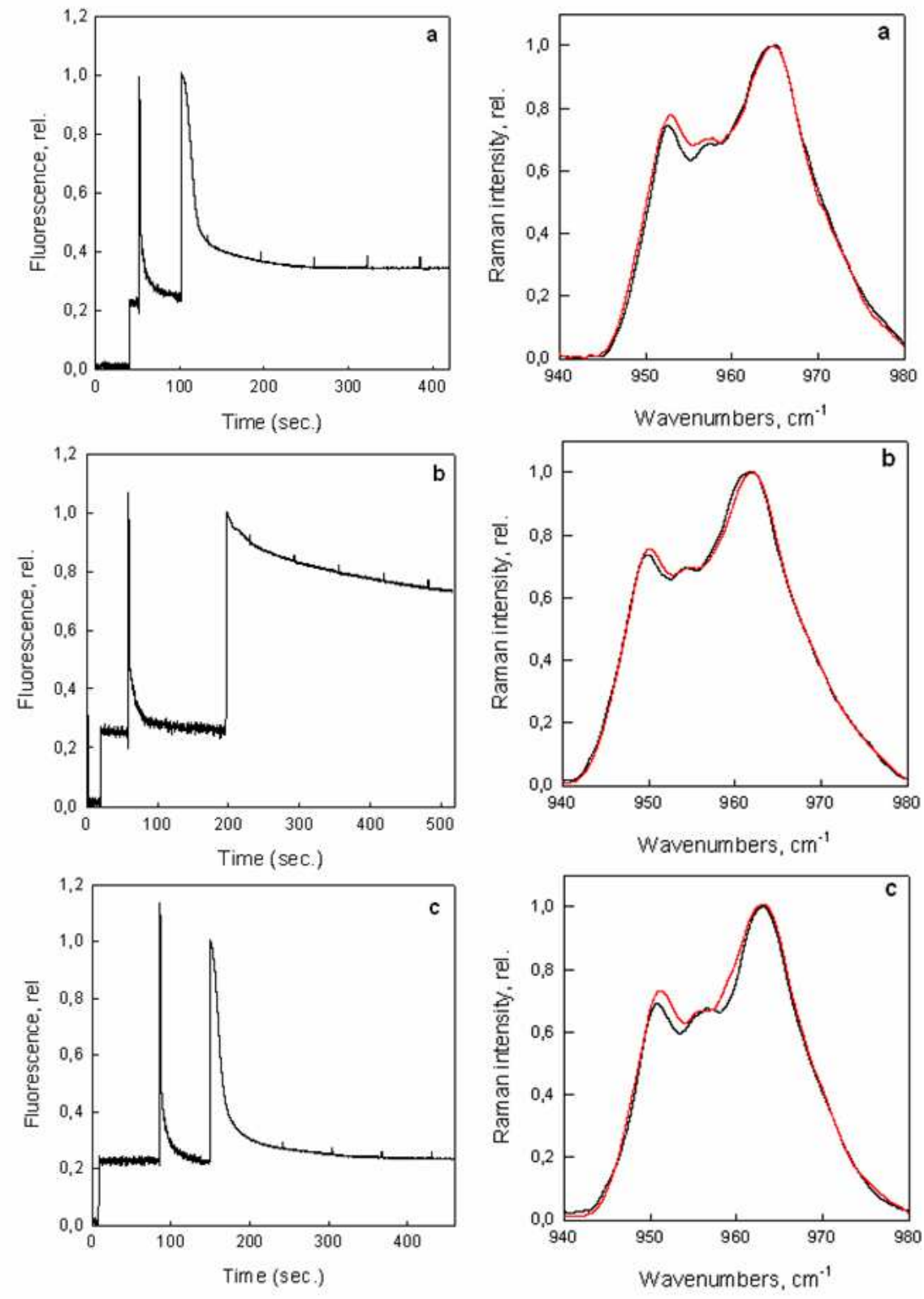

Figure 7. Chlorophyll fluorescence traces (left panel) and the corresponding resonance Raman spectra in ν_4 region (right panel) for wt (a), *npq4* (b) and L17 (c) leaves. Light intensity was 1500 µmol m^{-2} s^{-1}. Right panel shows spectrum after illumination (+qE, red) and following dark relaxation (-qE, black). Spectra are averages of 31, 22, 13 (+qE) and 28, 16, 21 (-qE) repetitions for wt, *npq4* and L17 respectively. Normalisation was made at 964 cm^{-1}. Excitation was at 488 nm.

Figure 8 shows the extent of the relative enhancement of the 953 cm^{-1} band as a function of the magnitude of NPQ for chloroplasts isolated from wt and L17 plants and for wt, *npq4*, and L17 leaves. Clearly, there was a positive correlation between the extent of the change in Raman signal and the amplitude of qE, the dark-reversible component of NPQ. The calculated maximum change in the samples from the L17 plants was approximately 8 %. It is concluded that the formation of qE was associated with a change in configuration of the LHCII-bound carotenoid neoxanthin, identical to that associated with quenching of the isolated complex. This, therefore, suggests that at least a part of qE observed *in vivo* was due to a conformational change in LHCII.

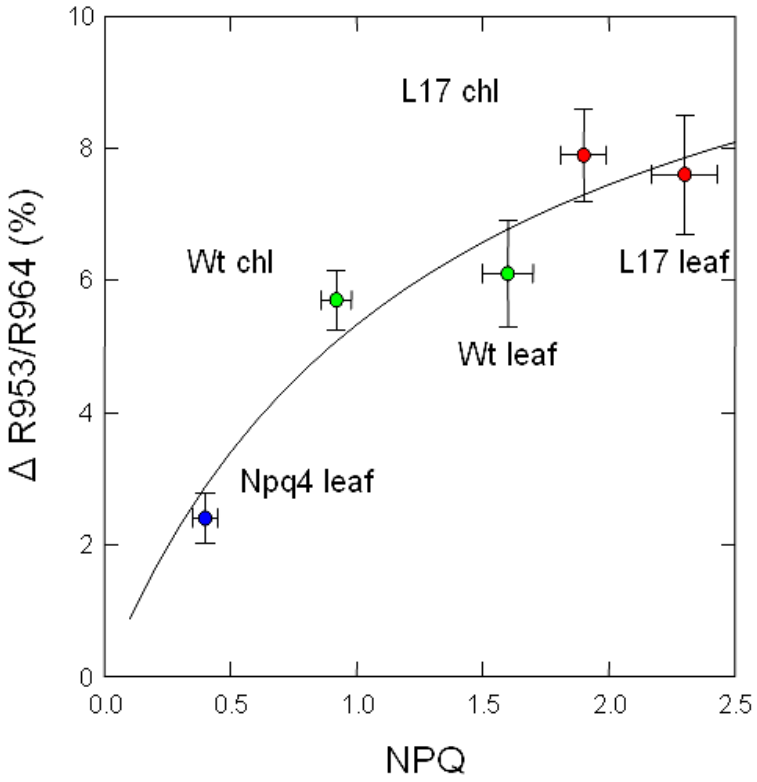

Figure 8. Extent of NPQ compared to the relative change in Raman intensity at 953 cm^{-1}. Data were obtained from chloroplasts (chl) isolated from wild type (wt) and L17 plants, and leaves of wild type (wt), *npq4* and L 17 plants. Data are the means of separate replicated samples with 25 spectra recorded for each sample. The number of separate samples were 17 (wt chl), 8 (L17 chl), 3 (npq4 leaf), 4 (wt leaf) and 3 (L17 leaf). Error bars are ±SEM. Line shown is the best fit (95% confidence by t-test).

In order to validate this conclusion at a more quantitative level, it was important to determine the size of the relative change in Raman intensity that would be expected *in vivo*, if all of the qE observed was due to the LHCII conformational change. Therefore, the relationship between the relative amplitude of the 953 cm^{-1} band and the extent of fluorescence quenching for the LHCII samples in different quenched state was determined (Figure 9). Note that these are the same data as plotted in Figure 3b, but here

quenching has been plotted as the k_d parameter, numerically equivalent to the measure of qE used in Figure 8. The results from this estimation were compared with the size of the changes found in chloroplasts and leaves (see Figure 8) in order to discover whether the two sets of data (*in vitro* and *in vivo*) were consistent with each other.

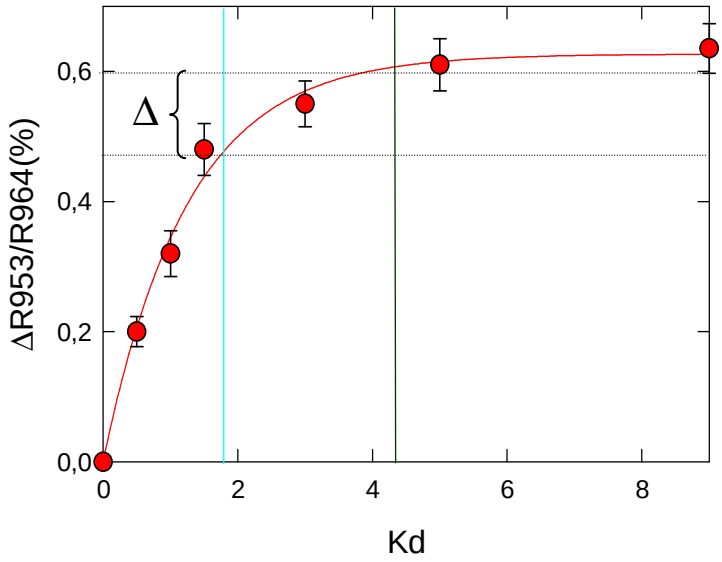

Figure 9. Relative change in Raman intensity at 953 cm^{-1} as a function of the extent of fluorescence quenching, k_d. The parameter k_d was calculated as (F(unquenched) – F(quenched)) / F(quenched) - where $F_{unquenched}$ is the fluorescence intensity at the time 0 before addition of biobeads and $F_{quenched}$ is the fluorescence intensity at different incubation times. Vertical lines correspond to the estimated level of quenching of LHCII *in vivo*: in dark-adapted chloroplasts (cyan line) and for maximum NPQ (dark-green line), based on the data in Figure 3a, 5a and 8. Δ, between the two dotted horizontal lines, is the estimated range for the change in the resonance Raman signal of neoxanthin *in vivo*, which would be associated with the formation of qE.

It can be seen that the relative amplitude of the 953 cm^{-1} band was strongly nonlinear with increasingly smaltler changes in intensity when k_d reached higher values. Comparing the *in vivo* spectrum of the wt *Arabidopsis* chloroplasts in the unquenched state (Figure 5a, black trace) with the spectrum for isolated LHCII trimers (Figure 3a, red trace) it seems that LHCII present in the chloroplasts membranes was already in a partially quenched state (judging from the relative change in intensity of the 953/964 cm^{-1} bands). Thus, the state of the LHCII in chloroplasts corresponded to a k_d of around 1.5-2.0 (indicated by the cyan vertical line in Figure 9). Therefore, the change in k_d arising from qE, which is about 2.5 (Figure 8) would start from a k_d of 1.5-2.0 and would reach a maximum of 4.0 to 4.5 (dark-green vertical line Figure 9). Hence, the predicted increase in intensity of the 953 cm^{-1} neoxanthin band *in vivo*, was about 0.12,

the difference between the two horizontal dotted lines (Δ). Therefore, an increase of about 20% in the relative intensity of the 953 cm^{-1} band was predicted *in vivo* in order to account for the change in k_d arising from NPQ formation.

In isolated LHCII neoxanthin has the major contribution to the resonance Raman signal at 953 cm^{-1}. Lutein also contributed to the signal but only to a small extent. This would not be the case in isolated chloroplasts. Thus, although almost all of the neoxanthin in thylakoid membranes is bound to LHCII trimers (Bassi et al., 1993; Morosinotto et al., 2002), even when the excitation is chosen to selectively excite neoxanthin molecules, the Raman spectrum obtained will also contain contributions from other carotenoids present in the membrane (β-carotene, violaxanthin, zeaxanthin and lutein). The contribution of neoxanthin to the *in vivo* spectrum can be quantified because only this carotenoid is in a 9-*cis* conformation and it thus exhibits fingerprint Raman bands over the whole spectral range (Ruban et al., 2000).

The following procedure was used to estimate how much of the 953 cm^{-1} resonance Raman signal was due to neoxanthin. Firstly, curve-fitting of the ν_1 band of the resonance Raman spectrum of chloroplasts excited in the neoxanthin region (488 nm) was performed (Figure 10). In a previous study, Ruban et al. (2001) reported that the ν_1 region of spectra of thylakoids containing either violaxanthin or enriched in zeaxanthin could be fitted using the spectra of isolated carotenoids. The fit was verified by an alternative approach based upon the calculation of the difference zeaxanthin *minus* violaxanthin spectra. The position of υ_1 varies with the number of conjugated C=C's of the carotenoid as well as the presence of *cis*-*trans* isomerisations. Therfore the position of υ_1 is different for each of the carotenoids present in the membrane. Therefore, the υ_1 region is the most appropriate one for estimating the neoxanthin contribution. Individual contours corresponding to the isolated xanthophylls, violaxanthin, neoxanthin, lutein, β-carotene and zeaxanthin (in pyridine) were used for the fit. The fitting procedure was performed using Sigmaplot software. Only the amplitudes of the individual carotenoid peaks were varied, until the fit matched the chloroplasts υ_1 spectrum. The υ_1 regions of β-carotene and zeaxanthin are almost identical and therefore were added together (Ruban et al., 2001). The neoxanthin contribution to the ν_1 region of the chloroplast spectrum was found to be about 35%, with contributions of ~50% from violaxanthin, ~8% from lutein and ~7% from zeaxanthin/β-carotene (Figure 10).

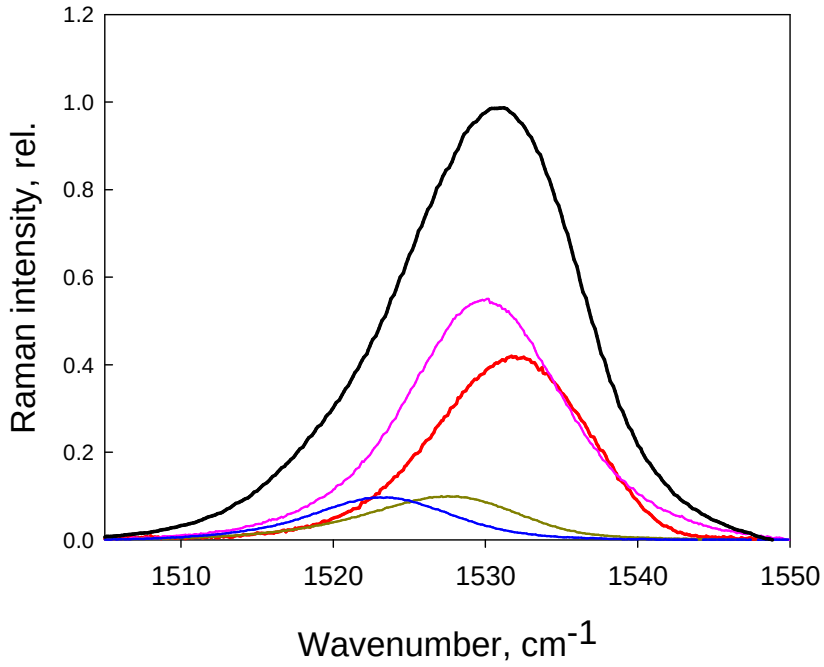

Figure 10. Curve fitting of the ν_1 band of the Raman spectrum of chloroplasts (black). Excitation was set at 488.0 nm. Individual contours correspond to isolated xanthophylls in pyridine: zeaxanthin/β-carotene (blue), lutein (dark-yellow), neoxanthin (red) and violaxanthin (pink). The curve fitting procedure was described in the text.

However, the contribution of neoxanthin to the ν_4 region will be different to its contribution to the ν_1 region since each xanthophyll has different ν_4/ν_1 ratio. The ν_4/ν_1 ratios were calculated from the spectra of the isolated carotenoids and found to be 0.12 for neoxanthin, 0.03 for violaxanthin, 0.07 for lutein, 0.06 for zeaxanthin and 0.02 for β-carotene. Therefore, the neoxanthin contribution to the ν_4 band was obtained by corrections using these ν_4/ν_1 ratios according to:

$$N(\%) = \left(\frac{\nu_4 neo}{\nu_1 neo} \cdot \frac{k_{neo}}{\sum \frac{\nu_4 i}{\nu_1 i} \cdot k_i} \right) \cdot 100 ,$$

where k_i is the fraction of the area of each xanthophyll in the ν_1 band of the resonance Raman spectrum of chloroplasts. Since the ν_1 spectrum for zeaxanthin and β-carotene are identical, but their ν_4 spectra are different, there are two values for the ν_4/ν_1 ratio of (zeaxanthin + β-carotene) and consequently for the estimated neoxanthin contribution to ν_4. Thus the contribution of neoxanthin to the ν_4 was calculated to be between 63 % and 66%. Similar, the contribution to ν_4 were estimated to be 22% and 23% for

violaxanthin, 8% and 8.6% for lutein, and 7% and 2.4% for zeaxanthin/β-carotene. Using the calculated estimate of the contribution of neoxanthin in the ν_4 region of 65%, the predicted change in intensity of the 953 cm^{-1} band associated with NPQ *in vivo* was corrected to give a value of 13 %. This value for the estimated change matched quite closely the 8 % change observed *in vivo* (Figure 5a), given the under-estimation due to the lutein contribution to the ν_4 region in LHCII spectrum. Although, the antenna complexes in the thylakoid membrane are not present simply as mixtures of LHCII and the same aggregates as *in vitro* can not be formed, it is highly significant that the predicted change in the resonance Raman signal from the *in vitro* curve (Figure 9) was found to be consistent with the one seen *in vivo*. Thus, it can be concluded not only that the quenching mechanism occurs in isolated LHCII as for NPQ *in vivo*, but that the magnitude of the change in LHCII conformation indicated that the amplitude of the change in Raman signal is sufficiently large to account for the majority of the *in vivo* quenching.

5.3 Discussion

The results presented in this chapter provide clear evidence that the qE process *in vivo* is caused by a conformational change that occurs in the major light-harvesting complex and that this conformational change results in an increase in energy dissipation. qE is induced and regulated by the ΔpH and the de-epoxidation state of the xanthophyll cycle carotenoids in a process modulated by the PsbS protein (Horton et al., 2005). The LHCII conformational change was previously reported to occur *in vitro* in LHCII aggregates (Horton et al., 1996) and in its crystallised form (Pascal et al., 2005), leading to a change in the configuration of the pigments bound to the complex. However, no experimental proof was provided that this occurs *in vivo*, or that it is correlated with the major component of NPQ. Using LHCII in different quenching states, as well as chloroplasts and leaves with different qE, it is shown here that the extent of the changes in the resonance Raman signal *in vivo* is consistent with the *in vitro* changes.

The twist in the neoxanthin configuration that gives rise to an altered Raman signal at 953 cm^{-1} indicates that LHCII can be present in different conformations, each conformation having different capacities of energy dissipation. Neoxanthin is present in a locus enriched in chlorophyll *b* (Liu et al., 2004) and it was shown to have strong

electronic interaction with these molecules (Croce et al., 1999). Changes in the chlorophyll *b* region are also present in the resonance Raman spectra of the quenched forms as compared to trimers (Ruban et al., 1995; Pascal et al., 2005). As discussed by Pascal et al. (2005), the Chl *b*606/Chl *b*607 dimer is close to neoxanthin and is a potential site of energy quenching in LHCII along with the site where the Chl *a*611/Chl *a*612 pair, lutein 620 and Chl *a*610 are present.

Although it can not be excluded that other quenching processes may contribute to qE to some extent, such as the quenching reported to occur in the minor complexes CP24, CP26 and CP29 (Morosinotto et al., 2002) or quenching via formation of carotenoid radicals (Holt et al., 2005), the data presented here show that the LHCII conformation change mechanism can account completely for the *in vivo* process of energy dissipation both qualitatively and quantitatively. The data presented also provide new insights into the structure, function and dynamics of the PSII light-harvesting antenna. It is well known that the incorporation of the LHCII trimer into the thylakoid membrane creates a macro-organisation that is necessary for efficient light collection and light energy transfer to the reaction centres. It also seems that LHCII in the thylakoid membrane is in a slightly quenched state in the dark, but at a level where there is a negligible effect on the quantum yield of photosynthesis. From this state, only small structural changes may be required in order to give rise to the large changes in energy dissipation needed for photoprotection. Thus, it seems that, when integrated into the membrane, LHCII is finely poised not only for carrying out its role of light-harvesting, but also for its regulatory role in the dissipation of excess energy.

5.4 Conclusions

The results presented in this chapter provide new evidence that the change in configuration of neoxanthin and the formation of NPQ both arise from the light-induced, ΔpH-dependent conformational change in LHCII. Moreover, because the NPQ-related change in neoxanthin configuration appears to be identical to that observed when fluorescence quenching is induced in isolated LHCII, it is further concluded that NPQ arises from the same quenching mechanism.

CHAPTER SIX

Transient absorption measurements on LHCII in different quenching states

6.1 Introduction

Under conditions of excess illumination the PSII light-harvesting antenna is switched into a photoprotective mode in order to dissipate the harmful excitation energy, a process known as non-photochemical quenching of chlorophyll fluorescence (NPQ) (Horton et al., 1996; Pascal et al., 2005). Despite the fact that the process of energy dissipation has been well-documented in recent years (Horton et al., 1996; Demmig-Adams & Adams, 1996; Niyogi, 1999; Horton et al., 2005; Pascal et al., 2005; Holt et al., 2005) the underlying molecular mechanism is still under debate. A principal role in the process of NPQ is played by the xanthophylls, in particular the xanthophyll cycle carotenoids (Frank et al., 1994; Demmig-Adams & Adams, 1996). It has been proposed that the conversion of violaxanthin (a 9 double bond carotenoid) into zeaxanthin (an 11 double bond carotenoid), which occurs when plants are exposed to strong light intensities, changes the carotenoid molecule from a non quencher into a quencher of the chlorophyll excited state. In this case the quenching occurs either via energy transfer (Berera et al., 2006; Ma et al., 2003), or through a charge transfer state (Holt et al., 2005). Alternatively it was proposed that zeaxanthin has mainly a structural role (Horton et al., 1994; Robert et al., 2004) in the creation of the quenched structure, acting as an allosteric activator of quenching (Horton et al., 1991). Recent studies of the quenching mechanism in LHCII crystals used for structural determination give new insights into the quenching process (Pascal et al., 2005), highlighting the possible significance of specific chlorophyll-xanthophyll domains within the complex. These studies suggested that the process involves changes in configuration of certain pigments, resulting from a protein conformational change. Experiments conducted on LHCII aggregates show that the *in vitro* quenching state resembles the *in vivo* NPQ state (Horton et al., 1991; Horton et al., 1996), providing a model system for understanding the mechanism underlying NPQ.

In order to determine the mechanism of quenching, it is necessary to track completely the pathway of excitation energy transfer in a quenched sample of LHCII and compare it to an unquenched sample. Recently, Berera et al. (2006) reported an investigation of artificial light-harvesting dyads, in which chlorophyll-like molecules are quenched by the optically forbidden, low-lying S_1 state of carotenoids. A low transient concentration of the latter molecular species is detected using transient absorption spectroscopy. The objective of the work described in this chapter is to apply

this methodology to determine whether similar carotenoid excited states are involved in the quenching in aggregated LHCII.

Transient absorption or 'pump-probe' spectroscopy is a method which allows the monitoring of the dynamics of extremely fast events in real time. The principle of a transient absorption experiment is rather simple. An intense pulse, the so-called pump pulse, is used to excite the molecules in the sample. Then the second, probe pulse passes through the sample and the intensity of the probe is monitored as a function of the time delay with respect to the pump pulse. Practically, one spectrum is recorded at several delay times between the pump and the probe, and then each spectrum is subtracted from that recorded when the pump pulse was absent. As the absorption spectrum of the sample is a signature of the molecules present in the sample, modifications in the absorption of the sample after the pump pulse, reflect pump-pulse-induced changes in the sample. By recording these absorption changes, the transfer of excitations between the different species present in the sample can be monitored. The detected signal in the transient absorption measurement is the change in absorption, $\Delta A\ (\lambda,t)$. The absorbance or optical density (O.D.) of a sample is defined as:

$$A(\lambda) = -\log \frac{I(\lambda)}{I_0(\lambda)}$$

where $I_0(\lambda)$ is the intensity of the incident light which hits the sample, $I(\lambda)$ is the intensity of the light transmitted through the preparation and λ is the wavelength of light. Now, the difference in absorption at time t after the start of the pump-induced events is given by the formula:

$$\Delta A(\lambda,t) = \Delta A(\lambda,t)_{on} - \Delta A(\lambda,t)_{off} = \log \frac{I(\lambda)_{off}}{I(\lambda,t)_{on}}$$

where $I(\lambda,t)_{on}$ and $I(\lambda,t)_{off}$ denote the intensities of the transmitted light with and without the pump pulse, respectively.

In a pump-probe experiment different signals can be observed. Figure 1 shows a schematic outline of the contributions to the transient absorption signal. When a chromophore is promoted to an excited state by absorption of the pump pulse, is loses its ground state absorption and a negative signal is observed, a process called photobleaching (PB). The pump pulse may create either new species with a different absorption spectrum (e.g. oxidised/reduced forms) or simply molecules in an excited

state which show excited state absorption (ESA) i.e. in the excited state, the chromophore may absorb more photons from the probe pulse and consequently go to a higher excited level. These 2 processes have a positive contribution (enhancement) to the absorption signal. The probe pulse may also stimulate a molecule in an excited state to decay back to the ground state by emitting photons, a process called stimulated emission (SE). SE gives rise to an apparent additional bleaching signal and its spectrum is similar to a fluorescence spectrum.

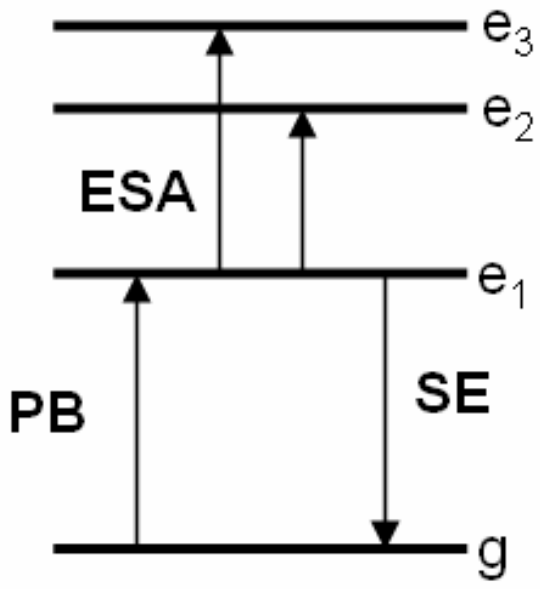

Figure 1 Schematic representation of the possible contributions to a transient absorption signal. PB=photobleaching (from ground state (g) to an excited state (e_1)); SE=stimulated emission (from e_1 to g); ESA= excited state absorption (from e_1 to e_2, e_3 …)

A schematic outline of the transient absorption (pump-probe) apparatus used to perform the measurements presented in this chapter is shown in Figure 2. Briefly, femtosecond laser pulses were obtained from a titanium:sapphire oscillator-regenerative amplifier (Coherent MIRA seed and RegA 9050) working at a repetition rate of 40 kHz, which provided initial pulses of ~50 fs at 800 nm (FWHM 30 nm). The laser beam was split into two parts: one was focused on a BBO (β -barium borate) crystal to generate a white light continuum (the probe beam); and the other was used to pump an optical parametric amplifier (OPA 9850, Coherent) to obtain the pump beam at 675 nm (~100 fs). The delay between the two beams was achieved by taking advantage of the speed of light: knowing the finite light speed ($3x10^8$ m/s), and using a translation stage to vary the distance that the probe beam travels with respect to the pump beam, a variable delay

was induced between the probe and the pump pulses. For instance, a 3 mm difference in distance travelled introduced a 1 ps time delay between the pulses. The polarization between the pump and probe beams was set at magic angle (54.7^0) with respect to the probe beam. The instrument response function was fitted to a Gaussian of 120 fs (FWHM).

An excited singlet state may also decay as a result of a process called singlet-singlet annihilation. Annihilation occurs when two excitons arise in the same pigment molecule and it is therefore dependent on the excitation pulse intensity, being present mainly at high excitation intensities. For this reason, to avoid this unwanted phenomenon, the pump intensity used was reduced to ~10 nJ. However, even at this low intensity annihilation may occur and this had to be taken into account in the analysis of the data.

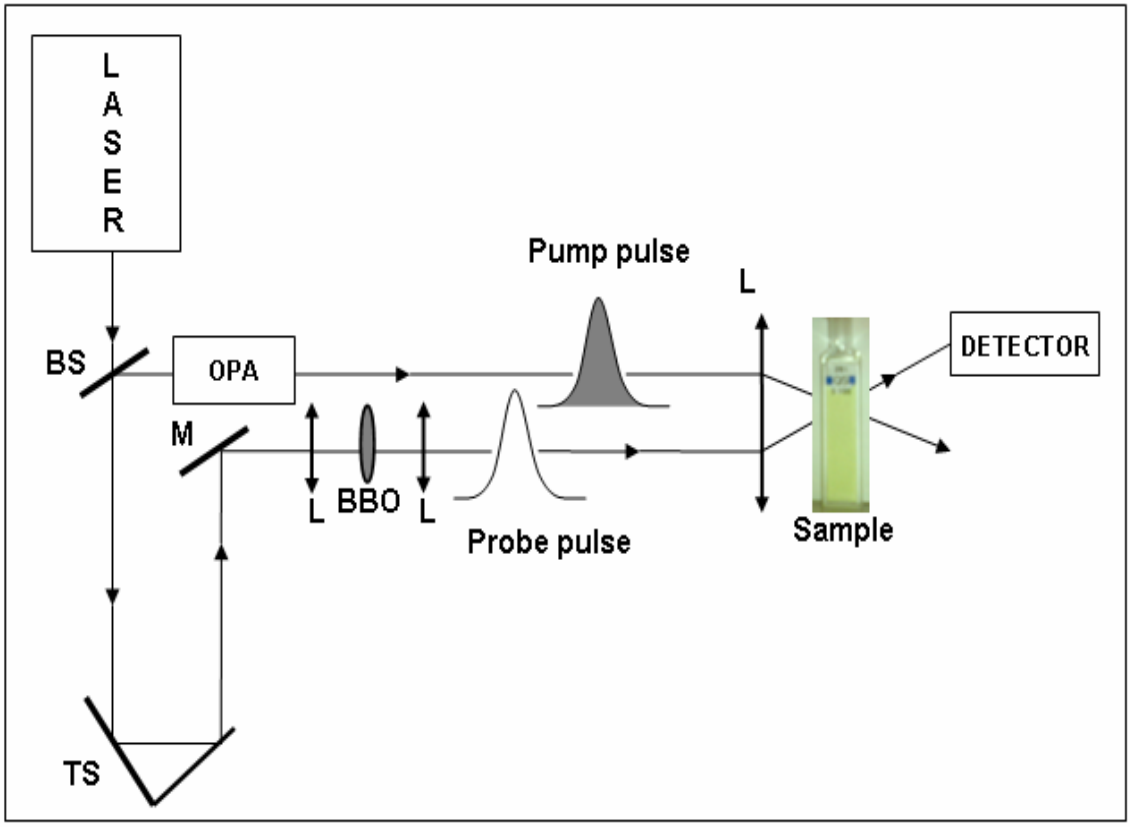

Figure 2. Schematic outline of a transient absorption setup. The pump pulse is used to excite the sample and the induced absorption changes are monitored with the white probe pulse, which is delayed in time. BS=beam splitter; TS=translation stage; M-mirror; BBO= β-BaB_2O_4 crystal used to generate white light; L=lenses.

A typical time-resolved experiment consists of collecting thousands of spectra (see Appendix for an example of transient difference absorption traces). In order to select only a small part of the information and to be able to interpret the dynamics and

kinetics of the experiment, data were analyzed by making use of global analysis techniques (van Stokkum et al., 2004). In this approach, data are described by a number of compartments with specific spectral properties. For example at time zero the excitation is situated in compartment 1. This compartment decays into compartment 2 with a rate constant k_1 (i.e. compartment 2 is populated with rate k_1), which decays with a rate constant k_2 into compartment 3, which populates compartment 4 with rate k_3 (Figure 3a). The number of compartments is increased until the addition of a new component does not lead to an improvement of the quality of the fit, finally obtaining for each compartment a rate constant and a spectrum. The obtained spectra are called Evolution-Associated Difference Spectra (EADS) and they represent in general a mixture of molecular states. For this reason in order to obtain the spectra of the corresponding pure molecular species (Species-Associated Difference Spectra, or SADS), a target analysis is also applied to the data whereby a specific kinetic scheme is applied (van Stokkum et al., 2004). At this stage the sequential model is branched in such a way as to reflect the true photophysics and/or photochemistry of the system. For example, considere the reaction scheme represented in Figure 3b: an initial excited state A can decay into two different states B and C with the rates k_B and k_C; the C state then, decays into D with the rate k_D; and both states B and D are relatively long-lived within the timescale of the measurement. When the measurement is performed, changes in the absorption spectrum of the system will occur reflecting the presence of these different states. Considering now the spectral evolution of the whole system, represented in Figure 3a, an attempt is made to fit the data to a number of events, in a way that (1) gives rise to (2), then to (3) and finally to (4). Upon excitation, the majority of the absorption difference (1) will be due to the formation of A, but a small proportion of A will have decayed into B and/or C. In (2), depending on the varying rate constants k_B and k_C, there will be a certain proportion of each, while a small amount of A will still remain. In addition, some of C may already have decayed in D on this timescale. In (3) depending on the constant k_D part of C will still be present and a very small part of A, the major component being D. Finally, in (4) it will be mainly D, with a small part of C and probably nothing of A.

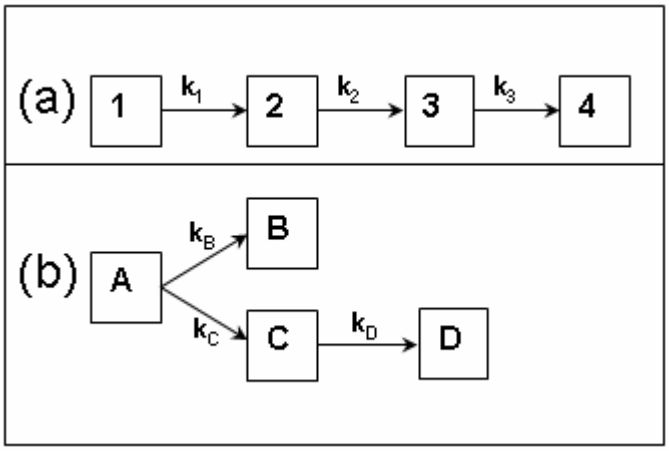

Figure 3. Schematic representation of global (a) and target (b) analysis models for a four-compartment system.

The aim of the work presented in this chapter is to explore the mechanisms of excited energy dissipation by using femtosecond transient absorption spectroscopy applied to LHCII in different quenching states. This work was carried out in the laboratory of Professor Rienk van Grondelle (VU University of Amsterdam), in collaboration with R. Berera and J. T. M. Kennis. Data analysis was carried out by I. van Stokkum.

6.2 Results

LHCII trimers were prepared from dark-adapted spinach leaves. PSII-enriched membranes (BBY particles) were solubilised with *n*-dodecyl *β*-D-maltoside (see section 2.3.4 for details) and fractioned by IEF. The dark-green band, which contains mainly LHCII trimers was collected and for a further purification was loaded onto a sucrose gradient, as described in 3.2.1 section. To obtain the quenched samples, trimeric LHCII was incubated in a 2 ml cuvette in the presence of *n*-dodecyl *β*-D-maltoside and biobeads were added in order to gradually remove the detergent. The quenching state was monitored by fluorescence measurements, and expressed as k_d ($k_d = \frac{F_{unquenched} - F_{quenched}}{F_{quenched}}$; where $F_{unquenched}$ is the fluorescence intensity at the time 0 before addition of biobeads and $F_{quenched}$ is the fluorescence intensity at different incubation times). The quenched aggregates and trimeric LHCII were then subject to transient absorption measurements.

Figure 4 shows the results of global analysis (EADS) of the data for the three samples used: trimeric LHCII, quenched aggregates with k_d=2 and quenched aggregates with k_d=9 (see also the raw data in Appendix where the transient difference absorption traces for the three samples recorded at 45 wavelengths are presented). Four components were needed to fit the data for all samples. The first one (black trace) appeared at time zero after correction for coherent artefacts and displayed the same features for all samples: bleaching of the chlorophyll Qy region at 677 nm, bleaching of the chlorophyll Qx region at about 620 nm superimposed with a chlorophyll excited state absorption; and below 600 nm, a positive signal originating from chlorophyll excited state absorption. This spectrum decayed in 975 fs for trimers, 1 ps for the sample with k_d=2 and 550 fs for sample k_d=9, to the second (red) trace which showed a drop in the chlorophyll Qy bleach and a small drop in the excited state absorption below 600 nm. Also, in the carotenoid ground state absorption region (below 530 nm) it appeared that the drop in amplitude was slightly bigger than in the region situated at higher wavelengths, suggesting that a carotenoid ground state might have been depopulated at this stage. This spectrum decayed in 21.7 ps for trimeric sample, in 26.6 ps for the sample having k_d=2 and in 18.3 ps for sample with k_d=9 to the third component (blue trace). This third set of spectra showed further bleaching in the chlorophyll Qy region with an overall small decrease of the chlorophyll excited state absorption present in all the samples. The region below 530 nm showed a slight decrease at this stage but, interestingly, for the quenched samples in the region situated between 530 and 600 nm the signal seemed to have the same amplitude, suggesting that the decay of the chlorophyll excited state absorption was compensated by the rise of another species, possibly a carotenoid excited state. For the trimeric samples the next evolution (blue to dark-cyan) took place in 505 ps and was characterised by a drop in the chlorophyll Qy region and a decrease of the chlorophyll excited state absorption. In the region below 530 nm the spectrum displayed a typical carotenoid triplet state superimposed with the chlorophyll excited state absorption, indicating that this last spectrum was a mixture of long-living (unquenched) singlet chlorophyll and carotenoids triplet. In the samples with an intermediate degree of quenching (k_d=2) the blue to dark-cyan evolution took place in 285 ps and was characterised by a drop in the chlorophyll Qy region and a decrease of the chlorophyll excited state absorption. As for the trimeric sample this spectrum was a mixture of carotenoid triplet and long living singlet

chlorophyll. The same evolution for the sample with highest quenching degree took place in 138 ps. For this sample the chlorophyll Qy bleach had disappeared, the spectrum being almost flat except a small part in the carotenoid triplet region (around 510 nm), suggesting that the triplet population was very small in this case.

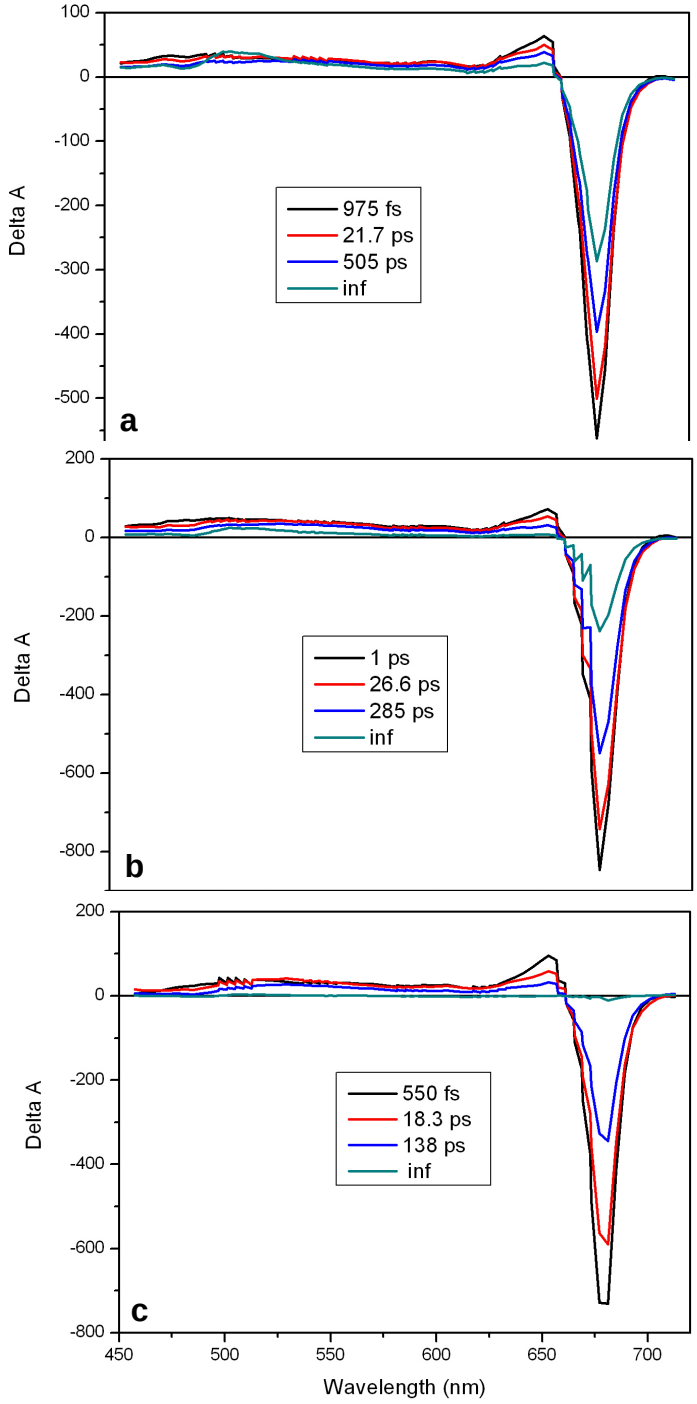

Figure 4. EADS for the trimeric (a), k_d=2 (b) and k_d=9 (c) LHCII. Dark-cyan trace presented as 'inf' refers to a component which does not decay on the timescale of the experiment (i.e. 20 ns).

Figure 5 shows the results obtained for the first 3 EADS (black, red and blue spectra, Figure 4) after normalisation in the Qy region. The rationale for normalization in this region was the following: assuming the carotenoid contribution to the spectrum in the Qy region (~680 nm) to be negligible, normalization in this region was expected to give a similar contribution to the spectrum from the chlorophyll bleach and chlorophyll excited state absorption, so that any spectral change (differences in amplitudes) could be assigned to a different species. For all three samples, in the region situated below 510 nm, there was a decrease in the amplitude from the black to the blue trace, the decrease being more pronounced as the samples are more quenched. This region corresponds to the carotenoid $S_0 \rightarrow S_2$ transition, thus suggesting that a depopulation of the carotenoid ground state absorption occured during the quenching process. In the region between 510 and 590 nm (region of excited state absorption from carotenoid S_1 state) there was an increase in the amplitude of the spectra from black to blue, this increase becoming more pronounced as the degree of quenching increased. The results obtained from the global analysis of the data along with the normalised EADS suggest the involvement of a carotenoid excited state during the quenching process.

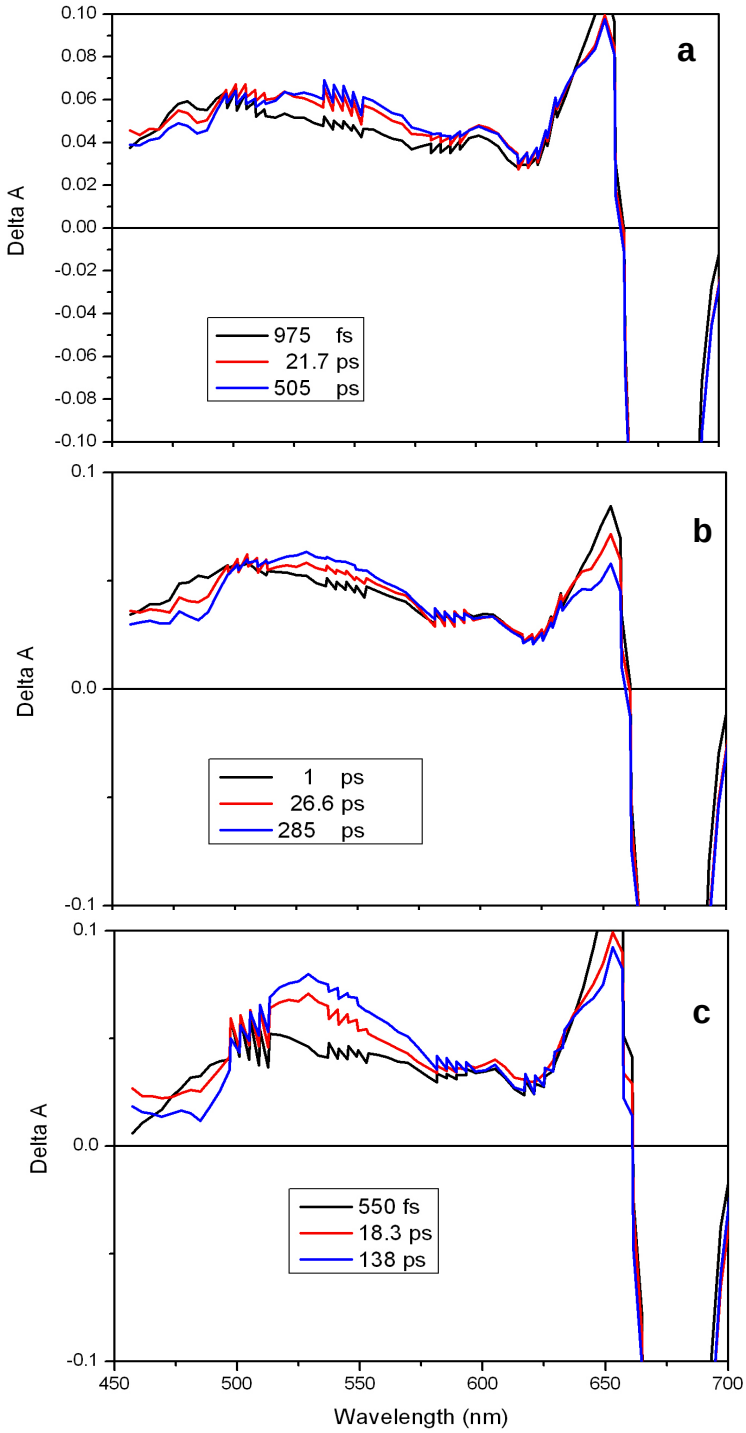

Figure 5. EADS after normalisation in the chlorophyll Qy region (see text for detailed explanation). The traces are the same as presented in Figure 4. The noise present is due to the overlapping of the windows when were added together.

In order to identify the spectrum of the quenching state, target analysis was applied to the data. The kinetic model applied for analysis of the samples is depicted in

Figure 6 and consists of 6 compartments. The model is not unique, presented here is the one which gave the best fit of the data. Four pools of chlorophylls are needed in order to take account of the heterogeneity of the sample: Chl 1, Chl 2, Chl 3 and Chl. Chl 4 pool represents the unquenched chlorophylls present in the trimeric unquenched state and in the sample with k_d=2.

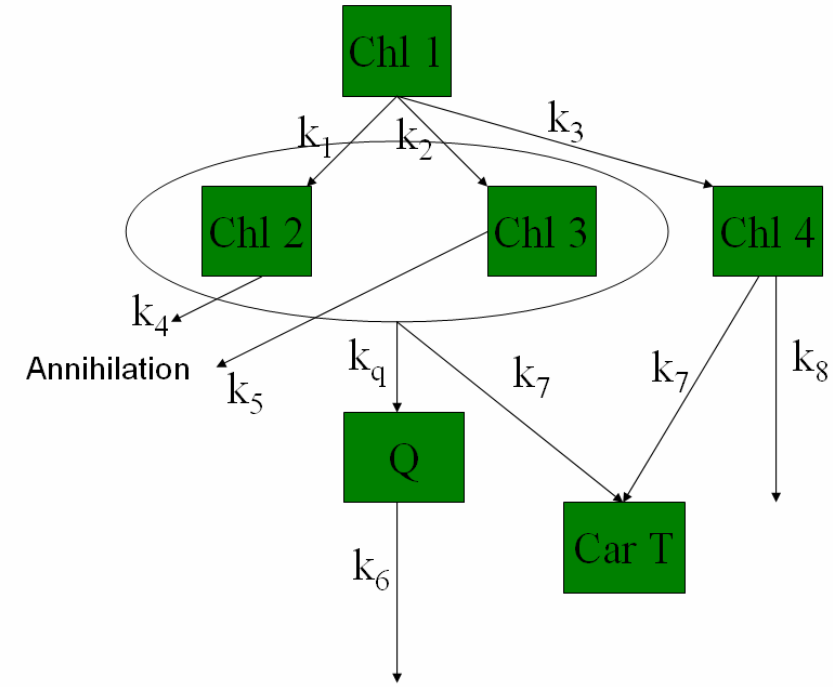

Figure 6. The kinetic model used to fit the data. For the sample with k_d=9 the Chl 4 pool (unquenched chlorophylls) was not considered. For further details see the text.

The excitation at time zero resides in the Chl1 compartment, and is distributed into the three compartments Chl 2, Chl 3 and Chl 4 (in about 1 ps) with rate constants k_1, k_2 and k_3 respectively. In the fitting process k_1, k_2 and k_3 were allowed to vary, to reflect the change in quenching and annihilation in the various samples upon aggregation. Chl 2 and Chl 3 are quenched via the quenching state Q (quencher) with a rate constant k_q. Both Chl 2 (fast) and Chl 3 (slow) contain an annihilation channel to account for the multi-exponential character of singlet-singlet annihilation that may occur (rate constants k_4 and k_5 respectively). Both compartments also populate the long-living triplet state with a rate constant k_7 corresponding to a very small yield. Chl 4 represents unquenched chlorophyll, which is present in the unquenched and mildly quenched (k_d=2) samples, but not in the highly quenched (k_d=9) sample. Chl 4 populates the long-living triplet state with rate constant k_7 and decays to the ground state with rate constant k_8. Rate

constant k_8 is also present from Chl2 and Chl3, but has been omitted from the scheme, for clarity. The rate constants that were obtained from the data-fitting process are shown in Table 1.

	trimers	K_d=2	K_d=9
k_1	$(15.87ps)^{-1}$	$(8.54ps)^{-1}$	$(2.39ps)^{-1}$
k_2	$(17.85ps)^{-1}$	$(3.74ps)^{-1}$	$(1.3ps)^{-1}$
k_3	$(2.87ps)^{-1}$	$(4.38ps)^{-1}$	$(51.8ps)^{-1}$
k_4	$(25ps)^{-1}$	$(25ps)^{-1}$	$(25ps)^{-1}$
k_5	$(400ps)^{-1}$	$(400ps)^{-1}$	$(400ps)^{-1}$
kq	$(770ps)^{-1}$	$(670ps)^{-1}$	$(217ps)^{-1}$
k_6	$(8ps)^{-1}$	$(8ps)^{-1}$	$(8ps)^{-1}$
k_7	$(10ns)^{-1}$	$(10ns)^{-1}$	$(10ns)^{-1}$
k_8	$(10ns)^{-1}$	$(10ns)^{-1}$	$(10ns)^{-1}$

Table 1 Rate constants obtained from the kinetic model in Figure 6 for the three samples. Estimated error in the rate constants k_1, k_2, k_3, and k_q is about 10%, the other rate constants were fixed.

Figure 7 shows the kinetic traces at different wavelengths for each of the samples and their corresponding fits obtained from the kinetic model described above.

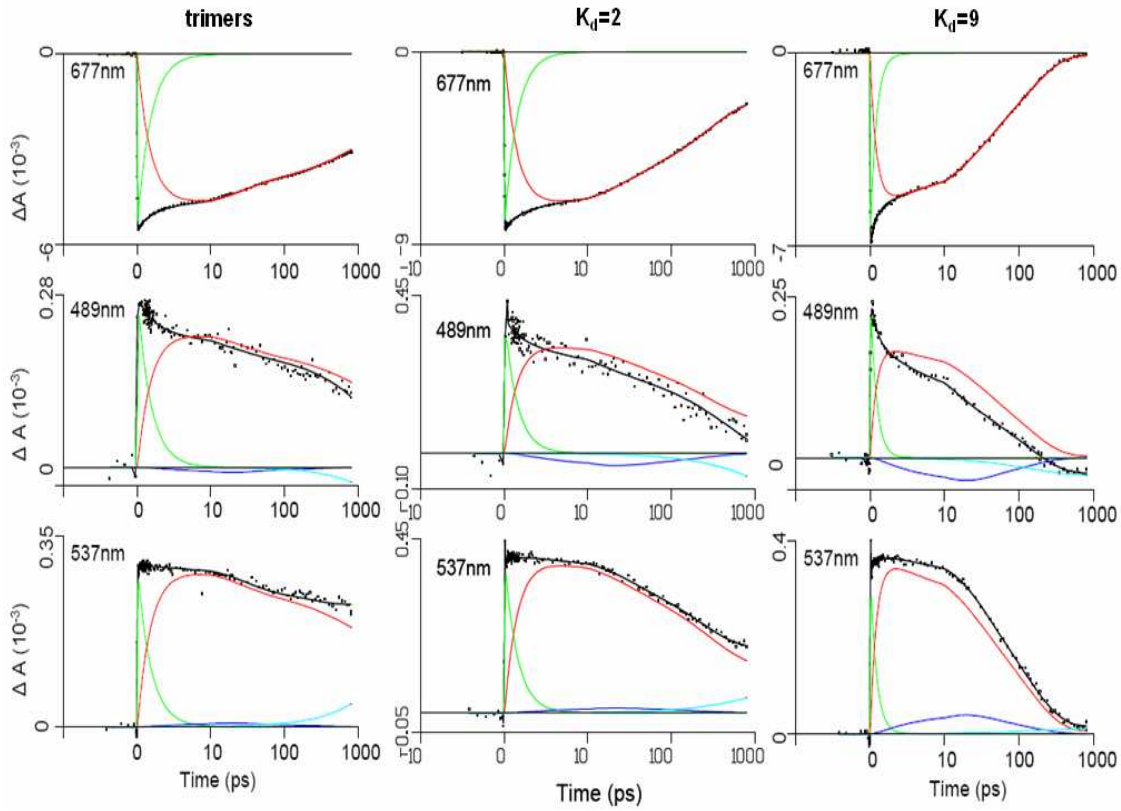

Figure 7 Transient absorption traces. ΔA=absorption changes; X=axis is linear from -10 to 10 and logarithmic thereafter. The black curves represent the fit using the model depicted in Figure 6. Green represents 1ps phase due to chlorophyll excited state relaxation; red=chlorophyll excited state decay; cyan=development of the carotenoid triplet state; blue=absorption changes due to the quencher Q.

At 677 nm, the traces show an initial bleach of the chlorophyll ground state absorption. This bleach relaxed(green trace) as chlorophyll excited state decayed (red line) to its ground state. As expected, the decay of the chlorophyll excited state was faster as the degree of quenching increases. The traces at 489 nm, situated in the region where the ground state of the carotenoid bleaches, and at 537 nm, corresponding to carotenoid excited state absorption, were very similar for the trimer. In contrast, for the quenched samples the traces at these two wavelengths differed significantly. This difference was accounted for in the model by the presence of the chlorophyll excited state decay contributing to the trace at 489 nm on the 10-20 ps timescale, but which is not present in the 537 nm traces. A comparison between the chlorophyll excited state decays reflected in the traces at 677 nm and 537 nm shows a slower decay for the latter, indicating that, simultaneously with the chlorophyll excited state decay, another species is transiently populated. This species has the excited state absorption in this region and is likely to be a carotenoid S1 state- its appearance and decay are shown by the blue trace in Figure 7. The same feature is present in the samples with an intermediate degree of quenching in the traces at 537 nm but the amplitude of this absorption change is much lower. Its contribution is negligible in the unquenched trimeric sample. In order to verify the importance of including this feature in the model, for the samples with k_d=9, the 489 nm and 537 nm traces were fitted without including quenching via the carotenoid excited state (Figure 8). It can be clearly seen that the quality of the fitting was reduced significantly when the quenching via a carotenoid excited sate was not taken into account in the model.

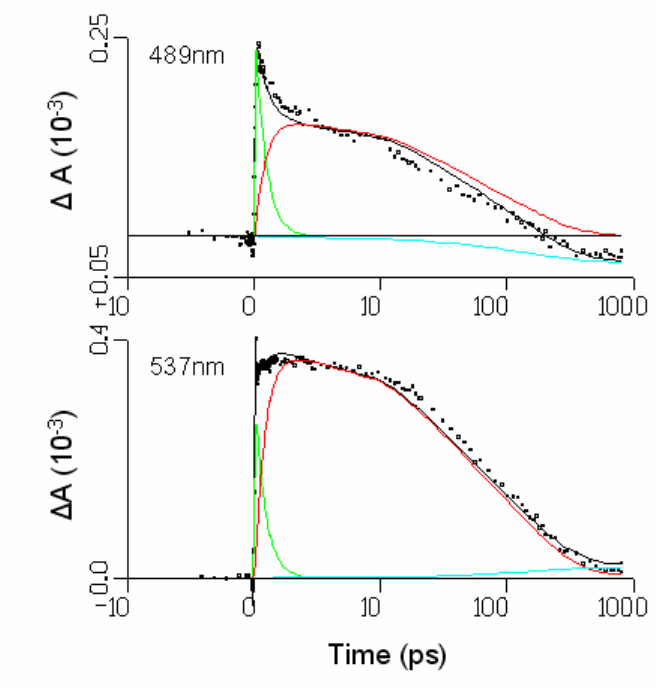

Figure 8 Selected kinetic traces at 489 and 537 nm for the sample having k_d=9. The corresponding fit was obtained by applying a kinetic model without quenching via a carotenoid excited state.

In order to investigate whether quenching occurs via energy transfer and/or a charge-separated state (Holt et al., 2005), extensive probing of the 900-1000 nm region was made. Figure 9 shows selected kinetic traces in the near-IR region (963 nm) for the quenched sample. The fit of the data was obtained from a model consisting of three lifetimes: a ~100 fs component to account for ultrafast relaxation, a ~12 ps component to account for singlet-singlet annihilation of chlorophyll excited states and a 160 ps component which corresponds to the lifetime of the chlorophyll excited state. The signal in this region was flat and followed the same dynamics as the chlorophyll excited state absorption, revealing no changes that could be assigned to the presence of a carotenoid radical formed during the quenching process.

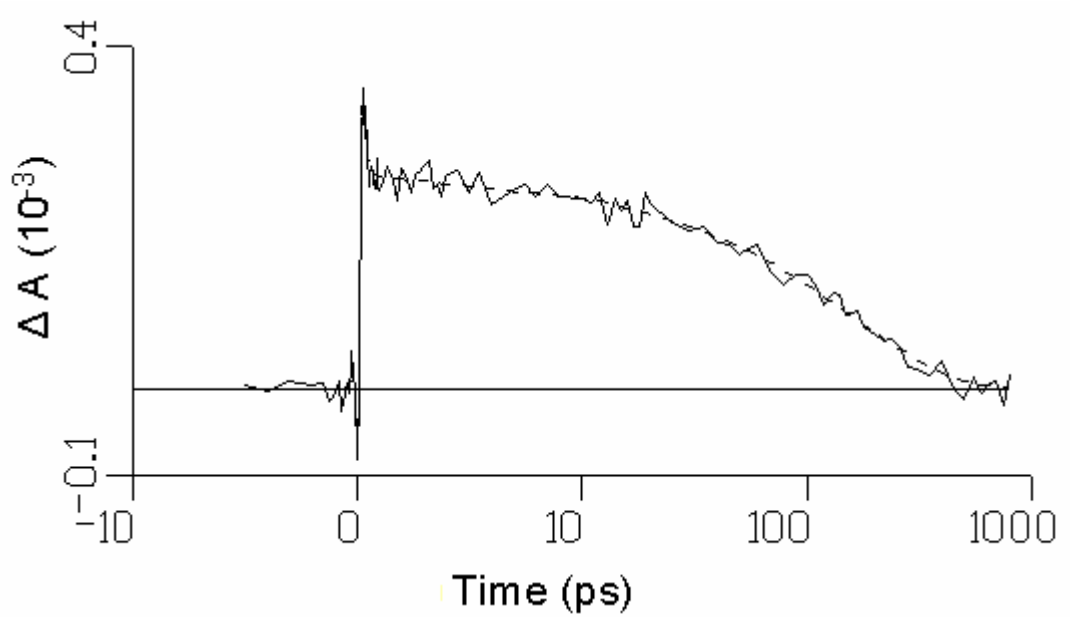

Figure 9 Selected kinetic traces in the near-IR (963 nm) region for the quenched sample (see text for details).

From these results it can be concluded that the chlorophyll fluorescence quenching in the quenched LHCII samples occurs via a carotenoid excited state.

Taking into account that the samples used contain only traces of violaxanthin and no zeaxanthin or antheraxanthin (see also 3.2.1 for detailed information), the only possible candidates to which the absorption changes can be assigned are neoxanthin and lutein. In order to identify which of these two carotenoids was involved, species associated spectra (SADS) for the sample with k_d=9 were obtained according to the model presented in Figure 6. Figure 10 shows the SADS of the 5 compartments of the model. The dark-green spectrum represents the first (Chl 1) pool of chlorophyll and the dark-yellow spectrum represents the Chl 2 and Chl 3 pools (the latter two are identical and represented by one spectrum). The cyan spectrum corresponds to the long-living carotenoid triplet state and the red spectrum is that of the quenching state, Q.

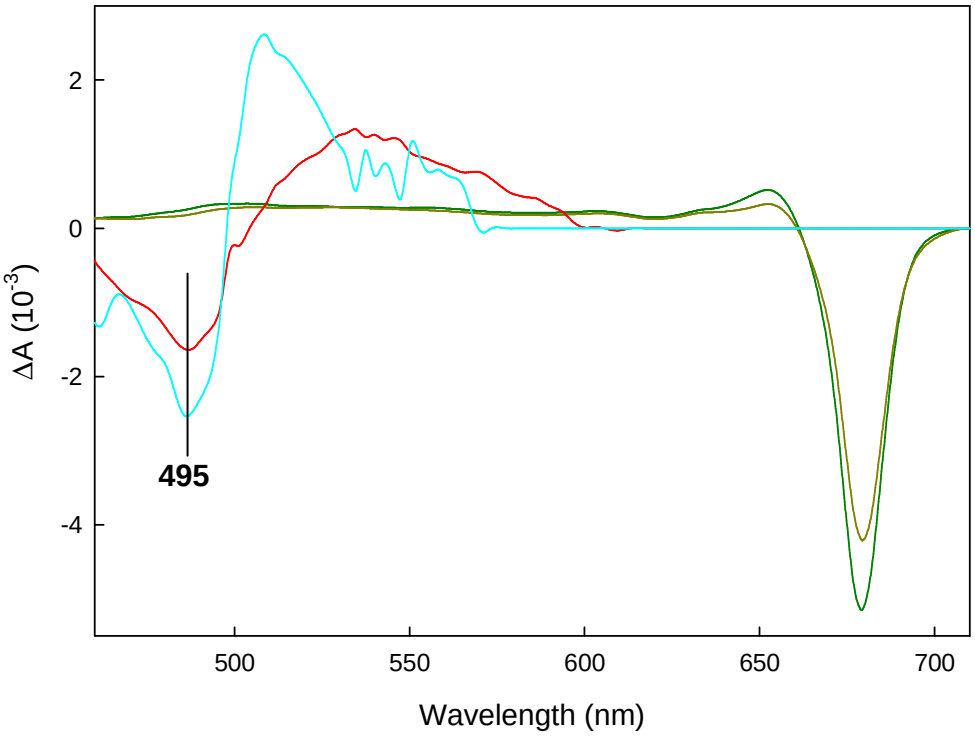

Figure 10. SADS for the sample with k_d=9 after target analysis model depicted in Figure 6. Dark-green spectrum represents the Chl 1 (chlorophyll) compartment, dark-yellow spectrum Chl 2 and Chl 3. Cyan spectrum represents the carotenoid triplet and the spectrum of the quencher is represented in red. By vertical line is shown the bleaching of the carotenoid triplet and of the quencher.

It can be seen that the bleach of the carotenoid triplet and the bleach of the quencher both peak at ~495 nm (negative peaks indicated by vertical line, Figure 10), which is known to belong to lutein 1 (Lampoura et al 2002). Thus, it may be concluded that lutein 1 is likely to be the quencher.

6.3 Conclusions

Time-resolved absorption spectroscopy was applied to LHCII in different quenching states. The results of the measurements showed that in the aggregated samples a carotenoid excited state was populated concomitant with the decay of the chlorophyll excited state, indicating energy transfer from chlorophylls to carotenoid. This excited state was identified as a low-lying S1 state of the LHCII-bound carotenoid lutein 1. The spectral evolution in the carotenoid absorption region showed the same features as those observed before by Berera et al. (2006) in artificial carotenoid-phthalocyanine dyads, in which it was demonstrated that quenching occurs via the population of this carotenoid excited (S1) state.

CHAPTER SEVEN

General discussion

7.1 Introduction

Photosynthesis in plants is an efficient process, collecting light energy even in extremely low light conditions and transferring this energy towards the reaction centres of the two photosystems, where primary photochemistry takes place. However, this process is also regulated when the incoming light energy is above that which can be used in electron transport (high light conditions), the light-harvesting antenna is able to switch into a photoprotective mode, dissipating the excess energy as heat. This dissipative process is known as non-photochemical quenching of chlorophyll fluorescence (NPQ). In higher plants the major component of NPQ is qE (feed-back de-excitation or energy dependent quenching) and this is dependent upon the formation of a ΔpH across the thylakoid membrane (Briantais et al., 1979). qE is facilitated by the de-epoxidation of violaxanthin to zeaxanthin during the xanthophyll cycle (Demmig-Adams, 1990) and additionally a crucial role has been shown to be played by the PsbS protein, since elimination of the protein results in a drastic reduction in qE (Li et al., 2000). Carotenoids have been found to play a vital role in photoprotection of the photosynthetic apparatus, by quenching chlorophyll triplets as well as scavenging harmful singlet oxygen. They are also involved in the mechanism of NPQ especially via the xanthophyll cycle. The mechanism of how the xanthophyll cycle zeaxanthin is involved in NPQ in not completely resolved and zeaxanthin may have either a direct or an indirect role in NPQ. Lutein is also proposed to have a role in NPQ (Lockstein et al., 2002).

Presented in this thesis is a detailed analysis of LHCII *in vitro* and *in vivo* using different spectroscopic approaches, in order to give a better understanding of the energy transfer between its bound pigments. Although several hypotheses have been proposed, the precise mechanism of excess energy dissipation has not been conclusively determined. New results presented in this thesis provide a step forward in the understanding of this non-photochemical mechanism(s).

7.2 Efficiency of energy transfer from xanthophylls to chlorophylls

Chapter 3 of this thesis presented a new approach to determine the contribution in the 77K absorption spectrum of lutein 2. This lutein molecule in trimeric LHCII has a red-shifted absorption (510 nm) compared to lutein 1 (495 nm). The absorption feature situated at around 510 nm was originally thought to arise from the xanthophyll violaxanthin. Peterman et al. (1997) reported the 4K absorption spectra of the

monomeric and trimeric LHCII, along with their calculated second derivative. It was found that during the monomerisation process the 510 nm transition disappeared. As pigment analysis by HPLC indicated that violaxanthin was (a) present in substoichiometric amounts in the trimer (thus potentially explaining the low intensity of the band) and (b) completely lost upon monomerisation, the authors concluded that this band arose from violaxanthin. However, using the highly selective resonance Raman technique it was found that the band could in fact be attributed to one of the luteins (lutein 2), this molecule being found in a twisted conformation in the trimer (Ruban et al., 2000). This twist was followed by analysing the ν_4 region of the spectrum where enhanced modes can be observed when excitation was set at 501, or at 514 nm (exciting mainly the lutein 2 molecules). Upon monomerisation some of the Raman modes are not observed, suggesting relaxation of this twisting. It was suggested that the new modes present in the resonance Raman spectrum of trimers may be induced by conformational changes in each monomer upon trimerisation (Ruban et al., 2000). In a later study (Ruban et al., 2001) it was suggested that the difference in the amplitude of the 495 nm band (lutein 1) and the 510 nm (lutein 2) may arise from a smaller extinction coefficient of the latter pigment, but the authors also stated that a more likely explanation was the observation that the 510 nm band is at least 70% broader than the one at 495 nm.

This hypothesis was tested in Chapter 3. A mathematical calculation of the second derivative performed on a Gaussian function showed that the amplitude of the second derivative was smaller for broader bands. Curve-fitting analysis performed on the absorption spectrum of LHCII trimer, showed that the 510 nm band was not a minor component of the spectrum, but had almost the same contribution as the 495 nm band. Interestingly, the red-shifted lutein was found in the newly-synthesised trimers of the antisense *asLhcb2 Arabidopsis* plants, which lack the Lhcb1 and Lhcb2 proteins of LHCII. These Lhcb5- and Lhcb3-containing trimers apparantly provide the same environment for lutein 2 (lut2) as in the major LHCII in the wild type. The origin of the red-shift may be new interaction between pigments during the trimerisation process. It can be proposed in this case that trimerisation creates an intermonomer lutein 2-Chl *a*603 (the closest pigment) associate (Figure 1a). Lutein 2 and Chl *a*603 are in van der Waals contact (3.35 Å) in the newly created associate and that could red-shift the lutein absorption band.

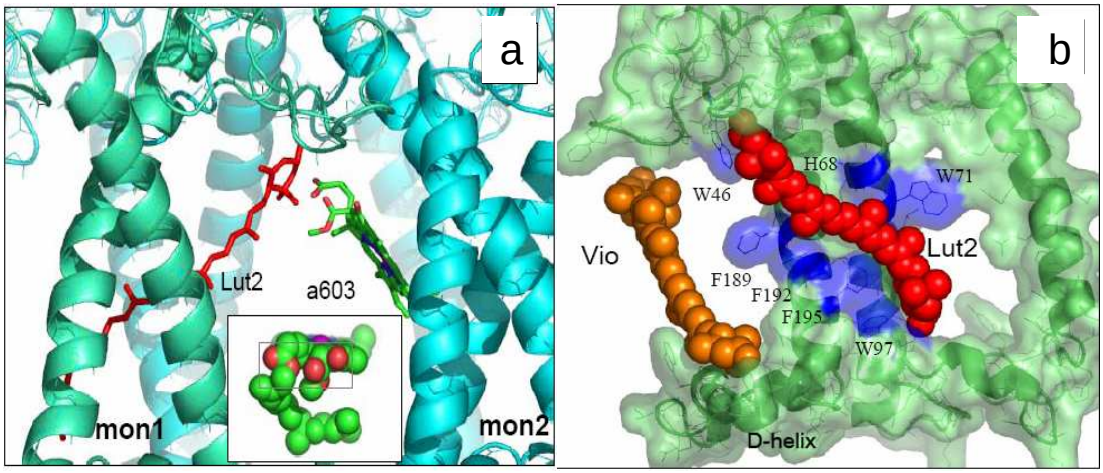

Figure 1. Lutein 2 – Chl *a*603 locus. Red is lutein 2 and green Chl *a*603 (a). Inset Chl *a*603 with all 5 polar oxygen-containing groups (red) facing lutein 2; (b) Lutein 2 (red) and violaxanthin (brown) binding sites. Highly conserved aromatic residues are indicated and highlighted in blue (Liu et al., 2004).

Shown in the inset to Figure 1a are the oxygens from the Chl *a*603, which faces the head group of the lutein molecule. The oxygens can exert a strong polarising field, leading to an increase in the xanthophyll dipole moment, which was indeed found to be large (Palacios et al., 2003), and consequently induce the shift of the lutein absorption. An alternative explanation for the red-shift may be found in the lutein environment on the monomer of the trimeric LHCII. There are 7 closely located aromatic residues (W46, W71, W97, F189, F192, F195, and H78) that have delocalised π-electron systems and these may affect the excited state energy level of lutein 2 and consequently red shift its absorption (Figure 1b).

The energy transfer efficiency from xanthophylls to chlorophyll *a* was estimated by comparing the absorption and excitation spectra. It was found that xanthophylls exhibited an efficiency of energy transfer of 80-90 %, consistent with previous data (van Amerongen & van Grondelle, 2001).

Comparative studies of the absorption and fluorescence excitation of the wild type and *asLhcb2* thylakoids revealed that there were no major alterations in xanthophylls to chlorophyll energy transfer. However, the 510 nm (lutein 2) band, exhibited a slight increase of the amplitude in the fluorescence excitation spectra, indicating that lutein 2 has higher energy transfer efficiency in the antisense plants. Because of the instability of the trimers isolated from the antisense plants, an exact estimation of energy transfer efficiencies for all of the xanthophylls was not possible, and estimation of these coefficients from the thylakoid spectra was impossible because of the complexity of the spectra.

Thylakoid membranes containing only violaxanthin or enriched in zeaxanthin were studied. Comparison of the absorption and fluorescence excitation spectra suggested that a conformational change in the antenna may occur as a result of the high-light treatment and the appearance of zeaxanthin. The light *minus* dark 1-T difference spectrum was a typical zeaxanthin *minus* violaxanthin spectrum, but, surprisingly, the excitation difference spectrum was differently structured. The difference between these two spectra could be explained by a change in the energy transfer coefficients of some pigments present in the thylakoid membrane after the light treatment. Upon illumination no differences in the chlorophyll *a*, chlorophyll *b*, neoxanthin, or lutein content were observed. Hence, the changes must have arisen because of the change in the xanthophyll cycle content and possible from a resulting conformational change in the antenna proteins. The double difference spectrum calculated by substracting the 1-T difference spectrum from the excitation difference spectrum, resembled a violaxanthin spectrum, suggesting that a population of the violaxanthin pool (which is not de-epoxidised) may become involved in energy transfer to the PSII cores after light treatment. It was shown that violaxanthin molecules are relatively strongly bound to the light-harvesting antenna, and therefore not all of the violaxanthin pool is easily accessible to the VDE enzyme for de-epoxidation (Ruban et al., 1994; Ruban et al., 1999). Violaxanthin was shown to bind tightly to CP29 (Ruban et al., 1999) and therefore a proportion of the above mentioned changes may be associated with this xanthophyll pool. It can be suggested that, during the illumination, changes occurred in the thylakoid membrane that triggered the movement of the CP29 complexes in the vicinity of the PSII cores (Figure 2), simultaneously with a conformational change in the protein, giving violaxanthin a more favourable position to transfer energy to the PSII cores. Alternatively, a conformational change in the LHCII domain following de-epoxidation may have co-operatively altered all of the V1 sites, so changing the configuration of the remaining violaxanthin, enhancing its ability to transfer energy to PSII.

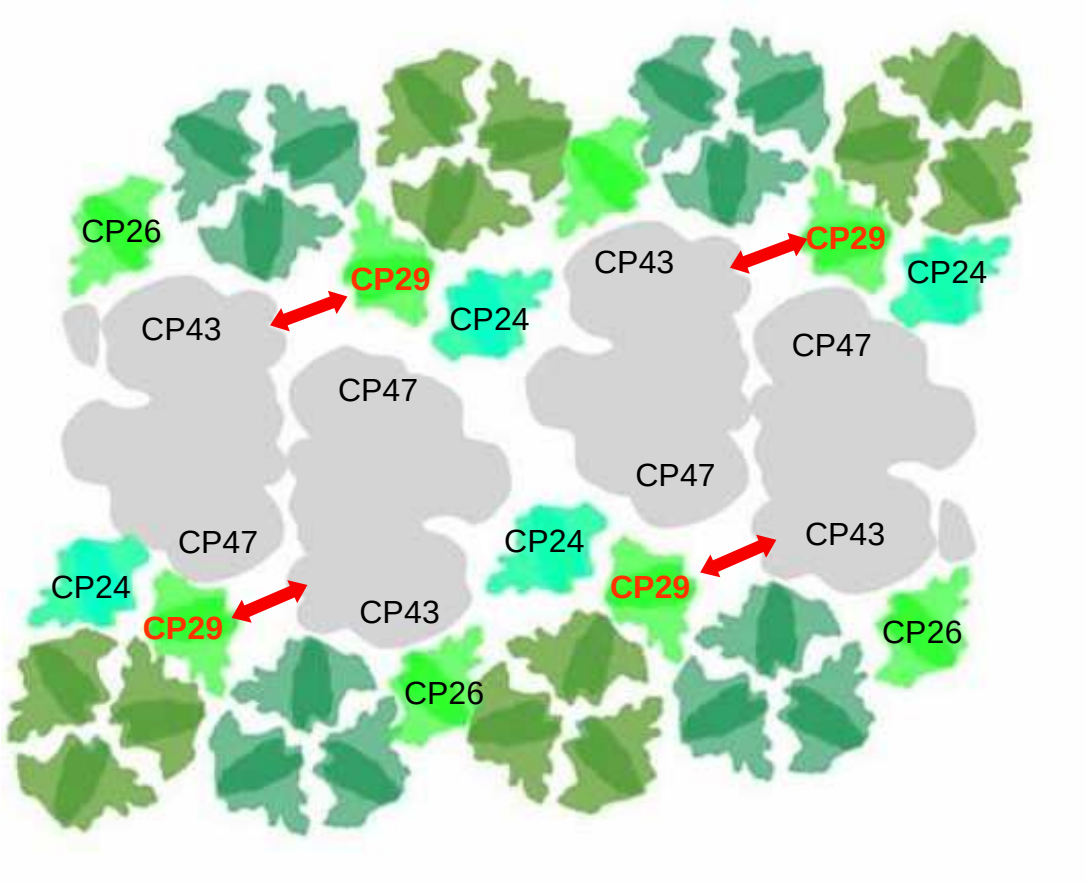

Figure 2. Possible mechanism of CP29 relocation caused by de-epoxidation within PSII macrostructure. The double headed red arrows indicated the possible CP29 relocation towards the PSII supercomplexes

7.3 Quenching without protein aggregation involves a conformational switch in LHCII subunits

Spectroscopic and biochemical analysis of isolated LHCII complexes incorporated in a solid gel system were performed during the transition to a photoprotective (low fluorescence) state (Chapter 4). These results strengthen the evidence that quenching does not require protein-protein interaction, but, instead, is caused by a conformational change within the monomeric (or trimeric) subunits of the complexes. Several lines of evidence indicated that quenching occured in the absence of aggregation in this system. Firstly, analysis of room temperature absorption spectra revealed the absence of the typical red 'tail' associated with the presence of large aggregates. Secondly, LHCII in the gel system, present in a variety of quenched and unquenched states, was completely mobile when ran in an electrophoresis gel, mirroring the behaviour of trimers/monomers rather than aggregates.

The occurrence of a conformational change in the protein during the transition to this low fluorescence state was also investigated in the gel system. The cross-linker

glutaraldehyde affected both the transition to the quenched state (when the detergent was diluted from the complex) and the relaxation from this state (when detergent was added). This suggested again that the protein underwent a conformational change during the transition to the photoprotective state, the cross-linker effectively "freezing" the complex in one conformation or the other. The absorption and CD changes, together with the twisted configuration that LHCII-bound neoxanthin exhibited in the quenched LHCII (Ruban et al., 1995; Pascal et al., 2005), indicated an involvement of this xanthophyll binding site in the conformational switch to the quenched state. This suggestion is consistent with the strong excitonic structure in the quenched LHCII state in the chlorophyll *b* region (Ruban et al., 1997), which could be explained by the formation of a stable rigid dimer of *b*606 and *b*607 potentiated by two water molecules (Pascal et al., 2005, see Figure 3). Chlorophyll *a*604 is located in very close contact with the *cis*- 'leg' of the neoxanthin molecule and thus could also be involved in the dynamics of this domain in LHCII. The observed changes in absorption and CD in the region (around 662 nm) where this chlorophyll peaks (van Grondelle & Novoderezhkin, 2006), indicated that this chlorophyll was affected during the establishment of the quenching state.

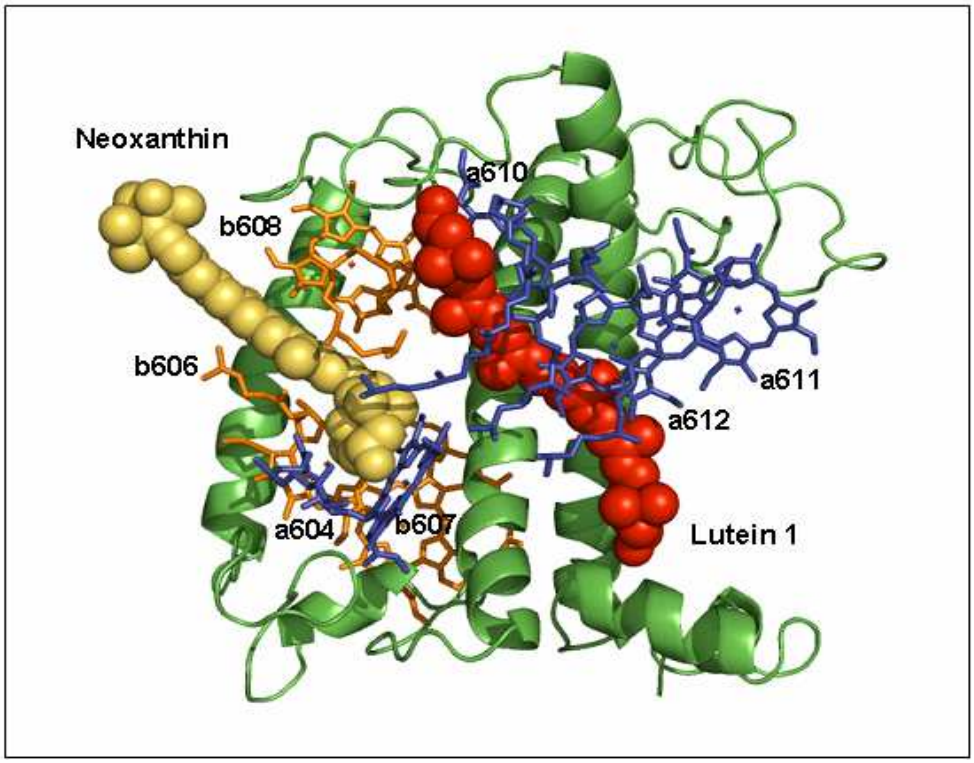

Figure 3. Possible sites of quenching in LHCII: neoxanthin and lutein 1 domain. Chlorophyll *a* are shown in purple, chlorophyll *b* in orange, neoxanthin in yellow, lutein 1 in red and the polypeptide bones in green (Liu et al., 2004).

Other changes were observed in the chlorophyll *a* pigments in both Soret and Qy region of the absorption spectrum, which indicate that the terminal emitter domain consisting in the chlorophylls *a*610, *a*611 and *a*612 was also affected during the transition to the quenched state. These changes, which were correlated with the alteration in the CD spectrum indicate that another domain was involved in the quenching-associated dynamics. Even during the very first stages of quenching, there was a change in the absorption spectrum (681 nm), attributed to the chlorophylls within the terminal emitter domain. Further quenching was followed by an enhancement and then a decrease of this feature, overtaken by a strong drop in oscillator strength of this group of pigments and a decrease in the corresponding CD feature (678 nm). As the quenching state became stronger, the absorption change in the carotenoid region became broader and more complex, indicating the involvement of lutein 1 in the process. It had previously been suggested that this domain is the likely site of quenching (Wentworth et al., 2003; Pascal et al., 2005) due to chlorophyll *a*-chlorophyll *a* and/or chlorophyll *a*-lutein 1 interaction. The data indicated that the transition into the quenching mode was progressive and gradual. Previously, it had been assumed that LHCII switched between just two states, and that the extent of quenching is determined by the proportion of the LHCII population in each state. However, here evidence was obtained that the formation of the quencher evolved through a number of different conformational states of LHCII.

7.4 *In vivo* detection of a light-induced conformational change of LHCII

It had been suggested from studies on aggregates of LHCII (Horton & Ruban, 1992), LHCII crystals (Pascal et al., 2005) and here the aggregation-free LHCII-gel that, during the transition to the dissipative state, LHCII undergoes a conformational change. This change appears to be an intrinsic feature of each LHCII (sub)unit, which results in a modification of pigment orientation, leading to formation of a quenching centre and hence an increase in energy dissipation. Many features of the quenching in aggregated state of LHCII resemble the NPQ process *in vivo* (Horton et al., 1996), but there was no experimental proof that this conformational state occurred *in vivo*.

Chapter 5 describes how the highly selective resonance Raman technique revealed a light-induced conformational change *in vivo* in chloroplasts and leaves after NPQ induction. This conformational change was monitored by a twisting of the LHCII-bound neoxanthin molecule, and it was found that the extent of the change in the Raman

signal was correlated with the amount of NPQ, when compared to the *in vitro* model system (LHCII aggregation). The predicted value of the Raman change associated with qE *in vivo*, was very similar to that observed *in vitro*, consistent with the hypothesis that quenching occurs through the same mechanism in each case.

7.5 Identification of the quencher in LHCII present in dissipative state

Femtosecond transient absorption spectroscopy performed on LHCII in a highly dissipative state showed that a carotenoid S1 excited state was populated on the same timescale as the chlorophyll excited state decay (Chapter 6). This carotenoid was identified as lutein 1. Thus, it can be suggested that the conformational change detected by resonance Raman spectroscopy opens up a pathway for energy dissipation within LHCII whereby chlorophyll(s) *a* transfers energy to a low-lying S1 excited state of lutein 1. Although a mechanism in which lutein 1 excited state acts as the chlorophyll fluorescence quencher can completely account for qE *in vivo*, other processes could be involved, but perhaps only to a relatively small extent. One of these processes may involve formation of a zeaxanthin cation. Transient absorption spectroscopy of isolated thylakoids suggest that the mechanism of qE is the energy transfer from the chlorophyll excited state to zeaxanthin followed by the formation of a zeaxanthin radical cation (Ma et al., 2003; Holt et al., 2005). It has been suggested that the zeaxanthin cation radical is preferentially formed in the CP29, CP26, CP24 minor complexes, which are hence the main sites of qE (Avenson et al., 2007).

7.6 How does the conformational change give rise to quenching?

The results described in this thesis add considerably to the evidence for the dynamic nature of the light-harvesting antenna in which conformational changes control the properties of the bound pigments. Recently, based on the crystal structure of the cucumber LHCII at 2.66 Å it was hypothesized how a conformational change involving lutein 1 might take place (Yan et al., 2007). LHCII crystals of different age show a decrease of the crystal unit cell as a result of dehydration. The dehydration of the crystals is accompanied by a shift of the maximum fluorescence emission peak from 680 nm to 700 nm (Yan et al., 2007), the feature associated with the quenched state, not only in LHCII crystals but also in LHCII aggregates (Ruban et al., 1991), in the LHCII-gel system (see Chapter 4) and even *in vivo* (Tang et al., 2007; Horton et al., 1996). The extent of quenching of chlorophyll fluorescence correlates with crystal age, the older

crystals being more quenched and their fluorescence maximum more red-shifted. It was then concluded that dehydration, which could mimic the effect of ΔpH formation across the thylakoid membrane, induces a conformational change within the LHCII crystal. This conformational change would result in a rotation of the lutein 1 molecule towards the Chl *a*612-Chl *a*611 dimer to form a hetero-trimer of pigments, lutein 1 becoming more twisted than lutein 2 (as found in the highly quenched crystals). The identification of lutein 1 as the quencher is entirely consistent with this model.

However, it is interestingly that in the resonance Raman measurements the predicted twist of the lutein 1 was not found when comparing quenched and unquenched samples (Pascal et al., 2005). There are enhanced modes in the ν_4 region of the Raman spectrum when the excitation (496, 501 and 514 nm) is set to selectively excite the lutein molecules, but these modes have been assigned to the other lutein (lutein 2) present in LHCII (Ruban et al., 2000; Ruban et al., 2001). This molecule is distorted during the trimerisaton process (associated with the 510 nm band discussed above). In the quenching process only neoxanthin exhibits a clear twisting as compare to free trimers and it can be suggested that the lutein 1 molecule perhaps needs only a very small (undetectable) change in its configuration to become the quencher. This change could result from a possible electrostatic effect created by the twisting of neoxanthin, causing lutein 1 to move closer to the terminal emitter chlorophylls *a*610, *a*611 and *a*612. Such transmission of conformational "information" from the neoxanthin domain to the quenching domain is depicted in Figure 4. The resulting small modification in the configuration of the lutein 1 then allows its S1 state to accept energy from the chlorophyll Qy state and then decays to its ground state dissipating the energy as heat.

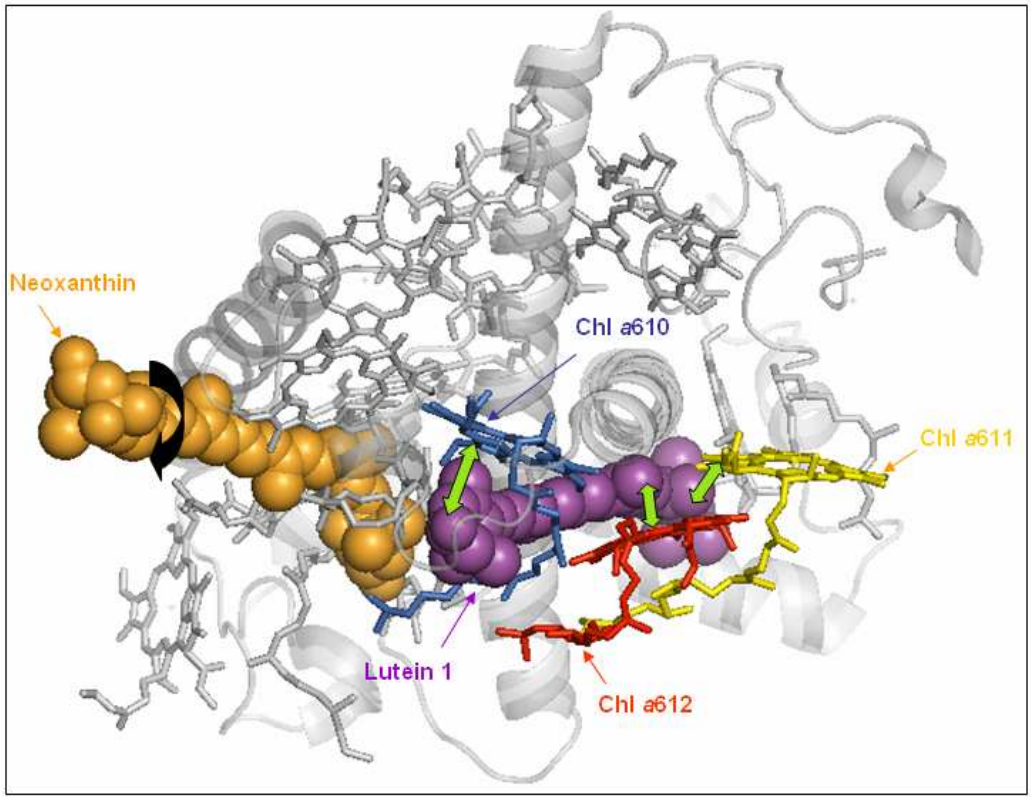

Figure 4. Model for mechanism of NPQ, showing the quenching site with the pigments involved. Lutein 1 (magenta) present in the vicinity of the terminal emitter domain consisting in Chl *a*610 (blue), Chl *a*611 (yellow) and Chl *a*612 (red). Green arrows indicate the possible movement of the lutein 1 towards chlorophylls. Also shown neoxanthin (orange) twisting (black arrow). In gray are depicted the other chlorophylls and the polypeptides residues present in LHCII monomer (Liu et al., 2004).

In the future it should be possible to further determine the molecular details of the conformational change in LHCII. At present, only the changes in the configuration of some pigments have been identified, and there is no understanding of how the protein changes conformation. Furthermore, how these changes are triggered by the ΔpH, how they are regulated by the xanthophyll cycle, and how these events are dependent upon PsbS remain unknown.

7.7 Prospects for future research

Isolated light-harvesting complexes are a good model for study NPQ process; as shown in this thesis the results from the *in vitro* studies were consistent with the *in vivo* measurements. It is now clear that insights into the molecular mechanism(s) of the conformational change that occur in the light-harvesting antenna would be revealed by further studies of the isolated complexes for which fine detailed structures and functions can be determined.

The exact role of the xanthophylls in the control of energy dissipation may be revealed by detailed characterization of the isolated complexes with different carotenoid content. These complexes may be isolated by mild solubilisation techniques (FPLC, sucrose gradient centrifugation) from the available mutants (*npq1*, *npq2*, *lut1*, *lut2*, or double/triple mutants of these) and/or antisense plants, followed by *in vitro* oligomerisation and analysis of the systems in different dissipative states. Also, isolation by mild detergent solubilisation of the intact oligomeric LHC antenna would provide a new system for studying quenching mechanism *in vitro,* where the proteins are present in an environment which resembles more closely their natural one. The role of the PsbS protein may be further investigated by following the isolation of the LHCII with and without PsbS, via oligomers prepared from the *npq4* mutant and L17 overexpressor plants. In parallel all these complexes mentioned above can be further studied by immobilisation in the newly developed gel system.

The nature of the chlorophyll fluorescence quencher in LHCII and *in vivo* has to be further studied, for example, to determine whether there is more than one mechanism involved. This study should include investigations of different isolated complexes (as suggested above) and intact systems such as chloroplast membranes or whole leaves using the spectroscopic techniques used here (transient absorption, resonance Raman, CD, steady-state fluorescence etc).

.

REFERENCES

Abrahams JP, Buchanan SK, van Raaij MJ, Fearnley IM, Leslie AGW, Walker JE (1994) Structure at 2.8Å resolution of F1-ATPase from bovine heart mitochondria. Nature **370**, 621-628

Adams WW, Demmig-Adams B, Winter K (1990) Relative Contributions of Zeaxanthin-Related and Zeaxanthin-Unrelated Types of 'High-Energy-State' Quenching of Chlorophyll Fluorescence in Spinach Leaves Exposed to Various Environmental Conditions. Plant Physiology **92**, 302-309

Andersson J, Wentworth M, Walters RG, Howard CA, Ruban AV, Horton P, Jansson S (2003) Absence of the Lhcb1 and Lhcb2 Proteins of the Light-Harvesting Complex of Photosystem II - Effects on Photosynthesis, Grana Stacking and Fitness. Plant Journal **35**, 350-361

Arntzen CJ, Ditto CL (1976) Effects of cations upon chloroplast membrane subunit. Interactions and excitation energy distribution. Biochim Biophys Acta **449**, 259–274

Aro E-M, Virgin I, Andersson B (1993) Photoinhibition of Photosystem II. Inactivation, Protein Damage and Turnover. Biochemica et Biophysica Acta **1143**, 113-134

Arvidsson PO, Bratt CE, Andreasson LE Åkerlund HE (1996) Purification and identification of the violaxanthin de-epoxidase as a 43 kDa protein. Photosynthesis Research **44**, 81-91

Aspinall-O'Dea M, Wentworth M, Pascal A, Robert B, Ruban A, Horton P (2002) In Vitro Reconstitution of the Activated Zeaxanthin State Associated with Energy Dissipation in Plants. PNAS **99,** 16331-16335

Avenson TJ, Ahn TK, Zigmantas D, Niyogi KK, Li Z, Ballottari M, Bassi R, Fleming GR (2008) Zeaxanthin Radical Cation Formation in Minor Light-harvesting Complexes of Higher Plant Antenna. J. Biol. Chem. **283**, 3550-3558

Bailey S, Walters RG, Jansson S & Horton P (2001) Acclimation of *Arabidopsis thaliana* to the Light Environment: the Existence of Separate Low Light and High Light Responses. Planta **213**, 794-801

Barber J (1998) Photosystem II. Biochimica et Biophysica Acta **1365**, 269-277

Barry B, Boerner RJ, De Paula JC (1994) The Use Of Cyanobacteria In The Study Of The Structure And Function Of Photosystem II. In The Molecular Biology of Cyanobacteria (Bryant, Da Ed). Kluwer Academic, Dordrecht, 217-257

Barzda V, de Grauw CJ, Jurrien Vroom J, Kleima FJ, van Grondelle R, van Amerongen H, Gerritsen HC *(2001)* Fluorescence Lifetime Heterogeneity in Aggregates of LHCII Revealed by Time-Resolved Microscopy. Biophysical Journal **81**, 538-546

Bassi R, Pineau B, Dainese P, Marquardt J (1993) Carotenoid-binding Properties of Photosystem II. European Journal of Biochemistry **212**, 297-303

Bassi R. (1996) Biochemistry and molecular biology of pigment binding proteins. In *Light as an energy source and information carrier in plant physiology* (Jennings, Zucchelli, Ghetti, Colobbetti. Eds.), Plenum Press New York, 41-63

Bassi R, Croce R, Cugini D, Sandona D (1999) Mutational Analysis of a Higher Plant Antenna Protein Provides Identification of Chromophores Bound into Multiple Sites. PNAS **96**, 10056-10061

Ben-Shem A, Frolow F, Nelson N (2003) Crystal Structure of Plant Photosystem I. Nature **426**, 630-635

Berera R, Herrero C, van Stokkum IHM, Vengris M, Kodis G, Palacios RE, van Amerongen H, van Grondelle R, Gust D, Moore TA, Moore AL, Kennis JTM (2006) A Simple Artificial Light – Harvesting Diad as a Model for Excess Energy Dissipation in Oxygenic Photosynthesis. PNAS **103**, 5343-5348

Berg JM, Tomoczko JL Streyr L (2002) In *The light reactions of photosynthesis* In: Biochemistry (eds Berg J.M., Tomoczko J.L. and Streyr L.) Freeman and Company, New York, **5**, 527-547

Bergantino E, Dainese P, Cerovic Z, Sechi S, Bassi R (1995) A Post translational Modification of The Photosystem-II Subunit CP29 Protects Maize from Cold Stress. Journal of Biological Chemistry **270**, 8474-8481

Bergantino E, Segalla A, Brunetta A, Teardo E, Rigoni F, Giacometti GM, Szabo I (2003) Light- and pH-dependent Structural Changes in the PsbS Subunit of Photosystem II. Proceedings of the National Academy of Sciences, **100**, 15265-15270

Bilger W, Bjorkman O, Thayer SS (1989) Light-Induced Spectral Absorbance Changes in Relation to Photosynthesis and the Epoxidation State of Xanthophyll Cycle Components in Cotton Leaves. Plant Physiology **91**, 542-551.

Boekema EJ, Hankamer B, Bald D, Kruip J, Nield J, Boonstra AF, Barber J, Rögner M (1995) Supramolecular Structure of the Photosystem II Complex from Green Plants and Cyanobacteria. Proceedings of the National Academy of Sciences **92**, 175-179

Boekema EJ, Van Roon H, Calkoen F, Bassi R, Dekker JP (1999) Multiple Types of Association of Photosystem II and its Light-Harvesting Antenna in Partially Solubilized Photosystem II Membranes. Biochemistry **38**, 2233-2239

Boekema EJ, Van Roon H, Van Breemen JFL, Dekker JP (1999) Supramolecular Organization of Photosystem II and its Light- Harvesting Antenna in Partially Solubilized Photosystem II Membranes. European Journal of Biochemistry **266**, 444-452

Boekema EJ, van Breemen JFL, van Roon H, Dekker JP (2000a) Arrangement of photosystem II supercomplexes in crystalline macrodomains within the thylakoid membrane of green plant chloroplasts. Journal of Molecular Biology **301**, 1123-1133

Boekema EJ, van Roon H, van Breemen JFL, Dekker JP (2000b) Supramolecular organisation of PSII and its light harvesting antenna in partially solubilised PSII membranes. European Journal Biochemistry **266**, 444-452

Bouvier F, D'Harlingue A, Hugueney P, Marin E, Marion-Poll A, Camara B (1996) Xanthophyll biosynthesis. Cloning, expression, functional reconstitution and regulation of β-cyclohexanyl carotenoid epoxidase from pepper. Journal of Biological Chemistry **271**, 28861-28867

Bradbury M & Baker NR (1981) Analysis of the Slow Phases of the in vivo Chlorophyll Fluorescence Induction Curve - Changes in the Redox State of Photosystem II Electron-Acceptors and Fluorescence Emission from Photosystem I and Photosystem II. Biochimica et Biophysica Acta **635**, 542-551

Brangeon J & Mustardy LA (1979) The ontogenic assembly of intra-chloroplast lamellae viewed in 3-dimensions. Biology of the Cell **36,** 71-80

Briantais JM, Vernotte C, Picaud M, Krause GH (1979) A Quantitative Study of the Slow Decline in Chlorophyll *a* Fluorescence in Isolated Chloroplasts. Biochimica et Biophysica Acta **548**, 128-138

Bricker TM, Frankel LK (2002) The Structure And Function Of CP47 And CP43 In Photosystem II. Photosynthesis Research **72,** 131-146

Burbridge A, Grieve T, Terry C, Corlett J, Thompson A, Taylor I (1997) Structure and expression of a cDNA encoding zeaxanthin epoxidase, isolated from wilt-related tomato library. Journal of Experimental Botany **48**, 1479-1750

Burgi R, Suter F & Zuber H (1987) Arrangement of the Light-Harvesting Chlorophyll a/b Protein Complex in the Thylakoid Membrane. Biochimica et Biophysica Acta **890**, 346-351

Caffarri S, Croce R, Breton J, Bassi R (2001) The Major Antenna Complex of Photosystem II Has a Xanthophyll Binding Site Not Involved in Light Harvesting. Journal of Biological Chemistry **27**, 35924–35933

Cape JL, Bowman MK, Kramer DM (2006) Understanding the cytochrome bc complexes by what they don't do. The Q-cycle at 30. Trends in Plant Science **11**, 46-55

Cogdell RJ & Frank HA (1987) How carotenoids function in photosynthetic bacteria. Biochimica et Biophysica Acta **895,** 63-79

Connelly JP, Muller MG, Hucke M, Gatzen G, Mullineaux CW, Ruban AV, Horton P, Holzwarth AR (1997) Ultrafast spectroscopy of trimeric light harvesting complex II from higher plants. Journal of Physical Chemistry B **101**, 1902-1909

Croce R, Weiss S, Bassi R (1999) Carotenoid-binding sites of the Major Light Harvesting Complex II of Higher Plants. The Journal of Biological Chemistry **274 (42)**, 29613-29623

Croce R, Muller MG, Bassi R, Holzwarth AR (2001) Carotenoid-to-chlorophyll energy transfer in recombinant major light-harvesting complex (LHCII) from higher plants. Biophysical Journal **80**, 901-915

Croce R, Canino G, Ros F, Bassi R (2002) Chromophore Organization in the Higher-Plant Photosystem II Antenna Protein CP26. Biochemistry **41**, 7334-7343

Crouchman S, Ruban AV, Horton P (2006) PsbS Enhances Nonphotochemical Quenching in the Absence of Zeaxanthin. FEBS Letters **580**, 2053-2058

Dall'Osto L, Caffarri S, Bassi R (2005) A Mechanism of Nonphotochemical Energy Dissipation, Independent from PsbS, Revealed by a Conformational Change in the Antenna Protein CP26. Plant Cell **17**, 1217-1232.

Dall'Osto L, Cazzaniga S, North H, Marion-Poll A, Bassi R (2007) The Arabidopsis aba4-1 Mutant Reveals a Specific Function for Neoxanthin in Protection against Photooxidative Stress. The Plant Cell **19**,1048-1064

Davison PA, Hunter CN, Horton P (2002) Overexpression of β-carotene hydroxylase enhances stress tolerance in Arabidopsis. Nature **418**, 203-206

Deisenhofer J, Epp O, Miki K, Huber R, Michel H (1985) Structure of the protein subunits in the photosynthetic reaction centre of *Rhodopseudomonas viridis* at 3Å resolution. Nature **318**, 618 - 624

Dekker JP, van Roon H, Boekema EJ, (1999) Heptameric association of light-harvesting complex II trimers in partially solubilized photosystem II membranes, FEBS Letters **449,** 211– 214

Dekker P & Boekema EJ (2005) Supramolecular Organization of Thylakoid Membrane Pproteins in Ggreen Plants. Biochimica et Biophysica Acta **1706,** 12-39

Demmig B, Winter K, Krüger A, Czygan F-C (1987) Photoinhibition and Zeaxanthin Formation in Intact Leaves. Plant Physiology **84**, 218-224

Demmig-Adams B (1990) Carotenoids and Photoprotection in Plants: A Role for the Xanthophyll Zeaxanthin. Biochimica et Biophysica Acta **1020**, 1-24

Demmig-Adams B & Adams WW (1992) Photoprotection and Other Responses of Plants to High Light Stress. Annual Review of Plant Physiology and Plant Molecular Biology **43**, 599-626

Demmig-Adams B & Adams WW (1996) The role of xanthophyll cycle carotenoids in the protection of photosynthesis. Trends in Plant Science **1,** 21-26

Demmig-Adams B, Gilmore AM, Adams WW (1996) In Vivo Functions of Carotenoids in Higher Plants. The FASEB Journal **10**, 403-412

de Weerd FL, van Stokkum IHM, van Amerongen H, Dekker JP, van Grondelle R. (2002) Pathways for Energy Transfer in the Core Light-Harvesting Complexes CP43 and CP47 of Photosystem II Biophysical Journal **82**, 1586-1597

Dominici P, Caffarri S, Armenante F, Ceoldo S, Crimi M, Bassi R (2002) Biochemical Properties of the PsbS Subunit of Photosystem II Either Purified From Chloroplast or Recombinant. Journal of Biological Chemistry **277**, 22750-22758

Dreuw A, Fleming GR, Head-Gordon M (2003) Charge-Transfer State as a Possible Signature of a Zeaxanthin-Chlorophyll Dimer in the Non-photochemical Quenching Process in Green Plants. Journal of Physical Chemistry **107**, 6500-6503

Du M, Xie X, Mets L, Fleming GR (1994) Direct observation of ultrafast energy-transfer processes in light harvesting complex II. J. Phys. Chem. **98**, 4736-4741

Edge R & Truscott GT (1999) Carotenoid radicals and the interaction of carotenoids with active oxygen species. In *The photochemistry of carotenoids*, (eds H.A. Frank, A.J. Young and R.J. Cogdell), Kluwer Academic Publishers, 223-234.

Eskling M, Arvidsson PO, Åkerlund HE (1997) The xanthophyll cycle, its regulation and components. Physiologia Plantarum **100**, 806-816

Ferriera KN, Iverson TM, Maghlaoui K, Barber J (2004) Architecture of the Photosynthetic Oxygen – Evolving Centre. Science **303**, 1831-1838

Finazzi G, Johnson GN, Dallosto L, Joliot P, Wollman F-A, Bassi R (2004) A Zeaxanthin – independent Nonphotochemical Quenching Mechanism Localised in the Photosystem II Core Complex. PNAS **101**, 12375-12380

Fiore A, Dall'Osto L, Fraser PD, Bassi R, Giuliano G (2006) Elucidation of the β-carotene hydroxylation pathway in *Arabidopsis thaliana.* FEBS Letters **580**, 4718-4722

Frank HA, Cua A, Chynwa TV, Young AJ, Gosztola D, Wasielewski MR (1994) Photophysics of the carotenoids associated with the xanthophyll cycle in photosynthesis. Photosynthesis Research **41**, 389-395

Frank HA, Bautista JA, Josue JS, Young AJ (2000) Mechanism of non-photochemical quenching in green plants. Energies of the lowest excited singlet state of zeaxanthin and violaxanthin. Biochemistry **39**, 2831-2837

Frank H.A. & Brudvig G.W. (2004) Redox Functions of Carotenoids in Photosynthesis. Biochemistry, **43**, 8607 -8615.

Funk C, Schroder W, Napiwotzki A, Tjus S, Renger G, Andersson B (1995) The PSII-S Protein of Higher-Plants - A New-Type of Pigment-Binding Protein. Biochemistry **34**, 11133-11141

Genty B, Briantais JM, Baker NR (1989) The relationship between the quantum yield of photosynthetic electron transport and quenching of chlorophyll fluorescence. Biochimica et Biophysica Acta **990**, 87-92

Gilmore AM & Yamamoto HY (1992) Dark Induction of Zeaxanthin-Dependent Nonphotochemical Fluorescence Quenching Mediated by ATP. PNAS **89**, 1899-1903

Gilmore AM, Bjorkman O, (1994) Temperature-sensitive coupling and uncoupling nonradiative energy dissipation: Similarities between chloroplasts and leaves of ATPase-mediated. Planta **197**, 646-654

Gilmore AM, Hazlett TL, Govindjee (1995) Xanthophyll cycle dependent quenching of photosystem II chlorophyll a fluorescence: formation of a quenching complex with a short fluorescence lifetime, Proc. Natl Acad. Sci. USA **92**, 2273–2277

Gilmore AM (1997) Mechanistic Aspects of Xanthophyll Cycle – Dependent Photoprotection in Higher Plant Chloroplasts and Leaves. Physiologica Plantarum **99**, 197-209

Gounaris K, Barber J, Harwood JL (1986) The Thylakoid Membranes of Higher Plant Chloroplasts. Journal of Biochemistry **237**, 313-326

Goussias C, Boussac A, Rutherford AW (2002) Photosystem II and photosynthetic oxidation of water: an overview. Philosophical Transactions of the Royal Society of London B **357,** 1369–1381

Gradinaru CC, Ozdemir S, Gulen D, Van Stokkum IHM, Van Grondelle R, Van Amerongen H (1998) The Flow of Excitation Energy in LHCII Monomers: Implications for the Structural Model of the Major Plant Antenna. Biophysical Journal **75**, 3064-3077

Gradinaru CC, van Stokkum IHM, Pascal AA, van Grondelle R, van Amerongen H (2000) Identifying the pathways of energy transfer between carotenoids and chlorophylls in LHCII and CP29, A multi-color, femtosecond pump probe study. Journal of Physical Chemistry **104**, 9330-9342

Grimm B, Kruse E, Kloppstech K (1989) Transiently expressed early light inducible thylakoid proteins share transmembrane domains with light harvesting chlorophyll binding proteins. Plant Molecular Biology **13**, 583-593

Groth G & Pohl E (2001) The Structure of the Chloroplast F_1-ATPase at 3.2Å Resolution. Journal of Biological Chemistry **276**, 1345-1352

Gruszecki W I, Grudzinski W, Banaszek-Glos A, Matula M, Kernen P, Krupa Z, Sielewiesiuk J (1999) Xanthophyll pigments in light-harvesting complex II in monomolecular layers: localisation, energy transfer and orientation. Biochimica et Biophysica Acta **1412**, 173-183

Hankamer B, Barber J, Boekema EJ (1997) Structure And Membrane Organization Of Photosystem II In Green Plants. Annual Review of Plant Physiology And Plant Molecular Biology **48**, 641-671

Harrer R, Bassi R, Testi MG & Schafer C (1998) Nearest-Neighbor Analysis of a Photosystem II Complex from *Marchantia polymorpha L.* (liverwort), which Contains Reaction Center and Antenna Proteins. European Journal of Biochemistry **255**, 196-205

Havaux M, Gruszecki WI, Dupont I, Leblanc RM (1991) Increased Heat Emission And Its Relationship To The Xanthophyll Cycle In Pea Leaves Exposed To Strong Light Stress. Journal Of Photochemistry And Photobiology B-Biology **8**, 361-370

Havaux M, Tardy F, Ravenel J, Chanu D, Parot P (1996) Thylakoid Membrane Stability To Heat Stress Studied By Flash Spectroscopic Measurements Of The Electrochromic Shift In Intact Potato Leaves: Influence Of The Xanthophyll Content. Plant Cell And Environment **19**, 1359-1368

Havaux M & Niyogi K (1999) The violaxanthin cycle protects plants from photooxidative damage by more than one mechanism. Proceedings of the National Academy of Sciences, USA **96**, 8762-8767

Havaux M & Tardy F (1997) Thylakoid membrane fluidity and thermostability during the operation of the xanthophyll cycle in higher-plant chloroplasts. Biochimica et Biophysica Acta. **1330**, 179-193

Heber U (1969) Conformational changes of chloroplasts induced by illumination of leaves in vivo. Biochim. Biophys. Acta **180**, 302–319

Holt NE, Kennis JTM, Dall'Osto L, Bassi R, Fleming GR (2003) Carotenoid to chlorophyll energy transfer in light harvesting complex II from Arabidopsis thaliana probed by femtosecond fluorescence upconversion. Chemical Physics Letters **379**, 305-313

Holt NE, Fleming GR, Niyogi KK (2004) Toward an Understanding of the Mechanism of Nonphotochemical Quenching in Green Plants. Biochemistry **43**, 8281-8289

Holt NE, Zigmantas D, Valkunas L, Li X-P, Niyogi KK, Fleming GR (2005) Carotenoid Cation Formation and the Regulation of Photosynthetic Light Harvesting. Science **307**, 433-436

Horton P & Hague A (1988) Studies on the Induction of Chlorophyll Fluorescence in Isolated Barley Protoplasts 4. Resolution of Non-Photochemical Quenching. Biochimica et Biophysica Acta **932**, 107-115

Horton P, Ruban AV, Rees D, Pascal AA, Noctor G, Young AJ (1991) Control of The Light-Harvesting Function of Chloroplast Membranes by Aggregation of the LHCII Chlorophyll Protein Complex. FEBS Letters **292**, 1-4

Horton P, Ruban AV (1992) Regulation Of Photosystem-II. Photosynthesis Research **34**, 375-385

Horton P, Ruban AV, Walters RG (1994) Regulation of Light Harvesting in Green Plants. Plant Physiology **106**, 41 5-420

Horton P, Ruban AV, Walters RG (1996) Regulation of Light Harvesting in Green Plants. Annual Review of Plant Physiology and Plant Molecular Biology **47**, 655-684

Horton P (1999) Are Grana Necessary for Regulation of Light Harvesting? Australian Journal of Plant Physiology **26**, 659-669

Horton P, Ruban AV, Wentworth M (2000) Allosteric Regulation of the Light-Harvesting System of Photosystem II. Philosophical Transactions of the Royal Society of London Series B-Biological Sciences **355**, 1361-1370

Horton P, Murchie EH, Ruban AV, Walters RG (2001) Increasing rice photosynthesis by manipulation of the acclimation and adaptation to light. Novartis Foundation Symposium **236**, 117- 134

Horton P, Ruban AV, Wentworth M (2005) Allosteric Regulation of the Light – Harvesting System of Photosystem II. Philosophical Transactions of the Royal Society of London B **355**, 1361-1370

Horton P, Wentworth M, Ruban AV (2005) Control of the Light Harvesting Function of Chloroplast Membranes: The LHCII – Aggregation Model for Non-photochemical Quenching. FEBS Letters **579**, 4201-4206

Ide JP, Klug DR, Kuhlbrandt W, Giorgi LB, Porter G (1987) The state of detergent solubilised light harvesting chlorophyll a/b protein complex as monitored by picosecond time-resolved fluorescence and circular diochroism. Biochim Biophys Acta **893**, 349–364

Jackowski G, Kacprzak K, Jansson S (2001) Identification of Lhcb1/Lhcb2/Lhcb3 heterotrimers of the main light-harvesting chlorophyll a/b-protein complex of photosystem II (LHCII) Biochemica et Biophysica Acta. **1504**, 340-345.

Jahns P & Miehe B (1996) Kinetic Correlation of Recovery from Photoinhibition and Zeaxanthin Epoxidation. Planta **198**, 202-210

Jansson S (1994) The Light-Harvesting Chlorophyll a/b Binding-Proteins. Biochimica et Biophysica Acta-Bioenergetics **1184,** 1-19

Jansson S (1999) A Guide to the LHC Genes and Their Relatives in Arabidopsis. Trends In Plant Science **4**, 236-240

Jansson S, Andersson J, Kim SJ, Jackowski G (2000) An *Arabidopsis thaliana* protein homologous to Cyanobacterial high light inducible proteins. Plant Molecular Biology **42**, 345-351

Jensen PE, Rosgaard L, Knoetzel J, Scheller HV (2002) Photosystem I Activity Is Increased In The Absence Of The PSI-G Subunit. Journal Of Biological Chemistry **277**: 2798-2803

Johnson MP, Havaux M, Triantaphylides C, Ksas B, Pascal AA, Robert B, Davison PA, Ruban AV, Horton P (2007) Elevated Zeaxanthin Bound to Oligomeric LHCII Enhances the Resistance of *Arabidopsis* to Photooxidative Stress by a Lipid-Protective, Antioxidant Mechanism. Journal of Biological Chemistry **282**, 22605-22618

Joliot P, Beal D, Joliot A (2004) Cyclic electron flow under saturating excitation of dark-adapted *Arabidopsis* leaves. Biochimica et Biophysica Acta **1656,** 166–176

Jordan P, Fromme P, Witt HT, Klukas O, Saenger W, Krauss N (2001) Three-dimensional structure of cyanobacterial photosystem I at 2.5Å resolution. Nature **411**, 909-917

Junge W, Lill H, Engelbrecht S (1997) ATP synthesis: an electrochemical transducer with rotary mechanics. Trends in Biochemical Science **22**, 420-423

Kamiya N, Shen JR (2003) Crystal Structure Of Oxygen-Evolving Photosystem II From Thermosynechococcus Vulcanus At 3.7-Angstrom Resolution. PNAS **100**, 98-103

Kim S, Pichersky E, Yocum CF (1994) Topological Studies of Spinach 22 kDa Protein of Photosystem II. Biochimica et Biophysica Acta **1188**, 339-248

Klimmek F, Ganeteg U, Ihalainen JA, van Roon H, Jensen PE, Scheller HV, Dekker JP, Jansson S (2005) Structure of the Plant Light Harvesting Complex I: In Vivo characterisation and structural interdependence of Lhca proteins. Biochemistry **44**, 3065-3073

Kok B, Forbush B, Mcgloin M (1970) Cooperation Of Charges In Photosynthetic O_2 Evolution - I. A Linear Four Step Mechanism. Photochemistry And Photobiology **11**, 457-475

Kovács L, Damkjær J, Kereïche S, Ilioaia C, Ruban AV, Boekema EJ, Jansson S, Horton P (2006) Lack of the Light – Harvesting Complex CP24 Affects the Structure and Function of the Grana Membranes of Higher Plant Chloroplasts. The Plant Cell **18**, 3106-3120

Krause GH (1973) The High-Energy State of the Thylakoid System is Indicated by Chlorophyll Fluorescence and Chloroplast Shrinkage. Biochimica et Biophysica Acta **292**, 715-728

Krause GH, Vernotte C, Briantais JM (1982) Photoinduced Quenching of Chlorophyll Fluorescence in Intact Chloroplasts and Algae - Resolution Into 2 Components. Biochimica et Biophysica Acta **679**, 116-124

Krause GH & Behrend U (1986) ΔpH-dependent Chlorophyll Fluorescence Quenching Indicating a Mechanism of Protection Against Photoinhibition of Chloroplasts. FEBS Letters **200**, 298-302

Krause GH & Weis E (1991) Chlorophyll Fluorescence and Photosynthesis - The Basics. Annual Review of Plant Physiology and Plant Molecular Biology **42**, 313-349

Krieger A, Moya I, Weis E (1992) Energy-dependent Quenching of Chlorophyll a Fluorescence : Effect of pH on Stationary Fluorescence and Picosecond-relaxation Kinetics in Thylakoid Membranes and Pphotosystem II Preparations. Biochemica et Biophysica Acta **1102,** 167-176

Krieger A & Weis E (1993) The Role of Calcium in the pH-Dependent Control of Photosystem- II. Photosynthesis Research **37**, 117-130

Kühlbrandt W & Wang DN (1991) Three-dimensional structure of plant light-harvesting complex determined by electron crystallography. Nature **350,** 130–134

Kuhlbrandt W, Wang DN, Fujiyoshi Y (1994) Atomic Model of Plant Light-Harvesting Complex by Electron Crystallography. Nature **367**, 614-621

Kurisu G, Zhang H, Smith JL, Cramer WA (2003) Structure of the Cytochrome b_6f Complex of Oxygenic Photosynthesis: Tuning the Cavity. Science **302**, 1009-1014

Lambrev PH, Várkonyi Z, Krumova S, Kovács L, Miloslavina Y, Holzwarth A, Garab G (2007) Importance of trimer–trimer interactions for the native state of the plant light-harvesting complex II. Biochimica et Biophysica Acta **1767**, 847–853

Lampoura SS, Barzda V, Owen GM, Hoff AJ, Amerongen H (2002) "Aggregation of LHCII leads to a redistribution of the triplets over the central xanthophylls in LHCII" Biochemistry **41**, 9139-9144

Lee ALC & Thornber JP (1995) Analysis of the Pigment Stoichiometry of Pigment-Protein Complexes from Barley (Hordeum vulgare) Plant Physiology, **107**, 565-574

Li XP, Bjorkman O, Shih C, Grossman A, Rosenquist M, Jansson S, Niyogi K (2000) A Pigment-Binding Protein Essential For Regulation Of Photosynthetic Light Harvesting. Nature **403**, 391-395

Li XP, Gilmore AM, Niyogi KK (2002a) Molecular and Global Time-Resolved Analysis of a PsbS Gene Dosage Effect on pH- and Xanthophyll Cycle-Dependent Nonphotochemical Quenching in Photosystem II. Journal of Biological Chemistry **277**, 33590-33597

Li XP, Müller-Moule P, Gilmore AM, Niyogi KK (2002b) PsbS – dependent Enhancement of Feedback De – excitation Protects Photosystem II from Photoinhibition. PNAS **99**, 15222-15227

Li XP, Phippard A, Pasari J, Niyogi KK (2002c) Structure-Function Analysis of Photosystem II Subunit S (PsbS) In Vivo. Functional Plant Biology **29**, 1131-1139

Li XP, Gilmore AM, Caffari S, Bassi R, Golan T, Kramer D, Niyogi KK (2004) Regulation of Photosynthetic Light Harvesting Involves Intrathylakoid Lumen pH Sensing by the PsbS Protein. Journal of Biological Chemistry **279,** 22866-22874

Liu Z, Yan H, Wang K, Kuang T, Zhang J, Gui L, An X, Chang W (2004) Crystal structure of spinach major light harvesting complex at 2.72Å resolution. Nature **428**, 287-292

Lokstein H, Tian L, Polle JEW, DellaPenna D (2002) Xanthophyll biosynthetic mutants of Arabidopsis thaliana: altered nonphotochemical quenching of chlorophyll fluorescence is due to changes in Photosystem II antenna size and stability. Biochmica et Biophysica Acta. **1553**, 309-319

Lokstein H, Härtel H, Hoffmann P, Woitke P, Renger G (2004) The Role of Light-harvesting Complex II in Excess Energy Dissipation: an in-vivo Fluorescence Study on

the Origin of High-energy Qquenching. Journal of Photochemistry and Photobiology **26**, 175-184

Loll B, Kern J, Saenger W, Zouni A, Biesiadka J (2005) Towards Complete Cofactor Arrangement in the 3.0Å Resolution Structure of Photosystem II. Nature **438**, 1040-1044

Lunde C, Jensen PE, Haldrup A, Knoetzel J, Scheller HV (2000) The PSI-H Subunit Of Photosystem I is Essential for State Transitions in Plant Photosynthesis. Nature **408**, 613-615

Lutz M (1977) Antenna chlorophyll in photosynthetic membranes. A study by resonance Raman Spectroscopy. Biochimica et Biophysica Acta **460**, 408-430

Ma Y-Z, Holt NE, Li X-P, Niyogi KK, Fleming GR (2003) Evidence for Direct Carotenoid Involvement in the Regulation of Photosynthetic Light Harvesting. PNAS **100**, 4377

Mathis P (1969) Triplet-triplet energy transfer from chlorophyll a to carotenoids in solution and in chloroplasts. Photosynthesis Research **2**, 818-822

Mathis P, Butler WL, Satoh H (1979) Carotenoid triplet state and chlorophyll fluorescence quenching in chloroplasts and subchloroplast particles. Photochemistry and Photobiology **30**, 603-614

McCarty RE, Evron Y, Johnson EA, (2000) Annu. Rev. Plant Physiol. Plant Mol. Biol. **51**, 83–109

Morishige DT, Anandan S, Jaing JT, Thornber JP (1990) Amino terminal sequence of the 21kDa apoprotein of a minor light harvesting pigment protein complex of the PSII antenna (LHCIId/ CP24). FEBS Letters **264**, 239-242

Morosinotto T, Baronio R, Bassi R (2002) Dynamics of Chromophore Binding to LHC Proteins In Vivo and In Vitro During Operation of the Xanthophyll Cycle. Journal of Biological Chemistry **277**, 36913-36920

Moya I, Silvestri M, Vallon O,| Cinque G, Bassi R (2001) Time-Resolved Fluorescence Analysis of the Photosystem II Antenna Proteins in Detergent Micelles and Liposomes. Biochemistry **40**, 12552-12561

Mullet JE & Arntzen CJ (1980) Simulation of grana stacking in a model membrane system. Mediation by a purified light harvesting pigment-protein complex from spinach. Biochem Biophys Acta **589**, 100–107

Muller DJ, Dencher NA, Meier T, Dimroth P, Suda K, Stahlberg H, Engel A, Seelert H, Matthey U (2000) Progress in atomic force microscopy of F0-ATPase. Biochimica et Biophysica Acta Bioenergetics-EBEC short reports **11**, 182

Muller P, Li XP, Niyogi KK (2001) Non-Photochemical Quenching. A Response to Excess Light Energy. Plant Physiology **125**, 1558-1566

Mullineaux CW, Pascal AA, Horton P, Holzwarth AR (1993) Excitation energy quenching in aggregates of the LHCII chlorophyll-protein complex- a time resolved fluorescence study. Biochimica et Biophysica Acta, **1141**, 23-28

Mullineaux CW, Ruban AV, Horton P (1994) Prompt Heat Release Associated with ΔpH-Dependent Quenching in Spinach Thylakoid Membranes. Biochimica et Biophysica Acta **1185,** 119-123

Murata N & Sugahara K (1969) Control of excitation transfer in photosynthesis and light induced decrease of chlorophyll a fluorescence related to photophosphorylation system in spinach chloroplasts. Biochimica et Biophysica Acta **189**, 182-192

Mustárdy L & Garab G (2003) Granum Revisited. A Three-dimensional Model – Where Things Fall into Place. Trends in Plant Science **8**, 117–122

Naqvi KR, Melo TB, Bangar Raju B, Javorfi T, Garab G (1997) Comparison of the absorption spectra of trimers and aggregates of chlorophyll a/b light-harvesting complex LHC II. Spectrochimica Acta Part A **53**, 1925-1936

Neubauer C & Yamamoto HY (1994) Membrane barriers and Mehler peroxidase reaction limit the ascorbate available for violaxanthin de-epoxidase activity in intact chloroplasts. Photosynthesis Research **39**, 137-147

Nield J, Kruse O, Ruprecht J, DA Fonseca P, Buchel C, Barber J (2000) Three-Dimensional Structure of *Chlamydomonas Reinhardtii* and *Synechococcus Elongatus* Photosystem II Complexes Allows for Comparison of their Oxygen-Evolving Complex Organization. Journal of Biological Chemistry **275**, 27940-27946

Niyogi KK, Grossman AR, Bjorkman O (1998) Arabidopsis Mutants Define a Central Role for the Xanthophyll Cycle in the Regulation of Photosynthetic Energy Conversion. Plant Cell **10**: 1121-1134

Niyogi, KK (1999) Photoprotection revisited: genetic and molecular approaches. Annual Review Plant Physiology Plant Molecular Biology **50,** 333-359

Niyogi KK, Shih C, Chow WS, Pogson BJ, DellaPenna D, Bjorkman O (2001) Photoprotection in a zeaxanthin and lutein deficient double mutant of Arabidopsis. Photosynthesis Research **67**, 139-145

Noctor G, Rees D, Young A, Horton P (1991) The Relationship Between Zeaxanthin, Energy-Dependent Quenching of Chlorophyll Fluorescence, and Trans-Thylakoid pH Gradient in Isolated-Chloroplasts. Biochimica et Biophysica Acta **1057,** 320-330

Noctor G, Ruban AV, Horton P (1993) Modulation of Delta-pH-Dependent Nonphotochemical Quenching of Chlorophyll Fluorescence in Spinach Chloroplasts. Biochimica et Biophysica Acta **1183**, 339-344

Noji H, Yasuda R, Yoshida M, Kinosita K (1997) Direct Observation Of The Rotation Of F-1-ATPase. Nature **386**, 299-302

Novoderezhkin VI, Palacios MA, van Amerongen & van Grondelle (2005) Excitation Dynamics in the LHCII Complex of Higher Plants: Modeling Based on the 2.72 Angstrom Crystal Structure. Journal of Physical Chemistry **109**, 10493-10504

Nussberger S, Dörr K, Wang DN, Kühlbrandt W (1993) Lipid-Protein Interactions in Crystals of Plant Light- Harvesting Complex. Journal of Molecular Biology **234,** 347-356

Ono T & Inoue Y (1984) Reconstitution of Photosynthetic Oxygen Evolving Activity by Rebinding of 33-kDa Protein to $CaCl_2$-Extracted PSII Particles. FEBS Letters **166,** 381-384

Owens TG (1994) Excitation energy transfer between chlorophylls and carotenoids. A proposed molecular mechanism for non-photochmeical quenching. In *Photoinhibition of Photosynthesis from molecular mechanisms to the field*. (eds N.R. Baker and J.R. Bowyer). Bios Scientific publishers, London, 95-107

Pagano A, Cinque G, Bassi R (1998) In Vitro Reconstitution of the Recombinant Photosystem II Light-harvesting Complex CP24 and its Spectroscopic Characterisation. Journal of Biological Chemistry **273**, 17154-17165

Paolillo DJ (1970) The Three-Dimensional Arrangement of Intergranal Lamellae in Chloroplasts. Journal of Cell Science **6**, 243-255

Papageorgiou G & Govindjee (1968) Light-Induced Changes in the Fluorescence Yield of Chlorophyll a In Vivo. Biophysical Journal **8**, 1316-1328

Pascal AA, Caron L, Rousseau B, Lapouge K, Duval J.-C, Robert B (1998) Resonance Raman Spectroscopy of a Light-Harvesting Protein from the Brown Alga *Laminaria saccharina*. Biochemistry **275**, 22031–22036

Pascal AA, Liu Z, Broess K, van Oort B, van Amerongen H, Wang C, Horton P, Robert B, Chang W, Ruban AV (2005) Molecular Basis of Photoprotectiona and Control of Photosynthetic Light Harvesting. Nature **437**, 134-137

Pesaresi P, Sandona D, Giuffra E, Bassi R (1997) A Single Point Mutation (E166Q) Prevents Dicyclohexylcarbodiimide Binding to the Photosystem II Subunit CP29. FEBS Letters **402,** 151-156

Peter GF & Thornber JP (1991) Biochemical-Composition and Organization of Higher-Plant Photosystem-II Light-Harvesting Pigment-Proteins. Journal of Biological Chemistry **266**, 16745-16754

Peterman EJG, Gradinaru CC, Calkoen F, Borst JC, van Grondelle R, van Amerongen H (1997) Xanthophylls in Light-Harvesting Complex II of Higher Plants: Light Harvesting and Triplet Quenching. Biochemistry **36**, 12208-12215

Pfündel EE (1993) Is zeaxanthin capable of energy transfer to chlorophyll α in partially greened leaves? A study of fluorescence excitation spectra during violaxanthin deepoxidation Photochemistry and Photobiology **57**, 356-361

Phillip D, Ruban AV, Horton P, Asato A, Young AJ (1996) Quenching of chlorophyll fluorescence in the major light harvesting complex of photosystem II. Proceedings of the National Academy of Science **93,** 1492-1497

Phillip D, Hobe S, Paulsen H, Molnar P, Hasimoto H, Young AJ (2002) The Binding of Xanthophylls to the Bulk Light-harvesting Complex of Photosystem II of Higher Plants. Journal of Biological Chemistry 28, 25160-25169

Pierre Y, Breyton C, Kramer D, Popot JL (1995) Purification And Characterization Of The Cytochrome *b6f* Complex From Chlamydomonas-Reinhardtii. Journal Of Biological Chemistry **270**, 29342-29349

Plumley FG & Schmidt GW (1987) Reconstitution of chlorophyll a/b light-harvesting complexes: xanthophyll dependent assembly and energy transfer. Proceedings of the National Academy of Science **84**, 146-150

Pogson BJ, Niyogi KK, Bjorkman O, DellaPenna D (1998) Altered xanthophyll compositions adversely affect chlorophyll accumulation and non-photochemical quenching in Arabidopsis mutants. Proceedings of the National Academy of Science **95**, 13324-13329

Polivka T, Herek JL, Zigmantas D, Akerlund HE, Sundstrom V (1999) Direct Observation of the (Forbidden) S_1 State in Carotenoids. PNAS **96,** 4914-4917

Polivka T, Zigmantas D, Sundstrom V, **Formaggio E, Cinque G, Bassi R** (2002) Carotenoid S_1 State in a Recombinant Light – Harvesting Complex of Photosystem II. Biochemistry **41**, 439-450

Porra R, Thompson W, Kriedmann P (1989) Determination of Accurate Extinction Coeffiecients and Simultaneous Equations for Assaying Chlorophylls a and b Extracted with Four Different Solvents: Verification of the Concentration of Chlorophyll Standards by Atomic Absorption Spectroscopy. Biochimica et Biophysica Acta **975,** 384-397

Quick WP & Horton P (1984) Studies on the Induction of Chlorophyll Fluorescence in Barley Protoplasts 2.Resolution of Fluorescence Quenching by Redox State and the Transthylakoid pH Gradient. Proceedings of the Royal Society of London Series B-Biological Sciences **220**, 371-382

Rees D, Young A, Noctor G, Britton G, Horton P (1989) Enhancement of the Delta-pH-Dependent Dissipation of Excitation Energy in Spinach Chloroplasts by Light Activation - Correlation With the Synthesis of Zeaxanthin. FEBS Letters B **256,** 85-90

Rees D, Noctor G, Ruban AV, Crofts J, Young A, Horton P (1992) pH Dependent Chlorophyll Fluorescence Quenching in Spinach Thylakoids from Light Treated or Dark Adapted Leaves. Photosynthesis Research **31,** 11-19

Remy R, Tremolieres A, Duval JC, Ambard-Bretteville F, Dubacq J P (1982) Study of the supramolecular organization of the light-harvesting chlorophyll protein (LHCP). Conversion of the oligomeric form into the monomeric one by phospholipase A2 and reconstitution with liposomes, FEBS Letters **137,** 271-275

Rhee KH, Morriss EP, Barber J, Kuhlbrandt W (1998) Three-Dimensional Structure Of The Plant Photosystem II Reaction Centre At 8 Angstrom Resolution. Nature **396**, 283-286

Ricci M, Bradforth SE, Jiminez R, Fleming GR (1996) Internal conversion and energy transfer dynamics of spheroidene in solution and in the LH1 and LH2 light-harvesting complexes. Chem. Phys. Lett. **259,** 381-390

Rimai L, Heyde ME, Gill D (1973) Vibrational spectra of some carotenoids and related linear polyenes. A Raman spectroscopic study. J. Am. Chem. Soc. **95**, 4493-4501

Robert B, Lutz M (1986) Structure of the Primary Donor of *Rhodopseudomonas sphaeroides:* Difference Resonance Raman Spectroscopy of Reaction Centers. Biochemistry **25**, 2303-2309

Robert B (1996) In *Biophysical Techniques in Photosynthesis* (Amesz, J., and Hoff, A. J., eds), Kluwer Academic Publisher, Dordrecht, Netherlands, 161–176

Robert B (1999) In *The Photochemistry of Carotenoids* (Frank, H. A., Young, A. J., Britton, G., and Cogdell, R. J., eds), Kluwer Academic Publishers, Dordrecht, Netherlands, 189–201

Robert B, Horton P, Pascal AA, Ruban AV (2004) Insights into the molecular dynamics of plant light-harvesting proteins in vivo. Trends in Plant Science **9**, 385-390

Rockholm DC, Yamamoto HY (1996) Violaxanthin De-Epoxidase - Purification Of A 43 kDa Lumenal Protein From Lettuce By Lipid-Affinity Precipitation With Monogalactosyldiacylglyceride. Plant Physiology **110**, 697-703

Ruban AV, Rees D, Noctor GD, Young AJ, Horton P (1991) Long wavelength chlorophyll species are associated with amplification of high energy state quenching in higher plants. Biochimica et Biophysica Acta **1059,** 355-360

Ruban AV & Horton P (1992) Mechanism of Delta-pH-Dependent Dissipation of Absorbed Excitation-Energy by Photosynthetic Membranes 1. Spectroscopic Analysis of Isolated Light-Harvesting Complexes. Biochimica et Biophysica Acta **1102**, 30-38

Ruban AV, Rees D, Pascal AA, Horton P (1992) Mechanism of pH-dependent dissipation of absorbed excitation energy by photosynthetic II. The relationships between LHCII aggregation in vitro and qE in isolated thylakoids. Biochimica et Biophysica Acta **1102,** 39-44

Ruban AV, Horton P, Young AJ (1993a) Aggregation of Higher-Plant Xanthophylls - Differences in Absorption-Spectra and in the Dependency on Solvent Polarity. Journal of Photochemistry and Photobiology B-Biology **21**, 229-234

Ruban AV, Young AJ, Horton P (1993b) Induction of Nonphotochemical Energy-Dissipation and Absorbency Changes in Leaves - Evidence for Changes in the State of the Light-Harvesting System of Photosystem-II In Vivo. Plant Physiology **102**, 741-750

Ruban AV & Horton P (1994) Spectroscopy of Nonphotochemical and Photochemical Quenching of Chlorophyll Fluorescence in Leaves - Evidence For a Role of The Light-Harvesting Complex of Photosystem-II in the Regulation of Energy-Dissipation. Photosynthesis Research **40**, 181-190

Ruban AV, Young AJ, Pascal AA, Horton P (1994b) The Effects Of Illumination On The Xanthophyll Composition Of The Photosystem-II Light-Harvesting Complexes Of Spinach Thylakoid Membranes. Plant Physiology **104**, 227-234

Ruban AV, Horton P, Robert B (1995) Resonance Raman Spectroscopy of the photosystem I1 Light-Harvesting Complexof Green Plants: A Comparison of Trimeric and Aggregated States. Biochemistry **34**, 2333-2337

Ruban AV & Horton P (1995) An Investigation of the Sustained Component of Nonphotochemical Quenching of Chlorophyll Fluorescence in Isolated Chloroplasts and Leaves of Spinach. Plant Physiology **108**, 721-726

Ruban AV, Calkoen F, Kwa SLS, van Grondelle R, Horton P, Dekker JP (1997) Characterisation of LHCII in the aggregated state by linear and circular dichroism spectroscopy. Biochimica et Biophysica Acta **1321**, 61–70

Ruban AV & Horton P (1999) The Xanthophyll Cycle Modulates the Kinetics of Nonphotochemical Energy Dissipation in Isolated Light- Harvesting Complexes, Intact Chloroplasts, and Leaves of Spinach. Plant Physiology **119,** 531-542

Ruban AV, Lee PJ, Wentworth M, Young AJ, Horton P (1999) Determination of the Stoichiometry and Strength of Binding of Xanthophylls to the Photosystem II Light Harvesting Complexes. Journal of Biological Chemistry **274,** 10458-10465

Ruban AV, Pascal AA, Robert B (2000) Xanthophylls of the major photosynthetic light-harvesting complex of plants: identification, conformation and dynamics FEBS Letters **477,** 181-185

Ruban AV, Pascal AA, Robert B, Horton P (2001) Configuration and Dynamics of Xanthophylls in Light-Harvesting Antennae of Higher Plants - Spectroscopic Analysis of Isolated Light-Harvesting Complex of Photosystem II and Thylakoid Membranes. Journal of Biological Chemistry **276**, 24862-24870

Ruban AV, Pascal AA, Lee PJ. Robert B, Horton P (2002a) Molecular configuration of Xanthophyll Cycle Carotenoids inPhotosystemII Antenna Complexes. Journal of Biological Chemistry **277**, 42937-42942

Ruban AV, Pascal AA, Robert B, Horton P (2002b) Activation Of Zeaxanthin Is An Obligatory Event in the Regulation of Photosynthetic Light Harvesting. Journal of Biological Chemistry **277**, 7785-7789

Ruban AV, Wentworth M, Yakushevska AE, Andersson J, Lee PJ, Keegstra W, Dekker JP, Boekema EJ, Jansson S, Horton P (2003) Plants Lacking the Main Light – Harvesting Complex Retain Photosystem II Macro – Organisation. Nature **421**, 648-652

Ruban AV, Solovieva S, Lee PJ, Ilioaia C, Wentworth M, Ganeteg U, Klimmek F, Chow WS, Anderson JM, Jansson S, Horton P (2006) Plasticity in the Composition of the Light Harvesting Antenna of Higher Plants Preserves Structural Integrity and Biological Function. Journal of Biological Chemistry **281,** 14981-14990

Salverda JM, Vengris M, Krueger BP, Scholes GD, Czarnoleski AR, Novoderezhkin V, van Amerongen H, van Grondelle R (2003) Energy Transfer in Light-Harvesting Complexes LHCII and CP29 of Spinach Studied with Three Pulse Echo Peak Shift and Transient Grating. Biophysical Journal **84**, 450-465

Sandona D, Croce R, Pagano A, Crimi M, Bassi R (1998) Higher Plant Light Harvesting Proteins. Structure and Function as Revealed by Mutation Analysis of Either Protein or Chromophore Moieties. Biochimica et Biophysica Acta-Bioenergetics **1365**, 207-214

Schansker G, Tóth SZ, Strasser RJ (2006) Dark Recovery of the Chl a Fluorescence Transient (OJIP) after Light Adaptation: The qT-component of Non-photochemical Quenching is Related to an Activated Photosystem I Acceptor Side. Biochemica et Biophysica Acta **1757**, 787-797

Schreiber U (1986) Detection of Rapid Induction Kinetics with a New Type of High-Frequency Modulated Chlorophyll Fluorometer. Photosynthesis Research **9**, 261-272

Shi LX, Lorkovic ZJ, Oelmuller R, Schroder WP (2000) The Low Molecular Mass PsbW Protein Is Involved In The Stabilization Of The Dimeric Photosystem II Complex In Arabidopsis thaliana. Journal Of Biological Chemistry **275**, 37945-37950

Siefermann D & Yamamoto HY (1974) Light – Induced De – epoxidation of Violaxanthin in Lettuce Chloroplasts III. Reaction Kinetics and Effec of Light Intensity on De – epoxidase Activity and Substrate Availability. Biochimica et Biophysica Acta **357**, 144-150

Siefermann D & Yamamoto HY (1975) Properties of NADPH and Oxygen-Dependent Zeaxanthin Epoxidation in Isolated Chloroplasts. A Transmembrane Model for the Violaxanthin Cycle. Archives of Biochemistry and Biophysics **171**, 70-77

Standfuss J, Terwisscha van Sceltinga AC, Lamborghini M, Kühlbrandt W (2005) Mechanisms of Photoprotection and Nonphotochemical quenching in Pea Light-Harvesting Complex at 2.5Å Resolution **24,** 919-928

Stewart DH & Brudvig GW (1998) Cytochrome b559 of Photosystem II. Biochimica et Biophysica Acta **1367**, 63-87

Takeguchi CA & Yamamoto HY (1968) Light induced 18O2 uptake by epoxy xanthophylls in new Zealand spinach leaves. Biochimica et Biophyisica Acta. **153**, 459-465

Teardo E, Polverino de Laureto P, Bergantino E, Dalla Vecchia F, Rigoni F, Szabò I, Giacometti GM (2007) Evidences for Interaction of PsbS with Photosynthetic Complexes in Maize Thylakoids. Biochemica et Biophysica Acta **1767**, 703-711

Telfer A, Dhami S, Bishop SM, Phillips D, Barber, J (1994) β-Carotene Quenches Singlet Oxygen Formed by Isolated Photosystem I1 Reaction Centers. Biochemistry **33**, 14469- 14474

Thayer S.S. & Bjorkman O (1992) Carotenoid distribution and deepoxidation in thylakoid pigment-protein complexes from cotton leaves and bundle-sheath cells of maize. Photosynthesis Research **33**, 213-225

Tomo T, Enami I, Satoh K (1993) Orientation And Nearest-Neighbor Analysis Of PsbI Gene-Product In The Photosystem-II Reaction Center Complex Using Bifunctional Cross-Linkers. Febs Letters **323**, 15-18

Vasiliev S, **Irrgang KD**, **Schrötter T**, **Bergmann A**, **Eichler HJ**, **Renger G**. (1997) Quenching of chlorophyll a fluorescence in the aggregates of LHCII: steady state fluorescence and picosecond relaxation kinetics. Biochemistry **36**, 7503-12

Van Amerongen H & van Grondelle R (2001) Understanding the Energy Transfer Function of LHCII, the Major Light Harvesting Complex of Green Plants. Journal of Physical Chemistry **105,** 604-617

Van Grondelle R, Novoderezhkin VI (2005) Energy transfer in photosynthesis: experimental insights and quantitative models. Physical Chemistry Chemical Physics **8**, 793-807

Van Stokkum IHM, Larsen DS, van Grondelle R (2004) Global and target analysis of time-resolved spectra. Biochimica et Biophysica Acta **1657**, 82-104

Walters RG & Horton P (1991) Resolution of Components of Nonphotochemical Chlorophyll Fluorescence Quenching in Barley Leaves. Photosynthesis Research **27**, 121-133

Walters RG & Horton P (1993) Theoretical Assessment of Alternative Mechanisms for Non-photochemical Quenching of PSII Fluorescence in Barley Leaves. Photosynthesis Research **36,** 119-139

Walters RG, Ruban AV, Horton P (1994) Higher-Plant Light-Harvesting Complexes LHCIIa and LHCIIc are Bound by Dicyclohexylcarbodiimide During Inhibition of Energy-Dissipation. European Journal of Biochemistry **226**: 1063-1069

Wehner A, Graße T, Jahns P (2006) De-epoxidation of violaxanthin in the minor antenna proteins of photosystem II, Lhcb4, Lhcb5 and Lhcb6. Journal of Biological Chemistry **281**, 21924-21933

Weis E & Berry JA (1987) Quantum Efficiency of photosystem II in relation to energy dependent quenching of chlorophyll fluorescence. Biochimica et Biophyisica Acta. **894**, 198-208

Wentworth M, Ruban AV, Horton P (2000) Chlorophyll Fluorescence Quenching in Isolated Light Harvesting Complexes Induced by Zeaxanthin. FEBS Letters **471**, 71-74

Wentworth M, Ruban AV, Horton P (2001) Kinetic Analysis of Nonphotochemical Quenching of Chlorophyll Fluorescence. 2. Isolated Light-Harvesting Complexes. Biochemistry **40**, 9902-9908

Wentworth M, Ruban AV, Horton P (2003) Thermodynamic investigation into the mechanism of the chlorophyll fluorescence quenching in isolated photosystem II light-harvesting complxes. Journal of Biological Chemistry **278**, 21845-21850

Whitmarsh J & Pakrasi HB (1996) Form And Function Of Cytochrome b_{559}. In Oxygenic Photosynthesis The Light Reactions (Ort Dr, Yocum Cf, Eds) Vol **4**. Kluwer, Dordrecht, 249-264

Widger WR, Cramer WA, Hermann RG, Trebst A (1984) Sequence Homology and structural similarities between cytochrome *b* of mitochondrial complex III and chloroplast b6/f complex. Proceedings of the National Academy of Science. **82**, 674-678.

Wraight CA & Crofts AR (1970) Energy dependent quenching of chlorophyll fluorescence in isolated chloroplasts. European Journal of Biochemistry **17**, 319-327

Yakushevska AE, Jensen PE, Keegstra W, Van Roon H, Scheller HV, Boekema EJ, Dekker JP (2001) Supermolecular Organization of Photosystem II and its Associated Light-Harvesting Antenna in *Arabidopsis thaliana*. European Journal of Biochemistry **268**, 6020-6028

Yakushevska AE, Keegstra W, Boekema EJ, Dekker JP, Andersson J, Jansson S, Ruban AV, Horton P (2003) The Structure of Photosystem II in Arabidopsis: Localization of the CP26 and CP29 Antenna Complexes. Biochemistry **42**, 608-613

Yamamoto HY, Nakayama TOM, Chichester CO (1962) Studies on the light and dark interconversions of leaf xanthophylls. Archives of Biochemistry and Biophysics **97**, 168-173

Yamamoto HY & Bassi R (1996) Carotenoids: Localization and function. In: Ort DR and Yokum CF (eds) Advances in Photosynthesis. Oxygenic Photosynthesis: The light reactions,. Kluwer Academic Publishers, Dordrecht, The Netherlands, 539–563

Yamamoto HY, Kamite L, Wang Y-Y (1972) An Ascorbate-Induced Absorbance Change in Chloroplasts from Violaxanthin De-epoxidation. Plant Physiology **49**, 224-228

Yamamoto HY (1999) Biochemistry and molecular biology of the xanthophyll cycle. In *Photochemistry of carotenoids* (Eds Frank H.A., Young A.J., Cogdell R.J.) Advances in Photosynthesis, vol **8**, Kluwer. Dordecht, 271-291

Yan H, Zhang P, Wang C, Liu Z, Chang W (2007) Two Lutein Molecules in LHCII Have Different Conformations and Functions: Insights into the Molecular Mechanism of Thermal Dissipation in Plants. Biochemical and Biophysical Research Communications **355**, 457-463

Zhang HM, Huang DR, Cramer WA (1999) Stoichiometrically Bound β-Carotene in the Cytochrome b_6f Complex of Oxygenic Photosynthesis Protects Against Oxygen Damage. Journal of Biological Chemistry **274**, 1581-1587

Zouni A, Witt HT, Kern J, Fromme P, Krauss N, Saenger W, Orth P (2001) Crystal Structure of Photosystem II from *Synechococcus Elongatus* at 3.8 Angstrom Resolution. Nature 409, 739-743

APPENDIX

Transient difference absorption traces at 45 wavelengths (indicated by the ordinate label) of the trimers (k_d=0). Time axis is linear from -1 to 1 ps and logarithmic thereafter. The dashed lines represent the fit using the model depicted in Figure 6, section 6.2. Insets depict residuals.

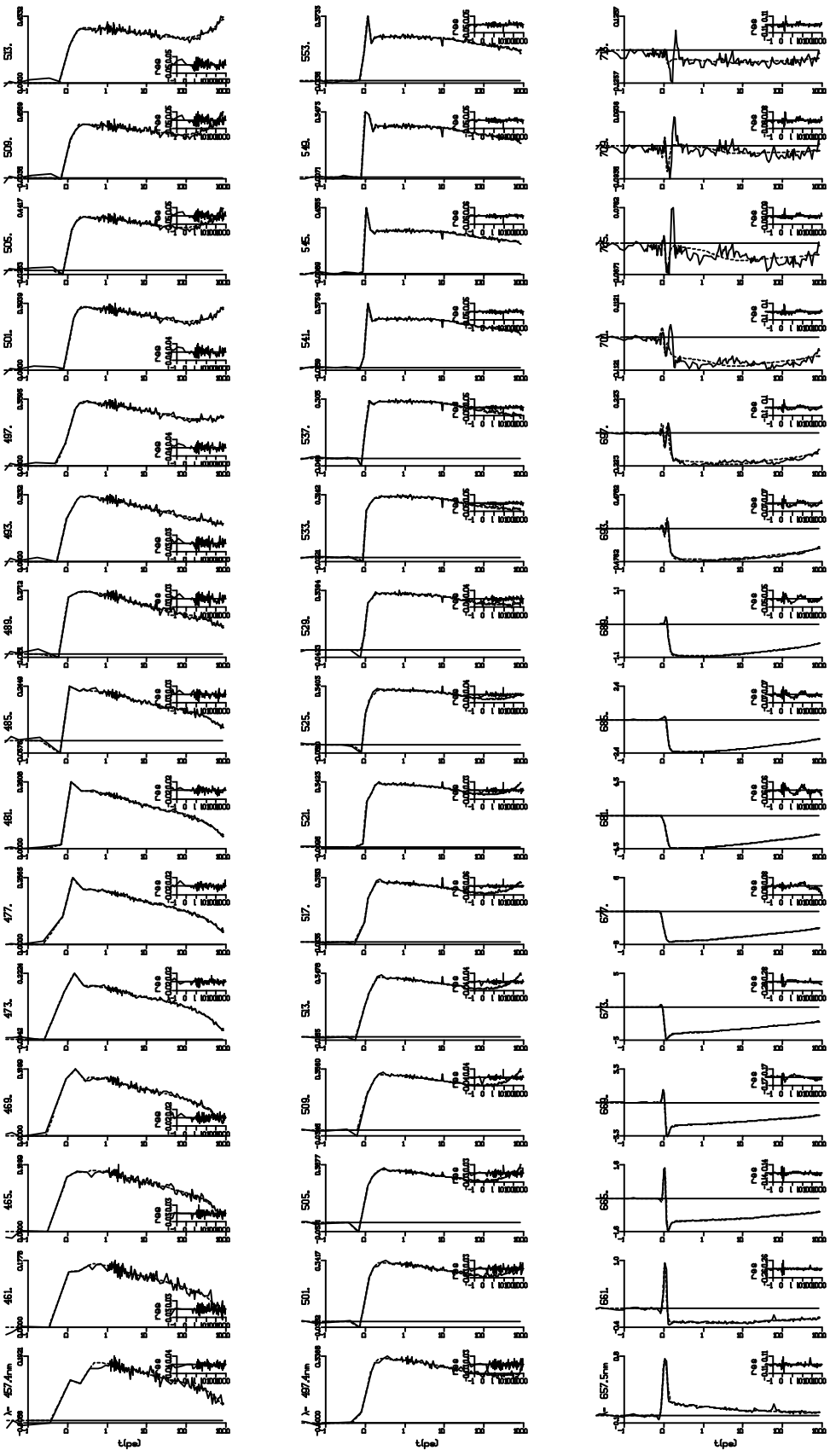
t (ps)

Transient difference absorption traces at 45 wavelengths (indicated by the ordinate label) of the sample with k_d=2. Time axis is linear from -1 to 1 ps and logarithmic thereafter. The dashed lines represent the fit using the model depicted in Figure 6, section 6.2. Insets depict residuals.

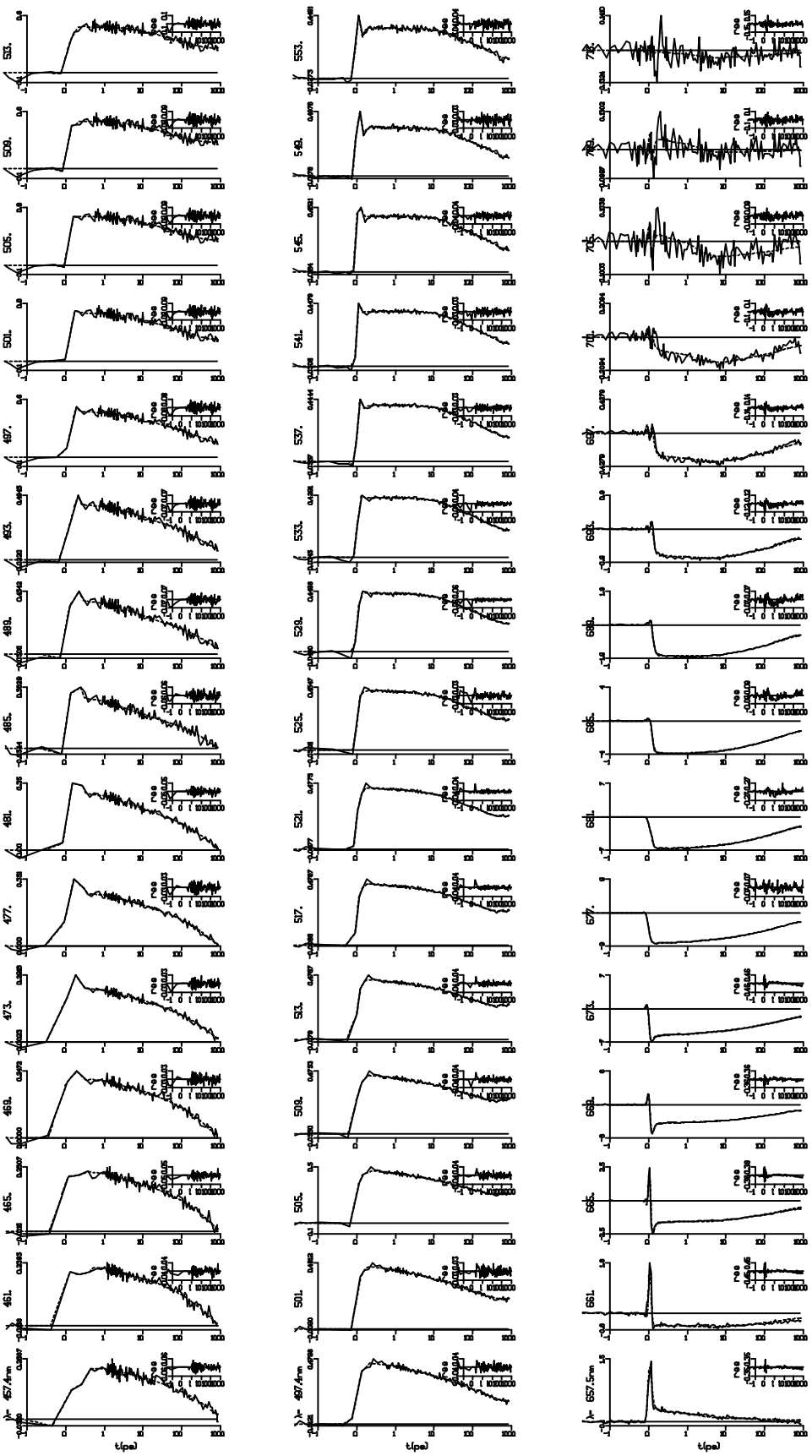
t(ps)

Transient difference absorption traces at 45 wavelengths (indicated by the ordinate label) of the sample with k_d=9. Time axis is linear from -1 to 1 ps and logarithmic thereafter. The dashed lines represent the fit using the model depicted in Figure 6, section 6.2. Insets depict residuals.

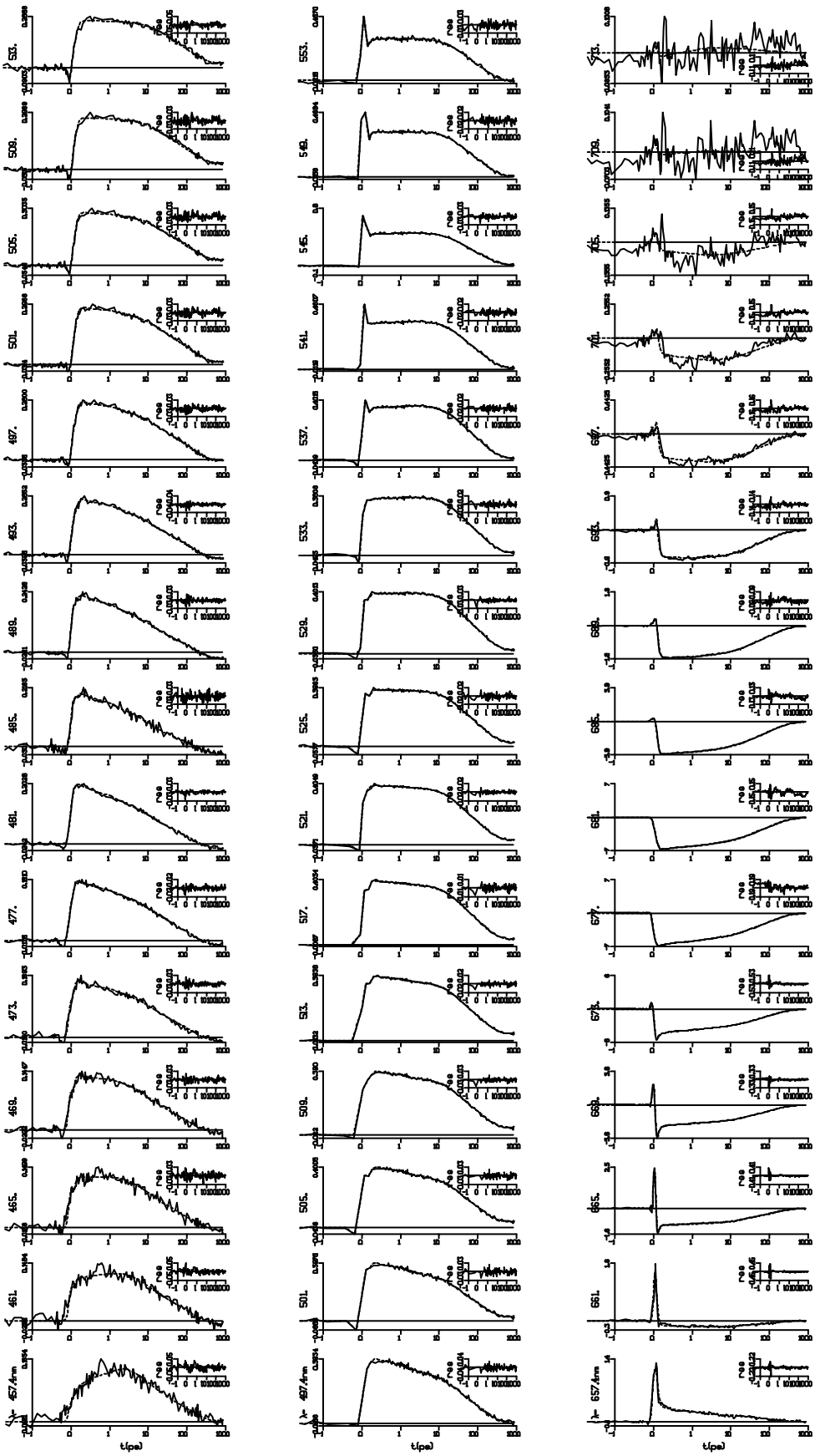

PUBLICATIONS